

For Reference

NOT TO BE TAKEN FROM THIS ROOM

EX LIBRIS
UNIVERSITATIS
ALBERTAENSIS



THE UNIVERSITY OF ALBERTA

HYDRAULICS OF END-DUMP CLOSURE OF ALLUVIAL CHANNELS

BY



BISHNU PRASAD DAS


A THESIS

SUBMITTED TO THE FACULTY OF GRADUATE STUDIES AND RESEARCH
IN PARTIAL FULFILLMENT OF THE REQUIREMENTS FOR THE DEGREE OF
DOCTOR OF PHILOSOPHY

DEPARTMENT OF CIVIL ENGINEERING

EDMONTON, ALBERTA

FALL, 1972



Digitized by the Internet Archive
in 2023 with funding from
University of Alberta Library

<https://archive.org/details/Das1972>

ABSTRACT

One method of river closure is by end-dumping loose non-cohesive materials from one or both banks progressively into the flow. This study was undertaken to experimentally develop comprehensive hydraulic design procedures for end-dump closure of alluvial channels.

A numerical measure defining stability, termed "efficiency of closure material", was introduced to denote the ratio of dumped material remaining within the dump zone at any stage of closure to the amount of material dumped. Efficiency of closure material, scour depth and backwater rise were correlated with the variables describing the characteristics of the fluid, the flow, the bed, and the closure material.

The most significant non-dimensional variables were found to be the Froude number of approach flow and the contraction ratio.

Experimental data was obtained from over 120 test runs with Froude numbers of 0.50, 0.29 and 0.10, using sand of median size 1.2 mm, 0.60 mm and 0.25 mm as bed material. Pebbles and rock chippings of 6.60 mm, 18 mm and 25 mm were used as closure material in a 7.5 foot wide flume fifty feet long.

Neither mean velocity through the constriction, nor velocity against the boundary was found to be a practical criteria for stability of the closure material. The stable size was found to correlate with

boundary shear stress as determined from measured velocity profiles.

Design curves for stable material size, maximum scour depth, backwater rise and rate of scour are presented. The design curve presented for stable material size is based upon a closure material efficiency of 90%. Comparison with the few available prototype closure data and with other studies of scour at constrictions are given.

The author is indebted to Mr. J. H. Smith of the Research Council of Alberta and Dr. J. Smith for the extremely fruitful discussions the author has with them throughout the investigation, to Dr. H. Hergenhahn, whose interest and research suggestions were helpful in initially framing and developing the study.

The author wishes to thank the staff of the Hydraulic Laboratory of the University of Alberta for their assistance in the execution of the experimental set-up.

The study was supported by the award of a scholarship to the author by the Commonwealth Scholarships and Fellowships Commission, Government of Canada. Partial financial support was also provided by the National Research Council of Canada. Technical support was provided in part by the Research Council of Alberta through the auspices of the Alberta Cooperative Research Program in Highway and River Engineering. Thanks are gratefully acknowledged.

ACKNOWLEDGEMENTS

The author is indebted to his supervisor Professor J.B. Nuttall for his suggestions, criticism and guidance provided throughout the course of the study. The author is thankful to Mr. C.R. Neill of the Research Council of Alberta and Dr. T. Blench for the extremely fruitful discussions the author had with them throughout the investigation, to Dr. N. Morgenstern, whose interest and research suggestions were helpful in initially framing and developing the study.

The author wishes to thank the staff of the Hydraulics Laboratory of the University of Alberta for their assistance in the erection of the experimental set-up.

The study was supported by the award of a scholarship to the author by the Commonwealth Scholarship and Fellowship Committee, Government of Canada. Partial financial support was also made available by the National Research Council Grant NRC A4334. Technical support was provided in part by the Research Council of Alberta through the auspices of the Alberta Cooperative Research Program in Highway and River Engineering. These are gratefully acknowledged.

TABLE OF CONTENTS

	<u>Page</u>
Title Page	i
Approval Sheet	ii
Abstract	iii
Acknowledgements	v
Table of Contents	vi
List of Tables	x
List of Figures	xi
Nomenclature	xv
 CHAPTER I INTRODUCTION	 1
1.1 Closure Methods	1
1.2 Characteristics of Closure Methods	3
1.3 Purpose and Scope	7
1.4 Outline of Contents	9
 CHAPTER II REVIEW OF LITERATURE	 12
2.1 Stability of Closure Material	12
2.2 Bed Scour due to End-Dump Constrictions	22
2.3 Maximum Backwater at End-Dump Constrictions	34
2.4 Concluding Remarks	41

TABLE OF CONTENTS (continued)

	<u>Page</u>
CHAPTER III THEORETICAL CONSIDERATIONS	42
3.1 Stability of Closure Material	42
3.2 Maximum Scour Depth	55
3.3 Maximum Backwater Rise	66
CHAPTER IV EXPERIMENTAL EQUIPMENT, MATERIALS AND PROCEDURE	69
4.1 Equipment	69
4.2 Materials	72
4.3 Procedure	80
CHAPTER V FLOW CHARACTERISTICS AND MATERIAL STABILITY: DATA ANALYSIS	87
5.1 Introduction	87
5.2 Flow Pattern Through End-Dump Constriction	89
5.3 Velocity Distribution Through Constriction	101
5.4 End-of-Closure Conditions	105
5.5 Stability of Closure Material	107
5.6 Concluding Remarks	131
CHAPTER VI ANALYSIS OF DATA ON BED SCOUR AND BACKWATER RISE	132
6.1 Introduction	132
6.2 Maximum Scour Depth	133
6.3 Time History of Scour	144
6.4 Check of Design Curves Against Previous Studies	154
6.5 Proposed Design Curves	161

TABLE OF CONTENTS (continued)

	<u>Page</u>
CHAPTER VI continued	
6.6 Maximum Backwater Rise	161
6.7 Concluding Remarks	167
CHAPTER VII SUMMARY, CONCLUSIONS AND RECOMMENDATIONS	169
7.1 Summary and Conclusions	169
7.2 Recommendations	177
LIST OF REFERENCES	179
APPENDIX A CHARACTERISTICS OF NORMAL FLOW	A1
A.1 Introduction	A2
A.2 Bed Forms	A2
A.3 Analysis	A3
APPENDIX B TURBULENT SEEPAGE THROUGH CLOSURE DAM	B1
B.1 Introduction	B2
B.2 Quantity of Seepage Through a Closure Dam	B5
B.3 Computation of K_f and Discussion	B7
APPENDIX C ANALYSIS OF DATA BY SHEAR-STRESS STABILITY CRITERIA	C1
C.1 Introduction	C2
C.2 Experimental Measurement of Drag on Advancing Boundary	C3
C.3 Effect of Hydrodynamic Lift	C8
C.4 Stability Analysis Considering Drag and Lift	C9

TABLE OF CONTENTS (continued)

	<u>Page</u>
APPENDIX C continued	
C.5 Analysis by Shields' Dimensionless Shear Stress	C12
C.6 Concluding Remarks	C14
APPENDIX D BASIC EXPERIMENTAL DATA	D1

LIST OF TABLES

<u>Table</u>		<u>Page</u>
4.1	Characteristics of Bed Material	75
4.2	Characteristics of Closure Material	79
4.3	Approach Flow Data of Some Rivers at Closure	81
4.4	Outline of Experimental Programme	83
5.1	Comparison of Experimental Stable Size with Values Given by Velocity Formulas	108
5.2	Particulars of Runs in Which Seepage Discharge Exceeded 10%	112
5.3	Effect of B/h Variation	120
5.4	Effect of d/h Variation	123
5.5	Particulars of Closure Tests from One Bank Only	125
5.6	Cross-Sectional Shape Effect	128
5.7	Verification of Design Curves	130
6.1	Experimental Data for Verification of Equation 3.31 with Coal and Pebbles as Bed Materials	140
6.2	Particulars of Runs Analysed for Rate of Scour	149
6.3	Comparison of Garde et al's (1961) Data and Liu et al's Data with This Study	160
A.1	Characteristics of Normal Runs	A5
B.1	Data for Computation of Coefficient of Turbulent Infiltration K_f of Closure Material	B7
C.1	Computation of Stable Size Considering Drag and Lift	C11
D.1	Basic Experimental Data	D1

LIST OF FIGURES

<u>Figure</u>		<u>Page</u>
1.1	Diagrammatic Illustration of Closure Methods	2
1.2	Definition Diagram for End-Dump Closure	6
2.1	Forces on a Stone on the Body of a Transverse-Dump Dam	13
2.2	Scour Patterns at an End-Dump Constriction	24
2.3	Relationship for Maximum Depth of Scour at an Abutment (Laursen, 1963)	28
2.4	Relationship for Maximum Depth of Scour in a Long Contraction (Laursen, 1963)	31
2.5	Comparison of Head Drop in Alluvial and Rigid Channel Constrictions (Liu, Chang and Skinner, 1961)	40
3.1	Definition Diagram for Efficiency of Closure Material	52
4.1	View of Experimental Flume Looking Upstream	73
4.2	Size-Distribution Curve for Bed Materials	74
4.3	Size-Distribution Curve for Closure Materials	77
4.4	Close View of the Closure Materials	78
5.1	Plot of Actual Contraction Ratio m_a versus Contraction Ratio m	88
5.2	Water Surface Topography for Flow Through an End-Dump Constriction	90
5.3	Flow Patterns Through End-Dump Constriction as Visualised by Confetti	91
5.4	General View of the End-Dump Dam and Scour Holes	93

LIST OF FIGURES (continued)

<u>Figure</u>		<u>Page</u>
5.5	Definition Diagram for Flow Contraction and Expansion	94
5.6	Plot of Coefficient of Contraction C_c , versus Contraction Ratio m	97
5.7	Relationships for Angle of Contraction ψ_1	98
5.8	Relationships for Angle of Expansion ψ_2	99
5.9	Non-Dimensional Profiles of the Live Stream Boundary	102
5.10	Velocity Distribution at Dump Line for Typical Contraction Ratios	103
5.11	Typical Velocity Distribution Along Flow	104
5.12	Plot of Mean Velocity at Dump Line V_2 , versus Contraction Ratio m	106
5.13	Relationship Between η , m , and D/h at F Values of 0.50, 0.29 and 0.10	114
5.14	Relationship Between D/h and m for $\eta = 0.97$ with F as the Third Parameter	116
5.15	Relationship Between D/h and m for $\eta = 0.90$ with F as the Third Parameter	117
5.16	Relationship Between D/h and m for $\eta = 0.80$ with F as the Third Parameter	118
5.17	Verification of Equations 3.15 and 3.19	121
5.18	Irregular Cross-Sections Tested	127
6.1	Typical Pattern of Bed Scour at a Low Contraction Ratio	134
6.2	Typical Pattern of Bed Scour at a High Contraction Ratio	135

LIST OF FIGURES (continued)

<u>Figure</u>		<u>Page</u>
6.3	Relationships for Maximum Scour Depth in Clear-Water Flow	137
6.4	Verification of Equation 3.31 for Maximum Depth of Scour in Clear-Water Flow	138
6.5	Design Curve for Maximum Scour Depth in Clear-Water Flow	141
6.6	Design Curve for Maximum Scour Depth in Sediment-Transporting Flow	143
6.7	Typical Scour Depth-Time Relationships During the Active Phase	146
6.8	Non-Dimensional Variation of Scour Depths with Time During the Active Phase	147
6.9	Verification of Equation 6.3 for Scour Depths During the Active Phase	150
6.10	Variation of $(d_t+h)/0.9(d_s+h)$ with t/t_{90}	152
6.11	Non-Dimensional Plots of Scour Profile	153
6.12	Comparison of this Study with Laursen's (1963) Analysis for Scour at Isolated Abutments	156
6.13	Comparison of this Study with a) Laursen's (1963) and b) Komura's (1966) Analyses for Scour in Long Contractions	157
6.14	Comparison of Garde et al's (1961) Data on Scour at Vertical Spur-Dikes and Liu et al's (1961) Data on Scour at Spill-Through Abutments, with this Study	159
6.15	Variation of Backwater Ratio H/h , with Contraction Ratio m	163
6.16	Relationships for Maximum Backwater Depth on Mobile Beds Correlating $(H/h)^3$ and $F^2(1/M^2 - 1)$	164
6.17	Relationship for Maximum Backwater Depth on Mobile Beds Correlating C , F and m	166

LIST OF FIGURES (continued)

<u>Figure</u>		<u>Page</u>
A.1	A General View of the Duned Bed; Bed Material Sand, $d_{50} = 0.25$ mm	A4
B.1	Relationship for Turbulent Seepage Through Closure Material	B6
B.2	Relationship Between Coefficient of Turbulent Infiltration and Material Size	B9
C.1	Experimental Measurements of Shear Stress on the End-Dump Boundary	C4
C.2	Non-Dimensional Boundary Shear-Stress ($\tau_o/\bar{\tau}_o$) Distribution in Constriction at $m = 0.56$	C6
C.3	Variation of Non-Dimensionalised Shear Maxima $\tau_{o_{max}}/\bar{\tau}_o$, on Advancing Boundary with Contraction Ratio m	C7
C.4	Variation of Efficiency of Closure η , with Shields Dimensionless Shear Stress Parameter τ_*	C13

NOMENCLATURE

A_f	= gross cross-sectional area of seepage, normal to flow
a	= length of closure dam normal to flow
B	= average width of approach channel
b	= width of opening at dump line computed as the mean of b_w and b_b
b_b	= width of opening measured at normal bed level
b_c	= average flow width (between live stream boundaries) at vena-contracta
b_{bs}	= width of opening measured at scoured bed level
b_w	= width of opening measured at water surface
C	= discharge coefficient (synonymous with C_d and C_m)
C_D	= drag coefficient
C_I	= empirical coefficient in Sandover's critical velocity formula (Eq. 2.15)
C_K	= Kindsvater and Carter's discharge coefficient
C_L	= correction factor to critical shear stress for cohesionless channel bank due to lift (Christensen)
C_T	= empirical coefficient in Sandover's logarithmic velocity formula (Eq. 2.16)
C_c	= coefficient of contraction = b_c/b
C_d	= discharge coefficient for constriction on rigid bed

- C_f = generalised Chezy coefficient for seepage (Eq. B.6)
 C_m = discharge coefficient for constriction on mobile bed
 C_z = Chezy coefficient in open-channel flow
 C_1, C_2 = coefficients in "velocity-stable size" relationships (Eqs. 2.4 and 2.8) due to Izbash
 D = representative size of closure material = D_{75} for sizes above 5 mm
 $D_{84}, D_{75}, D_{35}, D_{16}$ = grain sizes of which the given percent by weight of the closure material is finer
 D_1 = stable size of closure material from critical velocity formulae
 D_2 = stable size of closure material from shear stress considering drag and lift
 D_3 = stable size of closure material from shear stress considering drag only
 d = representative size of bed material = d_{50} for sizes up to 2 mm
 $d_{84}, d_{50}, d_{35}, d_{16}$ = grain sizes of which the given percent by weight of the bed material is finer
 d_s = limiting depth of scour below original bed level
 d_t, d_{ta} = depth of scour at time t during active phase of scour (Fig. 6.11)
 e = base of Napierian logarithms; porosity of coarse fill
 F = Froude number of normal (approach) flow = V/\sqrt{gh}
 F_D = drag force on a stone (closure material)

J_1, J_2, J_3 and J_4	= coefficients in relationships of closure material stability in eqs. 3.2 through 3.15
j_1, j_2	= exponents in " $\tau_{0\max}/\bar{\tau}_0 - m$ " relationship (eq. 3.6)
j_3, j_4	= exponents in " $\tau_{0\max}/\bar{\tau}_0 - m$ " relationship (eq. 3.26)
K	= a coefficient for closure material in Sandover's logarithmic velocity formula (eq. 2.16)
K_f	= coefficient of turbulent infiltration through closure material
K_m	= a multiplying factor in scour relationship (eq. 2.21) due to Izzard and Bradley, and Ahmad
K_s	= Strickler's coefficient
K_t	= surface area per unit volume of solids (eq. B.2) due to Wilkins
k_s	= Nikuradse effective sand grain roughness
L	= average width of closure dam along flow
L_b, L_f	= width of closure dam at base and at intermediate level
L_{01}	= length of backwater reach
L_{12}	= length from closure dam to the maximum backwater section
L_{23}	= length of contraction of live stream from dump line to vena-contracta
L_{34}	= length of expansion of live stream beyond vena-contracta
M	= opening ratio = $1 - m$
M_a	= actual or representative opening ratio (Biery and Delleur's equation 2.39)

m	= contraction ratio = $(B-b)/B$
m_a	= actual contraction ratio
n	= Manning's roughness coefficient
p	= an exponent in Garde's scour equation 2.27
Q	= normal (approach) discharge
Q_f	= seepage discharge through closure dam = $Q - Q_m$
Q_m	= measured discharge through the constriction over channel width b
q	= unit normal discharge
q_f	= unit seepage discharge through closure dam = $q_{f_1} + q_{f_2}$
q_{f_1}, q_{f_2}	= unit seepage in trapezoidal part and triangular part of closure dam (eqs. B.9 and B.10)
q_s	= unit sediment discharge for normal flow
q_{s_3}	= unit sediment discharge at section 33 (vena-contracta) out of scour hole for constricted flow
q_1, q_2, q_3 and q_4	= unit discharges at sections 11, 22, 33 and 44 respectively
R	= Reynolds number (Vh/ν or VD/ν or Vd/ν)
R_m	= hydraulic radius of the voids due to Taylor (eq. B.2)
R_n	= hydraulic mean radius for normal flow
R_*	= boundary Reynolds number = u_*d/ν
r	= ratio of depth of local scour at a constriction to depth of scour in equivalent long contraction (Laursen)
r_1, r_2, r_3 and r_4	= coefficients in turbulent seepage eq. B.1
s	= slope of the end-dump face = $\cot\theta$

- T, T' = coefficients in time-history of scour relationships (eq. 6.2) of Govindrao and Sharma
- t = time of scour
- t_e = characteristic time for scour to attain practical equilibrium
- t_{90} = time from commencement of scour to attain 90% of limiting scoured depth ($h + d_s$)
- U = free stream velocity in the flow direction
- u = velocity at depth y above theoretical bed
- u_1, u_2 = velocities at depths y_1 and y_2 for boundary layer flow
- u_{35} = velocity measured at $0.35 k_s$ above theoretical bed
- u_* = shear velocity ($=\sqrt{\tau_o/\rho_w}$)
- V = mean velocity of normal (approach) flow
- V_f = mean seepage velocity through porous fill
- V_t = velocity over closure material on a transverse-dump dam
- $V_{t_{min}}, V_{t_{max}}$ = minimum and maximum values of V_t that a stone can withstand (eqs. 2.4 and 2.8)
- V_v = mean seepage velocity through voids in the porous fill
- V_1, V_2, V_3 and V_4 = velocities at section 1-1, 2-2, 3-3 and 4-4 (subscript e refers to velocities after equilibrium scour is attained)
- V_{3_t} = velocity at section 3-3 (vena-contracta, location of deepest scour) at time, t
- V_* = shear velocity
- V_{*c} = critical shear velocity for bed material

V_{*t}	= shear velocity at time t
V_{*3e}	= shear velocity at section 3-3 (scour hole) after equilibrium
V_{*3t}	= shear velocity at section 3-3, at time t , during active scour phase
V_{\max}	= maximum velocity occurring against the end-dump face
W_s	= submerged weight of stone (closure material)
w	= fall velocity
x	= linear dimensions along scour hole
x_t, x_{ta}	= characteristic length of scour hole at time t (Fig. 6.11)
y, y_1 and y_2	= depths of flow normal to the boundary at which the instantaneous velocities are u, u_1 , and u_2
x_c, y_c	= Cartesian co-ordinates for live stream contraction (Fig. 5.9)
x_e, y_e	= Cartesian co-ordinates for live stream expansion (Fig. 5.9)
Z	= an expression relating unit seepage discharge q_f to coefficient of turbulent infiltration K_f (eq. B.11)
z	= a coefficient relating q_s and q_{s3} in sediment-transporting flow (eq. 3.34)
α	= angle of repose of closure material in water
α_e	= energy correction coefficient
β	= momentum correction coefficient
γ_D	= unit weight of closure material
γ_s	= unit weight of bed material
γ_w	= unit weight of water

η	= efficiency of closure material
λ	= an exponent in turbulent seepage equation B.1
ν	= kinematic viscosity
ρ_D	= specific density of closure material
ρ_S	= specific density of bed material
ρ_W	= specific density of water
$\Delta\rho_S$	= submerged specific density of bed sediment = $\rho_S - \rho_W$
σ_g	= geometric standard deviation of particle size (subscript d refers to bed material, subscript D refers to closure material)
τ	intensity of shear stress
τ_c	= critical shear stress for granular material on horizontal bed
τ_{cb}	= critical shear stress for granular material on a sloping bank
τ_o	= local intensity of shear stress on channel periphery or on end-dump face
$\tau_{o\max}$	= maximum intensity of shear stress on end-dump face
$\tau'_{o\max}$	= maximum intensity of shear stress on bed of the constricted channel
$\overline{\tau_o}$	= average intensity of shear stress on uncontracted channel periphery
τ_t	= intensity of shear stress on bed at time t from commence- ment of scour

- τ_* = Shields dimensionless shear stress = $\tau_o/(\rho_s - \rho_w)d$ or $\tau_o/(\rho_D - \rho_w)D$
- θ = angle of inclination of end-dump face with horizontal
- θ_1 = angle of inclination of the downstream slope of a transverse-dump dam (Fig. 2.1)
- θ_2 = angle of inclination of F_f with horizontal (Fig. 2.1)
- θ_3 = angle of inclination of F_D with horizontal (Fig. 2.1)
- ϕ = angle of repose of material
- ψ_1, ψ_2 = overall angle of contraction and expansion of the live-stream boundary with flow direction
- $\psi_{1\ell}$ = local angle of contraction at the dump line
- $\psi_{2\ell}$ = local angle of expansion just downstream of the vena-contracta
- ζ = total volume of material dumped over area 12341 (Fig. 3.1)
- ζ_* = useful volume of material remaining in closure area 1241 (Fig. 3.1)
- Φ = empirical coefficient in backwater rise equation 2.31 for rigid-bed channels, due to Liu, Bradley and Plate (1957)

CHAPTER I

INTRODUCTION

1.1 Closure Methods

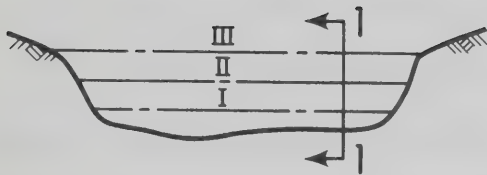
Prior to the construction of a major hydraulic structure on a flowing river a closure dam is usually built across the river, to divert the flow through an alternate waterway and dewater the work area. Closure dams are generally built with coarse, granular material varying in size from pebbles to loose rockfill. However, the use of earth or sand is possible where the situation permits. Closure of a river is accomplished by one or a combination of the following two basic methods:

(1) Transverse-dump method: - Closure material is dumped in more or less successive lifts uniformly across the river, until the closure dam emerges above water. (Fig. 1.1a).

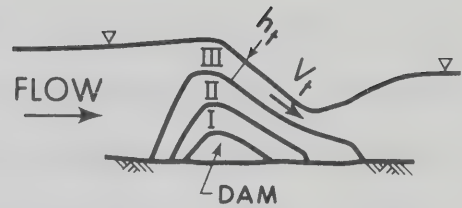
(2) End-dump method: - Closure material is pushed progressively from one or both banks to ultimately block the channel. (Fig. 1.1b).

A partial closure by the end-dump method is often used for building cofferdams for auxiliary works such as a powerhouse, a spillway, or a bridge abutment close to one bank. Construction of a spur on a flowing river is another example of partial closure by end-dumping. Diversion is not provided in such cases.

The construction engineer is required to assess in advance:

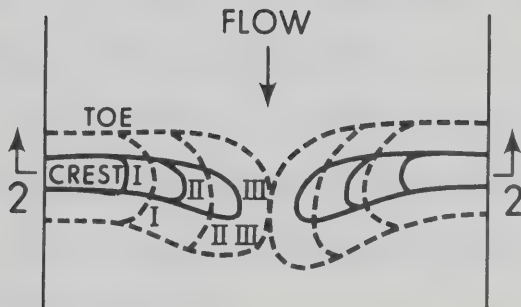


RIVER CROSS-SECTION
AT CLOSURE SITE

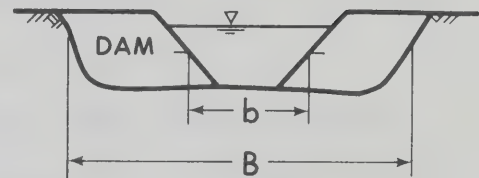


SECTION 1-1

(a) TRANSVERSE DUMP



PLAN OF RIVER AT
CLOSURE SITE



$$\text{Contraction Ratio } m = \frac{B-b}{B}$$

$$\text{Opening Ratio } M = \frac{b}{B}$$

SECTION 2-2

Note: I, II, III represent stage of
closure

(b) END DUMP

FIG. 1.1 DIAGRAMMATIC ILLUSTRATION OF CLOSURE METHODS

(1) the size of stable material at every stage of closure or alternatively, given the size of available closure material, to assess the critical height of the dam for transverse dump type or the critical gap width for the end-dump type,

(2) the quantity of material for the entire closure dam.

In the case of end-dump closure of alluvial rivers, considerable bed scour occurs at the dump area and downstream, particularly at high constriction. In such cases, the determination of the quantity of closure material becomes more involved.

Design procedures to arrive at the stable size of closure material at any stage of closure for both transverse and end-dump dams have until now (1972), been usually based upon the critical-velocity concept, the sequence being,

(1) assess the maximum velocity that occurs over the body of a transverse-dump dam or through the opening in an end-dump dam.

(2) compute the competent size of closure material on the basis of this velocity.

1.2 Characteristics of Closure Methods

1.2.1 Transverse-dump Method

From a trestle bridge or a cableway or a barge system, transverse-dumping is proceeded with uniformly across the full width of the river. The material upon dumping assumes and maintains a more or less trapezoidal shape under water (Fig. 1.1a). Continued dumping results in flattening of the downstream slope due to increased differential head and increased

flow velocity over the dam. The pertinent feature, however, is that the flow maintains a more or less uniform depth h_t , and a uniform transverse velocity, v_t , over the closure dam. The stability of the closure material is then predicted by correlation with the flow velocity close to the particle based on the studies of Blanchet (1946,1947), Izbash (1936), Izbash and Khaldre (1970), Izbash and Lebedev (1961), Olivier (1967) and design charts of U.S. Corps of Engineers (1970), all of which derive from the familiar Brahms-Airy Sixth power law (Leliavsky, 1955) for flow on a flat bed.

Straub (1953), and Neill (1967) have improved the procedure by relating the stable size on a channel bed to the depth of flow as well as to the mean flow velocity. It is indisputable that the mean velocity in a deep flow has to be greater than in a shallow flow to displace the same size of particle, because movement depends primarily on the shear or tractive stress on the stream bed. The mechanics of movement has been well summarized by the ASCE Task Committee on Sedimentation (1966)

"Thus it is seen that mean velocity alone cannot express the scouring action of the water at the bed and that to completely specify conditions the depth must also be given ... The advantage of using shear stress to specify critical conditions is that the one quantity suffices whereas if velocity is used one must also report the depth or the position at which the velocity is observed".

1.2.2 End-dump Method

(a) Closure of rigid-bed channels

Progressive lateral dumping to constrict the river from one or either banks dispenses with a bridge or a cableway and is a simple, economical scheme for closure of wide rivers (Fig. 1.1b). The definition sketches shown in Fig. 1.2 indicate the flow pattern through an end-dump constriction. These sketches illustrate the difference in water surface and bed configurations for closures on rigid-bed channels and alluvial channels. Increase in contraction ratio m , results in increased differential head and increased flow velocity through the constriction.

Lane (1919-20), Kindsvater and Carter (1955), Valentine (1958), Sandover (1969), and Izbash and Khaldre (1970), studying flow through open channel constrictions on rigid beds, have developed empirical coefficients for discharge, head loss and backwater rise. Using these coefficients mean flow velocity through the constriction (section 2-2 in Fig. 1.2b) can be calculated approximately, but no information was available for the velocity distribution either through the opening or against the advancing boundary (shown shaded in Fig. 1.2a) as the flow negotiates the constriction, Izbash and Lebedev (1961), and Izbash and Khaldre (1970), however, suggest that flow concentration to the extent of 20% over the mean velocity occurs against the end-dump face. They recommend the closure material to be competent against the increased velocity (using empirical correlations of transverse-

dump dams). For the curvilinear, rapidly accelerating flow through an end-dump constriction, this procedure is of questionable accuracy.

Pariset and Hausser (1959), and Sandover (1970) are probably the only researchers to have specifically reported on the stability of rockfill in end-dump closures on rigid-bed channels. They have presented empirical formulae for determining the stable size from relevant flow parameters and not by direct correlation with the flow velocity.

Pariset and Hausser's procedure involves predetermination of the head loss and the maximum backwater rise at the constriction. They have not suggested any method of evaluating these and presumably empirical coefficients of other researchers would have to be applied. Sandover's procedure involves a trial and error solution. As such both the procedures have limitations in practical application.

(b) Closure of alluvial channels

The coefficients of discharge and backwater determined for a constriction on a rigid-bed cannot be used to determine the velocity through an end-dump constriction on a mobile bed because of the possibility of bed scour. Sandover (1969) has determined similar coefficients for constrictions on a sand-bed channel in a laboratory flume (2 ft. wide), but his studies being inconclusive, the coefficients cannot be considered generally applicable.

1.3 Purpose and Scope

From the foregoing discussions it is obvious that knowledge even of end-dump closure on rigid-bed channels is by no means complete

and no specific procedure for alluvial channels has so far been formulated.

In the majority of cases where river closures are required, the bed is alluvium underlain by bedrock. The most general case is that in which the bedrock lies below the deepest scour level resulting from the constriction. This study was therefore framed to deal with the hydraulics of end-dump closure of alluvial channels. The specific objectives of this study are:

(1) to study the characteristics of flow through end-dump constrictions on an alluvial bed and to develop design curves which will directly determine the required stable size of closure material at each stage of the closure; and

(2) to develop design curves in respect of other associated phenomena of interest to the design and construction engineers, such as the configuration of the livestream boundary, the extent, pattern and time-rate of bed-scour at the dump line and the maximum backwater rise.

The key fact, however, is that all these flow phenomena mutually interact and the stability of the closure material is a composite effect. It needs to be mentioned that the mechanics of sediment movement in uniform flow over an alluvial bed is not fully understood yet; the difficulties and limitations inherent in the analysis of curvilinear, accelerating flow resulting from end-dump constrictions on alluvial channels, are thus obvious.

1.4 Outline of Contents

Previous studies relevant to end-dump river closures are reviewed in Chapter II. Studies on material stability in transverse-dump closures by Izbash (1936,1970) and the extension of such studies to end-dump closures by Sandover (1971) are examined. Specific studies either on bed scour or on backwater at end-dump constrictions, except for some qualitative informations by Sandover (1969,1970), do not appear to have been reported. Scour at an end-dump constriction is a combination of local and general scour. Investigations on local scour, such as due to bridge abutments or spur-dikes and on general scour due to channel contractions are reviewed. Studies on backwater due to different constriction geometry both on rigid-bed and alluvial channels are reviewed. The literature review revealed the lack of complete design procedures for end-dump closures, although valuable contributions have been made notably by Izbash and Sandover.

In Chapter III, comprehensive analyses of material stability, scour and backwater are made considering all the pertinent variables involved in an end-dump closure, such as the properties of the flow, fluid, closure material and bed material, and the constriction geometry. The role of shear stress in mobilizing the closure material and in scouring the bed, is specifically considered. Dimensional analysis is applied to derive non-dimensional parameters in respect of stability, scour and backwater. These analyses led to the formulation of the experimental programme for determining the parametric relations.

The experimental equipment, materials and procedure are detailed in Chapter IV. The tests were conducted in a 7.5 ft. wide flume and comprised over 120 runs utilising three sizes of closure material of 0.021, 0.059 and 0.082 ft., and three sizes of sand of 1.2 mm, 0.60 mm and 0.25 mm as bed material. The normal flow over the alluvial bed transported sediment in certain runs. The bed forms and the characteristics of normal test runs are described in Appendix A.

In Chapter V, the characteristics of flow through an end-dump constriction and its inter-relation with the stability of closure material are examined. Based on the analysis of data, design curves in respect of the flow contraction and expansion, and material stability are presented correlating the essential non-dimensional parameters developed in Chapter III. The hydrodynamic effect of the flow is analysed, giving due consideration to the reduction of the discharge through the constriction on account of the turbulent seepage through the porous closure material. An analysis of the turbulent seepage in the light of a non-linear flow law is made in Appendix B. Although correlation of the experimentally observed stable size with the velocity against the closure material was found to be unrealistic, a similar correlation with the experimentally observed shear stress against the closure material as shown in Appendix C, yields realistic results. The applicability of the design curves on stability developed from studies using rectangular and trapezoidal channels in the laboratory is tested against the few actual river closures for which data is

available.

In Chapter VI, analysis of the data in respect of scour and backwater, leading to the design curves is presented. The results of some check runs with coal and pebbles as bed material are discussed, indicating the satisfactory agreement of the experimental data with the analysis. Results of other researchers are compared with the findings of this study and satisfactory agreement is noted. A short summary, conclusion and recommendation for further studies is contained in Chapter VII. The complete experimental data is detailed in a tabular form in Appendix D.

CHAPTER II

REVIEW OF LITERATURE

2.1 Stability of Closure Material

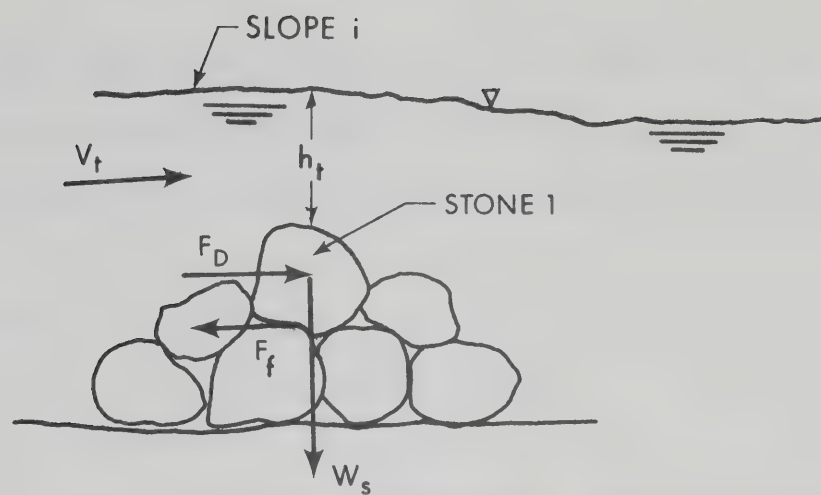
2.1.1 General

In order to be stable on the body of a closure dam the closure material has to withstand the hydrodynamic forces of the flow. Studies concerning the stability of rockfill forming a transverse-dump dam are based on the hydrodynamic effect of uniform or gradually varied flow on a level bed of coarse, non-cohesive, granular particles. Such analyses have been generally extended to end-dump closures. The available literature pertains to closures on rigid bed channels only.

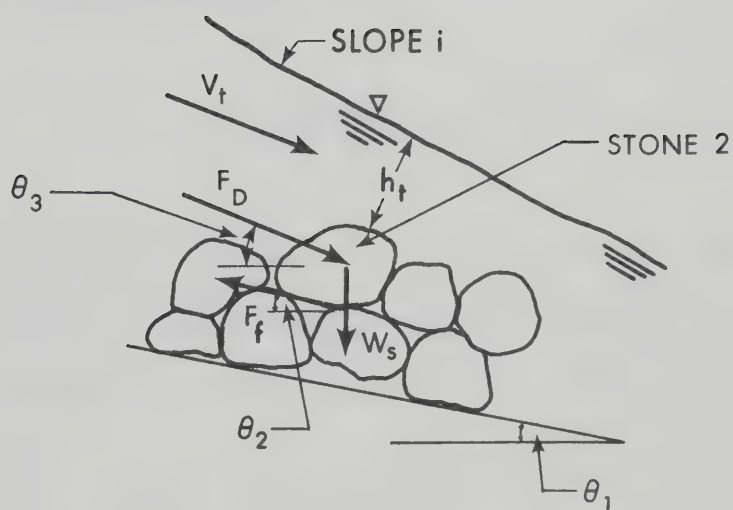
2.1.2 Analysis for Transverse-Dump Dams

Izbash (1936) and Blanchet (1947) are probably the earliest investigators to have analysed the stability of stones dumped to successfully close a channel transversely. Both considered the flow velocity over the closure material to be the most significant parameter. Their procedures and final equations correlating velocity with stable size are fairly similar.

Following Izbash (1970), the stability of a stone experiencing a velocity V_t (Fig. 2.1) requires analysis in two possible configurations on the body of the fill. For simplicity an equivalent spherical diameter D , is considered as the representative linear dimension of the stone.



(a) STONE ON CREST OF FILL



(b) STONE LYING PROTECTED ON SLOPE

FIG. 2.1 FORCES ON A STONE ON THE BODY OF A TRANSVERSE-DUMP DAM

In the first configuration (Fig. 2.1a) the stone 1, is lying exposed on the crest of the fill and is liable to slide down or overturn about an edge by the drag of the flow. The forces acting on the stone are

1) Drag,

$$F_D = C_D \gamma_w \left(\frac{\pi D^2}{4} \right) \cdot \left(\frac{V_t^2}{2g} \right) \quad (2.1)$$

in which C_D is a drag coefficient which depends upon the shape of the stone and a characteristic Reynold's number $V_t D / \nu$; ν being the kinematic viscosity of water; γ_w , the unit weight of water.

2) Submerged weight of the stone,

$$W_S = \left(\frac{\pi D^3}{6} \right) (\gamma_D - \gamma_w) \quad (2.2)$$

in which γ_D = unit weight of the stone.

3) Frictional Component of W_S ,

$$F_f = f \left(\frac{\pi D^3}{6} \right) (\gamma_D - \gamma_w) \quad (2.3)$$

in which f is the coefficient of friction of stone in water.

From statics, both for the limiting condition of equilibrium either by sliding or by overturning, algebraic manipulation will yield

$$V_{t_{\min}} = C_1 \left[2g \left(\frac{\gamma_D - \gamma_w}{\gamma_w} \right) \right]^{1/2} D^{1/2} \quad (2.4)$$

in which $V_{t_{\min}}$ represents the minimum flow velocity - capable of displacing the stone and C_1 is a coefficient which is a function of C_D and

f. Izbash evaluated C_1 empirically as 0.86.

In the second configuration (Fig. 2.1b) the stone 2, is lying in a pocket after sliding down the slope of inclination θ_1 . $V_{t_{\max}}$ is referred to the maximum stream velocity that this stone lying on the slope surrounded by other stones, can resist until limiting equilibrium is attained. The forces acting on the stone are

1) Drag acting at an angle θ_3 to the horizontal,

$$F_D = C_D \gamma_w \left(\frac{\pi D^2}{4} \right) \left(\frac{V_t^2}{2g} \right) \quad (2.5)$$

2) Submerged weight of the stone,

$$W_S = \frac{\pi D^3}{6} (\gamma_D - \gamma_w) \quad (2.6)$$

3) Frictional component of W_S ,

$$F_f = \frac{\pi D^3}{6} (\gamma_D - \gamma_w) \cdot \cos \theta_2 \quad (2.7)$$

in which F_f acts at an angle θ_2 to the horizontal.

Again from statics, for the limiting condition of equilibrium either by sliding or by overturning, algebraic manipulation will yield

$$V_{t_{\max}} = C_2 \left[2g \left(\frac{\gamma_D - \gamma_w}{\gamma_w} \right) \right]^{1/2} D^{1/2} \quad (2.8)$$

in which C_2 is a coefficient obviously higher than C_1 and depends upon

C_D , f , θ_1 , θ_2 and θ_3 and has been evaluated experimentally by Izbash to be 1.20.

Many rivers have been successfully closed by transverse dumping both in the U.S.S.R. and U.S.A. applying Izbash formula (Torpen, 1956, Linford, 1967).

Straub (1953) analysed the material stability from the theory of transportation in a wide channel. He evaluated the shear stress on the body of the dam for uniform flow and equated this to the critical tractive stress for the closure material. Referring to Fig. 2.1

shear stress on the body of the dam is,

$$\tau = \gamma_w \cdot h_t \cdot i \quad (2.9)$$

in which i = slope of the water surface.

τ_c , critical shear stress (Shields, 1936) for the closure material is given by

$$\tau_c = 0.06 (\gamma_D - \gamma_w) \cdot D \quad (2.10)$$

The slope of the water surface can be expressed in terms of flow velocity by applying Manning's formula,

$$V_t = \frac{1.486}{n} \cdot h_t^{2/3} \cdot i^{1/2} \quad (2.11)$$

in which n = the coefficient of roughness and is given by Chang (1939) as

$$n = 0.0432 D^{1/6} \quad (2.12)$$

Expressing equation 2-9 explicitly in terms of γ_w , h_t , V_t and D and, algebraically manipulating V_t , the mean velocity at which the closure material would get entrained is given by

$$V_t = 8.45 \left[\frac{\gamma_D - \gamma_w}{\gamma_w} \right]^{1/2} \left(\frac{h_t}{D} \right)^{1/6} \cdot D^{1/2} \quad (2.13)$$

In a transverse-dump dam the flow depth h_t and velocity V_t can be reliably computed, treating the flow as a friction controlled varied flow, from the energy and momentum principles.

2.1.3 Analysis for End-Dump Dams

In a transverse-dump dam, the closure material lies on a level bed, over which transversely uniform flow occurs. In contrast, in an end-dump dam, curvilinear accelerating flow occurs against the material lying on a slope (Fig. 1.2a). In spite of this, Izbash and Lebedev (1961) recommend the coefficients, correlating the stable size with velocity developed for transverse-dump dams, be applied to end-dump dams, although no information of laboratory studies by them, justifying such a procedure, are readily available. They however, recommend an arbitrary increase of 20% over the mean velocity through the opening, which accounts for flow concentration at the end-dump face, to be applied for predicting the stable size.

Izbash et al (1970) have presented non-dimensional curves for computing the discharge coefficient C_d , maximum backwater rise h^* , and head loss at the contraction along the centre line of flow ΔH for open channel constrictions (Fig. 1.2b). The mean velocity of flow through

the contraction which is to be closed by rockfill is then given by

$$V_2 = \frac{q_2}{H - \Delta H} = \frac{C_d [2g H]^{1/2}}{1 - \Delta H/H} \quad (2.14)$$

in which H , the depth of flow just upstream of the contraction is $h + h^*$, and q_2 is the unit discharge through the opening.

Equation 2.14 can be obtained by assuming weir flow through the contraction. The stable size corresponding to $1.20V_2$ can then be obtained from equation 2.4. For determining the stable size in an end-dump closure from Straub's equation 2.13, a similar semi-empirical approach as suggested by Izbash for obtaining the velocity and depth of flow will have to be resorted to. Depth of flow on the sloping boundary being variable, determination of the most critical combination of depth and velocity will involve a trial and error approach.

Sandover (1971) has recently developed two specific design procedures to arrive at the critical gap width for a particular size of closure material. In the first analysis, termed critical velocity method, Sandover assumed the instability to be caused by mean velocity through the gap. However, he experimentally determined the constant in equation 2.4 for computing the stable size instead of using Izbash's value of 0.86. For determining the mean velocity through the gap, he verified and accepted Valentine's (1958) discharge coefficient C_d for vertical sharp edged slot in rectangular channel as applicable to flow through an end-dump dam. The coefficient C_I , correlating the experimentally observed stable size with the mean velocity has been determined and curves pre-

sented by him. He has formulated a governing equation for stability to be balanced, in the form

$$C_I^2 = \frac{C_d^{4/3} \cdot Q^{2/3} \cdot \rho_w}{2g D b^{2/3} (\rho_D - \rho_w)} \quad (2.15)$$

in which C_I is Sandoover's empirical coefficient, Q = the discharge, ρ = specific gravity; suffix D refers to the dumped material and suffix w refers to water, $D = D_{75}$ = the nominal diameter of the dumped material defined herein as the sieve size passing 75% of the sample by weight and b = the gap width. The solution does not require determination of the flow velocity, but involves a trial and error procedure.

His second procedure termed the logarithmic velocity method is an improvement based on the concept that material entrainment starts after the maximum shear stress attained on the advancing boundary exceeds a critical value for the closure material. Sandoover determined the mean velocity through the gap using Valentine's C_d as in the first procedure. A logarithmic velocity distribution, normal to the curved boundary was assumed to obtain the velocity against the advancing face as a function of the mean velocity. From this the maximum shear stress on the advancing face was determined as another function of the mean velocity and was equated to a critical tractive stress for the material on the sloping boundary (Carter, 1953). In the analysis, coefficients were introduced and were determined empirically as in the first procedure. Curves for evaluating the coefficients have been presented. The governing equation for stability formulated in this case also needs

to be balanced by a trial and error procedure and takes the form

$$C_d^{2/3} \left(\frac{Q}{b}\right)^{1/3} = K \log \left(\frac{C_T b}{D}\right) \quad (2.16)$$

in which K is a constant for one size of closure material and C_T is an empirical coefficient.

Pariset and Hausser (1959) studied the stability for both straight and angled tip closure. Without elaborating the basis, they have developed an empirical relationship for stable closure material size (refer Fig. 1.2c) for straight closure as

$$D \cdot \frac{H_D^2}{H} = 0.80 \left(\frac{\Delta H}{H}\right)^{3/2} \quad (2.17)$$

in which H_D = height of the dam.

In the final stages of closure, the flow through the opening is minimal, when an alternate diversion is functioning. Then both ΔH and H_D approximate to H , which according to equation 2.17 results in an extremely uneconomical size of closure material given by

$$D = 0.8H \quad (2.18)$$

In this procedure, determination of the stable size needs in the first instance evaluation of the head loss at the contraction and the upstream backwater depth; both of which can only be evaluated by referring to other empirical coefficients. Hence this analysis seems to have limited applicability.

2.1.4 End-Dump Closures on Alluvial Channels

No systematic investigation of closures on alluvial channels appear to have been reported. Because considerable bed scour occurs at high contraction ratios in this type of closure, Izbash (1970) recommends rivers with rocky beds be closed preferably by end-dumping. Scanty qualitative information is available for end-dump closure on the alluvial Volga river (Izbash and Lebedev, 1961). Kuul (1970), Ovchinnikov (1970) have reported that the flow demanded an increase of stable size with increasing head-differential across the dam. Relevant analysis for determining the stable size has not been reported.

A protective blanket on the alluvial bed is generally provided prior to end-dump closure. In such cases if the bed scour is totally prevented, analysis for rigid bed channels would be applicable.

Sandover (1969) has obtained the discharge coefficient of end-dump constrictions on a coarse sand bed in a 2 ft. wide flume. These coefficients were consistently lower than the corresponding coefficients of Kindsvater and Carter (1953) obtained for similar sloping spill-through constrictions on rigid beds. Sandover has not advanced any reason for the lower coefficients, except rather inconclusively attributing it to closure material roughness, although it would be more reasonable to expect that the self-formed faces of the closure dam would tend to contract the flow as a venturi and thereby increase the discharge coefficient. In any case, a reasonably accurate determination of either the mean velocity or the velocity distribution against the end-dump face is not possible with the present knowledge. Sandover (1969) however states

without ample justification: "evidently the downstream scour will not affect the stability of the dam, unless it is sited on a very fine muddy ooze, which might move away from under the dam". Presumably based on this, he makes a statement (1971): "this scouring, however, did not appear to have any effect on the stability of the dam and consequently this work should be applicable to dams founded on loose erodible bed material".

2.2 Bed Scour Due to End-Dump Constrictions

2.2.1 Mechanics of Scour

A channel constriction generally results in two kinds of scour.

(a) Obstruction Scour or Local Scour

Small obstructions such as piers, abutments, or short spur dikes affect channel flow only in their vicinity. A vortex system forms near the obstacle and the increased bottom velocities associated with the vortices increase drag and lift on bed particles, which in turn causes local erosion (Neill, 1964, Vinje, 1967). Observations on abutments and piers by Laursen (1953), on vertical faced and other abutments by Liu, Chang and Skinner (1961), and on a vertical faced spur dike by Garde, Subramanya and Nambudripad (1961), show that deepest scour generally occurs around the upstream face of the obstacle.

(b) Contraction Scour or General Scour

A gradual contraction of a channel over sufficient length establishes a new regime of flow and causes a general degradation of the bed in the contracted reach, which is termed general scour. The depth of scour is then determined from consideration of the increased bed shear

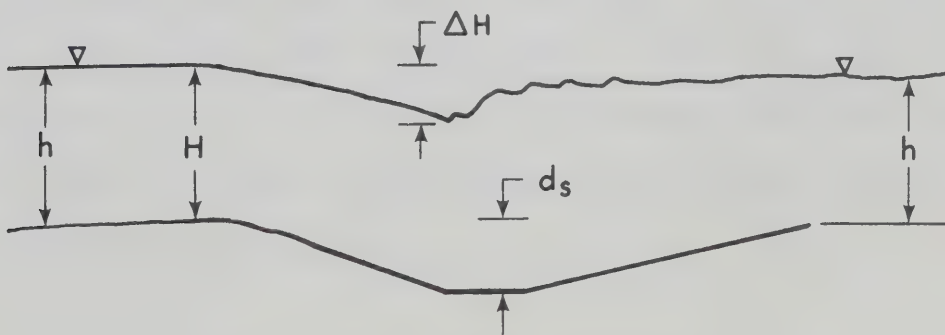
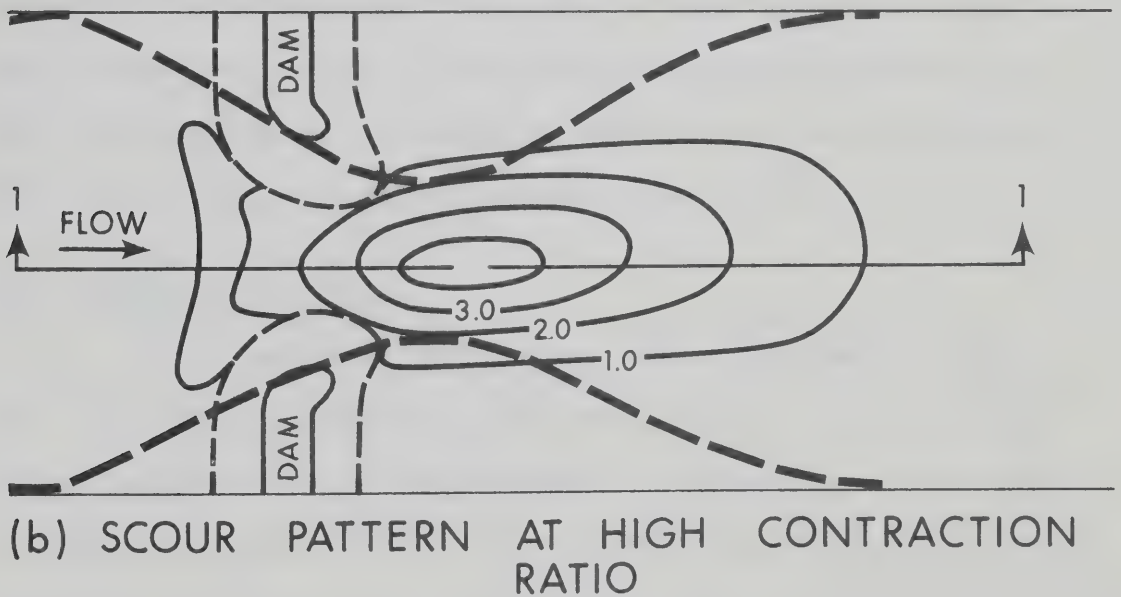
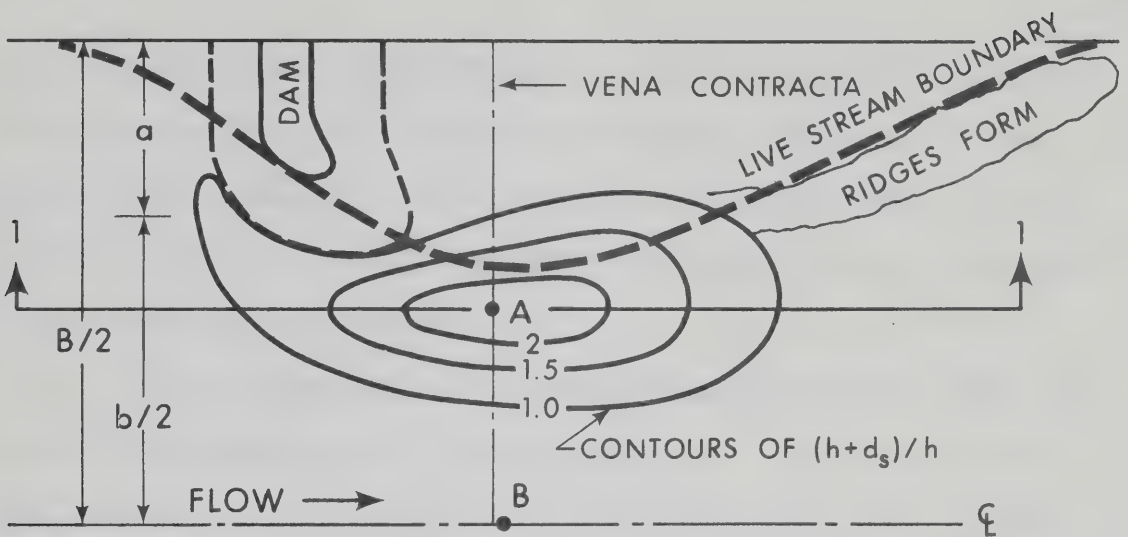
in the contracted reach. (Straub, 1936, Laursen, 1960 and 1963, Komura, 1966).

(c) Scour at End-Dump Closure Dams

The scour due to end-dump closure is essentially a combination of local scour and general scour. Typical scour patterns obtained experimentally in this study and shown in Fig. 2.2 attest to this.

At low contraction ratios, each wing of an end-dump dam behaves like a short spur-dike built out from one bank or like a projecting bridge abutment and creates local scour around its face. Because the geometry of the self-formed face of an end-dump dam is different from the rigid face of an abutment or a spur-dike, there is an essential difference in the scour patterns. Observations on abutments by Liu et al (1961), and on groins by Tison (1962), show that maximum scour around a vertical-face obstruction is deeper than that around a sloping-face or spill-through obstruction. These observations indicate the shape of the obstruction to be an important factor in local scour. The streamlined shape of the end-dump face in contrast to a blunt body produces a relatively weak wake and contracts the flow gradually in a venturi-shape from the dump line to the vena-contracta. This causes the deepest scour to move downstream of the dump line to the vena-contracta. The scour hole corresponds more or less to the inverted frustrum of an elliptical cone. (Fig. 2.2).

At higher degrees of contraction, the scour holes from the opposing sides overlap and a general pot hole scour pattern is observed over the entire gap as in a long-contraction. The deepest scour is also located downstream at the vena-contracta section.



(c) SECTION ALONG 1-1

FIG. 2.2 SCOUR PATTERNS AT AN END-DUMP CONSTRICTION

Location of the maximum scour at the vena-contracta section has been observed in the laboratory by Sandover (1970) for end-dump constrictions. Deepest scour was also observed downstream of the constriction for spill-through abutments in the studies of Liu, Chang and Skinner (1961) and Tutt (1972).

Although much analytical and experimental work has been done on scour, knowledge is still far from complete. The kinematics of flow, particularly vortex formation close to obstacles which produce local scour, has received little study. Design recommendations have been drawn largely from empirical data for specific constrictions. Useful summaries on scour at constrictions have been prepared by an ASCE Task Committee on Preparation of Sedimentation Manual (1962), by Neill (1964) and by the Highway Research Board (1970).

2.2.2 Maximum Scour Depth

A distinction is usually made between the "maximum scour depth" generally referred to in the context of the clear-water flow and the "equilibrium scour depth" generally referred to in the context of sediment-transporting flow. Komura (1966) describes these as static and dynamic equilibrium scour depth respectively. "Limiting scour depth" is also used to denote either of the terms. In this study the term "maximum scour depth" is used to denote the maximum depth below the original bed level whereas $(d_s + h)$ represents the maximum scoured depth below the original water surface.

Assessment of local scour as a consequence of an increase in the discharge intensity, has probably been the earliest approach. Lacey's studies on scour in alluvial rivers in regime, led to the formulation of a relationship by Khosla (1936) between d_s , the scour depth below the original bed and q , the discharge intensity per foot width of the main channel, as

$$h + d_s = 0.90 \left(\frac{q^{2/3}}{f_1^{1/3}} \right) \quad (2.19)$$

in which f_1 is Lacey's silt factor, which is a function of grain size of the bed sediment. The application of this formula to the calculation of scour at channel modifications such as bridge piers, bends or spur dikes, requires the use of a coefficient, which ranges from 1.0 to 3.5 to account for the flow concentration.

Blench (1957) reported an empirical correlation between $(h+d_s)$ and q developed from prototype data by Andru (1956) in the form

$$(h+d_s) F_b^{1/3} = 1.35 q^{0.74} \quad (2.20)$$

in which F_b is the bed factor. This is similar to Lacey's analysis.

Izzard and Bradley (1957) and Ahmad (1953) suggested relationships in the form

$$(h+d_s) = K_m (q_2)^{2/3} \quad (2.21)$$

in which K_m , a multiplying factor, is primarily a function of the spur-dike configuration and q_2 is the discharge intensity at the constriction, ($q_2 = q/l-m$).

The equations 2.24 through 2.27 indicate that the scour depth is primarily a function of the increased discharge intensity, which is a consequence of the constriction, but the functional relationship is complicated, being dependent upon other factors such as the geometry of the constriction, the bed material characteristics, the approach flow conditions and so on.

An analysis of scour in a long contraction by Straub (1934) and later by Laursen (1960) and Komura (1966) utilising the continuity equations for both discharge and sediment, have been based on the concept that the scour in a constricted reach would attain equilibrium after the sediment inflow balances the sediment outflow. Thus a distinction is made between the clear water scour and scour in sediment transporting flow. In the case of clear water scour the sediment inflow is nil and under equilibrium condition the boundary shear stress in the scoured region is the critical shear stress for the material. It is obvious that for the same approach flow conditions, the maximum scour depth for the clear-water case and the sediment-transporting case would be different from each other. Laursen's (1953) experimental observations indicate the maximum scour depth in the latter case to be largely independent of the flow intensity and size of the bed material but dependent principally upon the flow depth and length of the encroaching abutment.

Laursen (1960) considered a sudden constriction due to a

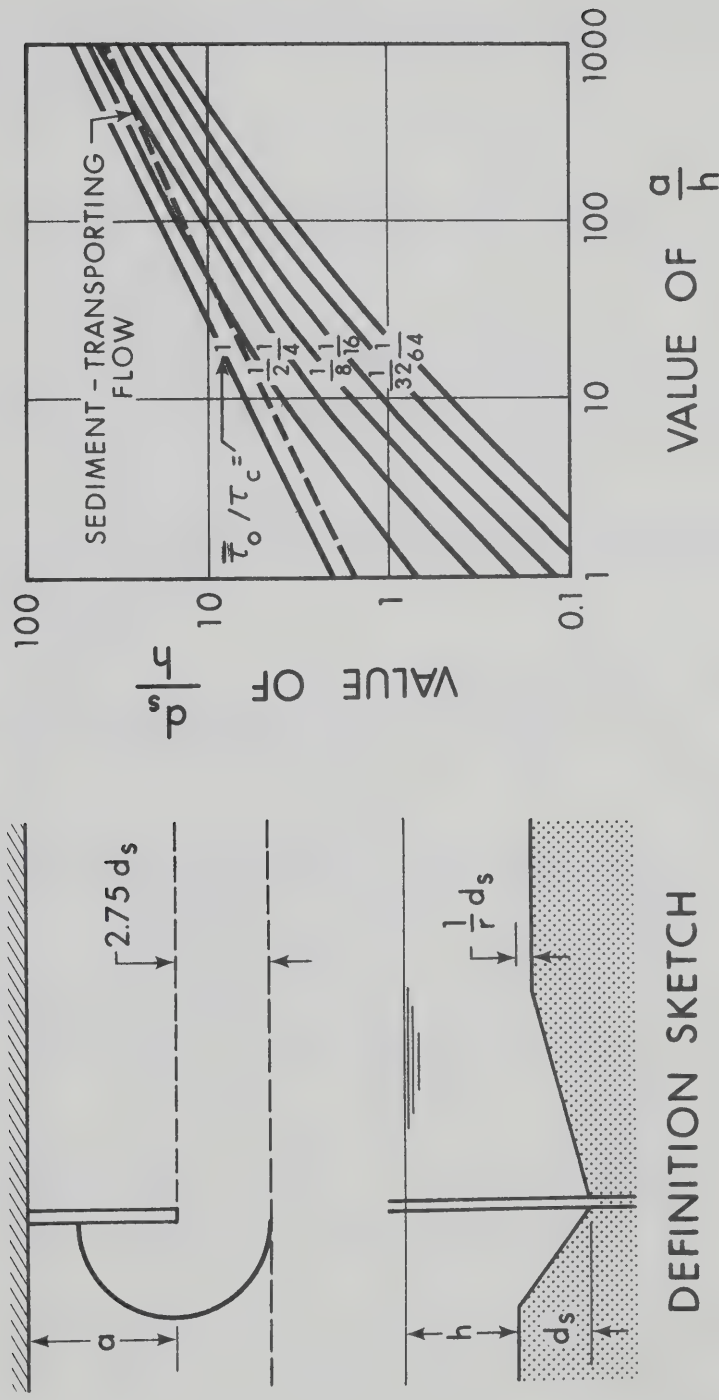


FIG. 2.3 RELATIONSHIP FOR MAXIMUM DEPTH OF SCOUR AT AN ABUTMENT (Laursen, 1963)

bridge as a "fore-shortened long contraction" (Fig. 2.3) and proposed a relationship for scour at an encroaching abutment under bed-load movement condition as

$$\frac{a}{h} = 2.75 \frac{d_s}{h} \left[\left\{ \frac{1}{r} \left(\frac{d_s}{h} \right) + 1 \right\}^{1.70} - 1 \right] \quad (2.22)$$

in which a = length of the encroaching abutment and r is a ratio of depth of scour at an abutment to depth of scour in a fictitious long contraction of width $a + 2.75 d_s$.

For the case of clear water scour at an encroaching abutment Laursen (1963) proposed

$$\frac{a}{h} = 2.75 \frac{d_s}{h} \left[\left\{ \frac{1}{r} \left(\frac{d_s}{h} \right) + 1 \right\}^{7/6} / \left(\frac{\bar{\tau}_0}{\tau_c} \right)^{1/2} - 1 \right] \quad (2.23)$$

in which $\bar{\tau}_0$ and τ_c are the boundary shear stress in the normal channel and the critical shear stress for the bed material respectively. Laursen does not consider the effect of the variation of r as significant. In Fig. 2.3 design curves to determine d_s from plots of equation 2.22 are drawn for $r = 12$ (based on experience of sediment-transporting flow) and for different values of $\bar{\tau}_0/\tau_c$. On Fig. 2.3 equation 2.23 is plotted in dashed line to determine d_s for sediment-transporting case. These curves are valid so long as the scour holes due to the two opposite abutments do not overlap. Laursen reasons that when the clear opening is more than $5.5 d_s$, interference is minimal. For further reduction in the opening, interference increases and at maximum interference the

scour depth is that due to a long contraction. In such a case the depth of scour for the clear water case is given by

$$\frac{(h+d_s)}{h} = \left(\frac{\bar{\tau}_0}{\tau_c}\right)^{3/7} \left(\frac{B}{b}\right)^{6/7} \quad (2.24)$$

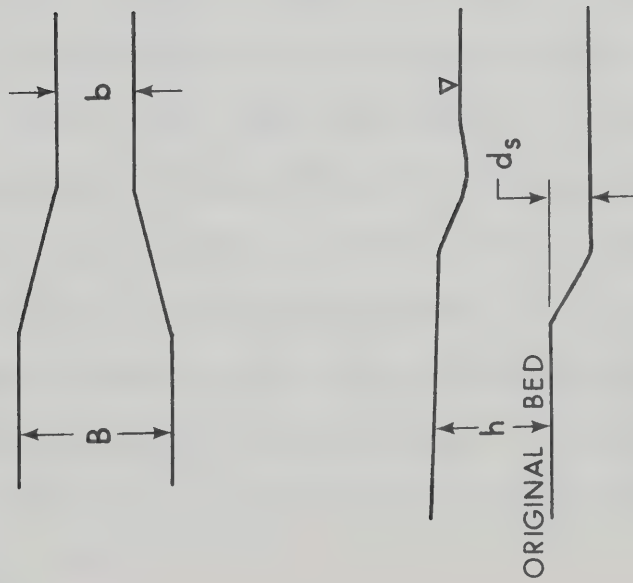
and for the sediment-transporting flow

$$\frac{(h+d_s)}{h} = \left(\frac{B}{b}\right)^{0.59 \text{ to } 0.69} \quad (2.25)$$

Design curves to determine d_s from equations 2.24 and 2.25 are shown in Fig. 2.4.

Considering the complexity of the problem, Garde, Subramanya and Nambudripad (1961), and Liu, Chang and Skinner (1961) have analysed the problem from a dimensional approach.

Garde, Subramanya and Nambudripad accepted the form of correlation of q_2 and $h + d_s$ (equation 2.21), but considered that logical dimensionless terms are inherent in the correlation and made dimensional analysis of all the pertinent variables. They studied scour around a spur-dike made of a vertical steel plate constricting an alluvial channel in the laboratory. Bed materials of median diameter 0.29 mm, 0.45 mm, 1.00 mm and 2.25 mm were used. They obtained a systematic correlation between the dimensionless scour depth $(h + d_s)/h$ and Froude number of the approach flow F and the opening ratio M for one size of the bed material. The variation of the three parameters for a sand of 0.29 mm was obtained by them as



DEFINITION SKETCH

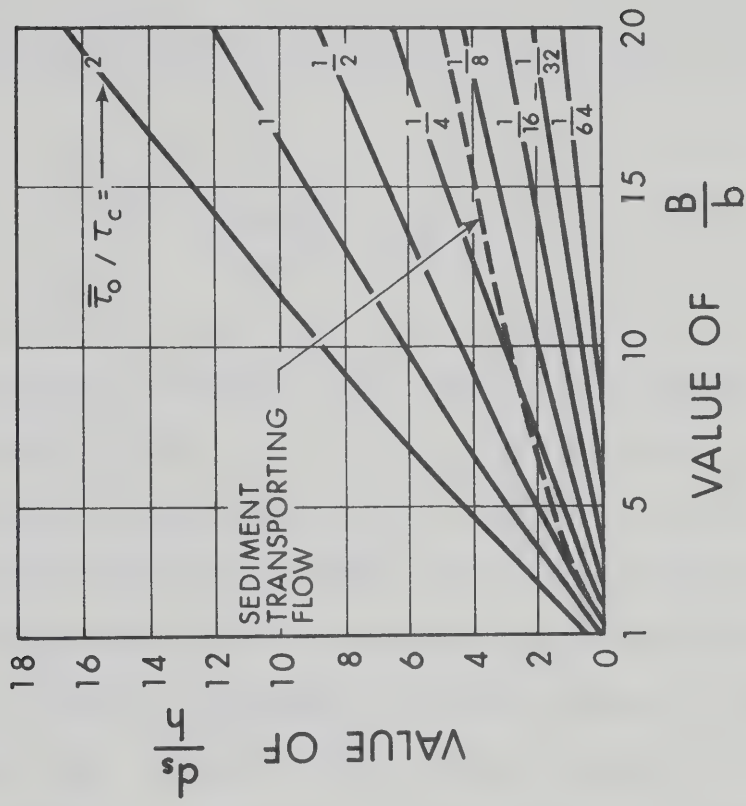


FIG. 2.4 RELATIONSHIP FOR MAXIMUM DEPTH OF SCOUR IN A LONG CONTRACTION (Laursen, 1963)

$$\frac{(h+d_s)}{h} = 4.0 \left(\frac{1}{M}\right) F^{2/3} \quad (2.26)$$

They concluded that in general a relationship exists in the form

$$\frac{(h+d_s)}{h} = J \left(\frac{1}{M}\right) F^p \quad (2.27)$$

in which J and p are functions of C_D , which is the drag coefficient of the bed sediment $= \{4/3(\gamma_s - \gamma_w) d\} / w^2 \rho_w$. They found that J varied in the range 2.75 to 5 and p varied in the range 0.67 to 0.90 for the bed sediment ranging from 0.29 to 2.25mm. Their experimental data convincingly indicated that even for sediment-transporting flow the depth of scour is not really independent of the flow intensity or the Froude number of the flow, although in most of their runs, prior to the introduction of the spur-dike either no movement, or only weak bed movement was occurring. Their data, however, showed a systematic trend when plotted on Fig. 2.3 thereby indicating that Laursen's equation 2.28 and 2.29 have merit. Neill (1962) argued that Garde et al's assumption that C_D adequately accounts for the sediment size is incorrect, because beyond a median size of 1.5 mm the fall velocity being proportional to the square root of size, C_D would be independent of the size and thus depth of scour would be same even for large boulders paving the bed. Neill (1962) basing on Blench's (1957) bed factor F_b , pointed out that an analysis of Garde et al's data indicated that the scoured depth might be expected to vary as $d^{-1/6}$.

Liu, Chang and Skinner have conducted extensive laboratory studies on the scour at bridge abutments of different shapes such as vertical wall, wing-wall, spill-through types. Their findings basically confirm those due to Garde et al, that the Froude number of approach flow F , as well as the opening ratio M are the most essential non-dimensional terms influencing scour.

For the case of sediment-transporting flow they obtained empirical equations for vertical wall models in the form

$$\left| \frac{(h+d_s)}{h} \right|_{\text{maximum}} = 0.3 + 2.15 \left(\frac{a}{h} \right)^{0.4} F^{1/3} \quad (2.28a)$$

and

$$\left| \frac{(h+d_s)}{h} \right|_{\text{equilibrium}} = 2.15 \left(\frac{a}{h} \right)^{0.4} F^{1/3} \quad (2.28b)$$

For the clear water scour the equation given was

$$\left| \frac{(h+d_s)}{h} \right|_{\text{limiting}} = 12.5 \left(\frac{F}{M} \right) \quad (2.29)$$

The scour depth for wing-wall and spill-through type abutments were lower than those for the vertical wall models for the same values of F and M .

Because only two sizes of sand of 0.56 mm and 0.65 mm were used in their experiments, no quantitative analysis of the effect of the sediment size has been done by Liu, Chang and Skinner.

2.3 Maximum Backwater at End-Dump Constrictions

2.3.1 Constrictions on Rigid Bed Channels

Lane (1920) is one of the earliest investigators to study open channel flow through sharp-edged vertical constrictions. His analysis was mainly based upon formulas by D'Aubuisson and Weisbach (Yarnell, 1934), where piers formed the obstruction to flow. He did indicate that a correlation may exist between the backwater ratio and coefficient of discharge, but no definite correlation was given.

Kindsvater and Carter (1953) and Tracy and Carter (1953) did extensive investigations of open channel flow through abutments of various shapes and geometry, using the approach of dimensional analysis. Their procedure of evaluating the maximum backwater can be summarized as follows.

Referring to Fig. 1.2b and applying the energy and continuity equation, a discharge equation is obtained as

$$Q = C_K b h_3 [2g(\Delta H + \alpha_e V_1^2 / 2g - h_{f_{1-3}})]^{1/2} \quad (2.30)$$

in which Q = discharge in cfs

C_K = Kindsvater's discharge coefficient

b = mean width of the contracted opening

h_3 = flow depth at section 3-3

$\alpha_e \frac{V_1^2}{2g}$ = weighted velocity head at section 1-1, where the mean velocity is V_1 and α_e is the energy coefficient

$h_{f_{1-3}}$ = head loss in friction between sections 1-1 and 3-3

By the aid of dimensional analysis C_K is found to be primarily dependent upon F_3 , the Froude number of the flow at section 3-3 ($F_3 = Q/bh_3[gh_3]^{1/2}$), m , the contraction ratio and L/b , the ratio of the length of the contraction in the flow direction to the opening width. Base curves to evaluate C_K correlated to m and L/b , for the case of vertical faced constrictions with square-edged abutments placed symmetrically at right angles to flow having $F_3 = 0.50$, have been presented. Curves for adjusting the discharge coefficient for other values of F_3 and other shape and angularity of constrictions have also been presented. The objective of the investigation was to predict the discharge through the constriction on natural rivers where h_3 and ΔH are known from field observations.

For similar vertical faced constrictions with square-edged abutments, Tracy and Carter have extended this study and have presented base curves for a dimensionless backwater rise $h^*/\Delta H$. By dimensional analysis $h^*/\Delta H$ was empirically correlated with the contraction ratio m and the Manning's roughness factor n . Adjustment curves for $h^*/\Delta H$ were also presented for other abutment shapes.

This method cannot be used to estimate directly the maximum backwater h^* from $h^*/\Delta H$ relationships because ΔH , which is dependent upon Q , h_3 and C_K , has to be evaluated in the first instance by a trial and error procedure.

Liu, Bradley and Plate (1957) recognizing the inherent difficulty in Tracy and Carter's procedure conducted studies for vertical-board, wing wall and sloping spill-through abutments. Analysis by

energy, momentum and continuity principles led to an equation for H , the depth of maximum backwater section, given by

$$\left(\frac{H}{h}\right)^3 = \frac{3}{2} F^2 \left(\frac{9\Phi}{4M^2} - 1\right) \quad (2.31)$$

in which F is the Froude number of the uncontracted normal flow; Φ is an empirical coefficient; M = opening ratio = $1-m$.

The empirical coefficient Φ was observed to depend upon the model type, F and M and is empirically correlated for a simple vertical board model as

$$\Phi = 1.33 \left[1 - \frac{2}{3} M^2 \left(2 - M - \frac{1}{3F^2} \right) \right] \quad (2.32)$$

The combination of equations 2.31 and 2.32 led to

$$\left(\frac{H}{h}\right)^3 - 1 = 4.83 F^2 \left[\frac{1}{M^2} - \frac{2}{3} (2.5 - M) \right] \quad (2.33)$$

The ultimate form of presentation of Liu, Bradley, Plate's data is a series of curves of $(H/h)^3$ plotted against $F^2(1/M^2 - 1)$. Their entire experimental data by dimensional analysis led to the inter-relation between essential dimensionless variables of the form

$$\frac{h^*}{h} = \text{function} \left(\frac{V}{\sqrt{gh}}, \frac{b}{B}, \text{model form} \right) \quad (2.34)$$

which the analytical relationship in equation 2.33 confirms.

The essential feature of their study is that the maximum backwater rise h^* , primarily a function of the uncontracted flow Froude number and the opening ratio, can be directly determined for different forms and shapes of constriction from their empirical correlations.

Studies similar to Liu, Bradley and Plate have been conducted for rectangular constriction plates by Valentine (1958) who also adopted a dimensional approach. Valentine assumed weir flow through the contraction to result in a discharge equation of the form

$$C_d = \frac{Q}{bH^{3/2}} \quad (2.35)$$

in which C_d = discharge coefficient, which Valentine determined empirically as a function of F and m and presented correlation curves of C_d and F with m as a third parameter.

Substituting $F(gh)^{1/2}$ for V , Q can be written as

$$Q = B.V.h. = B \cdot F(g)^{1/2} \cdot h^{3/2} \quad (2.36)$$

From equations 2.35 and 2.36

$$\left(\frac{H}{h}\right)^{3/2} = (g^{1/2}/C_d) \cdot \frac{F}{M} \quad (2.37a)$$

or
$$\left(\frac{H}{h}\right) = (g^{1/2}/C_d)^{2/3} \cdot \left(\frac{F}{M}\right)^{2/3} \quad (2.37b)$$

Biery and Delleur (1962) studied backwater rise through arch-

bridge constrictions. They postulated that equations 2.31 and 2.37b are similar, because if the leading term in equation 2.31 is only considered, both the equations indicate a generalised backwater equation of the form

$$\frac{H}{h} = f\left(\frac{F}{M}\right)^{2/3} \quad (2.38)$$

From their experimental results, Biery and Delleur presented an equation for any type of constriction in the form

$$\left(\frac{H}{h}\right) = 1 + 0.47 \left(\left(\frac{F}{M}\right)^{2/3}\right)^{3.39} \quad (2.39)$$

in which M' is the representative opening ratio. Liu, Bradley and Plate's data fitted equation 2.39 satisfactorily.

2.3.2 Constrictions on Alluvial Channels

Although considerable studies have been made to assess the maximum backwater on rigid bed channels, the only reported works on alluvial channels are those of Liu, Chang and Skinner (1961) and Sandover (1969).

Liu, et al's extensive study of the backwater rise at constrictions in alluvial channels is an extension of Liu, Bradley, and Plate's (1957) because Liu, Chang and Skinner accepted some form of correlation between the backwater ratio H/h and $F^2(1/M^2 - 1)$ (equation 2.31) even for alluvial channels, although energy and momentum equations for flow over the scoured bed at the constriction would be appreciably

different from rigid bed flow. They considered ΔH , the head differential to be a better representative term than h^* , the backwater rise and compared their $\Delta H/h$ with that due to Liu, et al (1957) as shown in Fig. 2.5. They made a rather qualitative conclusion that " ΔH for alluvial channels is about sixty per cent of that in a rigid channel".

Using a 2 ft. wide sand-bed flume, Sandover (1969) studied the backwater effects of end-dumped dams formed of materials of three nominal sizes ($D = 0.05$ inch, 0.22 inch and 0.44 inch). Sandover emphasized the difficulty of applying Carter and Tracy's method involving the unknown term ΔH . He therefore took the dimensional analysis approach also and obtained empirically the primary relationship between the non-dimensional variables of the form

$$\frac{h^*}{h} = \text{function} \left(\frac{V}{\sqrt{gh}}, \frac{b}{B}, \frac{b}{L}, \frac{b}{D} \right) \quad (2.40)$$

Sandover observed the terms b/L and b/D to be relatively unimportant and has presented curves for h^*/h versus m with V/\sqrt{gh} as the variable. Sandover's observed backwater coefficient h^*/h , when compared with Kindsvater's curves for similar type of sloping wall constrictions, were found to be consistently lower. Interestingly enough, Sandover did neither consider the size of bed material as an essential independent variable nor mention the effect of bed scour as pertinent, although he stated qualitatively that "deep scour hole just downstream of the toe of the dam and raised dunes on either side of this hole occurred when the larger materials were used as closure material.

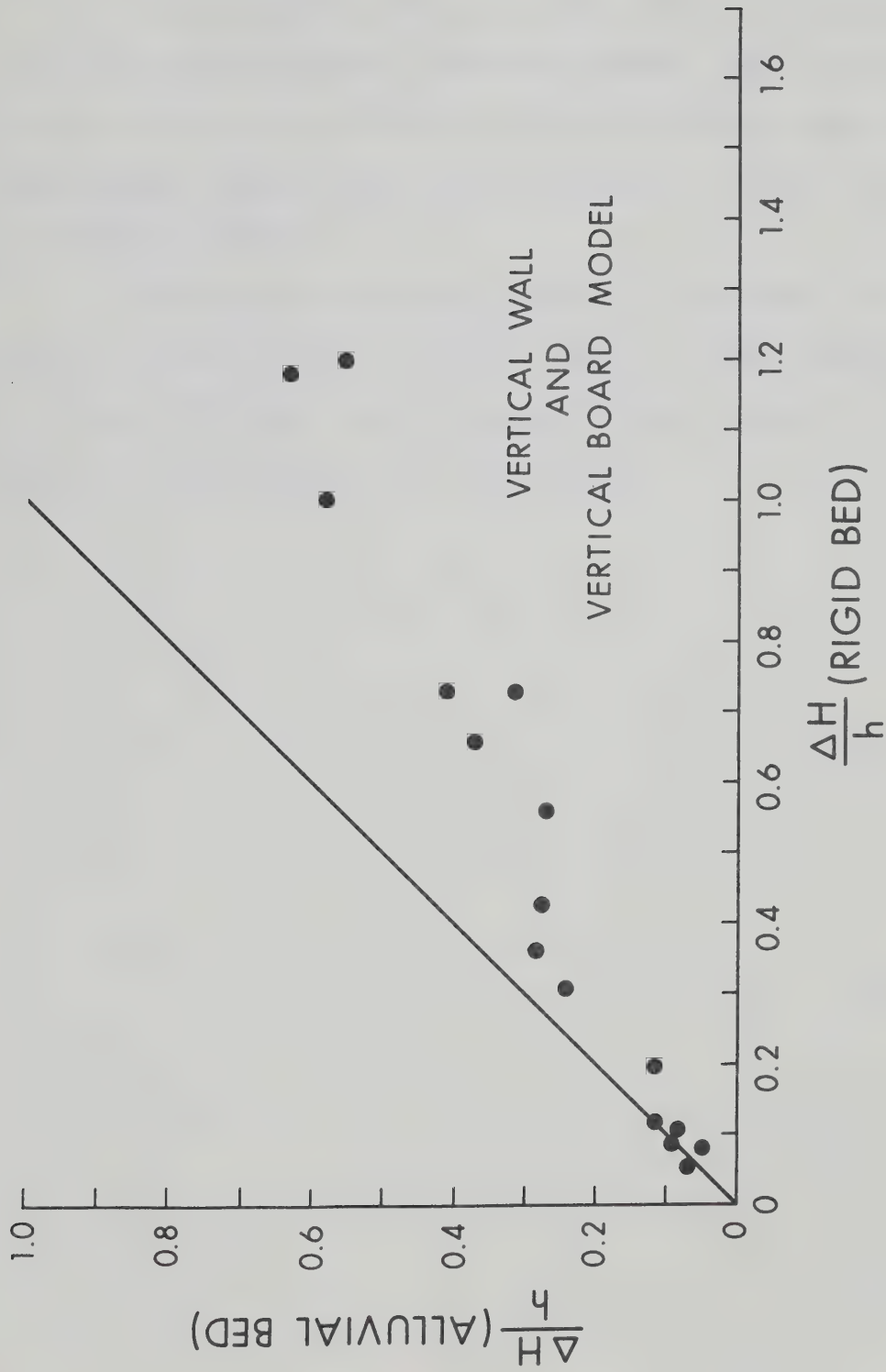


FIG. 2.5 COMPARISON OF HEAD DROP IN ALLUVIAL AND RIGID CHANNEL
CONSTRICTIONS (Liu, Chang and Skinner, 1961)

2.4 Concluding Remarks

In this chapter, previous studies relevant to the end-dump closure of alluvial channels have been reviewed. These studies pertain to the stability of closure material both in transverse-dump and end-dump closures, the bed scour, and the backwater rise due to constrictions in alluvials channels.

From review of previous research, it is evident that a systematic study of end-dump closure of alluvial channels has not been undertaken so far and that further study is needed in order to develop comprehensive hydraulic design procedures for such closures.

CHAPTER III

THEORETICAL CONSIDERATIONS

3.1 Stability of Closure Material

3.1.1 General

The present state of knowledge on the mobility of a stone end-dumped into the flow relies either on the maximum velocity against the stone (equation 2.4) or on the mean velocity and depth over the stone (equation 2.13). None of these quantities can be precisely determined for flow through an end-dump constriction even for a rigid-bed channel as clearly indicated in the foregoing discussions. The inaccuracies involved in computation of velocity and depth through the gap on alluvial channels would be even greater. A simple velocity approach, with the assumption that it accounts adequately for the entire hydrodynamic effect of the flow, suffers from a number of deficiencies.

3.1.2 Deficiencies of the Previous Design Methods

Detailed information regarding the flow velocity distribution through an end-dump constriction is not available. As such the recommendation of Izbash (1970), that a 20% increase over mean flow velocity occurs against the end-dump face cannot be considered as adequately representing the effect of the accelerating flow. Assuming that the maximum velocity against the boundary can possibly be evaluated empirically, no evidence appears to justify that velocity versus competent size relationships derived from criteria for incipient particle

movement on the level surface of a transverse-dump dam, are directly applicable for flow around an end-dump dam.

Raudkivi (1967) suggests that "impulse forces which are the consequence of turbulent agitation should be more important than mean boundary shear for entrainment of grains, whenever the boundary layer is turbulent." On a level bed, the turbulent fluctuations of drag force as high as twice the mean, occur due to velocity pulses up to 40% above the mean. Such fluctuations can cause instabilities at below-competent velocities. The turbulent velocity pulses, due to the accelerating flow on the extremely rough end-dump face are more intense than that on a level bed and cause substantial-increase in surface drag and lift forces. Hydrodynamic lift, which is not usually considered, can contribute substantially to instability as studies by Einstein and El Samni (1949) and Benedict and Christensen (1971) indicate.

The greatest single objection to a simple velocity criterion is that curvilinear flow with high local acceleration results in a higher surface drag than rectilinear flow. For flow through a curved trapezoidal channel bend, Ippen and Drinker (1962) have found boundary shear stress maxima 2.40 times of that on a straight level channel bed. Their conclusions for curvilinear flow can be summarised as

- (i) The boundary shear stress increases in intensity as well as in areal extent with conditions of increasing stream curvature presumably due to effects of local acceleration and secondary motion in the flow. Locations of shear maxima were generally found associated with the course of the filament of highest velocity and with the zones of locally

accelerated motion.

- (ii) The magnitude of shear maxima is not predictable from head loss (in terms of $V^2/2g$ i.e. by correlation with velocity) or by theory.

Because flow negotiating an end-dump dam is similar to flow in an acutely curved reach of channel, the advancing boundary would experience considerable increase of shear stress over the normal that occurs on the uncontracted channel boundary. Awazu's (1967) studies indicate that the shear stress on the bed of a rigid channel due to a symmetrically constricted flow increases to four times the normal, at a contraction ratio of 0.40 for an approach flow of Froude number around 0.50.

Relevant laboratory data or field observations of velocity and size are scarce and restricted.

Sandover's procedure, based primarily on the mean velocity consideration and using a trial and error solution offer an acceptable, but rather inconvenient design technique for closure of rigid-bed channels only. The limitations of Pariset and Hausser's procedure (1959) have already been stated.

An attractive and ideal solution would be to abandon the correlation of stable size with a maximum velocity, in favour a precisely determined maximum shear stress (ASCE Task Committee on Sedimentation, 1966) for coarse, granular closure material. Unfortunately it is not possible at present (1972) to predict analytically either the shear stress distribution or its maximum value for the accelerating flow.

In this study evaluation of the effect of shear stress on material entrainment is attempted by a semi-empirical analysis, although the design procedure recommended herein does not require any determination of shear stress. This is followed by dimensional analysis of all the relevant variables.

3.1.3 Theoretical Analysis by Critical Shear Stress Criteria

It is assumed that the threshold condition is attained after the maximum shear stress on the advancing boundary exceeds a critical value for the closure material. A semi-empirical analysis for closure of a simplified rectangular alluvial channel can be made as follows.

The uniform approach flow has a discharge Q , a mean velocity V , a uniform depth h and a uniform slope i_n (Fig. 1.2b). The bed material has a nominal diameter, d . From Manning's formula for uniform flow

$$V = K_S R_n^{2/3} i_n^{1/2} \quad (3.1)$$

in which K_S is the Strickler's coefficient, which for fully developed turbulence and hydraulically rough boundary can be considered as $(\text{Constant}/d^{1/6})$; R_n , the hydraulic radius can be considered equal to h for wide channels.

Equation 3.1 can therefore be written as

$$i_n = \frac{V^2 J_1^2 d^{1/3}}{h^{4/3}} \quad (3.2)$$

in which J_1 is a constant.

The shear stress on the bed for the normal uncontracted flow $\bar{\tau}_0$ is given by

$$\bar{\tau}_0 = \gamma_w \cdot h \cdot i_n \quad (3.3)$$

Substituting equation 3.2 in 3.3

$$\bar{\tau}_0 = \frac{\gamma_w \cdot h \cdot V^2 \cdot J_1^2 \cdot d^{1/3}}{h^{4/3}} = J_2 \cdot V^2 \left(\frac{d}{h}\right)^{1/3} \quad (3.4)$$

in which J_2 is a constant.

At a contraction ratio m , the maximum shear stress $\tau_{0_{\max}}$, on the end-dump face will appreciably exceed $\bar{\tau}_0$ (Ippen and Drinker, 1962).

Awazu (1967) proposes a relation between the ratio of the increased bed shear stress downstream of the contraction to the normal shear stress, and the contraction ratio m , in the form

$$\log_{10}(\tau_{0_{\max}}/\bar{\tau}_0) = 1.40 m - 0.021 \quad (3.5)$$

A similar exponential relationship is assumed for the maximum shear stress on the end-dump face, which gives

$$\left(\frac{\tau_{0_{\max}}}{\bar{\tau}_0}\right) = e^{j_1 m + j_2} \quad (3.6)$$

in which j_1 and j_2 are variable indices primarily dependant upon the Froude number of the approach flow F and closure material size D . In

actual practice the closure material is rarely a unigranular mass. In this study, the nominal size of the closure material which is a mixture, is taken as the D_{75} which is defined by the sieve size that passes 75% of the material by weight. U.S. Bureau of Reclamation (Lane and Carlson, 1953) recommends D_{75} as the representative size for coarse granular material. Sandover (1971) also considered D_{75} as the representative size.

The exponential increase of $(\tau_{o_{\max}}/\bar{\tau}_o)$ in relation to m was verified in this study, as reported in Section C.2, "Experimental measurement of drag on advancing boundary". From equations 3.4 and 3.6

$$\tau_{o_{\max}} = J_2 \cdot V^2 \left(\frac{d}{h}\right)^{1/3} \cdot (e^{j_1 m + j_2}) \quad (3.7)$$

From studies by Lane and Carlson (1953) the critical tractive stress on a sloping bank τ_{c_b} is given by

$$\tau_{c_b} = \tau_c \cdot \cos\theta \cdot (1 - \tan^2\theta/\tan^2\phi)^{1/2} \quad (3.8)$$

in which τ_c is the critical tractive stress for cohesionless, granular material on a horizontal bed, θ , is the angle of inclination of the slope, ϕ the angle of repose of the material:

τ_c for material of nominal size ≥ 0.03 ft. is given by (Shields, 1936)

$$\tau_c = 0.06 (\gamma_D - \gamma_w) D \quad (3.9)$$

Combining equation 3.8 and 3.9

$$\tau_{c_b} = 0.06 (\gamma_D - \gamma_w) \cdot \cos\theta (1 - \tan^2\theta / \tan^2\phi)^{1/2} \cdot D \quad (3.10)$$

Recent studies by Christensen (1971) indicate that the stable size determined by equation 3.10 is somewhat unsafe, because hydrodynamic lift has not been considered for the incipient motion. Christensen has proposed a correction factor L_r which when incorporated in equation 3.10 yields the correct form of the "size-critical shear stress relationship for a sloping bank" as

$$\tau_{c_b} = \{0.06(\gamma_D - \gamma_w) \cos\theta (1 - \tan^2\theta / \tan^2\phi)^{1/2} \cdot L_r\} \cdot D \quad (3.11)$$

L_r has a complex functional relationship with the particle size D_{35} , the roughness of the slope k_s , the angle of repose ϕ and the inclination of the slope θ . Christensen has proposed design charts correlating L_r with D_{35} , k_s , ϕ and θ . When the roughness/particle size ratio is small, L_r can be high enough to cause instability even on apparently stable flat slopes. L_r becomes insignificantly small as k_s/D_{35} increases.

Based on the foregoing considerations equation 3.11 can be written as

$$\tau_{c_b} = J_3 \cdot L_r \cdot D \quad (3.12)$$

in which J_3 is a coefficient functionally related to θ and ϕ . However J_3 varies within small limits because θ , the angle of inclination of the self-formed dam face is fairly constant and the variation of ϕ for

material coarser than 0.03 ft. is not appreciable (for example, for a typical slope of 2 horizontal to 1 vertical, the term $\cos\theta(1-\tan^2\theta/\tan^2\phi)$ varies from 0.63 to 0.774 for ϕ ranging from 35° to 45°). Considering the complex nature of variation of L_r , equation 3.12 can be further simplified to

$$\tau_{cb} = J_4 \cdot D \quad (3.13)$$

in which J_4 is a variable coefficient.

Equating 3.7 to 3.10 for the threshold condition

$$J_4 D = J_2 V^2 \left(\frac{d}{h}\right)^{1/3} \cdot e^{j_1 m + j_2} \quad (3.14)$$

Dividing both sides of equation 3.14 by gh for non-dimensionality and writing F^2 for V^2/gh

$$\frac{D}{h} = \left(\frac{J_2}{J_4}\right) \cdot F^2 \left(\frac{d}{h}\right)^{1/3} \cdot e^{j_1 m + j_2} \quad (3.15)$$

The functional relationship of the terms in equation 3.15 can only be evaluated by thorough experimental investigation. Assuming the variation of J_4 to be in a small range, a semi-logarithmic plot of $(D/h)(h/d)^{1/3}$ versus m should be linear for one Froude number of approach flow.

Equation 3.15 demonstrates that the mobility of the closure material on the end-dump face is a multidimensional problem. It was therefore considered pertinent to apply dimensional analysis to all the

variables involving flow, fluid, closure material, and channel bed material. At the outset of the experimental programme, in a series of preliminary runs, the velocity distribution and the maximum velocity occurring against the end-dump face were determined to study the effectiveness of the critical velocity criteria. In these runs a distinctive nature of the collective movement of the material, when pushed into the flow, was also observed.

3.1.4 Concept of Closure Material Efficiency

Before attempting dimensional analysis it was considered necessary to define the stability of closure material not merely qualitatively (for example by "first evidence of erosion" by Sandover (1971) or "beginning of entrainment of material" by Pariset and Hausser (1959) but rather quantitatively by introducing a numerical measure termed "efficiency of the closure material". The preliminary runs showed that at the threshold condition for a particular closure material the smaller sizes in the mixture become entrained rather selectively. Continued dumping of the same closure material (to constrict the channel further) resulted in the larger sizes becoming entrained at an increased rate and carried downstream. The advancing boundary slope flattened and progressed in a tongue-shape along the flow. However, some gain in contraction ratio over that corresponding to the threshold condition was attained. In an actual closure operation, where a mixture of quarry-run rock is pushed, a similar pattern of movement would probably occur. Therefore a term, efficiency of closure, is introduced to denote the

percentage by volume of closure material remaining stable within the limits of the dump line (i.e. within the useful area), out of the quantity dumped into the flow at any stage of closure. Figure 3.1 explains this with more clarity.

It is obvious that the efficiency of closure is unity until the onset of instability and that it decreases with increase in contraction ratio. The efficiency becomes nil when the closure material is completely carried downstream upon dumping and no longer results in any advance of the dam face.

3.1.5 Dimensional Analysis

The variables entering the problem can be grouped into the following categories.

(1) Geometry of the channel and the end-dump dam: B (approach channel mean width, b (mean gap width)). The geometry of the end-dump face is considered constant, because the face of the dam is self-formed. Constriction from one or both banks normal to the flow is considered.

(2) Flow characteristics: V (approach channel mean velocity), h (approach channel mean depth).

(3) Fluid characteristics: ρ_w (specific gravity of fluid (water)), ν (kinematic viscosity), g (gravitational acceleration).

(4) Bed material characteristics: d (median size), σ_{gd} (geometric standard deviation), ρ_s (specific gravity).

(5) Closure material characteristics: D (representing size, passing 75% by weight), σ_{gD} (geometric standard deviation), ρ_D (specific

gravity (assumed same as bed material)), α (angle of repose in water), η (efficiency of closure material).

As the flow against the coarse closure material will be fully rough turbulent, kinematic viscosity ν was considered unimportant and left out of the analysis.

Assuming that a particular size of closure material will have a particular efficiency of closure corresponding to a particular constricted width, the following function can be formulated.

$$\eta = f_1(B, V, h, \rho_w, g, d, \sigma_{gd}, \rho_D, \sigma_{gD}, \alpha, b) \quad (3.16)$$

Assuming repeating variables V, ρ_w and h , application of the π theorem yields the following combination of non-dimensional parameters.

$$\eta = f_2\left(\frac{B}{h}, \frac{b}{h}, \frac{D}{h}, \frac{d}{h}, \frac{\rho_D}{\rho_w}, \frac{V^2}{gh}, \sigma_{gd}, \sigma_{gD}, \alpha\right) \quad (3.17)$$

With the manipulation permissible within the theory of dimensional analysis, equation 3.17 can be rewritten as

$$\eta = f_2\left(\frac{B-b}{B}, \frac{V}{\sqrt{gh}}, \frac{B}{h}, \frac{d}{h}, \frac{D}{h}, \frac{\rho_D}{\rho_w}, \sigma_{gd}, \sigma_{gD}, \alpha\right) \quad (3.18)$$

As this study is limited to experimental closure material of specific gravity $\rho_D \approx 2.65$ and experimental fluid water, the ratio ρ_D/ρ_w will be a constant and is left out of analysis. The terms σ_{gd}, σ_{gD} , and α can be reasonably considered as secondary. As such their effects have

not been specifically studied. For these restricted conditions the stability equation reduces to

$$\eta = f_4 \left(\frac{B-b}{B}, \frac{V}{\sqrt{gh}}, \frac{D}{h}, \frac{d}{h}, \frac{B}{h} \right) \quad (3.19)$$

The principal non-dimensional terms influencing stability are considered to be m , the contraction ratio, V/\sqrt{gh} , the Froude number of approach flow, D/h , the ratio of closure material size to approach flow depth and d/h , the ratio of bed material size to approach flow depth. The effect of d/h which is a pertinent non-dimensional term for alluvial channels, is relatively minor in comparison to m , F and D/h , because the term $(h/d)^{1/3}$ appears in the stability equation 3.15. B/h is considered to have the least influence on stability.

In previous studies of flow through open channel constrictions, by Kindsvater and Carter (1955), Valentine (1958), Liu, Bradley and Plate (1957) and Liu, Chang and Skinner (1961), the Froude number of approach flow and the contraction ratio were observed to be the most significant variables. The ratio D/h in equation 3.19 can be considered as representative of the relative stability of the closure material against this approach flow.

Equations 3.15 and 3.19 led to the experimental investigation in the first instance, of the relationship between the principal non-dimensional terms F , m , D/h and η . The influence of d/h and B/h were studied in detail later.

3.2 Maximum Scour Depth

3.2.1 Clear Water Case

The literature review indicates that the maximum depth of either local scour or general scour is usually assessed;

(1) by relating to the increased discharge intensity (a regime type analysis) applying empirical coefficients, or

(2) from empirical correlations involving relevant non-dimensional variables describing the phenomenon; or

(3) from an analysis of sediment erosion in the constricted region by relating to the increased bed shear stress (Laursen 1960, 1963).

(This approach is strictly valid for a long contraction).

Each procedure has merit and has proved useful in practical applications (Highway Research Board, 1970). The principles of analysis involved in one procedure are not fundamentally different from that in the other procedures, but are really complimentary (Garde et al, 1961, Neill, 1962).

A regime type analysis requires the correct evaluation of the increased discharge intensity, which, however, is not possible for the non-uniform flow through a constriction. Use of empirical correlation of non-dimensional variables is justified if thorough studies have been made for the particular type of constriction, and if these variables describe the sediment characteristics completely. Shear stress approach can only be considered valid if the flow at the location of the deepest scour is two-dimensional.

Systematic scour studies at an end-dump constriction have

not been undertaken so far. It is not possible at present to determine the maximum depth of scour by a rigorous analysis of the three-dimensional flow at a bluff obstruction. An end-dump dam, however, behaves as a reasonably stream-lined obstacle. The contracting flow beyond the dump line, visualised by dye streaks in this study, indicated a predominantly two-dimensional pattern at all stages of closure. From the scour patterns obtained in this study it is obvious that the maximum scour that occurs close to the vena-contracta (at A in Fig. 2.2) is more a consequence of a two-dimensional flow with a high boundary shear (as in a long contraction) than of a vortex (as at a bluff obstruction).

Based on the foregoing discussions an analysis is made assuming the flow at A to be reasonably two-dimensional. The increased bed shear stress at the vena-contracta (Section 33 in Fig. 1.2) is considered primarily responsible for causing the deepest scour. The effect of sediment size and density is specifically considered in the analysis. For the clear-water case maximum scour depth is attained when the boundary shear in the scoured-hole is reduced to the critical tractive stress for the bed-sediment.

It is assumed that one-half of a channel having a normal flow width B , depth h and mean velocity V is blocked by an end-dump dam of length a . Laursen reasons that the obstructed flow hVa is restricted to flow over a width $2.75 d_s$ (Fig. 2.3) in addition to the normal flow. Therefore due to contraction of the flow, the discharge intensity q_3 at A (vena contracta location) would be the maximum to cause scour of depth d_s .

The mean velocity of flow V_{3_t} at A, at any time t ($t = 0$ at commencement of scour) is given by

$$V_{3_t} = q_3 / (h + d_t - \Delta H_t) \quad (3.20)$$

in which d_t is the depth of scour and ΔH_t is the head loss at time t . Because for subcritical flow $\Delta H_t \ll (h + d_t)$, (an assumption equivalent to neglecting the kinetic term as suggested by Laursen (1963), equation (3.17) can be approximated by

$$V_{3_t} = q_3 / (h + d_t) \quad (3.21)$$

and after maximum scour is attained, V_{3_e} , the mean velocity at A is given by

$$V_{3_e} = q_3 / (h + d_s) \quad (3.22)$$

For sediment - transporting flow, the equation of resistance can be approximated in a power form (Keulegan, 1938)

$$\frac{V}{V_*} = 7.66 \left(\frac{R}{k_s} \right)^{1/6} \quad (3.23)$$

in which V_* is the shear velocity, R = hydraulic radius \approx depth of flow. (Error introduced by this assumption is not significant for the two-dimensional flow at A), k_s = equivalent roughness (a function of V_* and d_{65}) $\approx d$.

From equation 3.23 at any time t

$$\frac{V_{3_t}}{V_{*3_t}} = 7.66 \left\{ \frac{(h + d_t)}{k_s} \right\}^{1/6} \quad (3.24a)$$

and after maximum scour is attained

$$\frac{V_{3e}}{V_{*c}} = 7.66 \left\{ \frac{(h+d_s)}{k_s} \right\}^{1/6} \quad (3.24b)$$

in which V_{*3t} and V_{*c} are the shear velocity at time t and critical shear velocity for the bed-sediment respectively. Because $V_{3e}(h+d_s) = V_{3t}(h+d_t)$, division of equation 3.24b by 3.24a yields

$$\left(\frac{V_{*3t}}{V_{*c}} \right)^2 = \left(\frac{\tau_{3t}}{\tau_c} \right) = \left\{ \frac{(h+d_s)}{(h+d_t)} \right\}^{7/3} \quad (3.25)$$

in which τ_{3t} is the bed shear stress at time t and τ_c is the critical shear stress for bed sediment.

At time $t = 0$, the depth of scour $d_t = 0$ and the bed shear stress is τ'_{0max} , which is the maximum attained as a result of the contraction. According to Awazu (1967) with the increase in contraction ratio m , τ'_{0max} increases exponentially and is related to the boundary shear stress for the uncontracted flow $\bar{\tau}_0$ in the form

$$\frac{\tau'_{0max}}{\bar{\tau}_0} = 10^{j_3 m + j_4} \quad (3.26)$$

in which j_3 and j_4 are coefficients primarily dependent upon F . (Base 10 instead of e is used for convenience in calculation).

Substitution of equation 3.26 in 3.25 corresponding to time $t = 0$, gives

$$\frac{\bar{\tau}_0 10^{j_3^{m+j_4}}}{\bar{\tau}_c} = \left\{ \frac{(h+d_s)}{h} \right\}^{7/3} \quad (3.27)$$

Substitution of d for k_s and h for R in equation 3.23 yields

$$\bar{\tau}_0 = V_*^2 \rho_w = \left(\frac{V^2 \rho_w}{7.66^2} \right) \left(\frac{d}{h} \right)^{1/3} \quad (3.28)$$

τ_c , assuming Shield's dimensionless critical shear stress (Laursen 1963) to be equal to 0.04, is given by

$$\tau_c = 0.04g (\rho_s - \rho_w) \cdot d \quad (3.29)$$

Division of equation 3.29 by 3.28 and substitution of F^2 for V^2/gh yields

$$\left(\frac{F^2}{2.34} \right) \left(\frac{h}{d} \right)^{2/3} \left(\frac{\rho_w}{\Delta \rho_s} \right) 10^{j_3^{m+j_4}} = \left\{ \frac{(h+d_s)}{h} \right\}^{7/3} \quad (3.30)$$

Equation 3.30 can be rewritten as

$$\frac{(h+d_s)}{h} = 0.695 F^{0.85} \left(\frac{h}{d} \right)^{0.29} \left(\frac{\rho_w}{\Delta \rho_s} \right)^{0.43} 10^{0.43(j_3^{m+j_4})} \quad (3.31)$$

According to Chitale (1967) for strict correspondence between the power law form in equation 3.23 and the logarithmic velocity distribution, the coefficient 7.66 and index $1/6$ are not constants, but variables in the range 3.2 to 7.66 and $1/12$ to $1/3$ respectively for

different bed regimes. The coefficient 7.66 is eliminated from this mathematical development. It is instructive to examine the form of the equation 3.31 for the index taking the extreme values of 1/12 and 1/3. For the index taking a value 1/12, equation 3.31 becomes

$$\frac{(h+d_s)}{h} = 0.675 F^{0.92} \left(\frac{h}{d}\right)^{0.384} \left(\frac{\rho_w}{\Delta\rho_s}\right)^{0.46} 10^{0.46(j_3^m+j_4)} \quad (3.32)$$

and for the index taking a value 1/3, equation 3.31 becomes

$$\frac{(h+d_s)}{h} = 0.725 F^{0.75} \left(\frac{h}{d}\right)^{0.13} \left(\frac{\rho_w}{\Delta\rho_s}\right)^{0.38} 10^{0.38(j_3^m+j_4)} \quad (3.33)$$

Because equations 3.32 and 3.33 are not significantly different from equation 3.31 and the law of resistance of sediment - transporting flow is not definitely established, equation 3.31 is considered appropriate for experimental investigation.

Considering the simplified assumptions made in this analysis it is expected that the indices in equation 3.31 would require some modification to comply with the experimental data.

3.2.2 Sediment-Transporting Case

The approach channel would transport bed load if $\bar{\tau}_o/\tau_c$ exceeds unity. In reality some movement commences earlier, around a $\bar{\tau}_o/\tau_c$ value in the range of 0.5 to 0.8, as Laursen's plots (Fig. 2.3) show. Several factors such as grain-size distribution of bed sediment, the variability of the critical tractive force particularly for fine sediments, and flow

characteristics are responsible for this. In this case, after introduction of the constriction, the flow as well the sediment input from the upstream from a channel width equal to a , (the length of the dam Fig. 2.3) would be carried over the scoured area in addition to the normal flow and sediment load. In other words, if q_s is the sediment discharge for the normal flow, then q_{s3} the sediment discharge out of the scour hole, after introduction of the constriction is given by

$$q_{s3} = q_s(1+z) \quad (3.34)$$

in which z , a coefficient, can reasonably be assumed to be a function of F and m .

Equation 3.34 can therefore be written as

$$q_{s3} = q_s \cdot f_1(F,m) \quad (3.35)$$

At A, corresponding to the equilibrium scour condition, the mean velocity V_{3e} and depth $h + d_s$, would just carry q_{s3} such that sediment output from the scour hole just balances the input. According to sediment discharge formula of Kalinske (1949)

$$q_{s3} = 10 V_{*3e}^2 d \left(\frac{V_{*3e}^2}{\Delta \gamma_s d} \right)^2 = 10 V_{*3e}^5 / \Delta \gamma_s d \quad (3.36)$$

and

$$q_s = 10 V_*^5 / \Delta \gamma_s d \quad (3.37)$$

in which V_{*3e} is the bed shear velocity in the scour hole at equilibrium.
From equations 3.36 and 3.37

$$\frac{V_{*3e}}{V_*} = \left(\frac{q_{s3}}{q_s} \right)^{1/5} \quad (3.38)$$

At time $t = 0$, (commencement of scour), V_{*3} , the bed shear velocity is related to the normal shear velocity by equation 3.26.

$$\frac{V_{*3}}{V_*} = (10^{j_3 m + j_4})^{1/2} \quad (3.39)$$

Application of equation 3.23 to the commencement and equilibrium scour conditions yield

$$\frac{V_{*3}}{V_{*3e}} = \left\{ \frac{(h+d_s)}{h} \right\}^{1/6} \left(\frac{V_3}{V_{3e}} \right) \quad (3.40)$$

Because $q_3 = V_3 \cdot h = V_{3e}(h+d_s)$, equation 3.40 can be rewritten as

$$\frac{V_{*3}}{V_{*3e}} = \frac{(h+d_s)^{7/6}}{h} \quad (3.41)$$

Eliminating V_{*3} between equations 3.39 and 3.41 and equating to equation 3.38

$$\frac{V_{*3e}}{V_*} = (10^{j_3 m + j_4})^{1/2} / \left\{ \left(\frac{h+d_s}{h} \right) \right\}^{7/6} = \left(\frac{q_{s3}}{q_s} \right)^{1/5} \quad (3.42)$$

Substituting 3.35 in 3.42 and algebraically manipulating

$$\frac{(h+d_s)}{h} = 10^{0.43(j_3^m + j_4)} / f_2(F, m) \quad (3.43)$$

Equation 3.40 indicates that $[(h+d_s)/h]$ is a unique function of F and m and the functional relationship can only be established by experimental investigation.

Equation 3.43 also substantiates the hypothesis postulated by Laursen (1953) that the sediment size is unimportant so far as the limiting scour depth in flows carrying appreciable sediment change is concerned.

3.2.3 Dimensional Analysis of Maximum Scour

The variables influencing maximum scour depth d_s can be grouped into the following categories:

(1) Flow Properties: V (approach channel mean velocity), h (approach channel mean depth).

(2) Geometry of the channel and the end-dump dam: B (approach channel mean width), b (mean gap width). Self-formed face of the dam is assumed to have a constant geometry.

(3) Fluid Properties: ρ_w (specific gravity of water), ν (kinematic viscosity), g (gravitational acceleration).

(4) Bed Material Properties: d (median size), σ_{gd} (geometric standard deviation), ρ_s (specific gravity), w (fall velocity to account for particle shape).

(5) Time of scour t : Closure material forming the dam is considered to have no significant effect on scour and is therefore left out of the analysis.

Assuming a particular maximum scour depth is attained at a particular time t , corresponding to a particular b , for particular approach flow conditions,

$$d_t = f_1(t, B, V, h, \rho_w, \nu, g, d, \sigma_{gd}, \rho_s, w, b) \quad (3.44)$$

Assuming V , ρ_w and h as repeating variables, π -theorem yields.

$$\frac{d_t}{h} = f_2\left(\frac{Vt}{h}, \frac{B}{h}, \frac{b}{h}, \frac{V^2}{gh}, \frac{V}{w}, \frac{d}{h}, \frac{\rho_w}{\rho_s}, \sigma_{gd}, \frac{Vh}{\nu}\right) \quad (3.45)$$

By manipulation of the dimensionless groups equation 3.45 can be written as

$$\frac{(h+d_t)}{h} = f_3\left(\frac{Vt}{h}, \frac{B-b}{B}, \frac{V^2}{gh}, \frac{V}{w}, \frac{d}{h}, \frac{\rho_w}{\rho_s}, \sigma_{gd}, \frac{Vh}{\nu}, \frac{B}{h}\right) \quad (3.46)$$

σ_{gd} has a definite effect on the depth of scour, as studies by Komura (1966) indicate, but because his experimental data showed the depth varied as $(\sigma_{gd})^{1/5}$ for the sediment-transporting case, and $(\sigma_{gd})^{1/2}$ for the clear-water case, variation in σ_{gd} over practical limits (1 to 2) would not be expected to significantly affect d_s . Hence in this study effect of variation of σ_{gd} is not specifically studied. Reynold's number of the flow Vh/ν is considered to have a secondary influence for

the turbulent flow in the low viscosity fluid (water). Variation of B/h is similarly considered to have insignificant effect. Although the fall velocity has been recognised by several investigators (Rouse, 1939) to be a characteristic parameter describing the shape and erosion characteristics of coarse sediments, it is established (Alger and Simons, 1968) that variability of shape can considerably affect the fall velocity. Correlations with equivalent spherical diameter, as is normally done are not reliable. From these considerations, the terms d/h and ρ_s/ρ_w are retained and V/w is left out of the analysis.

For these restricted conditions equation 3.43 can be re-written as

$$\frac{(h+d_t)}{h} = f_4\left(\frac{Vt}{h}, m, F, \frac{d}{h}, \frac{\rho_s}{\rho_w}\right) \quad (3.47)$$

From equation 3.47, the functional relationship for the maximum scour depth can be written as

$$\frac{(h+d_s)}{h} = f_5\left(\frac{Vt_e}{h}, m, F, \frac{d}{h}, \frac{\rho_s}{\rho_w}\right) \quad (3.48)$$

in which t_e is a characteristic time at which the scour practically ceases. It has been recognised (Neill 1964) that t_e for sediment - transporting flow is finite whereas for strictly clear-water flow, the limiting scour is attained asymptotically at infinite time. It is however reasonably correct to assume the non-dimensional scoured depth $(h+d_s)/h$ to be functionally related to m , F , d/h and ρ_s/ρ_w only

for both the clear water and sediment-transporting case, whereas a correct functional form of equation 3.47 for the clear water case should yield $(h+d_t)/h = 1$ at $t = 0$ and $(h+d_t)/h = (h+d_s)/h$ at $t = \infty$. (Govind Rao and Sharma, 1967). For the sediment transporting case the relationship should yield $(h+d_t)/h = 1$ at $t = 0$ and $(h+d_t)/h = (h+d_s)/h$ at $t = t_e$.

3.3 Maximum Backwater Rise

3.3.1 General

Analysis for rigid bed channels by Liu et al (1957), Valentine (1958), and Biery and Delleur (1962) have shown that the generalized backwater equation is of the form

$$\frac{H}{h} = f\left(\frac{F}{M}\right)^{2/3} \quad (3.49)$$

Unlike the rigid bed case, backwater rise in the case of a mobile bed is influenced by bed-scour. The bed scour downstream of the constriction (Fig. 2.2) is similar to a drop introduced in a sub-critical flow. It has been established from energy considerations that for subcritical flow through a constriction, a drop in the bed would result in a higher tail water or less head loss and less backwater than a flat bed. Because scour is related to the flow, fluid and sediment characteristics, the head loss or the backwater rise given by equation 3.49 would logically involve additional non-dimensional terms involving sediment size. The closure material size is also important, particularly in the case of dams with wide crest and base widths. The

effect of turbulent seepage when employing large irregular quarried blocks would also be appreciable on the backwater rise. It is thus obvious that any generalized backwater equation for end-dump closures involving a number of variables would be deficient and cannot be considered applicable to all situations.

3.3.2 Dimensional Analysis of Backwater Rise

The variables considered are the flow, fluid and sediment properties dealt with in section 3.1.5 and 3.2.3, as well as the depth of scour d_s and length of the dam L , along the flow. Dimensional analysis yields a relationship between the most essential variables in the form

$$\frac{H}{h} = f_1\left(m, \frac{B}{h}, F, \frac{d}{h}, \frac{D}{h}, \frac{d_s}{h}, \frac{L}{h}\right) \quad (3.50)$$

It has been established in equation 3.31 that d_s/h is a function of F , m and d/h . In the limited scope of experimental investigations L/h variation will not be significant and hence left out. Sandover's (1970) study supports this hypothesis. Similarly B/h and D/h are considered of secondary importance.

Equation 3.50 can therefore be rewritten as

$$\frac{H}{h} = f_2\left(F, m, \frac{d}{h}\right) \quad (3.51)$$

From the foregoing discussions, it is apparent that the experimental data can be analysed to develop correlations (1) between

$(H/h)^3$ and $F^2\{1/M^2 - 1\}$ according to the findings of Liu and Bradley and Plate (equation 2.19) and (2) between C and F with m as a third parameter, as suggested by Valentine (equation 2.23).

In both these analyses, the effect of d/h is critically examined to evaluate its effect as equation 3.51 indicates.

Because both clear-water flow and sediment-transporting flow will have the same essential non-dimensional terms given by equation 3.51, separate analysis for each case is not warranted.

CHAPTER IV

EXPERIMENTAL EQUIPMENT, MATERIALS AND PROCEDURE

4.1 Equipment

4.1.1 General

The equipment used in the testing may be divided into

- (1) the flume and the flow system, and
- (2) the measuring devices.

4.1.2 Flume and Flow System

(a) Main Flume

Experiments were carried out in a 60 ft. long non-recirculating flume (referred to as flume), 7.5 ft. wide by 4 ft. deep with a horizontal bottom resting on the laboratory floor. The side walls were built of 8 in. wide hollow-concrete blocks. Of the 4 ft. depth available in the flume, the bottom 1.5 ft. was filled with the bed material over 50 ft. length. A head tank, an upstream stilling pool between the head tank and the flume, and a drop box downstream of the tail gate took up an overall length of 10 ft.

The downstream end of the flume was designated as station 0 and the upstream end as station 50. Of the 50 ft. length of alluvial bed, a 30 ft. stretch between stations 7 and 37, where uniform water surface slope could be attained was used as the test area. The bed elevation (top of the alluvial bed) was arbitrarily designated as

1.500 ft. The bed fill of 1.5 ft. allowed for full vertical development of the scouring action around the end-dump dams, which were built symmetrically from both walls at station 26 for all the runs in series A, B, C and D and at station 25 in the other series. (Section 4.3.1).

Flow in the system to the extent of 3 cfs was provided by two centrifugal pumps, which drew supply from an underlying sump. The flow was received in a head tank and the discharge was measured by calibrating the overflow weir in the head tank. Baffles and wire mesh screens were provided in the head tank and in the upstream stilling pool of the flume. The downstream end of the flume was provided with a tail gate which could be cranked up or down about its bottom (horizontal axis) kept at the bed elevation. This tail gate regulated the stage-discharge pattern of the normal flow required in the study.

The flume had provision for a 2 ft. wide rectangular notch in the left wall at station 35 for effecting diversion of the flow during closure studies. Provision was made to modify the notch to a triangular shape if required. The bottom of the notch was kept at the bed elevation.

(b) Subsidiary Flume

Studies on stability, scour and back water were carried out in the main flume. To supplement the studies on scour, a few check runs were carried out with pebbles and coal as bed material (Section 4.2.1b). A small, 1 foot wide glass walled flume was used for this purpose.

4.1.3 Measuring Devices

The principal recording instruments comprised;

(1) A point gauge for measuring the water-surface elevation and the static bed elevation at any point within the flume. The point gauge was equipped with a vernier to measure to the nearest 0.001 ft.

(2) An electronically sensed propeller meter, for velocity measurement. The propeller meter was mounted on a special swivel, so that continuous velocity traverses could be taken at any inclination, particularly normal to the curved advancing boundary. The propeller meter was also equipped with a vernier to measure flow depth to the nearest 0.001 ft. The propeller meter was connected to an autograph recorder. This permitted measurement of velocity to the nearest 0.01 fps.

(3) An electronic bed probe for recording bed elevation under water as scour progressed. The probe maintained a constant distance above the bed and worked on an optical principle. Light was fed through optical fibres and reflected back from the bed into a photo cell, which operated a servo-mechanism. The bed probe was also connected to an autograph recorder and could be calibrated to read to the nearest 0.001 ft.

The point gauge, the propeller meter and the bed probe were mounted on a single carriage, which could travel along the flume on the rails fixed on the side walls.

Other recording instruments were two steel tapes, fixed on the two flume walls and a third steel tape fixed on the carriage to provide

readings for the longitudinal and transverse locations of the principal instruments.

A stationary point gauge was provided in the head tank to measure the head on the overflow weir. Another stationary point gauge was provided at the tail gate to record the tail water elevation. A third point gauge was provided at the diversion notch.

A view of the main flume looking upstream, (Fig. 4.1) shows the carriage with the point gauge, the propeller meter, the bed probe and the autograph recorders.

4.2 Materials

4.2.1 Bed Material

(a) Sand

Three sizes of sand of 1.20 mm, 0.60 mm and 0.25 mm median diameter, were used as bed materials to cover the applicability of this study to closure of alluvial channels. (U.S. Bureau of Reclamation recommends the size passing 75% of the material by weight as the representative size for coarse non-cohesive materials above 0.2 inch. For sizes up to 5 mm, it was arbitrarily decided to accept the median size and above 5 mm, the 75% size as the representative size in this study).

The size distribution curves are shown in Fig. 4.2. The characteristics of bed material are presented in Table 4.1.

(b) Other Bed Materials

The design recommendations of this study are based on the results of tests (runs 1 to 100) carried out in the main flume, with

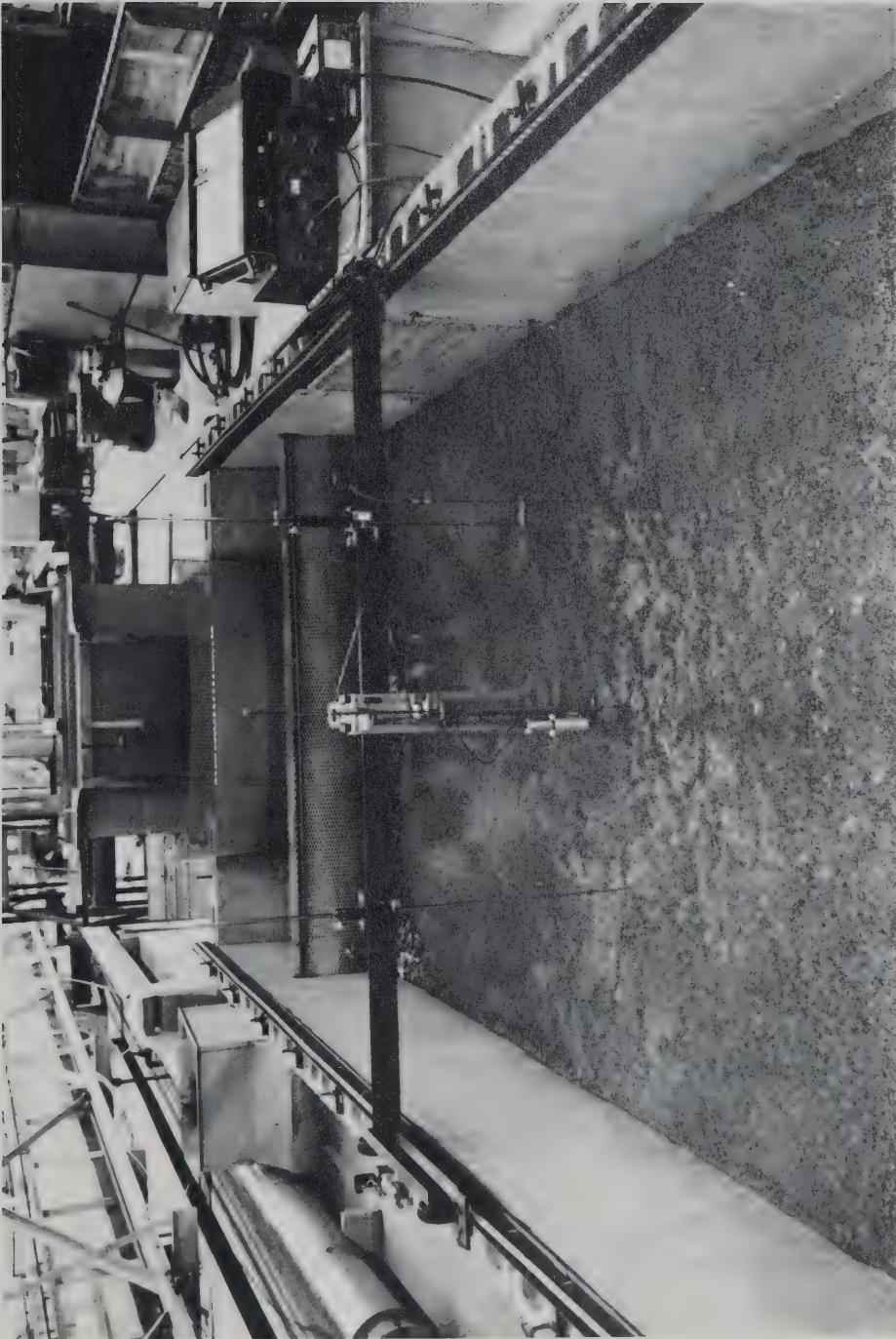


FIG. 4.1 VIEW OF EXPERIMENTAL FLUME LOOKING UPSTREAM (The point gauge, the optical bed probe, and the propeller-type current meter supported on the carriage, and the autograph recorders are seen)

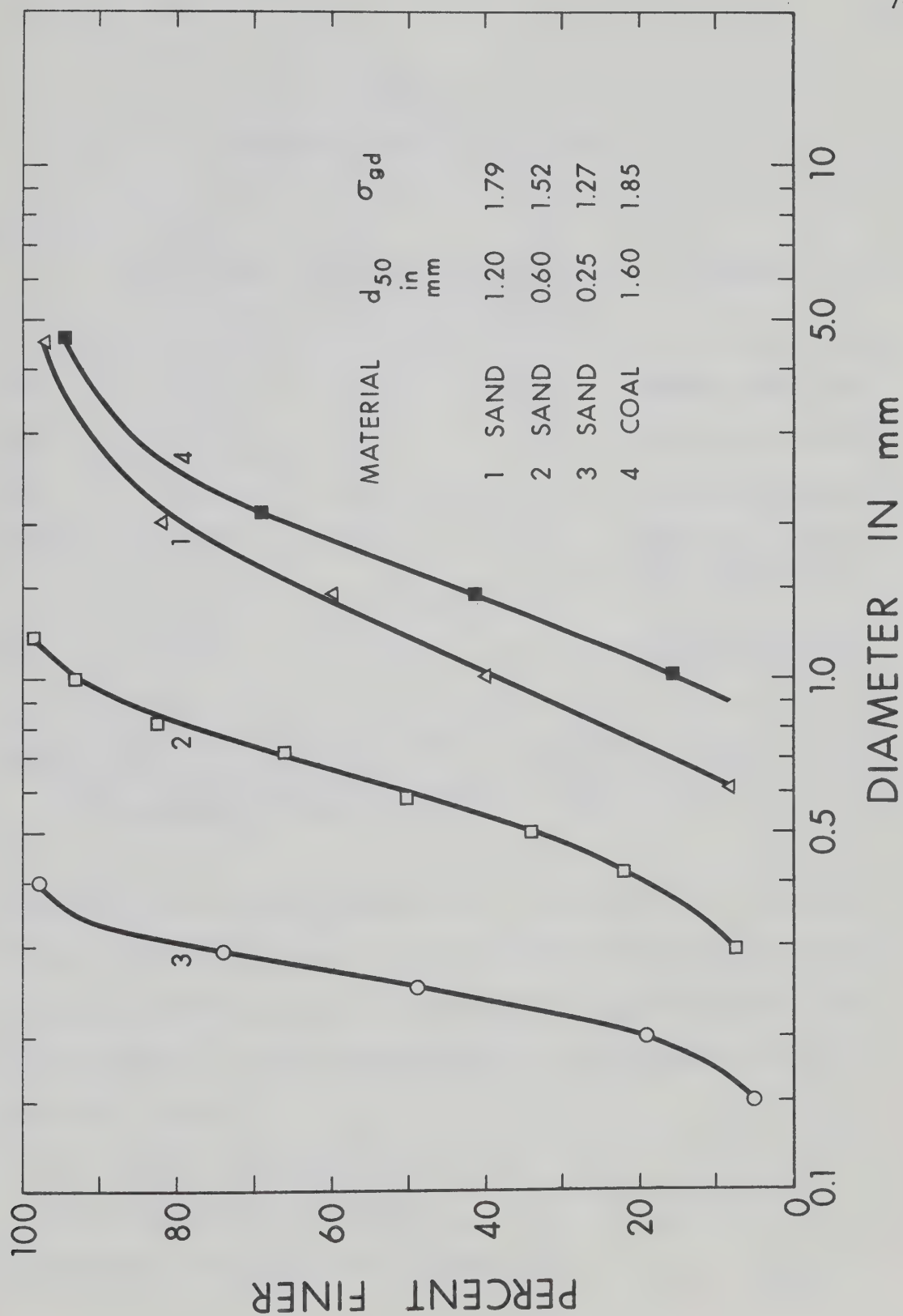


FIG. 4.2 SIZE-DISTRIBUTION CURVE FOR BED MATERIALS

TABLE 4.1
CHARACTERISTICS OF BED MATERIAL

Material	d_{50} Median Size in mm	ρ_s Specific Gravity	σ_{gd}^a Geometric Standard Deviation	Remarks
Sand	1.20	2.66	1.79	Natural river sand
Sand	0.60	2.65	1.52	Artificially sorted
Sand	0.25	2.67	1.27	Artificially sorted
Pebbles	$D_{75}=6.60$	2.68	1.51	Moderately angular shape (used only in check runs)
Coal	1.60	1.26		Crushed coal (used only in check runs)

^a σ_{gd} the geometric standard deviation is computed as $\frac{1}{2} \{d_{85}/d_{50} + d_{50}/d_{15}\}$
(ASCE Task Committee on Preparation of Sedimentation Manual, Committee
on Sedimentation, 1962)

the three sizes of sand as bed material. In section 3.2 the depth of scour has been derived as a complex function involving the size as well as the specific gravity of bed material. It was therefore considered essential to test the applicability of the design curves in a few check runs to

- (i) coarser bed material and
- (ii) light weight bed material.

The subsidiary flume was used for these runs.

Naturally worn pebble having d_{75} of 6.60 mm was used as coarse bed material in the check runs. This material was also used as closure material B (section 4.2.2) and its size distribution curve is shown on Fig. 4.3. Its specific gravity was close to 2.65.

Coal (anthracite) having d_{50} of 1.60 mm and specific gravity of 1.26 was used as the light weight bed material in the check runs. Size distribution curve for coal is shown in Fig. 4.2.

4.2.2 Closure Material

Three sizes of closure material having D_{75} of 6.60 mm (0.021 ft.), 18.00mm (0.059 ft.) and 25 mm (0.082 ft.) were used. These were designated as material B, C and D respectively. Closure material A was the natural river sand, of 1.20 mm median size, used as bed material. This was used only in four runs, for which the approach flow had a low Froude number of 0.10.

The size distribution curves are shown on Fig. 4.3. Figure 4.4 shows the materials B, C and D in close view. Their characteristics are presented in Table 4.2.

The angular shape of closure materials used in this study were considered representative of the natural quarried rocks used in river closures. It is obvious that extreme angularity or extreme roundness would change the material behaviour to a certain extent, which, however, may not be considerable, because ϕ varies in the range of 38° to 42° for variation from extremely rounded to extremely angular shape (U.S. Bureau of Reclamation, Sandover, 1971) in respect of materials

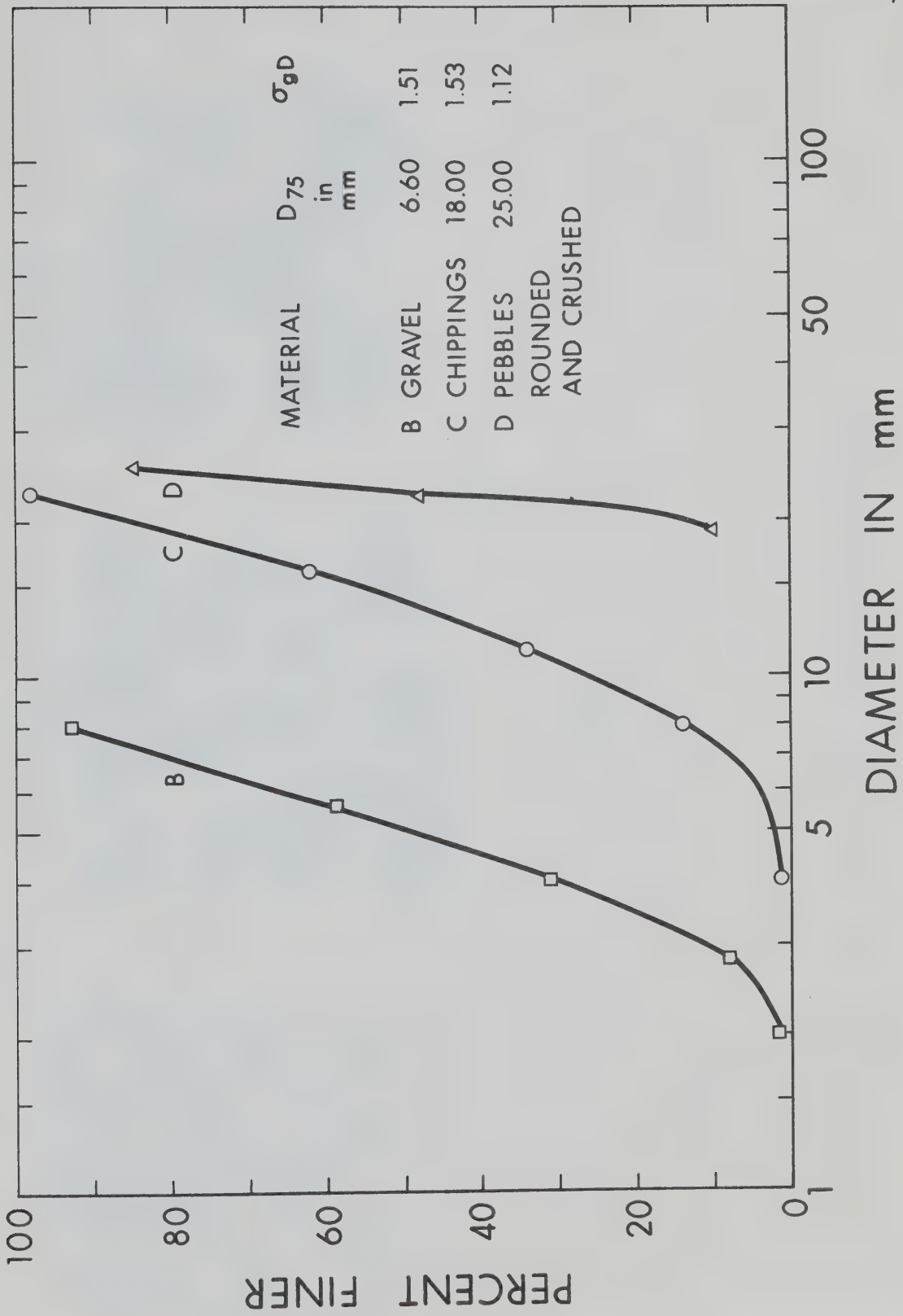
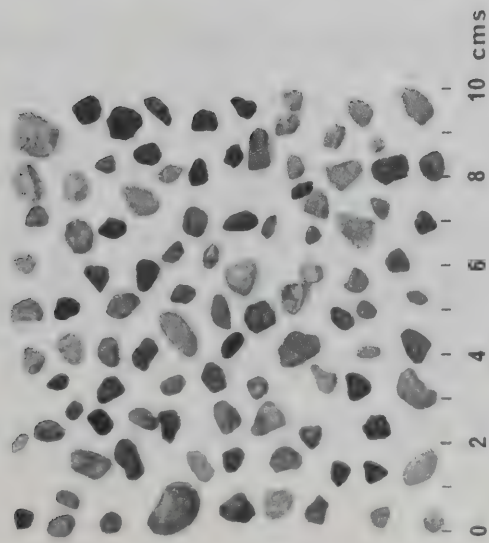
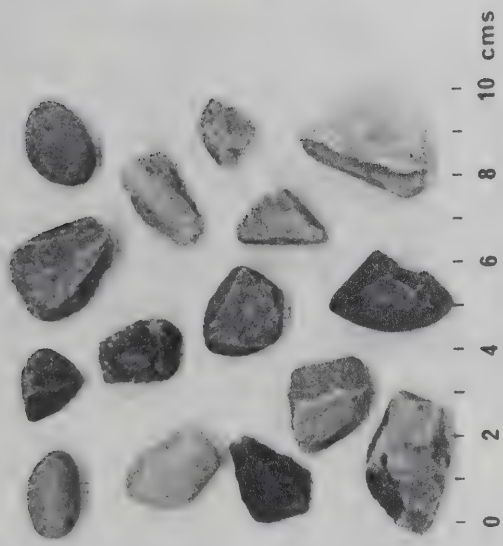


FIG. 4.3 SIZE-DISTRIBUTION CURVE FOR CLOSURE MATERIALS



MATERIAL B

$D_{75} = 6.60 \text{ mm}$



MATERIAL C

$D_{75} = 18.00 \text{ mm}$



MATERIAL D

$D_{75} = 25.00 \text{ mm}$

FIG. 4.4 CLOSE VIEW OF THE CLOSURE MATERIALS

TABLE 4.2
CHARACTERISTICS OF CLOSURE MATERIAL

Material	D_{75} in mm	ρ_D Specific Gravity	σ_{gD} Geometric Standard Deviation	Shape	ϕ Angle of Repose in degrees
A. Sand	$d_{50}=1.20$	2.66	1.79	Slightly angular	28-30
B. Naturally worn pebble	6.60	2.68	1.51	Moderately angular	31
C. Crushed Chippings	18.00	2.64	1.53	Moderately angular	34
D. Pebbles and chippings crushed	25.00	2.66	1.12	Slightly angular	38

in the size range of 2 in. to 2 ft. Sandover (1971) also observed that the angle of repose in water was consistently less than ϕ by 10° .

These observations do not imply that no advantage would be gained by the use of extremely jagged rocks, because such rocks by virtue of interlocking under the action of gravity and hydrodynamic effect of flow, tend to gain added stability.

This study attempts to make design recommendations in respect of closure materials of standard shape and specific gravity around 2.65.

4.3 Procedure

4.3.1 Arrangement of Test Series

In order to gain an insight into the role played by velocity in entrainment of closure material, the experimental programme at the outset comprised a series of preliminary runs in which the flow pattern, velocity distribution against the closure material and though the constriction were thoroughly studied.

The subsequent sixteen series of runs were conducted to yield data for empirical correlation of essential non-dimensional terms in respect of stability (section 3.1.3 to 3.1.5), scour (section 3.2.1 and 3.2.2) and backwater rise (section 3.3.2). These runs, covered the bulk of the experimental programme. The last four series of runs were check runs, meant to

- (1) assess the effect of rate of dumping on stability,
- (2) assess the applicability of design curves for stability to irregular channel cross-sections,
- (3) assess the applicability of the design curves on scour to
 - (a) coarse bed material (small values of the ratio of depth of flow to bed material size, h/d) and
 - (b) light weight bed material.

It has been shown in Chapter III, that dimensional analysis of independent variables describing stability, scour or backwater, indicated the Froude number of approach flow to be a significant non-dimensional parameter.

(a) Froude Number of Approach Flow

It was decided to conduct stability studies at three representative Froude numbers of 0.50, 0.29 and 0.10, on the consideration that in practical cases where closure is attempted, the Froude number rarely exceeds 0.30 and is mostly in the range 0.05 to 0.25. Table 4.3 summarizes the Froude number of normal flow in some rivers during actual closure operations.

TABLE 4.3
APPROACH FLOW DATA OF SOME RIVERS AT CLOSURE

Name of River	B Width in feet	h Nominal Depth of Flow	Q Discharge in Cubic ft/sec.	F Nominal Froude Number of Flow
Missouri at Fort Randall	1,000	12 ^a	28,600	0.12
Missouri at Oahe Dame Site	650	24	30,000	0.07
Columbia at Dalles Dam	520	50	108,000	0.103
River in USSR (Sandover 1971)	984	27.50	127,000	0.158
Mangla Dam closure	470	18.00	7,000	0.07

^a - Over the protection blanket on bed.

An outline of the experimental programme as split to different series is presented in Table 4.4. It can be seen from Table 4.4 and Table D.1 that each series (except the check runs) is a convenient group of runs corresponding to one Froude number of approach flow and one size of bed material. Thus concurrent variation of Froude number and bed material could be studied.

In general, corresponding to the Froude numbers of 0.50, 0.29 and 0.10, the uncontracted flow had normal depths of 0.18 ft., 0.26 ft. and 0.38 ft. respectively. These depths were chosen in order to limit the maximum scour depth to 1.50 ft. at the highest contraction ratio.

4.3.2 Data Taken

Experimental procedure involved gathering data for varying approach flow conditions, i.e. at the three Froude numbers of 0.50, 0.29 and 0.10, in respect of

- (1) flow pattern and velocity distribution through constriction,
- (2) stability of each size of closure material by obtaining closure efficiency - contraction ratio relationships,
- (3) maximum depth, pattern and time history of scour at varying contraction ratios,
- (4) maximum backwater rise and its location.

The general test procedure in each series was as follows.

The bed was screeded level in the test reach and an equilibrium steady flow condition was established by regulating the tail gate to

TABLE 4.4

OUTLINE OF EXPERIMENTAL PROGRAMME

Series Designation	Run Numbers	Froude Number	Bed Material	Scope
A	1 to 6	Around 0.50	Sand 1.2 mm	Preliminary runs for studying flow pattern and velocity distribution.
B	7 to 21	0.50	Sand 1.2 mm	(a) For obtaining data to develop design curves specifically for stability of closure material, (b) collecting data on scour and backwater.
C	24 to 38	0.10	Sand 1.2 mm	Stability studies with large closure material.
D	39 to 49	0.29	Sand 1.2 mm	Studying effect of B/h variation on stability
E	50 to 51	0.145	Sand 1.2 mm	Verification of the applicability to one side closure.
F	52 to 60	0.29	Sand 1.2 mm	(a) Studying effect of d/h variation on stability, (b) Development of design curves on scour and backwater considering bed material size. Series B through P considered for this purpose.
G	61 to 68	0.29	Sand 1.2 mm	Qualitative observations on the effect of rate of dumping on stability.
H ₁	69 to 70	0.29	Sand 1.2 mm	Checking of cross-sectional shape effect by undistorted modelling of natural rivers.
H ₂	71 to 73	0.525	Sand 1.2 mm	Verification of design curves on scour and backwater considering bed material size. Series B through P considered for this purpose.
H ₃	74	0.10	Sand 1.2 mm	Qualitative observations on the effect of rate of dumping on stability.
J	75 to 81	0.29	Sand 0.60 mm	Checking of cross-sectional shape effect by undistorted modelling of natural rivers.
K	82 to 85	0.110	Sand 0.60 mm	Verification of design curves on scour and backwater considering bed material size. Series B through P considered for this purpose.
L	86 to 89	0.50	Sand 0.60 mm	Qualitative observations on the effect of rate of dumping on stability.
M	90 to 93	0.29	Sand 0.25 mm	Checking of cross-sectional shape effect by undistorted modelling of natural rivers.
N	94 to 96	0.10	Sand 0.25 mm	Verification of design curves on scour and backwater considering bed material size. Series B through P considered for this purpose.
P	98 to 100	0.45	Sand 0.25 mm	Qualitative observations on the effect of rate of dumping on stability.
R	101 to 105	0.50	Three sizes of sand	Checking of cross-sectional shape effect by undistorted modelling of natural rivers.
S	107 to 111	--	--	Verification of design curves on scour for large bed material and light weight bed material.
T ₁	112 to 122	--	Pebbles	Verification of design curves on scour for large bed material and light weight bed material.
T ₂	123 to 127	--	6.6 mm Coal 1.60 mm	Verification of design curves on scour for large bed material and light weight bed material.

result in the desired depth of flow corresponding to the discharge and the Froude number. A uniform water surface slope in the test area was attained within a reasonable period of time, but the bed slope did not become parallel to the water surface slope, nor could this be achieved by shaping the alluvial bed prior to the run. As shown in section A.3, the theoretical bed slope for uniform flow was too small (0.002) to be maintained precisely in a small reach of 30 ft. Thus the normal flow referred to in this study, has a uniform water surface slope over a horizontal bed. The slightly accelerating flow did not result in any significant increase of velocity to alter the Froude number of the flow over the test area, upon which the analysis is primarily based. Uniform water surface slope over a horizontal bed was also the case in the investigations of Chang (1939) and Liu, Chang and Skinner (1961). It is, however, true that open channel flow through a constriction being predominantly a local phenomenon, the measured data (dependent variables) would not involve appreciable error with the slight difference in slope of the bed and water surface. Simons, Richardson and Nordin, Jr. (1965) have demonstrated that normal flow over a sedimentary bed can only be considered as being in equilibrium and not strictly uniform. The characteristic features of normal flow are detailed in Appendix A.

A series generally consisted of three sets of runs corresponding to the three sizes of closure material. The procedure for a set of runs was to keep the velocity and depth of the approach flow unchanged, thereby maintaining one Froude number of approach flow for

all runs, but increasing the contraction ratio from run to run. The closure material was dumped from both sides of the flume in equal quantities until the dam came up above water level and advanced into the flow.

The rate of dumping and the crest width of the dam approximately simulated the following typical prototype conditions:

- (i) 20 cubic yard dump trucks assumed dumping a load every five minutes,
- (ii) crest width 40 ft.,
- (iii) linear scale ratio 1:100, time scale ratio 1:10.

At an arbitrarily chosen contraction ratio, the dumping was stopped. The water surface levels, live stream boundary, and velocity profiles normal to the bed and advancing boundary slope were then recorded, starting at the section of maximum backwater upstream and ending where the flow widens to the parent channel width (section 11 to section 44 in Fig. 1.2a. The readings were taken fairly close in plan around the advancing boundary, and at one-foot intervals elsewhere. The bed profiles were also recorded by the probe at suitable intervals to complete the bed configuration, upon which the water surface configuration and velocity pattern could be superimposed to provide a detailed flow description.

The configuration of the crest above water and the toe location of the end-dump dam were carefully recorded, for computing the contraction ratio. These data were used to determine the volume

of material moved beyond the useful closure area required for computation of the closure efficiency (Fig. 3.1) corresponding to the particular contraction ratio.

By injecting dye from upstream and also using confetti, the flow pattern and eddy zones could be visualized. Photographs of the flow pattern, the closure material movement, the scour pattern and other pertinent features were taken during the tests.

The flow was continued until nearly equilibrium scour conditions were attained downstream. The scour holes were contoured in the dry for taking photographs and the scoured bed elevations were recorded.

The complete test data are presented in a tabular form in Appendix D.

CHAPTER V
FLOW CHARACTERISTICS AND MATERIAL STABILITY:
DATA ANALYSIS

5.1 Introduction

Based on the analysis of experimental data of this investigation, the characteristics of flow through an end-dump constriction, and the related problem of closure material stability are studied in this chapter.

The theoretical analysis in Chapter III indicate the contraction ratio, m , to be an important parameter in the hydraulic design. Due consideration was therefore given in defining and evaluating m , particularly for the closure of alluvial channels.

5.1.1 Computation of Contraction Ratio

In the previous studies on flow through constrictions, the contraction ratio, m , expressed in terms of width, ($m=1-B/b$) has been accepted as the representative measure of channel contraction. For closure of rigid-bed channels the representative b is generally evaluated (Izbash et al, 1970) as $\frac{1}{2} (b_w + b_b)$; b_w and b_b representing the water surface width and bed width respectively at the dump line (Fig. 1.2c). To account for the bed scour in the case of closure of alluvial channels, the representative b should be evaluated as $\frac{1}{2} (b_w + b_{bs})$; b_{bs} representing the width at the scoured bed level. How-

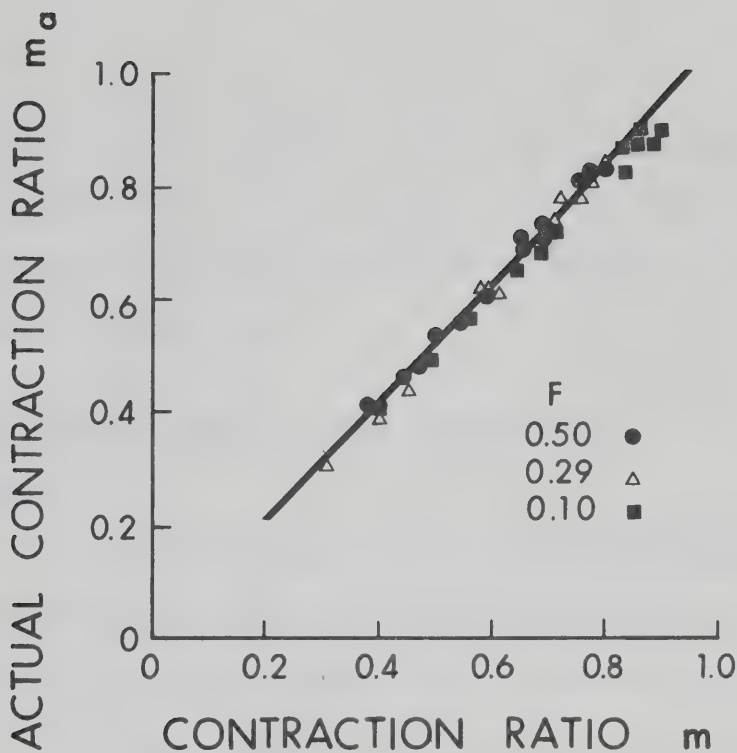


FIG. 5.1 PLOT OF ACTUAL CONTRACTION RATIO m_a VERSUS CONTRACTION RATIO m

ever, b_{bs} cannot be determined precisely for the variable scour conditions. In their study of bridge constrictions in alluvial channels, Lin et al (1961) have stated that " b = width of opening in constriction", but did not clarify as to how b was measured in their study.

For reasons stated above, it was considered practical to evaluate b in this study as $\frac{1}{2}(b_w + b_b)$, irrespective of the bed scour at the dump line. The contraction ratio m , is computed as $(1 - [b_w + b_b]/2B)$. It is obvious that the actual contraction ratio m_a , ($m_a = 1 - [b_w + b_{bs}]/2B$) for a scoured bed is slightly more than the computed value because b_{bs} is less than b_b .

From the measured values of b_w , b_b and b_{bs} in all the runs in series B, C and D of this study a plot of m , versus m_a is shown in Fig. 5.1. In spite of the considerable bed scour in the dump area,

particularly at higher values of m , the scatter is slight and the correlation is good. This illustrates that the consistent use of m , as the representative contraction ratio, in preference to m_a , does not involve any significant error.

5.2 Flow Pattern Through End-Dump Constriction

5.2.1 General

The longitudinal water surface variation along the centre line of the flume at a few typical contraction ratios are shown in Fig. 5.2. The water surface topography for a contraction ratio of 0.56, is also shown in Fig. 5.2. Rapid drop of water surface contours around the dump line in contrast to a flatter drop along the centre line indicates the flow to be accelerating more rapidly close to the advancing boundary. The patterns as visualised by dye streaks are shown in Fig. 5.3.

It was generally noted that the flow through an open channel constriction formed by end-dump dams on a mobile bed is quite similar to that on a rigid bed, as observed in the extensive experimental investigations by Kindsvater and Carter (1955) for various constriction geometries and by Biery and Delleur (1962) for semi-circular arch bridge constrictions.

The progressive closure by end-dumping resulted in a progressive rise of the backwater upstream of the dump line. The backwater level, which attained a maximum at the instant the dumping stopped, was observed to fall gradually, with progression of bed scour

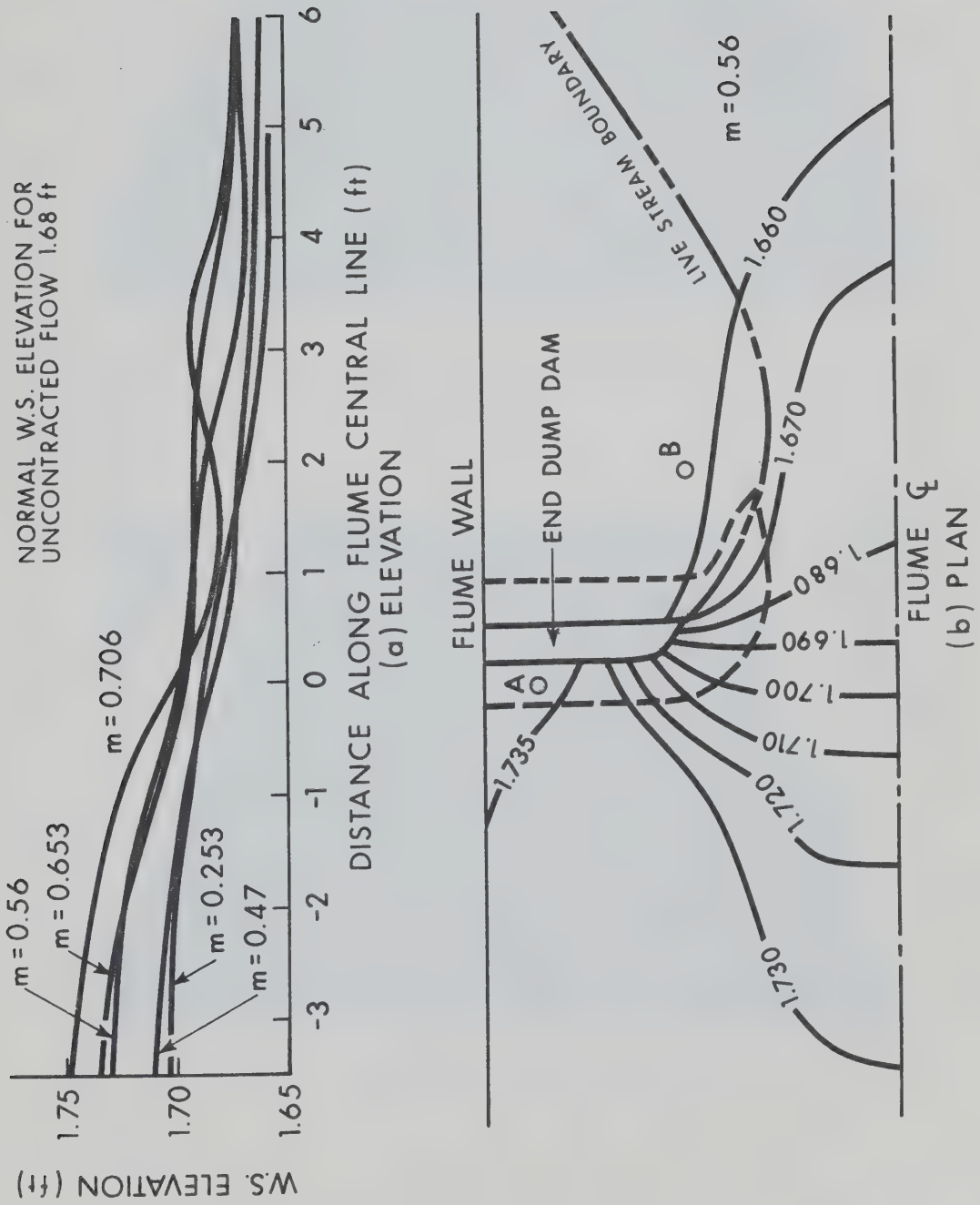
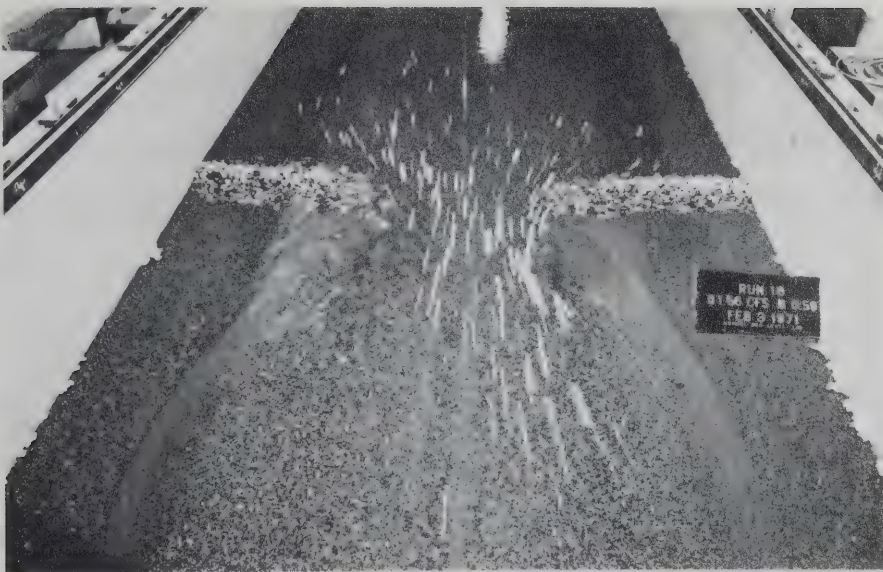
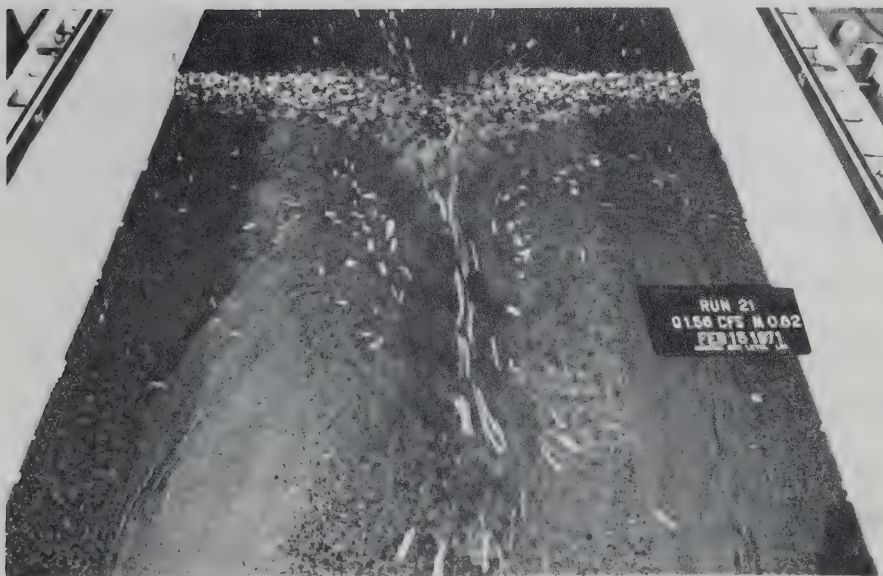


FIG. 5.2 WATER SURFACE TOPOGRAPHY FOR FLOW THROUGH AN END-DUMP CONSTRICTION



(a) At a low contraction ratio of 0.59



(b) At a high contraction ratio of 0.82

FIG. 5.3 FLOW PATTERNS THROUGH END-DUMP CONSTRICTION
AS VISUALISED BY CONFETTI
(M in photographs represent contraction ratio)

at the contraction, until both attained equilibrium.

The slope of the dam advancing into the flow was self-formed, as an interaction between the flow and gravity. Until the onset of instability, the slope more or less conforms to the angle of repose in water for the closure material, but beyond the threshold condition the slope flattens and the tongue at the end progressively extends along the flow. The general configuration of the advancing face and scour hole are shown in Fig. 5.4 for two typical contraction ratios of 0.59 and 0.77. At the contraction ratio of 0.77, it can be seen that the closure material has crossed the threshold condition and the efficiency of closure was 0.50.

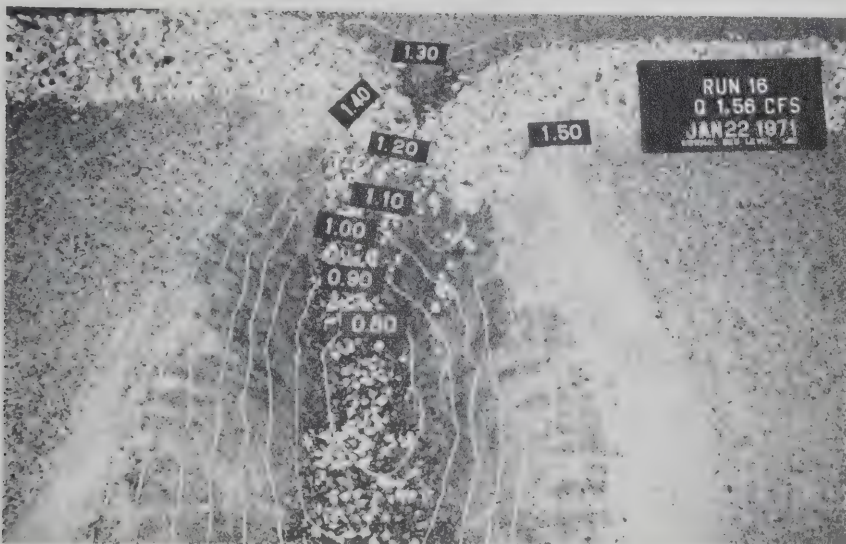
The upstream face of the advancing boundary more or less conforms to the contracting live stream. Instability of the dumped material was observed to occur predominantly over the upstream face (area pqrp shown cross-hatched in Fig. 1.2a). The balance area downstream on the advancing boundary is not subjected to the erosive action of the flow. This was also observed in the laboratory by Pariset and Hausser (1959) and Sandover (1969) and in the field in the actual closure of Dalles dam (1965). However, against Pariset and Hausser's observation that only the upstream 15% of the total width of the progressing face is subjected to severe erosion by flow, the present experiments indicated the proportion to be at least 60%.

5.2.2 Contraction and Expansion of the Live Stream Boundary

The flow contracts from section 1-1 through section 3-3 (Fig. 5.5)



(a) At a low contraction ratio $m=0.59$, $F=0.50$, $h=0.18$ ft, $d_s=0.45$ ft.



(b) At a high contraction ratio $m=0.77$, $F=0.50$, $h=0.18$ ft., $d_s=0.75$ ft.

FIG. 5.4 GENERAL VIEW OF THE END-DUMP DAM AND SCOUR HOLES
(M in photographs represent the contraction ratio, bed contour interval 0.10 ft.)

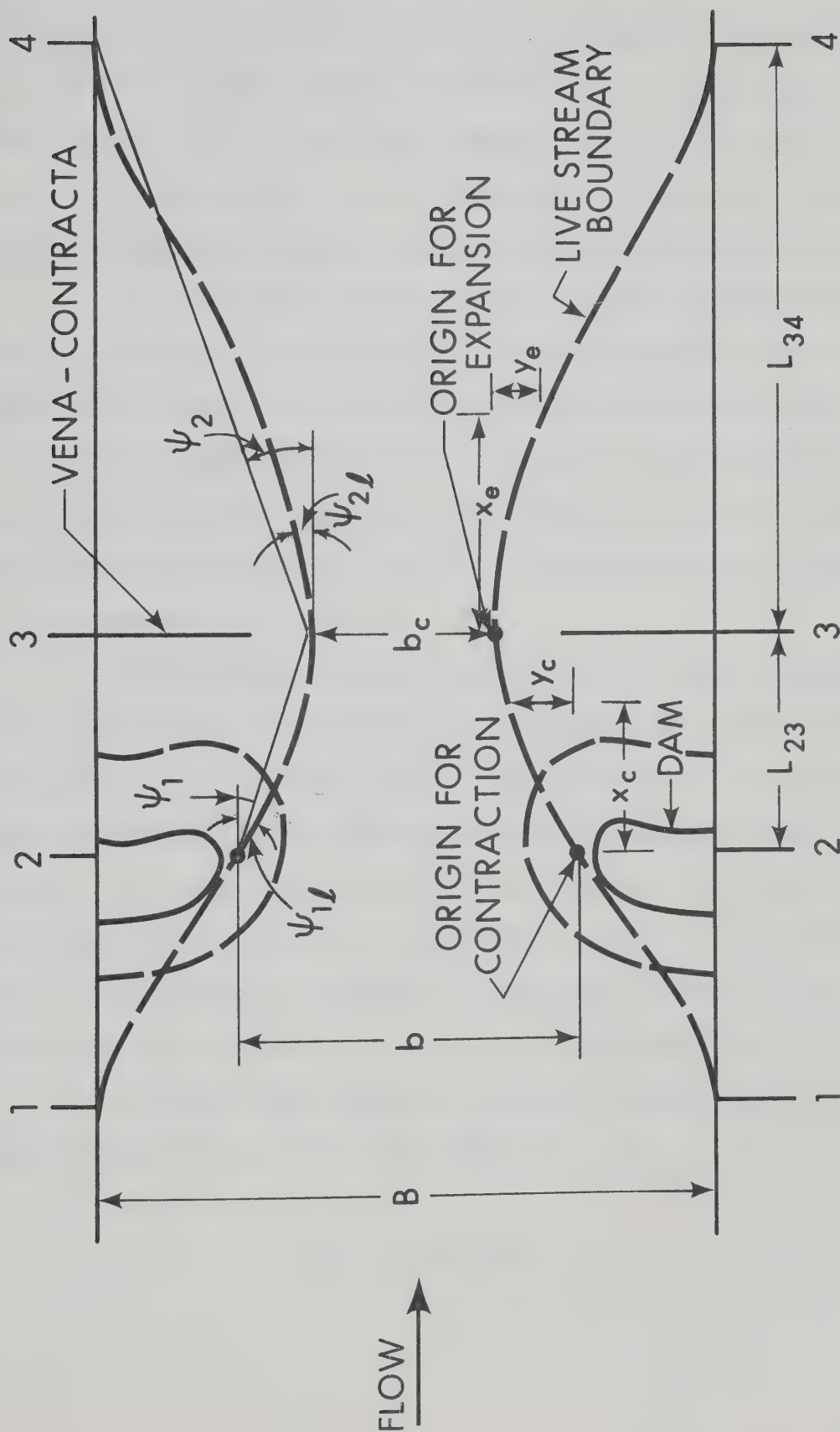


FIG. 5.5 DEFINITION DIAGRAM FOR FLOW CONTRACTION AND EXPANSION

and accelerates as it negotiates the end-dump boundary. In contrast to a relatively shorter length of contraction, the live stream expands gradually over a much longer length. The local angle of contraction $\psi_{1\ell}$ at the dump line was observed to be larger than the local angle of expansion $\psi_{2\ell}$ measured slightly downstream of the vena-contracta.

The flow width at vena-contracta b_c , was measured by introducing dye from the separation point along the advancing boundary. Because the boundary of the jet was not clearly defined, the data can not be considered as precise. The length of contraction L_{23} and the length of expansion L_{34} were also measured. The complete experimental data are presented in Table D.1. The coefficient of contraction C_c was computed as the ratio b_c/b .

In a rectangular constriction, the contracting stream maintains a more or less vertical edge. For the end-dump constriction, the contracting stream edge is more or less vertical on the upstream and downstream of the dam and hugs to the sloping end-dump face in-between. It is therefore likely that the geometry of the constriction has a decisive influence on the coefficient of contraction. Other factors upon which C_c may depend are the roughness of the closure and bed material and the B/h ratio of the uncontracted flow.

A logical relationship of principal non-dimensional terms denoting flow contraction can be assumed as

$$C_c = f_1(m, F, \tan\phi) \quad (5.1)$$

$\tan\phi$, the slope of end-dump face, represents effect of closure material. The length of contraction can be expressed as

$$\frac{L_{23}}{b} = f_2(m, F, \tan\phi) \quad (5.2)$$

Equation 5.2 can be written in an alternative form as

$$\tan\psi_1 = \frac{L_{23}}{(B-b)/2} = f_3(m, F, \tan\phi) \quad (5.3)$$

A similar relationship for flow expansion can be assumed in the form

$$\tan\psi_2 = \frac{L_{34}}{(B-b)/2} = f_4(m, F, \tan\phi) \quad (5.4)$$

Izbash (1970), based on experimental data, proposes a relationship for flow expansion in the form

$$\tan\psi_2 = f\left(\frac{m^2}{\log 1/M}\right) \quad (5.5)$$

which support the validity of equation 5.4.

Based on the experimental data of this study, a plot of C_c versus m is shown in Fig. 5.6. Because b_c could not be measured precisely, the scatter of the data is to be expected. The data differs from the hypothesis given by free streamline theory (Streeter, 1948) that C_c assumes a minimum value of 0.611 for a two-dimensional slot.

In Fig. 5.7, plots of $\tan\psi_1$ versus m and $\tan\psi_1$ versus $[m^2/\log(1/M)]$ are shown. In Fig. 5.8, plots of $\tan\psi_2$ versus m and $\tan\psi_2$ versus $[m^2/\log(1/M)]$ are shown. Variation of F and $\tan\phi$ are also

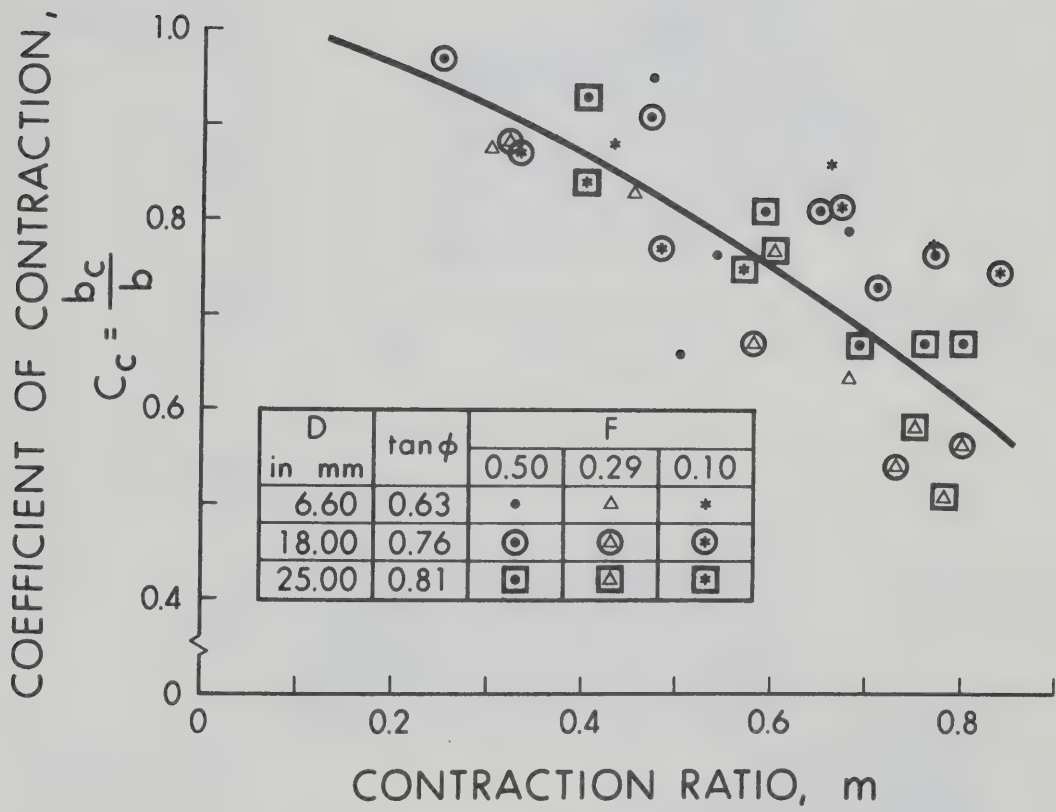


FIG. 5.6 PLOT OF COEFFICIENT OF CONTRACTION C_c ,
VERSUS CONTRACTION RATIO m

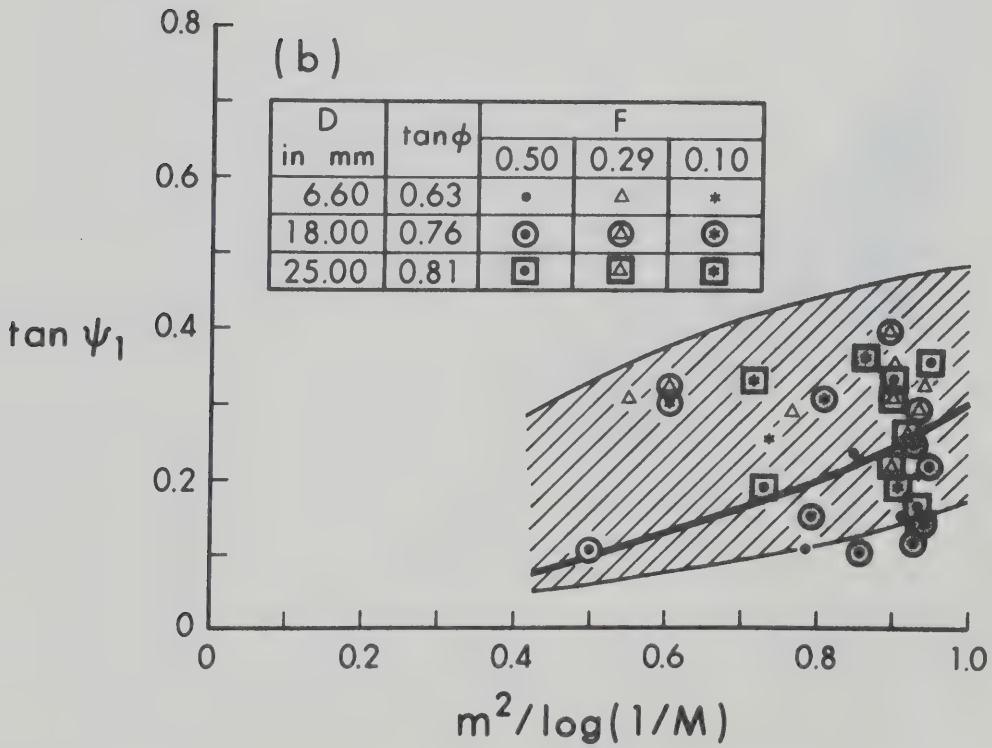
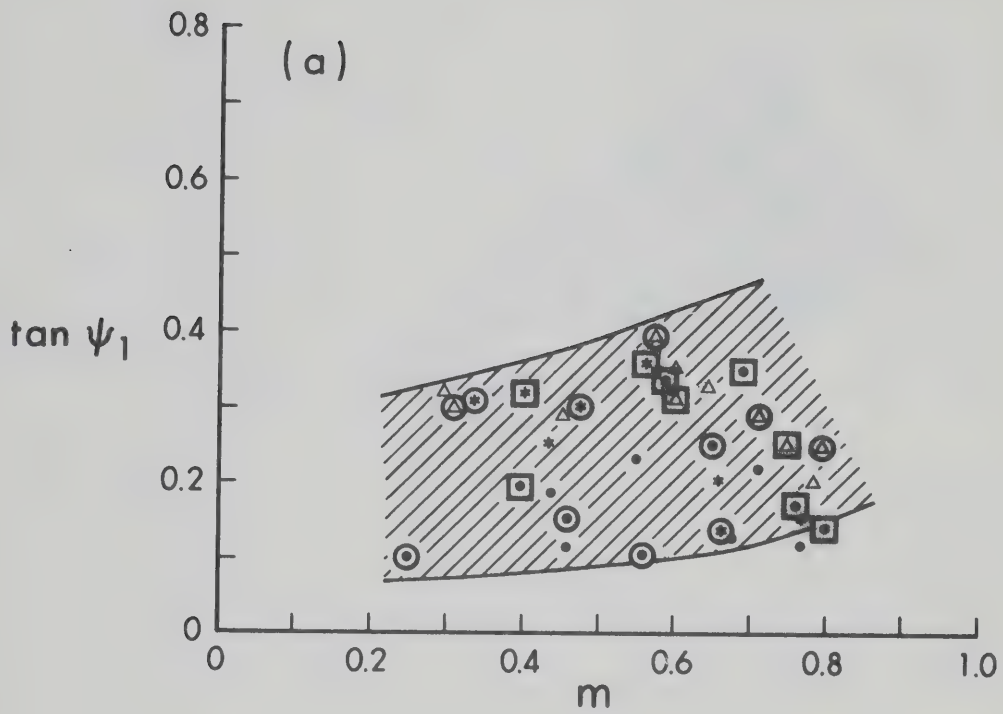


FIG. 5.7 RELATIONSHIPS FOR ANGLE OF CONTRACTION ψ_1

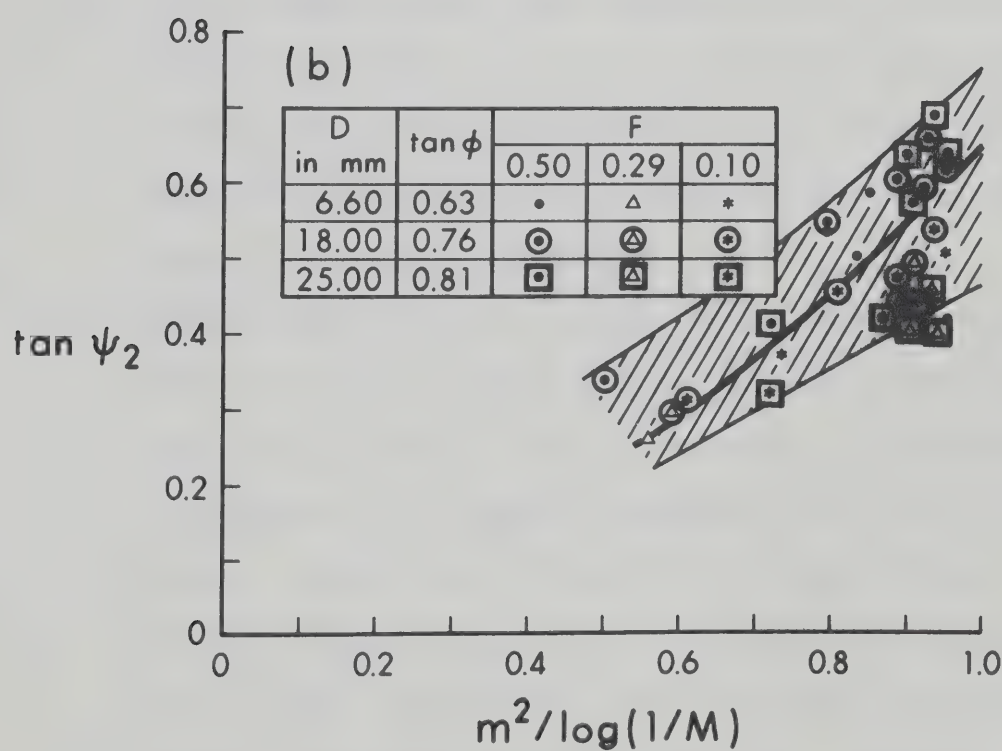
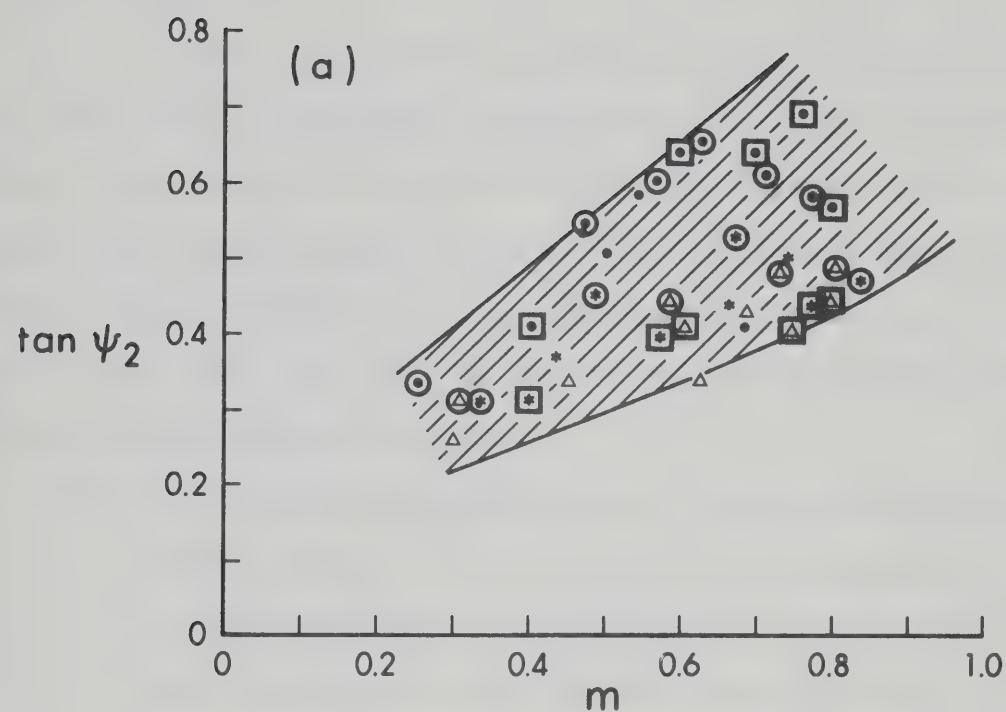


FIG. 5.8 RELATIONSHIPS FOR ANGLE OF EXPANSION ψ_2

shown in these plots.

As Figs. 5.6, 5.7 and 5.8 indicate, the correlations of $\tan\psi_1$ and $\tan\psi_2$ with m is only fair, whereas the correlation of C_c with m is good. The effect of variation of Froude number does not appear to be significant, but the size of closure material appears to have a significant effect both on C_c and $\tan\psi_1$. Although, no definite conclusion can be drawn from these plots because of considerable scatter, the following observations can be made.

- (i) C_c is primarily dependent upon m . The mean curve drawn through the data points in Fig. 5.6 can be used to determine C_c . Use of large and angular rocks can result in variation of C_c upto $\pm 10\%$ from the mean value read from Fig. 5.6.
- (ii) Angle of contraction ψ_1 , as indicated in Fig. 5.7 varies between 5° and 25° . Use of large rocks would result in increase of ψ_1 . Precise prediction of its variation with other flow parameters is not attempted in this study, because of limitations of the data.
- (iii) Angle of expansion ψ_2 as indicated in Fig. 5.8 varies between 15° and 35° . Closure material size has a lesser influence on ψ_2 than ψ_1 . This is reasonable, as the expanding stream does not remember the effect of the contraction pattern. Froude number of approach flow seems to have a greater influence on ψ_2 than ψ_1 . It appears that an approach flow of higher Froude number, having a higher velocity of the jet at the vena-contracta, tends to draw the ambient fluid

in the eddy zone more quickly and to cause the jet to diffuse more rapidly. The process of diffusion and velocity distribution downstream of the vena-contracta (Fig. 5.11) are similar to observations of Albertson et al (1950).

The mean curves drawn through data points in Figs. 5.7b and 5.8b can only be considered as useful guides for determination of the flow profile at any stage of closure.

5.2.3 Non-dimensional Plots of Contraction and Expansion Profiles

From the live-stream configuration measured in each run, non-dimensional plots of flow contraction and expansion are shown in Fig. 5.9. (Fig. 5.5 is to be referred to as the key diagram). A non-dimensional plot of expansion due to Izbash and Lebedev (1961) is shown on Fig. 5.9b for comparison.

Figure 5.9 indicates that the profiles are similar, irrespective of the contraction ratio and Froude number of flow.

5.3 Velocity Distribution Through Constriction

Figure 5.10 shows typical velocity distributions through the gap at the dam axis at increasing contraction ratios. Figure 5.11 shows velocity distribution along the flow at one contraction ratio. For the runs shown in Figs. 5.10 and 5.11 the uncontracted channel had a mean velocity of 1.15 fps, whereas the flow negotiating the closure dam attained a maximum point velocity of 1.81 to 2.05 fps. The interesting feature, however, is that although the contraction ratio increased from 0.30 to 0.75, the overall mean horizontal velocity

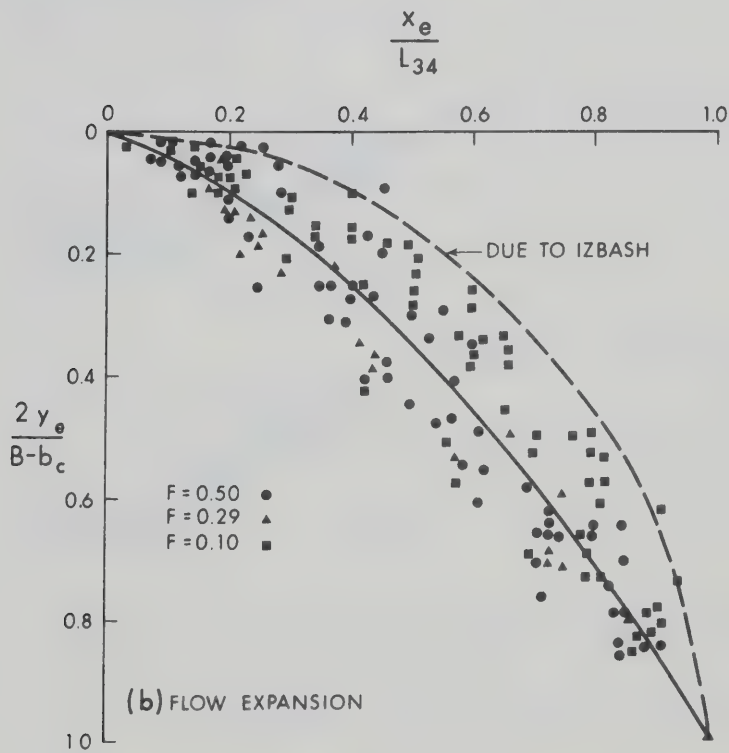
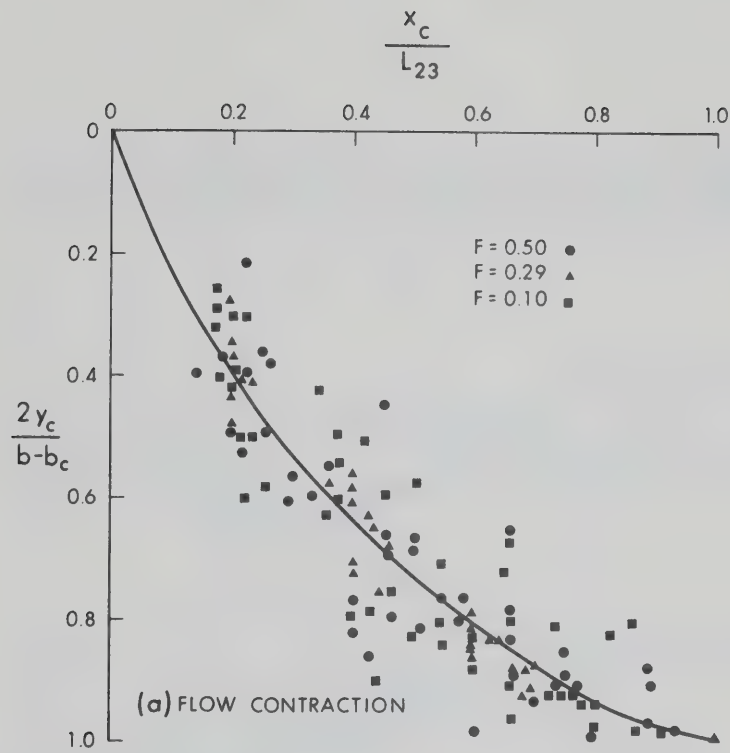
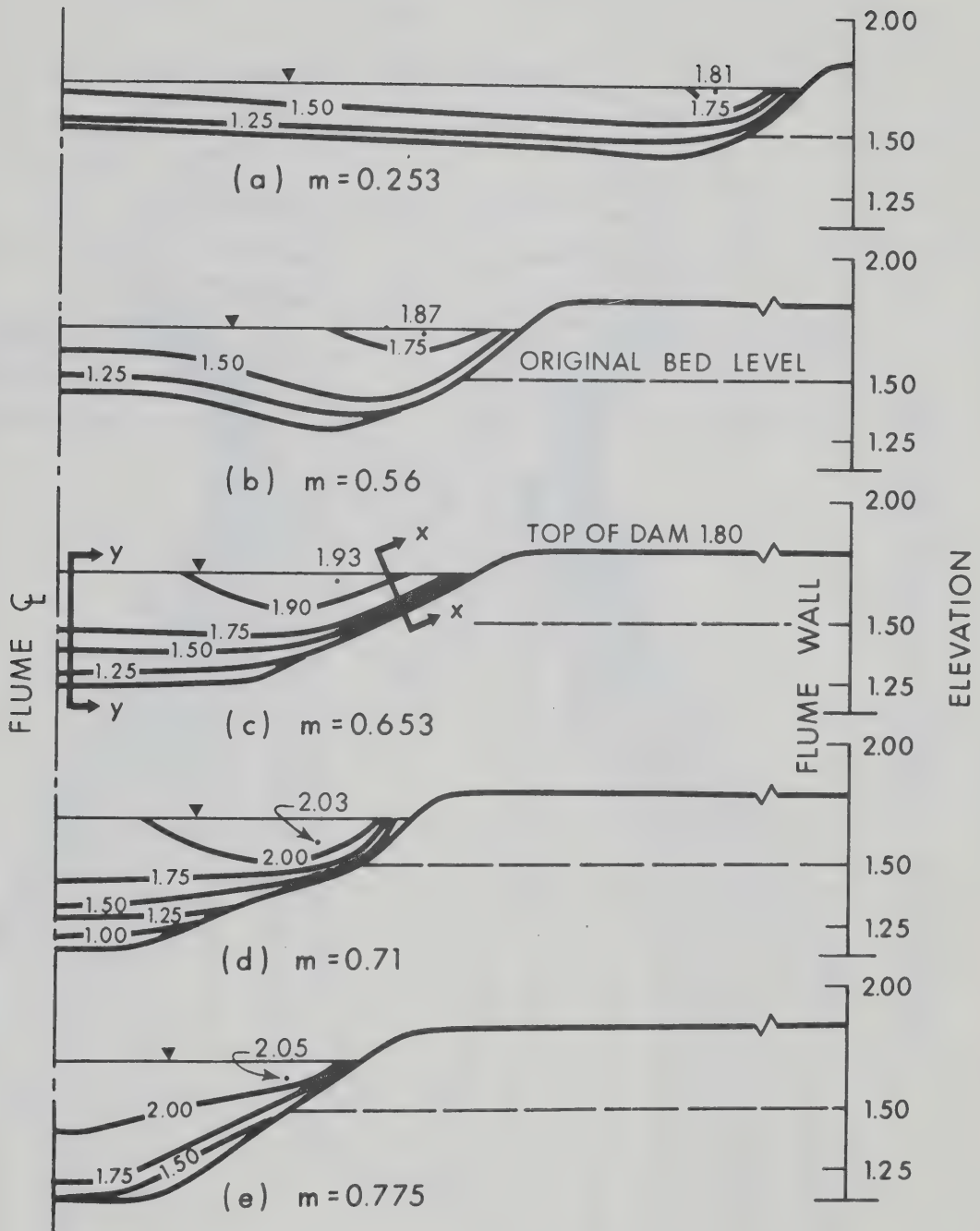


FIG. 5.9 NON-DIMENSIONAL PROFILES OF THE LIVE STREAM BOUNDARY



Note: Maximum point Velocity f.p.s. 1.93

Isovels f.p.s. — 1.75 —

FIG. 5.10 VELOCITY DISTRIBUTION AT DUMP LINE
FOR TYPICAL CONTRACTION RATIOS

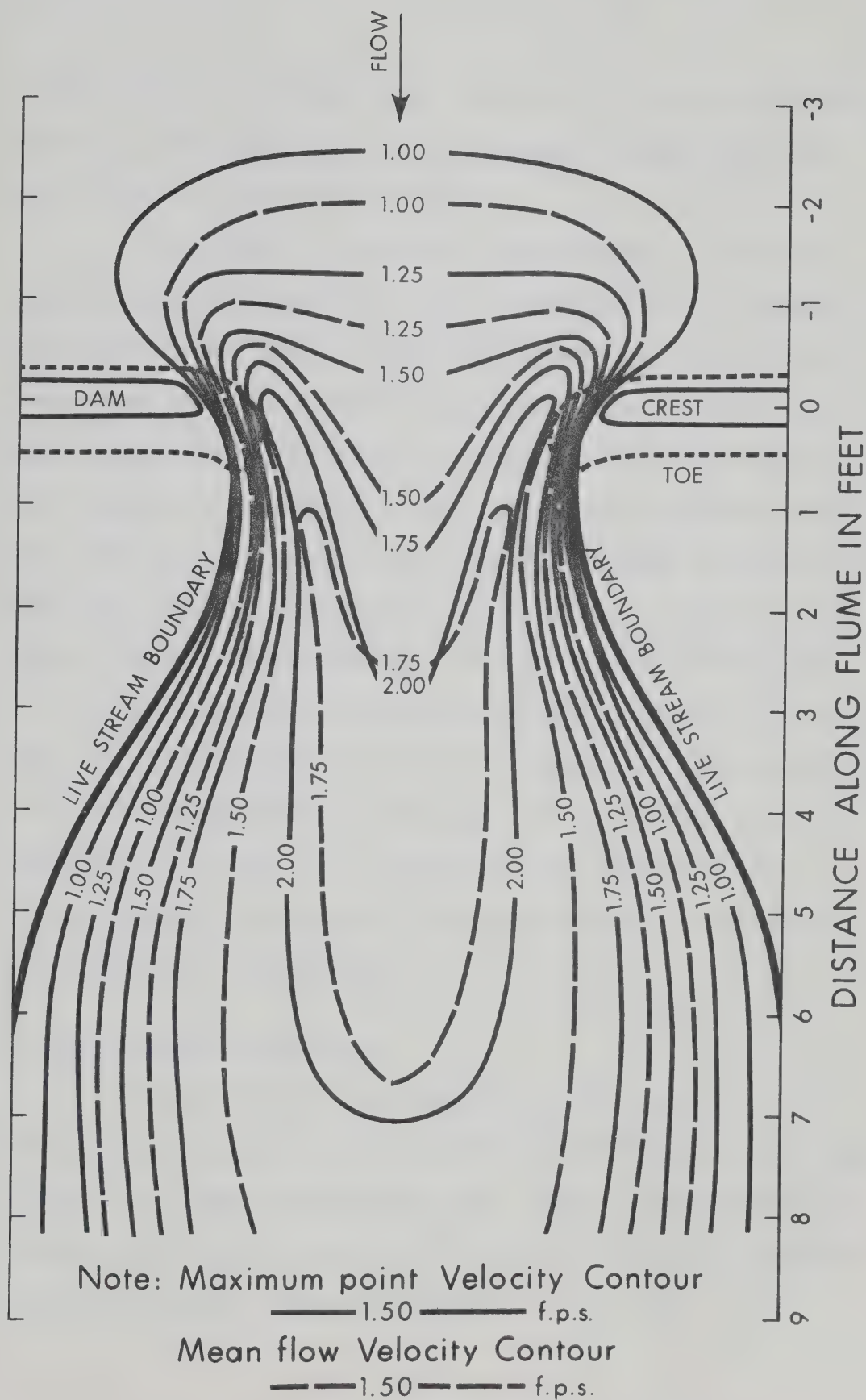


FIG. 5.11 TYPICAL VELOCITY DISTRIBUTION ALONG FLOW
 ($m=0.65$, $F=0.50$, $h=0.18$ ft., $V=1.15$ fps)

in the contraction, as can be seen from Fig. 5.12, did not materially change, but remained around 1.50 fps, because of considerable bed scour as shown in Figs. 5.10c, d and e.

A pertinent observation that needs emphasis is that the velocity against the boundary as well as the stability of the material was relatively unaffected by scour at the dump line or downstream. Elaborating, let it be assumed that one size of material was found to attain the threshold condition at a particular contraction ratio. At that instant, the dumping was stopped. The scour progressed, thereby redistributing the velocity through the gap (decrease in mean velocity). After scour attained equilibrium, attempt to advance the dam further into the flow with the same material did not succeed significantly.

The velocity distribution along typical sections such as XX and YY in Fig. 5.10c were observed to be logarithmic. (The mean velocities for the contraction ratio of 0.65 shown were 1.83 and 1.57 fps respectively). The conclusive evidence was that the overall mean velocity through the contraction does not govern the stability of closure material at section XX.

5.4 End-of-Closure Conditions

At a contraction ratio generally in the range of 0.85 to 0.90, the two wings of the closure dam join at the centre, after which the bed is no longer available for scour. Material instability then increases abnormally, because the afflux and flow velocity through the constriction suddenly increases abnormally (Fig. 5.12).

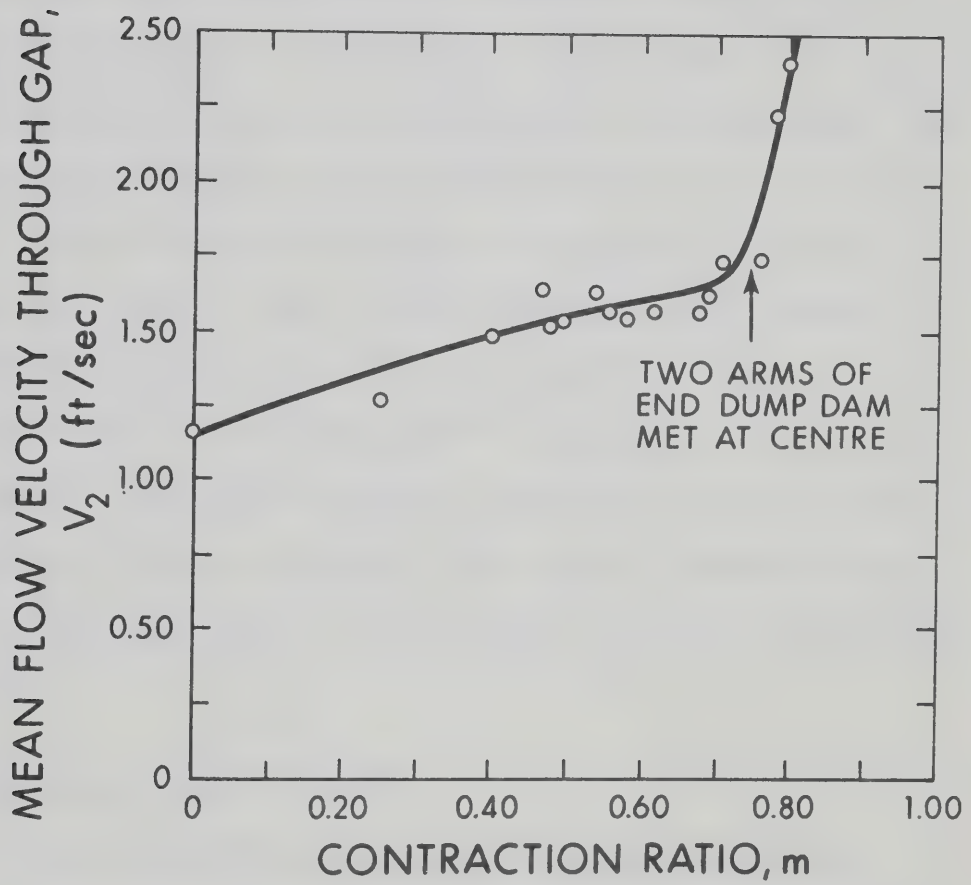


FIG. 5.12 PLOT OF MEAN VELOCITY AT DUMP LINE V_2 ,
VERSUS CONTRACTION RATIO m

Izbash (1970) has observed this in actual closure jobs in the U.S.S.R. and designates this as the most critical stage of closure. According to him the flow attains the maximum specific power, which is the product of unit discharge through the gap and the head loss at the contraction. He recommends employing special blocks like tetrapods, or very heavy reinforced concrete blocks, or cribbed and garlanded boulders, to successfully close the flow. The design curves developed in this research program apply up to a contraction ratio of 0.90 and cannot be used thereafter. It must be stressed here, however, that in actual practice at 90% closure, a very small fraction of flow really goes through the contraction, because most of it is diverted through the alternate waterway. In rapid closures, discharge through the constriction will be less by the discharge going into storage. These aspects, combined with the small gap remaining, make the final closure a practical but difficult proposition.

5.5 Stability of Closure Material

5.5.1 Analysis of Stability Data by Critical Velocity Criteria

In the preliminary runs, data at the threshold condition for each closure material were carefully collected to see whether instability could possibly be correlated with the experimentally observed maximum velocity occurring close to the boundary. A summary of three runs where threshold conditions were just attained is presented in Table 5.1, which incorporates a comparison of the experimentally observed stable size and the size computed from the velocity formulas previously

TABLE 5.1
COMPARISON OF EXPERIMENTAL STABLE SIZE WITH
VALUES GIVEN BY VELOCITY FORMULAS

M	V_{\max}	D_1		D
Contraction Ratio	Observed Maximum Velocity Against Boundary in feet per second	Stable material size in feet computed cor- responding to velocity V_{\max} by		Experimentally Observed Stable Size in feet
		Izbash (1970)	U.S. Corps of Engineers (1970)	
1	2	3	4	5
0.25	1.80	0.02	0.025	0.021
0.47	1.85	0.022	0.03	0.059
0.69	1.95	0.023	0.038	0.082

Note: For all the runs, $Q = 1.56$ cfs, $B = 7.50$ ft., $V = 1.15$ fps
 $F = 0.50$.

discussed herein. Correlation with mean velocity through the constriction (observed) has not been attempted, because this will indicate considerably smaller stable sizes.

Good agreement at the low contraction ratio of 0.25 and poor agreement at higher contraction ratios of 0.47 and 0.69 between the experimentally-observed stable size and the size computed according to velocity criteria can be noted in Table 5.1. This can be explained as follows.

At low contraction ratios, the increase in velocity and shear stress on the boundary over the normal values is minimal. The flow behavior is still similar to that of a uniform flow in a prismatic channel; whereas a higher contraction ratio results in increased flow curvature, flow velocity and acceleration close to the boundary and consequently results in a greater increase of shear stress (Ippen and Drinker, 1962), which demands a drastic increase in stable size. Experimental evidence (Table 5.1) substantiates the inadequacy of either the "mean velocity-through the constriction" or "velocity against the boundary" to govern the stability.

In Appendix C, shear stress maxima occurring against the dumped material have been computed from measured velocity distribution normal to the advancing boundary. Stable size of material has been computed from shear stress criteria, considering drag and lift (Christensen, 1971). Good agreement between experimentally observed stable size and computed stable size has been noted.

5.5.2 Proposed Design Curves

(a) Effect of Turbulent Seepage

It was observed that at high values of contraction ratio, seepage through the body of the closure dam became noteworthy because of increased head-differential across the dam. It was therefore considered necessary to analyse the stability data after accounting for the seepage through the body of the dam.

Detailed velocity measurements were taken at close intervals along the dump line from which, Q_m , the discharge through the opening was computed. Assuming the discharge going into storage as negligible, Q_s , the seepage discharge was computed as the difference of Q , the uncontracted flow discharge and Q_m .

Because seepage reduces the discharge through the opening, its primary effect is to enhance the stability of the material on the end-dump face. Seepage, however, has a destabilising effect on the downstream slope (Terzaghi and Peck 1948, Martin, 1970).

In this study, the effect of seepage is accounted for by assuming the approach discharge to be Q_m and not Q . It is, however, considered reasonable to disregard the effect of seepage on the stability of closure material, when Q_s is less than 10% of Q . This is, of course, an arbitrary decision.

It has been shown in section 3.1.5 that the essential non-dimensional parameters describing stability are F , D/h , m and η . It is obvious that a correct analysis of stability has to be based upon F and h values that correspond to Q_m as the normal or approach discharge.

Detailed velocity measurements were taken in Series B, C, D, F and G. For runs in which seepage discharge exceeded 10%, the hydraulic particulars for both Q and Q_m as approach flow, are presented in Table 5.2. B, the channel width is assumed the same for both cases. F and h corresponding to Q_m were obtained by referring to the stage-discharge curve of the channel for each series.

The seepage discharge exceeded 10% of the normal, for closure material size 0.059 ft. and 0.082 ft. only. From a comparison of column 9 with column 12 and column 10 with 13 in Table 5.2 it is obvious that even a reduction of approach channel discharge (up to 30%) due to seepage does not result in appreciable (less than 10%) reduction of either V or h or F . A natural river also exhibits this trend, because reduction in discharge results in reduction of both stage and velocity; Froude number of flow is thereby reduced to a lesser extent. Because F and h are specifically considered in the analysis it is reasonable to expect that correlation of non-dimensional parameters based on normal flow data would yield realistic results except in the case of runs 34, 35 and 36.

It needs to be mentioned that for all the runs in Table 5.2, the contraction ratio was in excess of 0.70 and the efficiency of closure was as low as 0.70 or even lower. As will be discussed in section 5.5.2b, the design charts are developed considering efficiency up to 0.80. Although the data of runs in Table 5.2 are included in analysing the stability of closure material, the error introduced is considered minimal.

TABLE 5.2
PARTICULARS OF RUNS IN WHICH SEEPAGE DISCHARGE EXCEEDED 10%

Run No.	m Contraction Ratio	D Closure Material Size in feet	Q Approach Flow Discharge in cfs	Q _m Measured Discharge Through Opening in cfs	Q _s Seepage Discharge in cfs	$\frac{Q_s}{Q}$	Approach flow data corresponding to Q			Modified data considering Q _m as approach flow		
							V	h	F	V	h	F
							in fps	in feet		in fps	in feet	
1	2	3	4	5	6	7	8	9	10	11	12	13
15	0.71	0.059	1.56	1.41	0.15	0.10	1.15	0.18	0.50	1.10	0.17	0.47
16	0.77	0.059	1.56	1.43	0.23	0.15	1.15	0.18	0.50	1.06	0.168	0.46
20	0.69	0.082	1.56	1.39	0.17	0.11	1.15	0.18	0.50	1.09	0.17	0.47
21	0.76	0.082	1.56	1.31	0.25	0.16	1.15	0.18	0.50	1.05	0.166	0.455
30	0.84	0.059	1.00	0.88	0.12	0.12	0.35	0.38	0.10	0.34	0.35	0.10
31	0.87	0.059	1.00	0.90	0.10	0.10	0.35	0.38	0.10	0.34	0.35	0.10
33	0.57	0.082	1.00	0.87	0.13	0.13	0.35	0.38	0.10	0.34	0.35	0.10
34	0.77	0.082	1.00	0.70	0.30	0.30	0.35	0.38	0.10	0.29	0.32	0.09
35	0.88	0.082	1.00	0.61	0.39	0.39	0.35	0.38	0.10	0.27	0.30	0.087
36	0.90	0.082	1.00	0.48	0.52	0.52	0.35	0.38	0.10	0.23	0.27	0.079
45	0.73	0.059	1.66	1.41	0.29	0.17	0.84	0.26	0.29	0.81	0.245	0.29
46	0.80	0.059	1.66	1.32	0.38	0.23	0.84	0.26	0.29	0.81	0.24	0.288
48	0.75	0.082	1.66	1.28	0.42	0.26	0.84	0.26	0.29	0.79	0.215	0.29
49	0.77	0.082	1.66	1.21	0.49	0.29	0.84	0.26	0.29	0.77	0.21	0.28
57	0.74	0.059	1.00	0.84	0.20	0.19	0.84	0.26	0.29	0.80	0.24	0.289
58	0.70	0.082	1.00	0.92	0.12	0.12	0.84	0.26	0.29	0.83	0.24	0.288
59	0.75	0.082	1.00	0.74	0.30	0.29	0.84	0.26	0.29	0.76	0.21	0.282
60	0.82	0.082	1.00	0.80	0.24	0.23	0.84	0.26	0.29	0.81	0.23	0.292
65	0.68	0.059	0.62	0.55	0.07	0.11	0.84	0.26	0.29	0.84	0.24	0.293
67	0.69	0.082	0.62	0.54	0.08	0.13	0.84	0.26	0.29	0.83	0.235	0.289
68	0.75	0.082	0.62	0.50	0.12	0.19	0.84	0.26	0.29	0.81	0.23	0.292

(b) Correlation of Essential Non-dimensional Parameters

The summary of the experimental results incorporating the salient data are presented in Table D.1. The maximum velocity V_{\max} , measured close to the boundary illustrates that its increase over increasing contraction ratios, is not as drastic as the increase in stable size demanded by the flow.

The dimensionless variables η , m and D/h yielded by each run of series B, C and D are plotted in Fig. 5.13 for each of the three Froude numbers of 0.50, 0.29 and 0.10. The experimental evidence vindicates the validity of the four essential parameters provided by dimensional analysis.

As the contraction ratio corresponding to the threshold condition could not be exactly determined experimentally, (and would also be a conservative estimate of material stability) a contraction ratio corresponding to an efficiency of 0.97 was arbitrarily considered as representating the onset of instability. However, the contraction ratio corresponding to an efficiency of 0.90 was accepted as the stable design condition for the closure material, because loss of 10% of closure material will be economically commensurate with the gain in contraction ratio. Pariset and Hausser (1959) also accepted a loss of 10% of the closure material as marking the onset of an unstable condition.

As has been mentioned earlier it is possible to obtain an improved closure of the waterway by sacrificing efficiency. This might well be the requirement in practical cases where only a partial closure is to be achieved by the economically available size. It can be seen

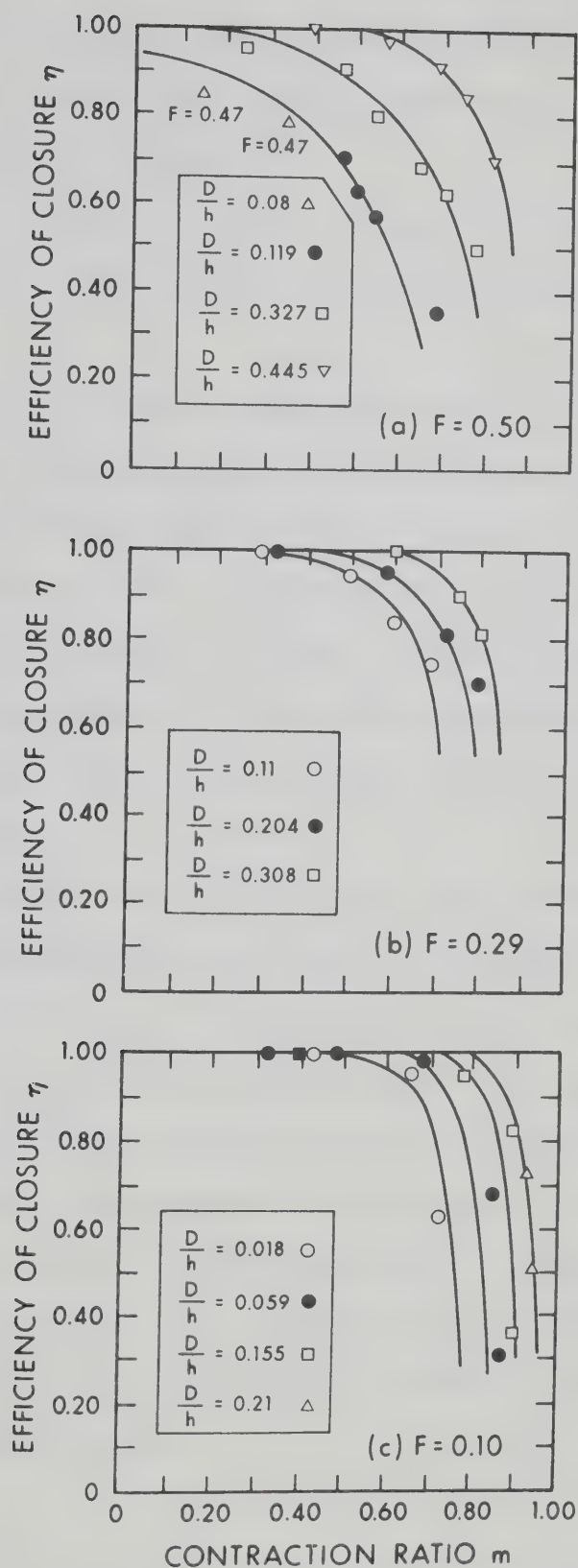


FIG. 5.13 RELATIONSHIP BETWEEN η , m , AND D/h AT F VALUES OF 0.50, 0.29 AND 0.10

from Fig. 5.13b that for a D/h value of 0.204, an increase in contraction ratio from 0.60 to 0.76 can be attained by allowing the efficiency to drop from 0.95 to 0.60.

As stated earlier, in section 3.1.5 "Dimensional Analysis", the omission of the term d/h is considered acceptable for practical design.

Interpolating by numerical techniques, Fig. 5.13 has been transformed into Figs. 5.14, 5.15, and 5.16 as a three parameter plot of F , m and D/h corresponding to efficiencies of 0.97, 0.90 and 0.80. (An efficiency of 0.80 is acceptable in situations where availability of large size material is limited. Lower values may not be economical in practice.) Figure 5.15 is proposed as the design chart for stability of the closure material. Use of Figs. 5.14 and 5.16 can also be made as required.

The data generally available for a closure job are Q , the river discharge, B , the river width, h , the normal depth and D , the closure material size. The information sought is b , the critical gap width. From the available information, F , the Froude number of approach flow and D/h can be computed and from Fig. 5.15, m , the stable contraction ratio corresponding to an efficiency of 0.90, can be directly read out to yield b , the stable gap width. Alternatively, if the gap width b is specified, the contraction ratio m is known. Stable size, D , can then be evaluated by reading out D/h for known values of F and m again from Fig. 5.15.

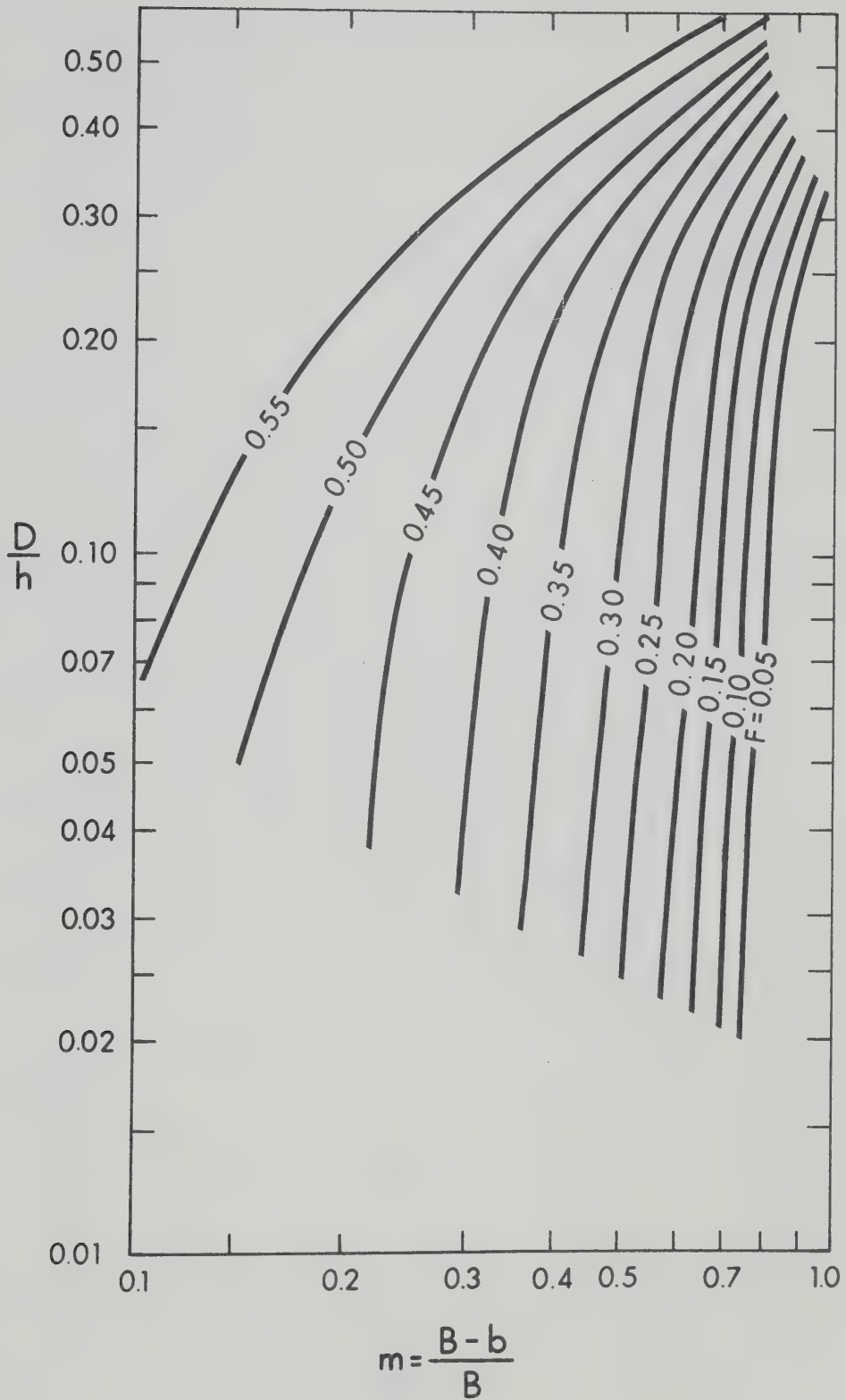


FIG. 5.14 RELATIONSHIP BETWEEN D/h AND m FOR $\eta = 0.97$ WITH F AS THE THIRD PARAMETER

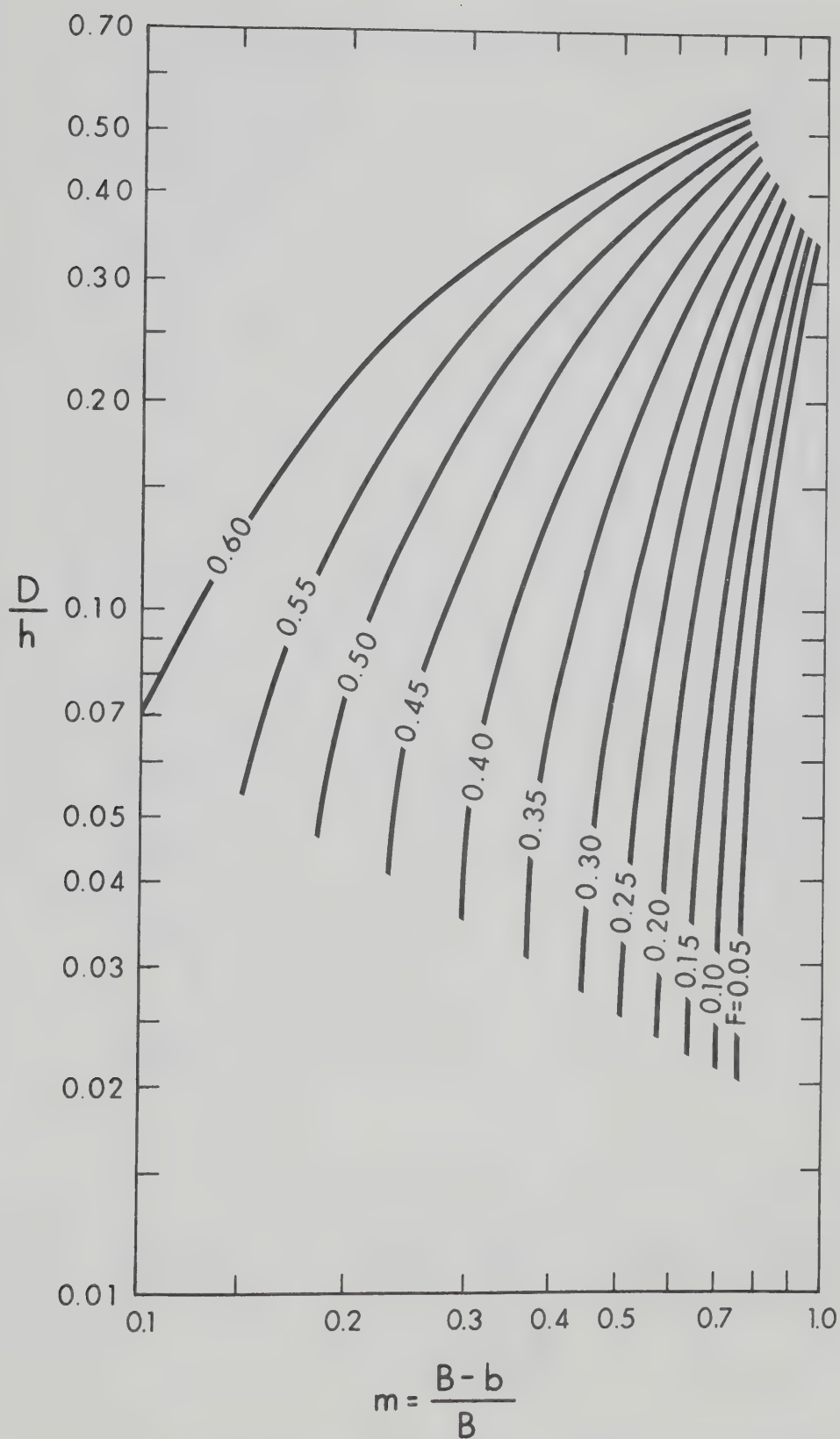


FIG. 5.15 RELATIONSHIP BETWEEN D/h AND m FOR $\eta = 0.90$ WITH F AS THE THIRD PARAMETER

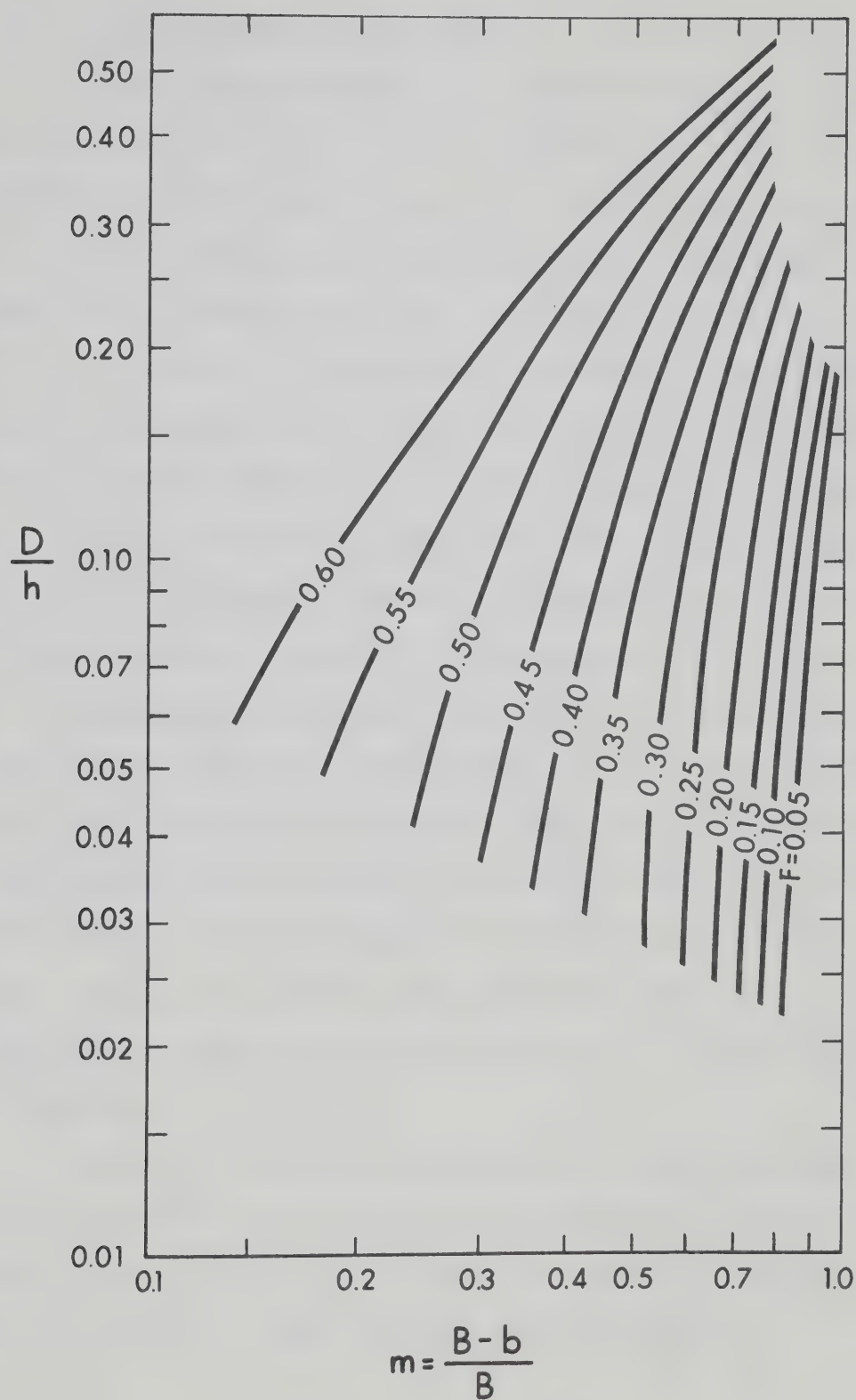


FIG. 5.16 RELATIONSHIP BETWEEN D/h AND m FOR $\eta = 0.80$ WITH F AS THE THIRD PARAMETER

(c) Effects of Neglected Parameters

Effects of B/h Variation - The suggested design curves have been developed at one value of B (full flume width of 7.50 ft.) and one value of d (median size 1.20 mm). The effect of variation of B/h upon stability, as indicated by dimensional analysis, was studied by systematically varying B from 7.50 ft. to 4.6 ft. in series F and then to 2.75 ft. in series G. The experimental procedure for these runs was identical to those previously described. Only one Froude number of 0.29 was studied, utilising all the three sizes of closure material. Table 5.3 compares the observed contraction ratio with values read from Fig. 5.13. Although B/h varied in the range 28.8 to 10.6, no significant difference in stability was observed over this range.

Effects of d/h Variation - The effect of variation of d/h was specifically studied at a Froude number of 0.29 by varying the bed material size first to 0.60 mm in series J and then to 0.25 mm in series M. Other series in this study were run at Froude numbers of 0.50 and 0.10 with 0.60 mm and 0.25 mm sand for collecting data specifically on scour. Because the stability data collected in those series were not very precise, effects of variation of d/h at $F = 0.50$ and 0.10 , are not examined.

To test the validity of equation 3.15, a semi-logarithmic plot of $(D/h)(h/d)^{1/3}$ versus stable m (corresponding to efficiency of 0.90 from data of series D, J and M) with F as a third parameter is shown in Fig. 5.17a. A linear correlation is indicated.

TABLE 5.3
EFFECT OF $\frac{B}{h}$ VARIATION

Run No.	$\frac{B}{h}^*$	$\frac{D}{h}$	Experimental Efficiency η	Values Contraction ratio m	Contraction ratio m from Fig. 5.13 corresponding to efficiency η in col. 4
1	2	3	4	5	6
52	17.70	0.081	0.95	0.435	0.45
53	17.70	0.081	0.65	0.65	0.64
54	17.70	0.081	0.30	0.68	0.69
55	17.70	0.227	0.98	0.54	0.50
56	17.70	0.227	0.80	0.69	0.75
57	17.70	0.027	0.60	0.74	0.78
58	17.70	0.31	0.95	0.70	0.72
59	17.70	0.31	0.65	0.75	0.82
60	17.70	0.31	0.30	0.82	0.83
61	10.60	0.081	0.90	0.49	0.51
62	10.60	0.081	0.90	0.57	0.63
63	10.60	0.227	0.98	0.44	0.50
64	10.60	0.227	0.90	0.60	0.65
65	10.60	0.227	0.50	0.68	0.77
67	10.60	0.31	0.90	0.69	0.74
68	10.60	0.31	0.60	0.74	0.81

* - $B/h = 28.80$ for previous runs

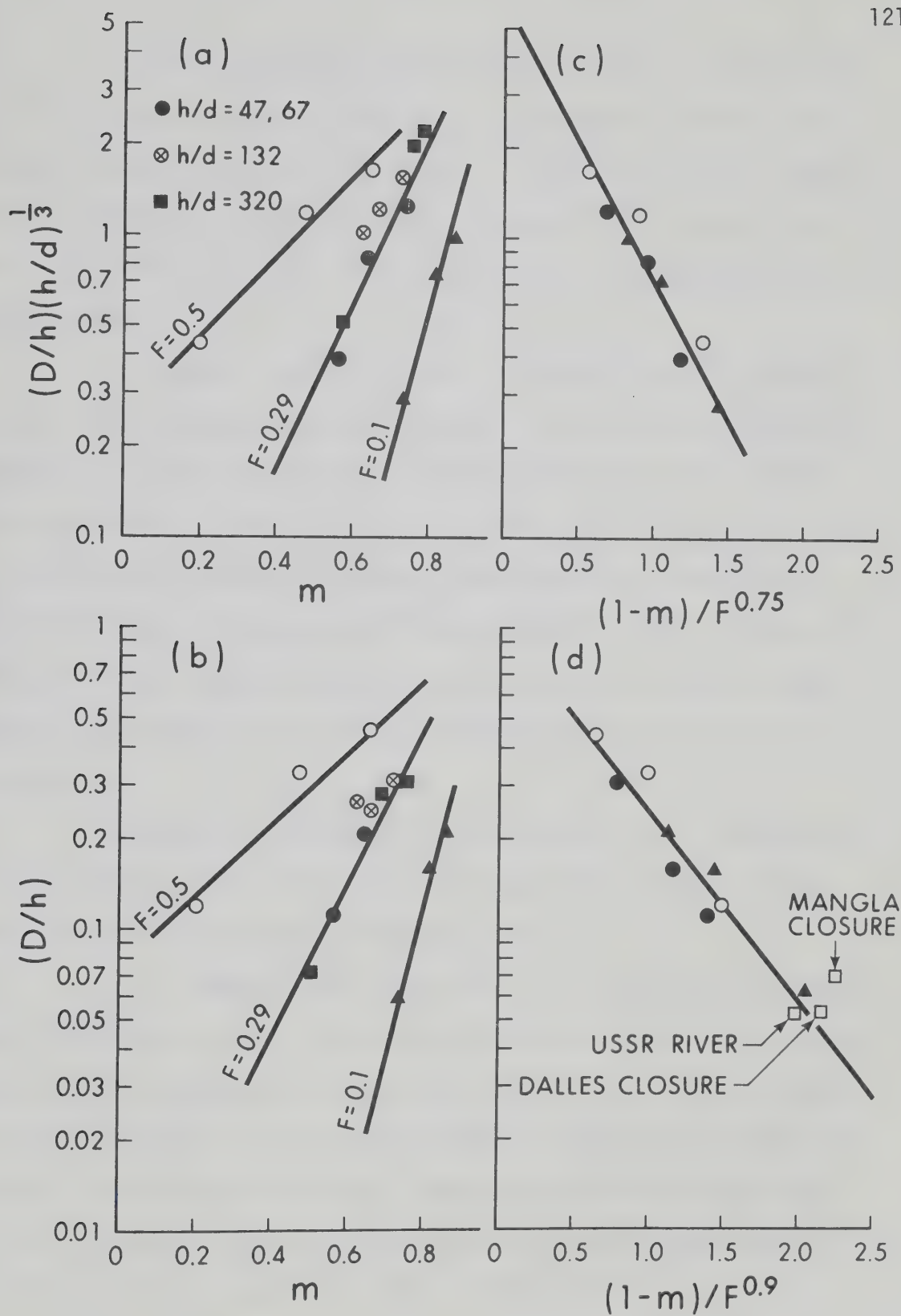


FIG. 5.17 VERIFICATION OF EQUATIONS 3.15 AND 3.19

To dissociate the effects of h/d variation, a similar plot of D/h , m and F is shown in Fig. 5.17b. Although h/d varied in the range 47 to 320, for the Froude number of 0.29, the stability appears to be relatively unaffected. Table 5.4 compares the observed contraction ratio with values read from Fig. 5.13. The agreement is indeed good.

It appears that for closure of alluvial channels the variation of bed material size (consequently, the variation of bed scour) does not influence the stability of closure material significantly. The use of D/h in place of a term like $(D/h) (h/d)^{1/3}$ (equation 3.15) is justified in practical interest. Purely empirical correlations combining F and m to one variable are attempted in Figs. 5.16c and d. Because of the complex variation of the constants in equation 3.10, these linear correlations cannot be considered exact, but merely as guides.

Figures 5.14 through 5.17 indicate that as the contraction ratio approaches unity, D/h values converge and the effect of the variation of Froude number is insignificant.

It is concluded that the effects of B/h and d/h are minimal over the range tested. A possible explanation is that the contraction ratio and the geometry of the end-dump constriction can be considered primarily responsible for the distribution of shear stress (Ippen and Drinker, 1962, Replogle and Chow, 1966) and hence for the stability of the closure material. Variation of B/h has no significant effect on the contraction ratio. Variation of d/h results in variation of

TABLE 5.4
EFFECT OF $\frac{d}{h}$ VARIATION

Run No.	$\frac{h^*}{d}$	$\frac{D}{h}$	Experimental Values		Contraction ratio m from Fig. 5.13 corresponding to efficiency η in Col. 4
			Efficiency η	Contraction ratio m	
1	2	3	4	5	6
75	132	0.081	0.98	0.39	0.38
76	132	0.081	0.90	0.61	0.68
77	132	0.31	0.90	0.74	0.76
79	132	0.227	0.90	0.65	0.66
80	132	0.31	0.80	0.80	0.81
90	320	0.081	0.98	0.35	0.38
91	320	0.081	0.90	0.50	0.52
92	320	0.227	0.90	0.65	0.64
93	320	0.31	0.90	0.72	0.72

* $h/d = 45$ and 66 for previous runs

the extent of bed scour, but as Fig. 5.1 indicates, the contraction ratio is not altered significantly due to bed scour. Hence the stability is relatively unaffected by variations of either B/h or d/h .

(d) Effects of Rate of Dumping

The rate of dumping though left out of the analysis, was varied widely in a few check runs to observe any effect on the stability. Until the onset of instability, the rate of dumping was observed to have no effect. After a particular closure material crossed the threshold condition, a higher dumping rate did not indicate significant improvement in efficiency, but merely resulted in the crest elongating along and not extending into the flow. In this study no quantitative assessment of the effect of either the rates of dumping or the variation of crest width has been made. It needs to be emphasized that a substantially wider crest would make the head loss occur over a longer length and the closure material would gain some measure of stability. This aspect was taken advantage of by maintaining a 250 ft. wide crest for the Dalles dam (1965) in the final stages of closure.

(e) Closure Tests from One Bank Only

In series H, six verification runs were made at the three Froude numbers of 0.525, 0.29 and 0.1 to test the applicability of the design curves to a closure from one bank only. The contraction ratio-efficiency relationships were found to agree satisfactorily with values for dual closures, as can be seen from the comparison presented in Table 5.5.

TABLE 5.5
PARTICULARS OF CLOSURE TESTS FROM ONE BANK ONLY

Run No.	F	$\frac{D}{h}$	Experimental Efficiency η	Values Contraction ratio, m	Contraction Ratio m from Fig. 5.13 Corresponding to η in Col. 4
1	2	3	4	5	6
69	0.29	0.081	0.90	0.455	0.49
70	0.29	0.227	0.90	0.60	0.63
71	0.525	0.117	0.90	0.23	0.22
72	0.525	0.327	0.90	0.40	0.46
73	0.525	0.445	0.90	0.65	0.67
74	0.10	0.056	0.90	0.74	0.73

5.5.3 Additional Tests to Check Effects of Channel Cross-Sectional Shape

It is well known that natural rivers rarely correspond to the rectangular or trapezoidal channel sections studied in the laboratory. It was therefore considered important to test closures in the laboratory on an undistorted model of a natural river. For this the Kitimat River, British Columbia, Canada, was modelled to 1:100 scale covering a stretch of over 3,000 ft. Closure was attempted with two sizes of material representing nominal diameters of 2.10 and 4.00 ft. at three discharges of 15,000, 30,000 and 50,000 cfs. Data for laboratory closure on a model of the outflow channel of Lake Athabasca, Alberta,

Canada (1971) are also available. A flow of 35,000 cfs was partially closed with stones representing nominal spherical diameter of 2.00 ft.

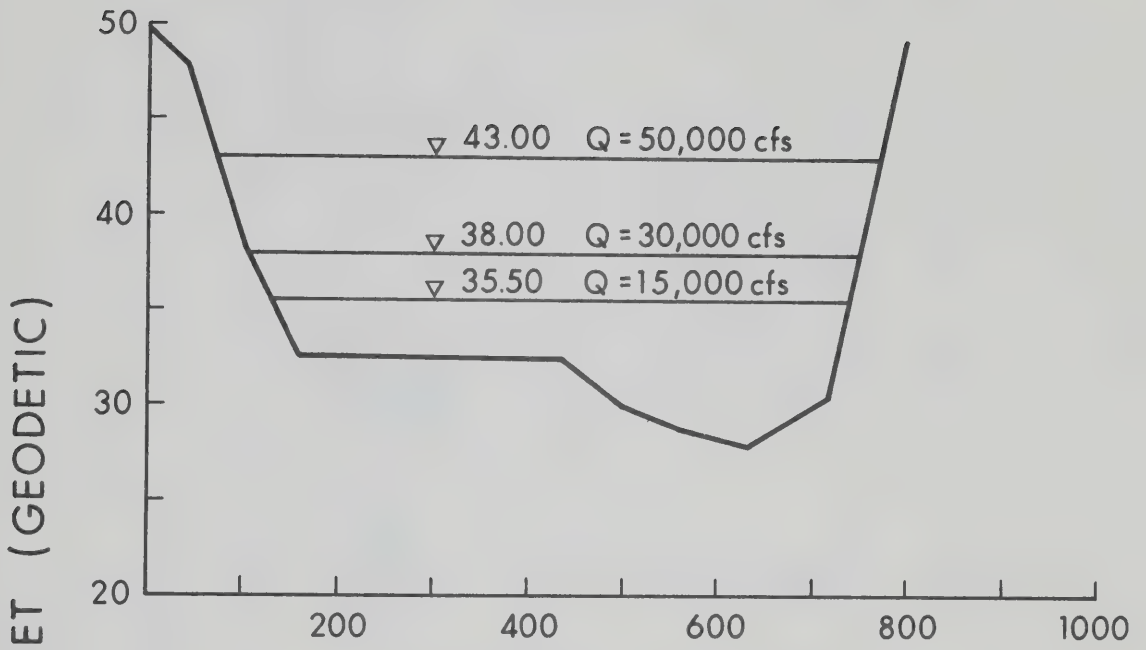
The cross-sections of Kitimat River and the outflow channel of Lake Athabasca are shown in Fig. 5.18. As these rivers have a markedly deep central channel with side berms, the normal flow depth was substituted by the hydraulic mean depth for computing D/h values.

A summary of the experimental data for these two cases are presented in Table 5.6. As can be seen, the agreement between the design value and the experimentally observed value of the critical gap width is quite satisfactory. It appears that the design curves can be applied to natural channels of irregular shape if hydraulic mean depth (R) is substituted for h , the normal flow depth.

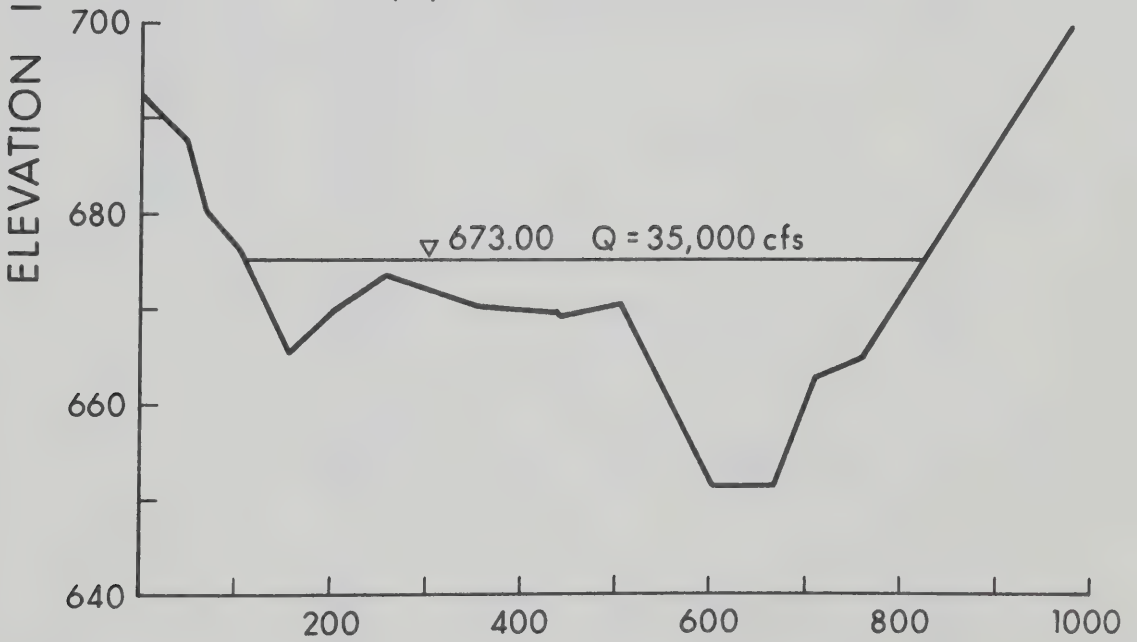
5.5.4 Checking of Design Curves

(a) Against Actual Closures

Comprehensive data of actual river closures or even partial closures by cofferdams are few due to lack of proper documentation. Many rivers in the U.S.S.R. (Linford, 1967) have been closed by either transverse-dump or end-dump methods, but exact data for end-dump dams pertaining to the threshold contraction ratio and the stable size are rarely available. Sandover (1971) quotes two cases, the first for a Russian river reported by Izbash, and the second for Mangla Cofferdam in Pakistan. A third case, Dalles dam on the Columbia river (1965), is also available, although it must be emphasized that the quoted value of critical gap width is rather approximate. A comparison of the critical



(a) KITIMAT RIVER



(b) OUTFLOW CHANNEL OF LAKE ATHABASCA

FIG. 5.18 IRREGULAR CROSS-SECTIONS TESTED

TABLE 5.6

CROSS-SECTIONAL SHAPE EFFECT

Flow Description	Q Discharge CFS	B River Width in feet	F Froude Number of Flow	h Depth of flow in feet Minimum	h Maximum	R Hydraulic Mean Depth in feet	D Closure Material Size in feet	$\frac{D}{R}$	Critical Gap width in feet From Design Curve (Fig. 5.15)	Exptly Observed
1	2	3	4	5	6	7	8	9	10	11
Kitimat River	15,000	600	0.40	3.0	7.50	5.00	2.10	0.42	195	175
"	30,000	600	0.43	6.5	10.50	7.50	2.10	0.20	312	292
"	50,000	600	0.33	11.50	15.50	12.50	2.10	0.168	270	275
"	50,000	600	0.33	11.50	15.50	12.50	4.00	0.32	210	180
Overflow channel of Athabasca Lake	35,000	700	0.28	2.00	22.00	9.10	2.00	0.22	205	170

gap width from the design curve presented herein (Fig. 5.15) with that actually attained at the site is made in Table 5.7.

(b) Against Data of Other Researchers

Quantitative data on the stability of rockfill in end-dump closure of rigid-bed channels is available due to Sandover (1971). This is probably the only reported study on end-dump closures. Sandover conducted the tests in a 10 ft. wide and 4 ft. deep flume, using two types of materials, rounded and angular (pebbles or chippings) in twelve different nominal diameters ranging from 0.3 inches for the pebbles and 0.3 to 8 inches for the chippings. Sandover's flume data are also utilized in Table 5.7.

The agreement between the suggested design values and the actual river closure data as well as Sandover's data is indeed good. The actual river closure data are also plotted on Fig. 5.17d for illustration.

However, all the closures verified were carried out on fixed-bed channels. The maximum contraction ratio attained in these cases was 0.89 for Mangla Cofferdam, but the Froude number was as low as 0.035; under which condition for a mobile bed channel the bed scour would not be substantial, according to the indications of this study. The closure material on the firm bed channel would have then behaved similarly to that on the mobile bed channel, used herein to develop the design curves.

TABLE 5.7

VERIFICATION OF DESIGN CURVES

Flow Description	Q Discharge in CFS	B Normal Flow Width in feet	h Normal Flow Depth in feet	F Froude Number of Normal Flow	D Nominal Size of Closure Material in feet	$\frac{D}{h}$	b, Critical Gap width in feet Scaled from Design Curve Fig.	b, Critical Gap width in feet Actually Observed at Site or Laboratory ^a
1	2	3	4	5	6	7	8	9
Due to Izbash (River in U.S.S.R.)	127,000	984	27.50	0.158	1.44	0.053	355	370
Mangala Cofferdam	7,000	470	18.00	0.035	1.25	0.070	44	50
Dalles Dam	56,000 ^b	520	48.00	0.058	2.50	0.052	73	60 - 70 ^c
Stop Point A	19.25	9.84	1.32	0.226	0.037	0.028	4.80	5.17
B	18.20	9.84	1.29	0.221	0.037	0.029	4.45	5.23
C	16.75	9.84	1.26	0.211	0.037	0.029	4.35	4.65
D	15.35	9.84	1.23	0.201	0.037	0.030	4.23	4.26
E	13.15	9.84	1.18	0.184	0.037	0.031	3.90	3.74
F	11.20	9.84	1.13	0.167	0.037	0.033	3.64	3.13
G	8.35	9.84	1.05	0.139	0.027	0.035	3.05	2.61

a - Based on Sandover's flume data for RUNS A through G

b - Approximate discharge assumed in main channel out of actual river discharge of 108,000 cfs; balance was diverted through skeleton power house units

c - Based on gap width on 16-17 October, 1956.

5.6 Concluding Remarks

In this chapter the characteristics of flow through an end-dump constriction built into an alluvial channel and the stability of closure material were critically analysed based on the experimental data. Application of critical velocity criterion to determine the stable size was found to yield unrealistic results.

A theoretical analysis of stability from shear stress criteria supported by dimensional analysis indicated the most important non-dimensional parameters to be the Froude number of approach flow, the contraction ratio, the ratio of nominal closure material size to depth of flow and the efficiency of closure. Experimental data corroborated the adequacy of these four parameters. Bed scour at the dump area, reflecting the effect of the bed material, was found to have a minor influence on the stability of closure material. Appendix C indicates satisfactory agreement between the observed stable size and the size computed from measured shear stress on the boundary.

Curves correlating the essential parameters have been presented as design curves for direct determination of stable size of closure material or of critical gap width at any stage of closure. These curves are not recommended for use at contraction ratios exceeding 0.90.

A few actual closures and closures in the laboratory were analysed in the light of the proposed design curves. Good agreement between the actual critical gap widths and the predicted values is noted.

CHAPTER VI

ANALYSIS OF DATA ON BED SCOUR AND BACKWATER RISE

6.1 Introduction

In this chapter, analyses of the experimental data on scour and backwater are made in the context of the theoretical developments made in Chapter III and the knowledge gained regarding the characteristics of flow through the constriction (section 5.2).

Although it is accepted that characteristics of the bed material play a decisive role in the pattern and extent of scour and backwater rise, definite conclusion or design recommendations regarding local scour have been scanty, as discussed in Chapter II. The analysis of data in this study is made giving specific consideration to the size and the specific gravity of the bed material.

Design curves correlating the essential non-dimensional parameters are presented. Conformity of the data of investigations on local scour by other researchers, with the proposed design curves, is examined. In such examinations, due consideration is given to the variation in the geometry and characteristics of the constriction from one situation to the other.

6.2 Maximum Scour Depth

6.2.1 Location of Deepest Scour

It has been shown earlier that at the vena-contracta the contracting flow attains the maximum velocity close to the live stream boundary and the flow velocity decreases towards the centre of the channel (Fig. 5.11). Two isolated elliptical scour holes with some general scour of the bed in the centre generally occur at low contraction ratios. As the contraction ratio increases the scour holes move to the centre and become deeper. Figures 6.1 and 6.2 illustrate the typical scour pattern at different degrees of contraction at a Froude number of 0.50, for the bed material of 1.2 mm. The same trend was observed at the Froude numbers of 0.29 and 0.10 and for the bed materials of 0.6 mm and 0.25 mm as well. From the definite trend in the location of the deepest scour close to the live-stream boundary, at the vena-contracta both for the clear water and the sediment-transporting flows, it is obvious that the increased bed shear stress due to the contracted flow is primarily responsible for maximum scour at the end-dump constrictions.

Figures 5.7 through 5.9 which define the live-stream configuration, can be used to determine the location of deepest scour.

6.2.2 Clear Water Case

The data for the runs 7 through 85 and 94 through 96 corresponding to the clear water case are presented in Table D.1.

The analysis of the data is based upon Eq. 3.31 and Eq. 3.48

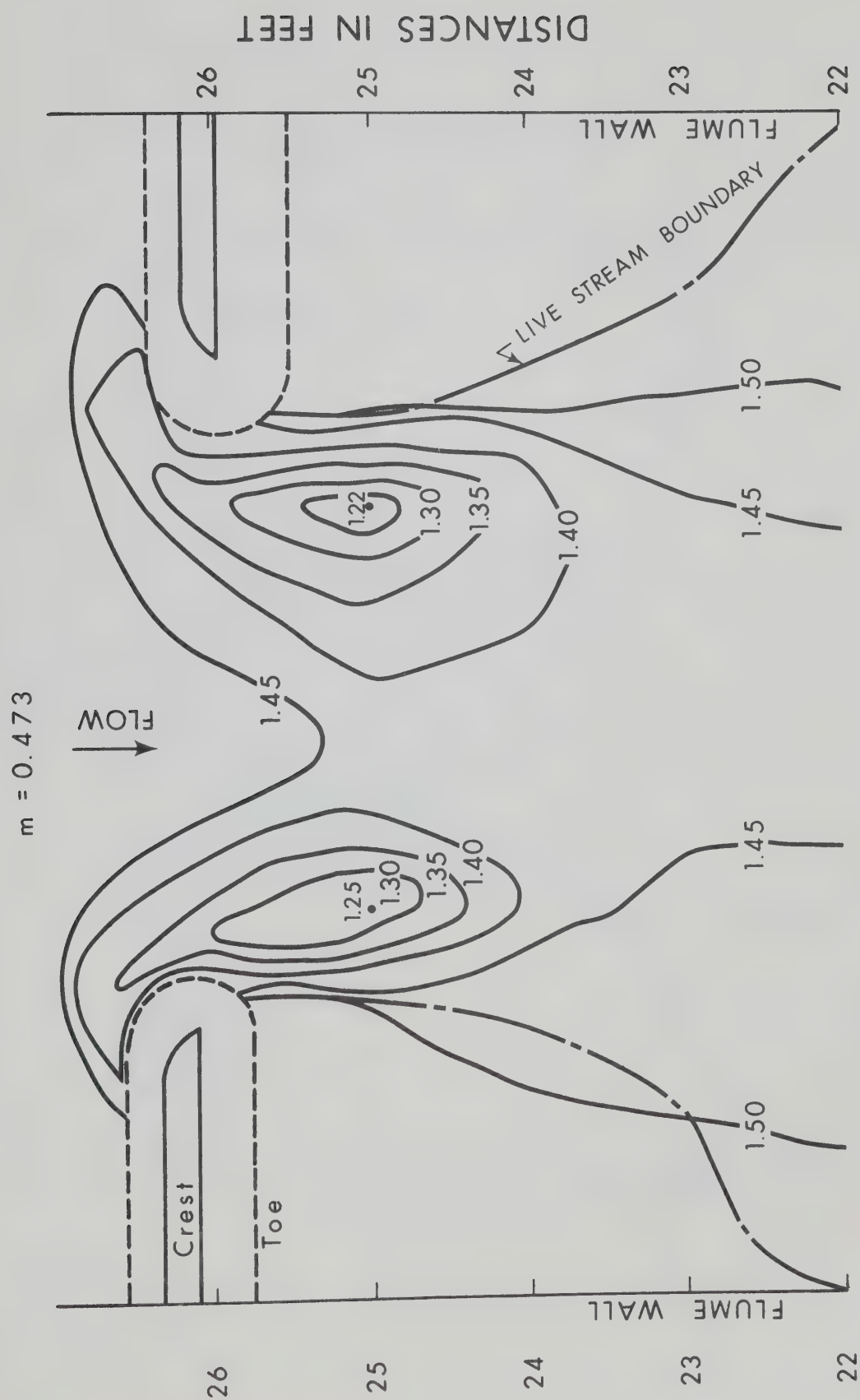


FIG. 6.1 TYPICAL PATTERN OF BED SCOUR AT A LOW CONTRACTION RATIO
 ($m=0.473$, $F=0.50$, $h=0.18$ ft., Normal Bed Level 1.50, Bed Contours in feet)

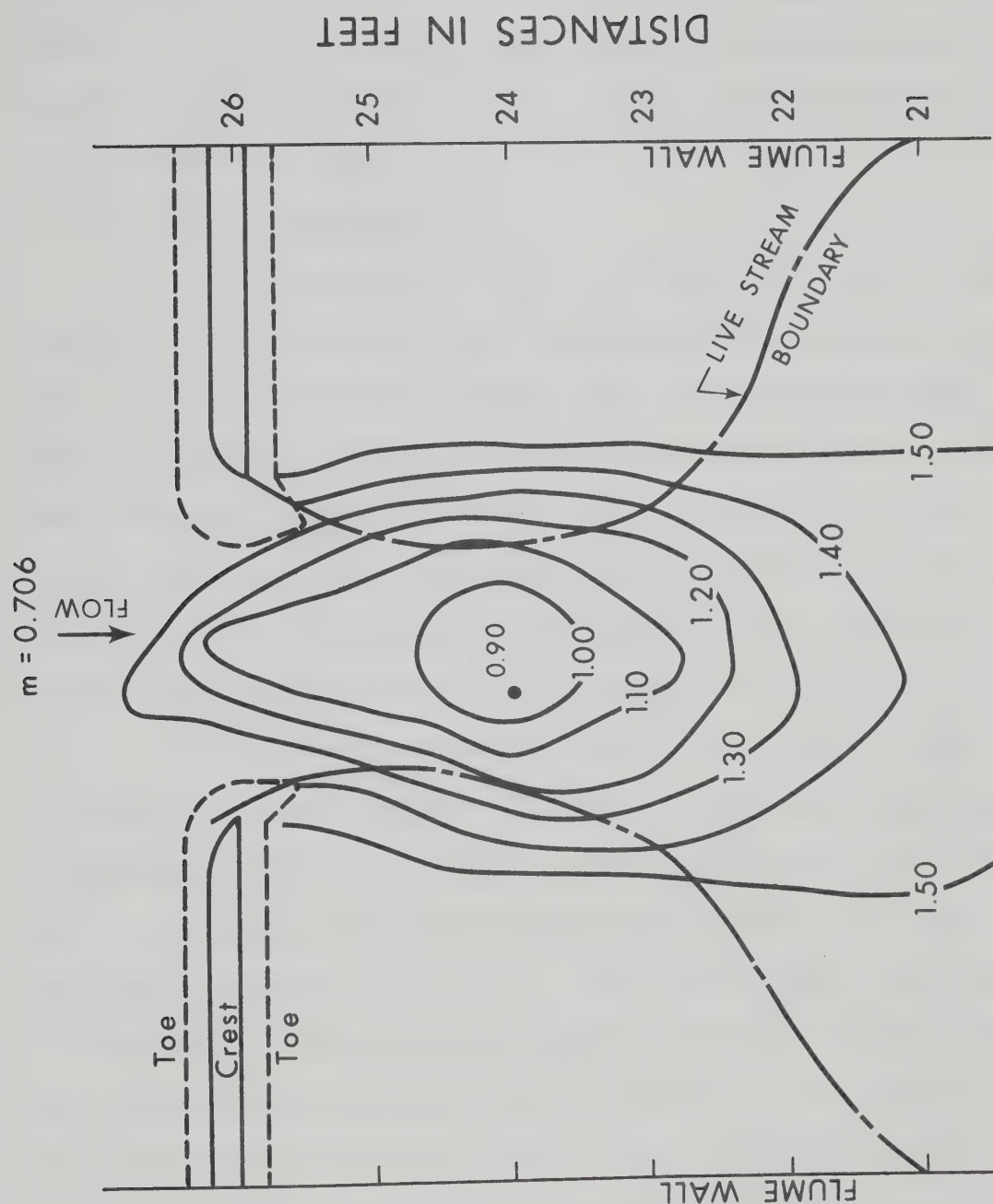


FIG. 6.2 TYPICAL PATTERN OF BED SCOUR AT A HIGH CONTRACTION RATIO
($m=0.706$, $F=0.50$, $h=0.18$ ft., Normal Bed Level 1.50, Bed Contours in Feet)

A semilogarithmic plot of $(h + d_s)/h$ versus m with F as the third parameter is shown in Fig. 6.3a. The plot indicates a definite correlation between $(h + d_s)/h$, m and F . On this figure, the variation of h/d is shown to illustrate that the sediment size has a definite influence on the maximum scour depth.

(a) Effect of Sediment Size

In Fig. 6.3b a plot of $\{(h + d_s)/h\}(d/h)^{0.29}$ versus m shows the data to coalesce at each Froude number which illustrates the validity of Eq. 3.28. The index 0.29 indicates that at a particular Froude number of the flow, the variation of the sediment size in the practical range from medium to coarse sand (say from 0.2 mm to 1.5 mm, 750% increase) would result in a decrease of the non-dimensional scour depth by only 75%. However the bed forms which would be more pronounced for the fine sand can cause variation of scour depth over time.

It has been recognized that the critical tractive stress for dune beds is higher than that for plane beds (ASCE Task Committee on Sedimentation, (1966)). As such Eq. 3.29, derived under the assumption of an invariant critical tractive stress related to size only, would not be completely realistic for flows over different bed forms. At low values of particle Reynolds number, Eq. 3.29 is not applicable. These considerations and factors such as the shape of sediment can cause the index of 0.29 to be as low as 0.16 as suggested by Neill (1962).

Figure 6.4 shows the non-dimensional plot of experimental data, based on Eq. 3.31. The theoretical analysis has thus a satisfactory agreement with the experimental data. The combined parameter

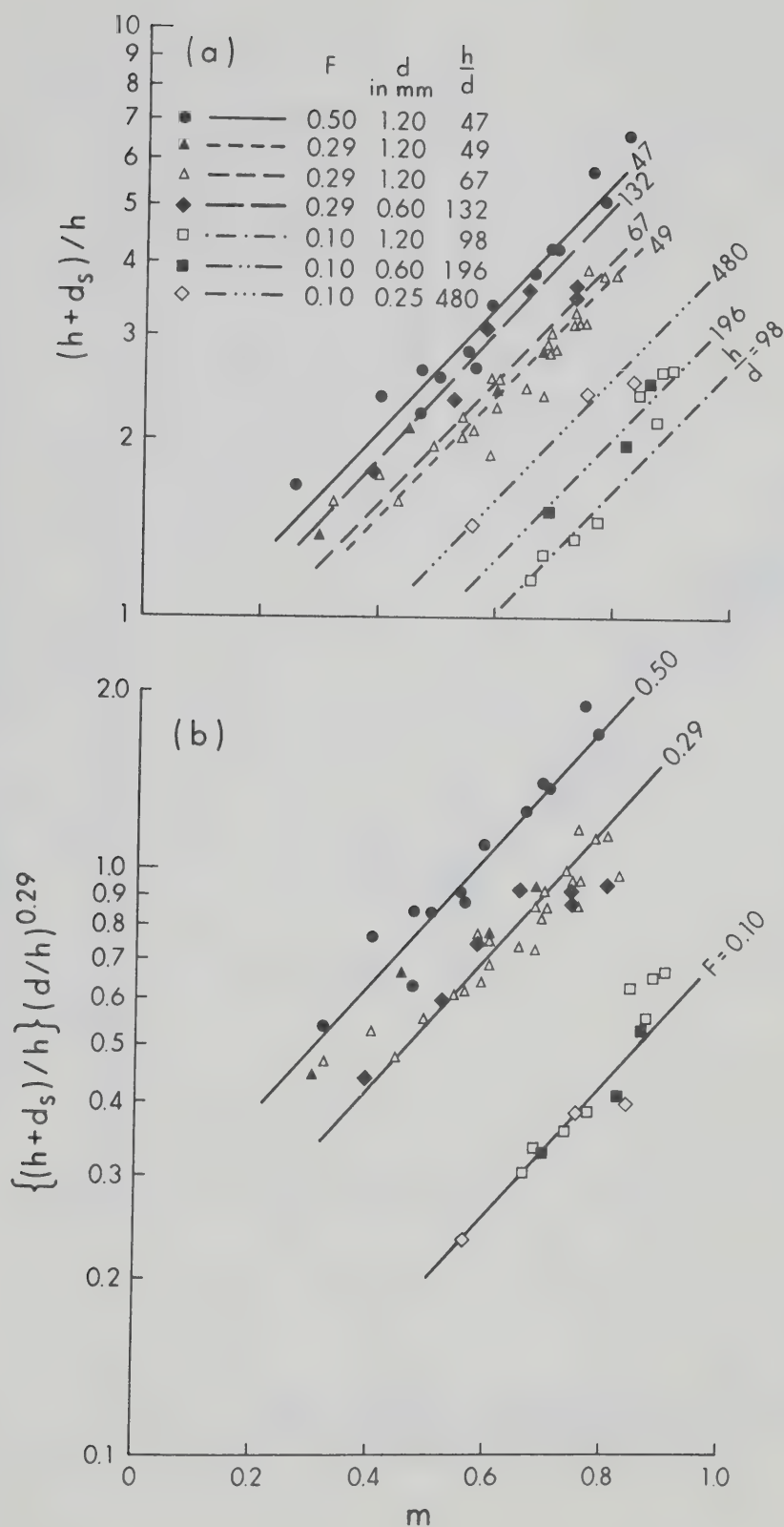


FIG. 6.3 RELATIONSHIPS FOR MAXIMUM SCOUR DEPTH IN CLEAR-WATER FLOW

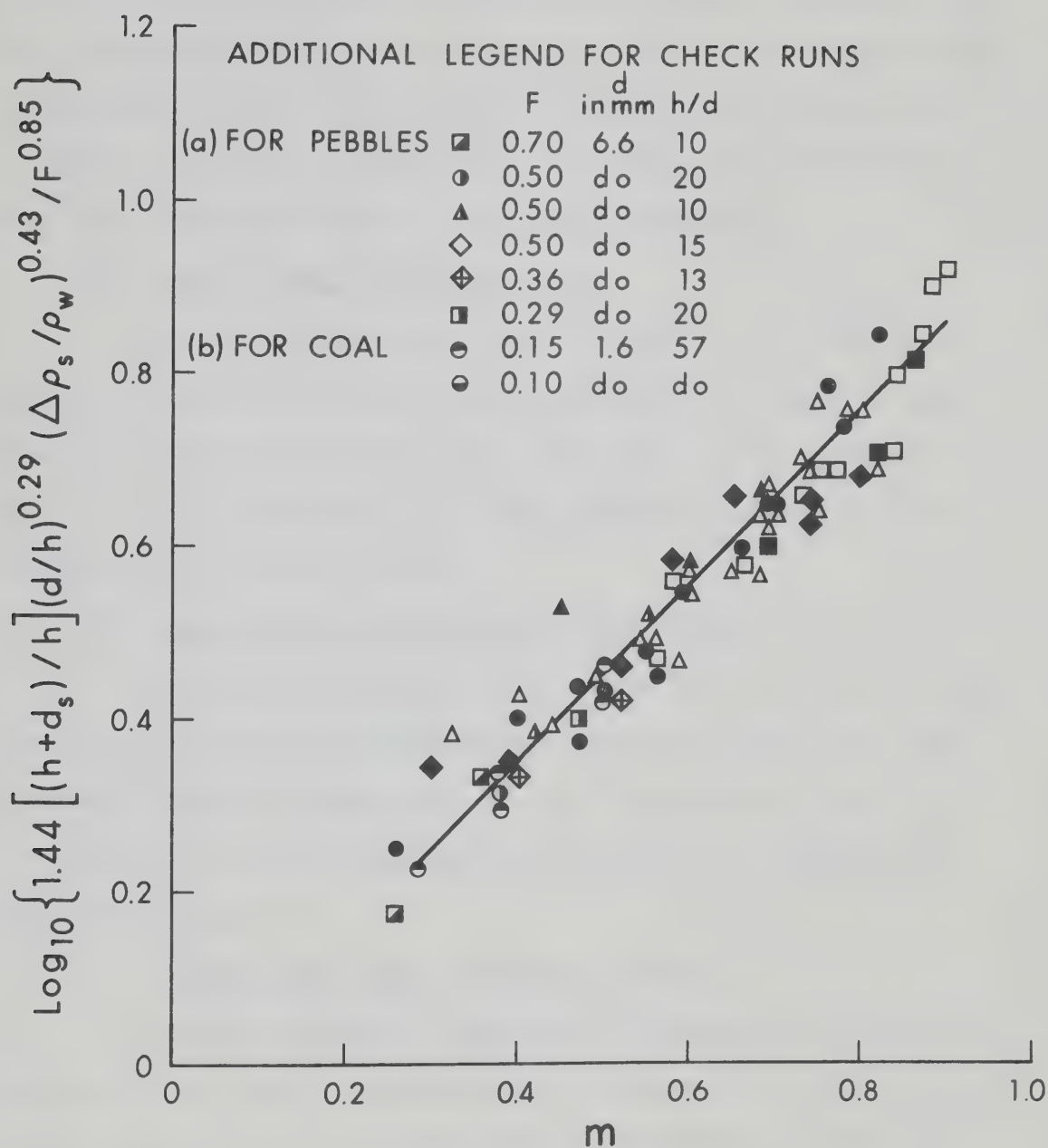


FIG. 6.4 VERIFICATION OF EQUATION 3.31 FOR MAXIMUM DEPTH OF SCOUR IN CLEAR-WATER FLOW

$\{(h + d_s)/h\}(d/h)^{0.29}$ seems to represent the effect of sediment size more adequately than C_d , the average drag coefficient of the sediment as proposed by Garde et al (1961). It was, however, considered desirable to check the validity of Eq. 3.31 with coarse bed material and light weight bed material for general applicability.

(b) Check of Data for Large Sediments

It was considered desirable to check Eq. 3.31 with pebbles of 6.6 mm (closure material B) as the bed material. Table 6.1 summarizes the data for the check runs. The data is also plotted on Fig. 6.4 for illustration. It is seen that the agreement is satisfactory for h/d values as low as 10.

(c) Check of Data for Light-Weight Bed Material

Crushed coal (anthracite) of median size 1.6 mm and specific gravity of 1.26 was used as bed material in a few check runs. The summary of the experimental data is also incorporated in Table 6.1. The data is also plotted on Fig. 6.4. Satisfactory agreement with Eq. 3.31 is noted.

(d) Maximum Scour Depth in Alluvial Channels

As the experimental data agrees with equation 3.28 which incorporates the essential dimensionless parameter given by Eq. 3.48, Fig. 6.4 can be used to determine the maximum depth of scour. To obviate tedious repetitive mathematical computations for determination of $(d_s + h)/h$ for alluvial channels from Fig. 6.4, convenient charts covering Froude numbers in the range 0.05 to 0.60 are presented in Fig. 6.5 for bed sediments of specific gravity 2.65.

TABLE 6.1

EXPERIMENTAL DATA FOR VERIFICATION OF EQUATION 3.31
WITH COAL AND PEBBLES AS BED MATERIALS

(a) For pebble ($d_{75} = 6.6 \text{ mm}$) as Bed Material

Run No.	Flume data				d_s in feet	$(h+d_s)/h$ Observed	Computed data $(h+d_s)/h$ from SFig. 6.4
	F	h in feet	d in feet	$\frac{h}{D}$	m		
112	0.70	0.21	0.021	10	0.25	0.03	1.24
113	0.70	0.21	0.021	10	0.35	0.16	1.63
114	0.50	0.42	0.021	20	0.37	0.25	1.69
115	0.50	0.21	0.021	10	0.27	No scour	No scour
116	0.50	0.21	0.021	10	0.55	0.20	1.84
117	0.50	0.315	0.021	15	0.42	0.14	1.60
118	0.36	0.27	0.021	13	0.30	No scour	No scour
119	0.36	0.27	0.021	13	0.40	0.02	1.07
120	0.36	0.27	0.021	13	0.52	0.05	1.28
121	0.29	0.42	0.021	20	0.37	No scour	No scour
122	0.29	0.42	0.021	20	0.47	0.08	1.25

(b) For Coal ($d_{50} = 1.6 \text{ mm}$, $\rho_s = 1.26$) as Bed Material

123	0.15	0.30	0.0052	57	0.28	0.10	1.34
124	0.15	0.30	0.0052	57	0.38	0.18	1.73
125	0.15	0.30	0.0052	57	0.50	0.35	2.28
126	0.10	0.30	0.0052	57	0.38	0.08	1.21
127	0.10	0.30	0.0052	57	0.50	0.16	1.60

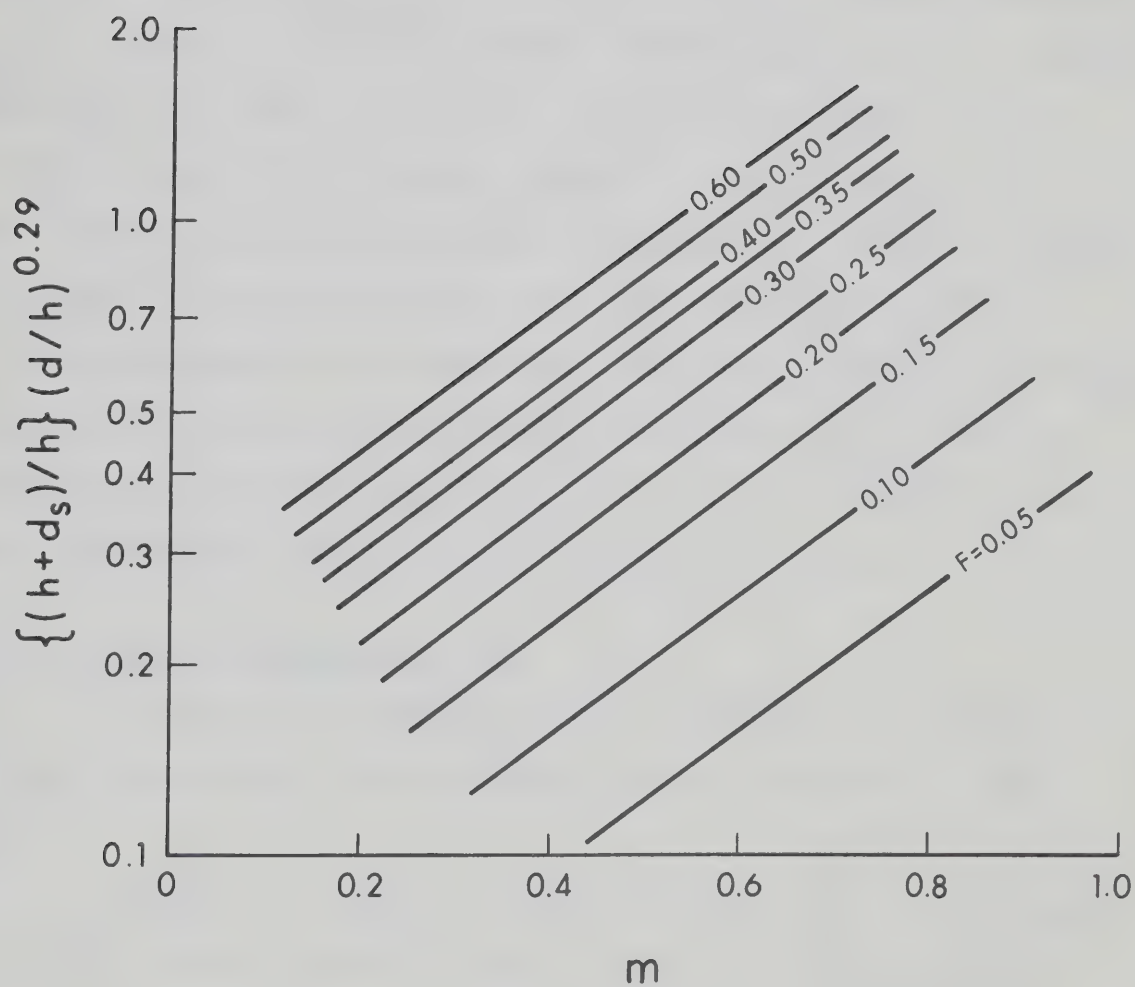


FIG. 6.5 DESIGN CURVE FOR MAXIMUM SCOUR DEPTH
IN CLEAR-WATER FLOW

(e) Evaluation of Indices j_3 and j_4 in " $\tau'_{o_{\max}}/\bar{\tau}_o$ -m" Relationship

Based on Eq. 3.31, the slope of the straight line fitting the entire data in Fig. 6.4 is $0.43 j_3$ and the intercept on the ordinate is $0.43 j_4$. Thus j_3 and j_4 are evaluated as 2.1 and - 0.17 respectively. Awazu (1967) measured $\tau'_{o_{\max}}$ at the centre line of the flume and evaluated j_3 as 1.40 and j_4 as - 0.021. Because velocity and shear at A is greater than that at B (centre of the gap) in Fig. 2.2, the results of this study are compatible with Awazu: however, it is seen that $\tau'_{o_{\max}}/\bar{\tau}_o$ in Eq. 3.26 is primarily dependent upon the contraction ratio and is largely independent of the Froude number of the flow. This was also observed in drag measurements on end-dump face (Appendix C). The other interesting observation is that up to a contraction ratio 0.10, $\tau'_{o_{\max}}/\bar{\tau}_o$ does not exceed unity. The exponential form of Eq. 3.26 can be assumed reasonably valid in the contraction ratio range of 0.15 to 0.85.

6.2.3 Sediment-Transporting Flow

In the runs 86 through 93 and 97 through 100 the flow was transporting sediment. The experimental data are presented in Table D.1.

Based on Eq. 3.43, a semilogarithmic plot of $(h + d_s)/h$ versus m with F as third parameter is shown in Fig. 6.6a. The data shows a systematic variation with F. Although the effect of d/h has not been studied specifically, it appears to be insignificant in the range tested. In fact for F remaining nearly constant (0.50 to 0.45), with the increase in h/d from 91 to 232, $(h + d_s)/h$ decreases, instead of

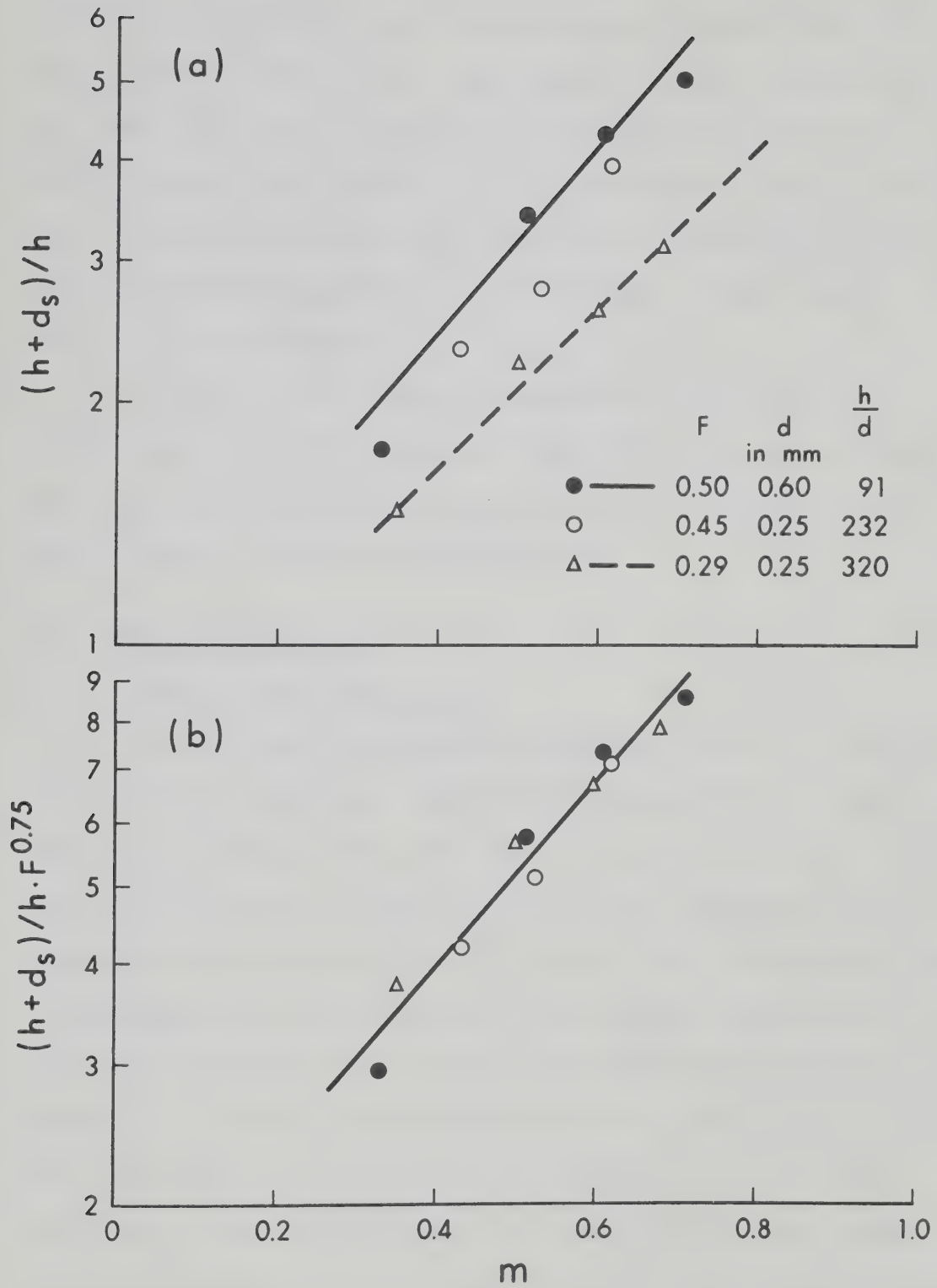


FIG. 6.6 DESIGN CURVE FOR MAXIMUM SCOUR DEPTH
IN SEDIMENT-TRANSPORTING FLOW

increasing as would have been the case with clear water flow. It needs to be mentioned that the experimental procedure for these runs was deficient, because of the non-circulating nature of the flow. Manual feeding of the sediment at the upstream as was actually done, can not be considered to maintain absolutely uniform flow and sediment discharge from upstream. In view of these a truly rigorous analysis is not attempted.

In Fig. 6.6b, a combined parameter $(h + d_s)/h F^{0.75}$ is plotted against m . (For clear water flow $F^{0.85}$ occurs in Eq. 3.31). The correlation being satisfactory, this figure is proposed as the design curve for sediment-transporting flow.

6.3 Time History of Scour

6.3.1 Characteristic Time of Scour

It has been recognized that the rate of scour is influenced by the sediment properties. Rouse (1939), Laursen (1953), Doddiah, Albertson and Thomas (1953), Feld (1968), Govindrao and Sharma (1967)'s analyses of scour due to jets indicated V/w as a significant parameter describing the rate of scour. Carsten (1966) indicated that Vt/h in combination with d/h describe the rate adequately where h is a characteristic length of the system. Many investigators (Ahmed, 1953, Breusers, 1967, Watkins, 1969) have verified that the depth of scour, after the initial transitional period (when the rate is extremely rapid) has a linear semilogarithmic relationship with time. However a definite relationship of the scour rate and the flow, fluid, characteristics and the geometry of the obstruction has still not been obtained, because

of the complexity of the problem. Dimensional analysis and experimental data have been used with judgement and as Breusers (1967) indicated, exact scaling of the model data to the prototype still remains unsolved particularly for fine sediments. Breusser indicated that the time scale of scour can be expressed as a function of the length scale, sediment size scale ($d_{\text{prototype}}/d_{\text{model}}$), density scale and velocity scale $[(V-V_{*c})_{\text{prototype}}/(V-V_{*c})_{\text{model}}]$. The functional relationship will vary from one situation to the other. However a similarity in the scour hole configuration does occur (Laursen, 1952, Breusers, 1967) and can be expressed as

$$\frac{d_t}{h} = f\left(\frac{t}{t_e}, \frac{x_t}{h}\right) \quad (6.1)$$

in which d_t and x_t represent the characteristic depth and length of the scour hole at time t . The determination of the equilibrium time t_e for any scouring process is the most difficult problem.

Bed profiles recorded in this study are analysed to develop relationships for the rate of scour for the clear water case only. A few typical plots of depth of scour versus time are shown in Fig. 6.7. Semilogarithmic plotting of the same data against the non-dimensional parameter Vt/h (Eq. 3.47) show a systematic trend (Fig. 6.8). This indicates that with F , m , d/h and ρ_s/ρ_w kept constant, $(h + d_t)/h$ should be uniquely related to Vt/h . Other researchers have made similar assumptions and have obtained compatible results. For example, Laursen (1963) postulated that d_t represents the hypothetical maximum

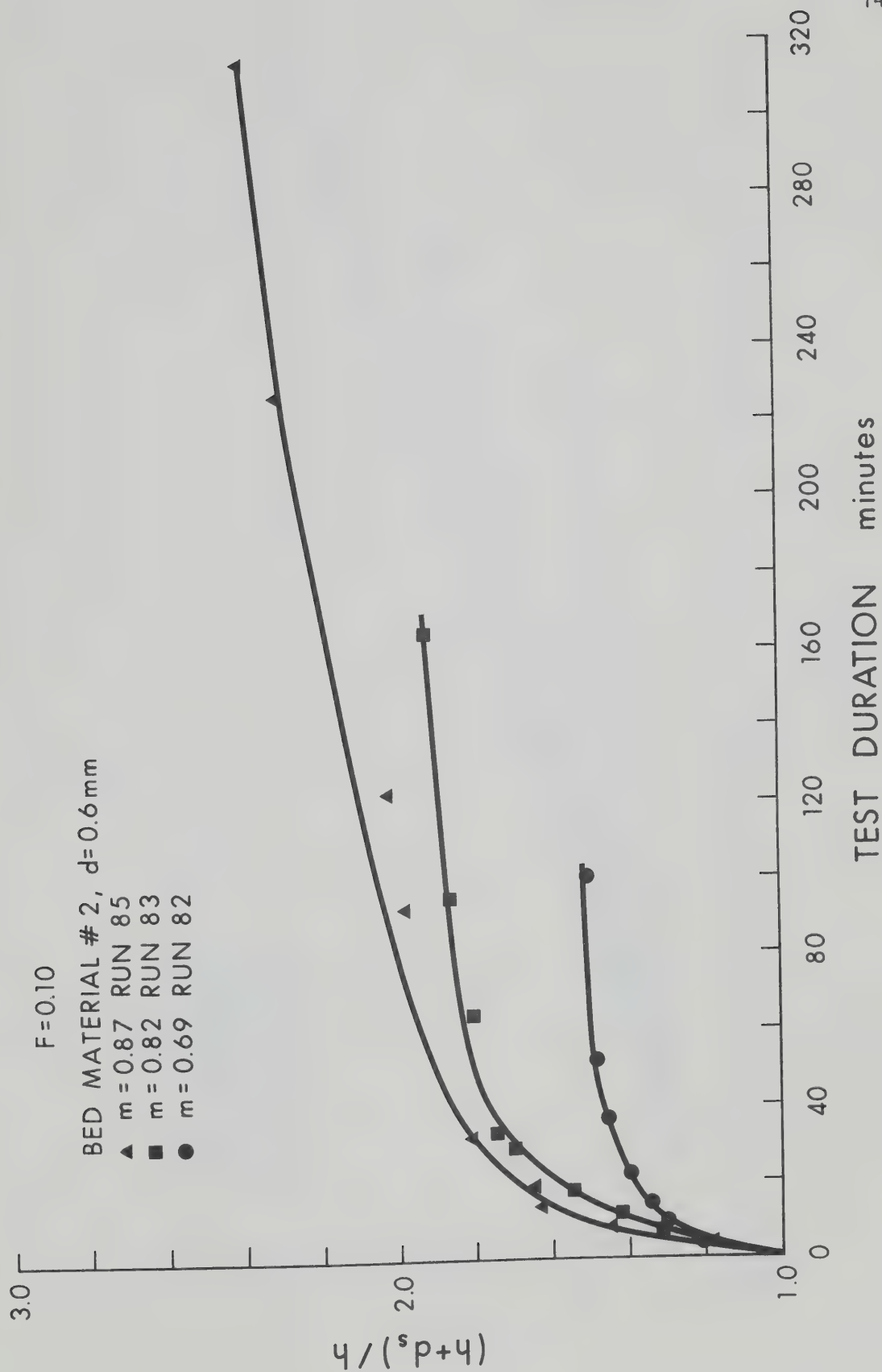


FIG. 6.7 TYPICAL SCOUR DEPTH-TIME RELATIONSHIPS DURING THE ACTIVE PHASE

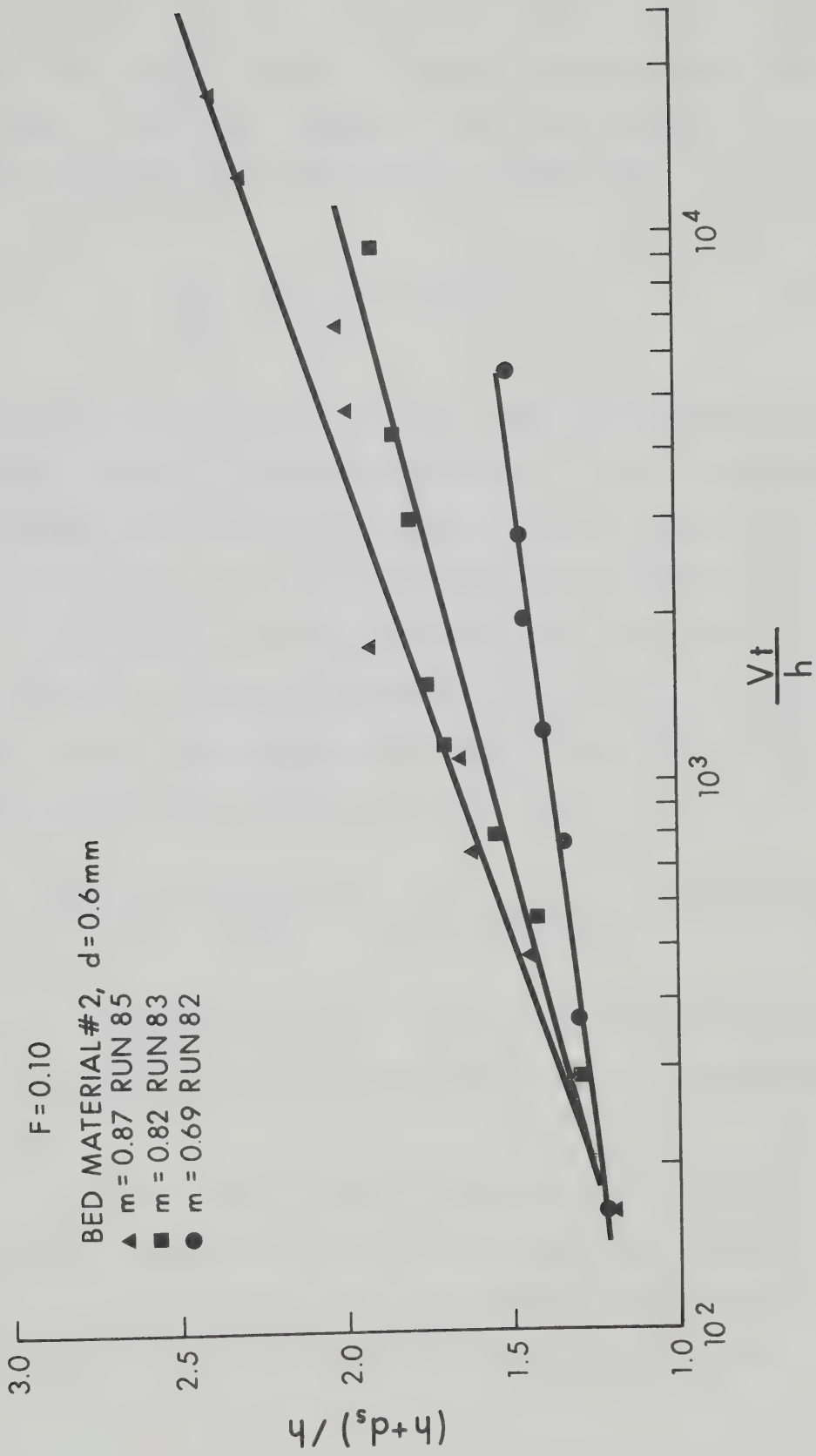


FIG. 6.8 NON-DIMENSIONAL VARIATION OF SCOUR DEPTHS WITH TIME DURING THE ACTIVE PHASE

scour depth for a coarser sediment to develop an expression for the rate of scour. Govind Rao and Sharma (1967) also accepted a similar hypothesis and proposed for scour due to a vertical jet

$$\frac{d_t}{h} = \frac{TV}{w} \tan^{-1} 0.4 \left(\frac{wt}{h}\right)^{0.4} - T' \quad (6.2)$$

in which T and T' are constants. A similar expression for scour due to a horizontal jet was also developed empirically. T and T' are evaluated from the boundary conditions of $d_t = 0$ at $t = 0$ and $d_t = d_s$ at $t = \infty$. Equation 6.2 satisfies the scour relationship over the entire period and has the advantage of yielding the maximum scour depth directly.

Based on the foregoing considerations and Eq. 3.47, a non-dimensional form of the transient-scour depth can be deduced from Eq. 3.31, with values of $j_3 = 2.1$ and $j_4 = -0.17$, as

$$1.44 \left[\left(\frac{h+d_t}{h}\right)\right] \left(\frac{d}{h}\right)^{0.29} \left(\frac{\Delta\rho_s}{\rho_w}\right)^{0.43} \left(\frac{1}{F^{0.85}}\right) \left(\frac{1}{10^{0.9m-0.08}}\right) = f\left(\frac{Vt}{h}\right) \quad (6.3)$$

Particulars of representative runs, covering three bed materials at three Froude numbers, chosen for verification of Eq. 6.3 are presented in Table 6.2.

A plot of Eq. 6.3 in Fig. 6.9 indicates a definite trend though showing a wide scatter. This is understandable because the scouring process is certainly not as simplified as assumed in this analysis. Figure 6.9 is not proposed as a design curve because of its

TABLE 6.2
PARTICULARS OF RUNS ANALYSED FOR RATE OF SCOUR

Run No.	Q in cfs	B in feet	V in fps	h in feet	d in mm	F	b in feet	m
71	0.62	2.75	1.22	0.176	1.20	0.525	2.35	0.23
72	0.62	2.75	1.22	0.176	1.20	0.525	1.65	0.40
19	1.56	7.50	1.15	0.18	1.20	0.50	2.30	0.69
44	1.66	7.50	0.84	0.26	1.20	0.29	3.15	0.58
42	1.00	7.50	0.72	0.19	1.20	0.29	2.35	0.69
48	1.66	7.50	0.84	0.26	1.20	0.29	1.90	0.75
75	0.94	4.15	0.84	0.26	0.60	0.29	2.52	0.39
81	0.94	4.15	0.84	0.26	0.60	0.29	1.98	0.52
78	0.94	4.15	0.84	0.26	0.60	0.29	0.93	0.74
34	1.00	7.50	0.35	0.38	1.20	0.10	1.90	0.74
31	1.00	7.50	0.35	0.38	1.20	0.10	0.97	0.87
82	0.56	4.25	0.35	0.38	0.60	0.10	1.30	0.69
83	0.56	4.25	0.35	0.38	0.60	0.10	0.75	0.82
94	0.48	3.60	0.35	0.38	0.25	0.10	1.60	0.56
95	0.48	3.60	0.35	0.38	0.25	0.10	0.90	0.75
96	0.48	3.60	0.35	0.38	0.25	0.10	0.60	0.83

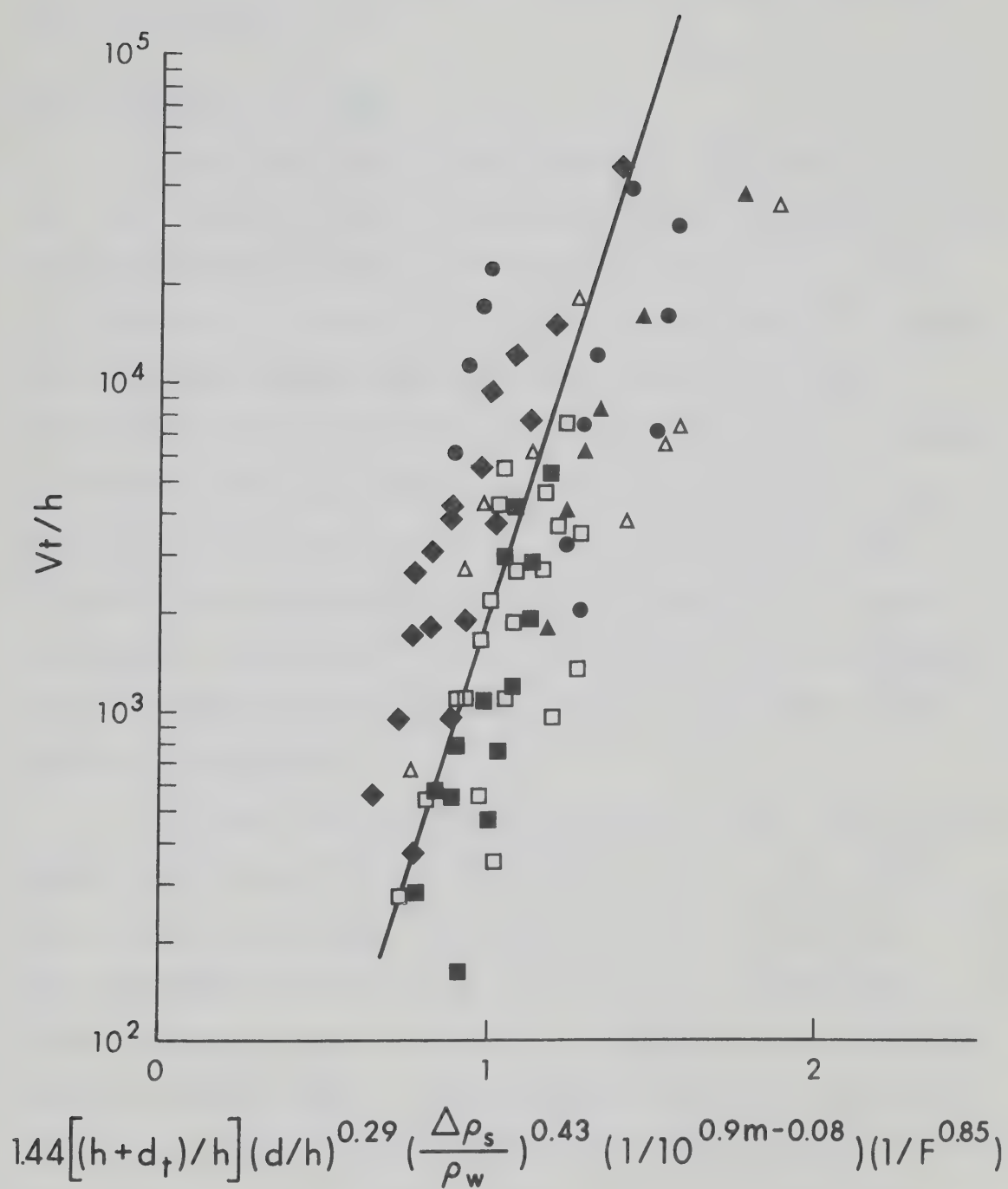


FIG. 6.9 VERIFICATION OF EQUATION 6.3 FOR SCOUR DEPTHS DURING THE ACTIVE PHASE

limitations. It can only be used as a guide to determine d_t approximately at any time t .

6.3.2 Similarity in Scour

From a mean curve plotted through the data points in Fig. 6.9, t_{90} , the time to attain 90% of the maximum scoured depth was read out for the runs in Table 6.2. A dimensionless plot of t/t_{90} versus $(d_t + h)/0.90(d_s + h)$ for all runs (Fig. 6.10) show that scour pattern for a particular geometry (end-dump constriction in this case) is similar irrespective of the bed material size. This was also observed by Breusers (1967). An important conclusion from Fig. 6.10 is that before $0.1 t_{90}$ is elapsed, 60% of the maximum scour occurs, which illustrates the necessity of execution of a closure job with minimum interruption. For practical purposes, an interruption of a few hours on the prototype, would be expected to result in development of full scour in the dump area.

A typical plot nondimensionalised with respect to the length and depth of the scour hole is shown in Fig. 6.11a. Similar plots were obtained for all runs. The different profiles of the scour hole with respect to time fall on one curve at all values of non-dimensional time as shown in Fig. 6.11b. This was also the conclusion reached by Laursen (1952). From the pattern of the scour profiles (Figs. 6.1 and 6.2), it would be reasonably correct to expect the deepest scour to occur at the vena-contracta section, close to the live-stream boundary. The contraction of the live stream and the

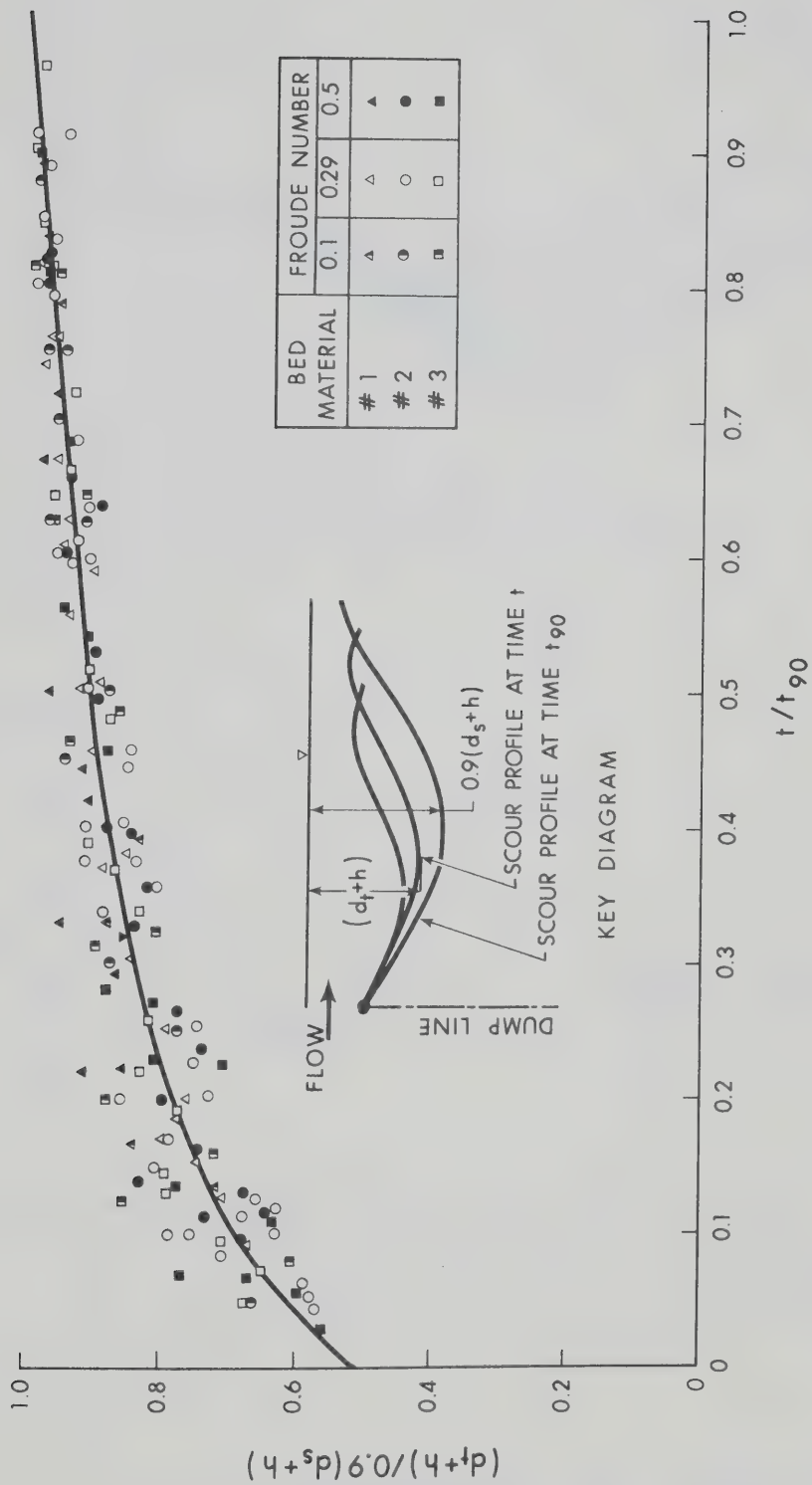


FIG. 6.10 VARIATION OF $(d_t + h) / 0.9(d_s + h)$ WITH t / t_{90}

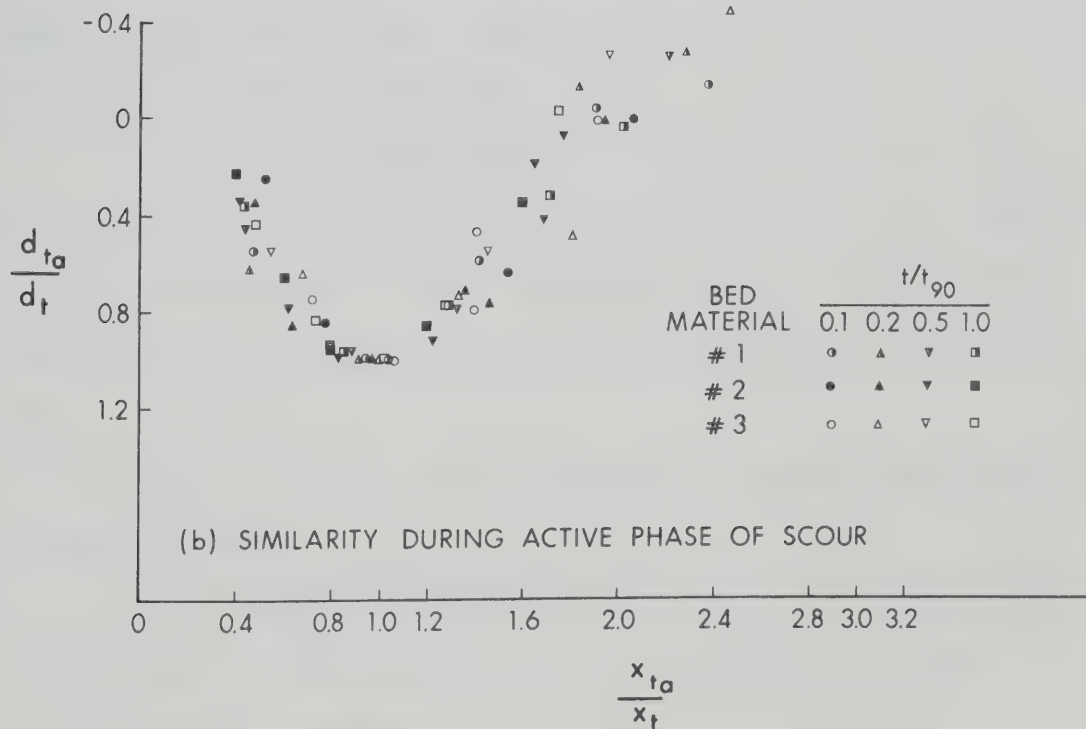
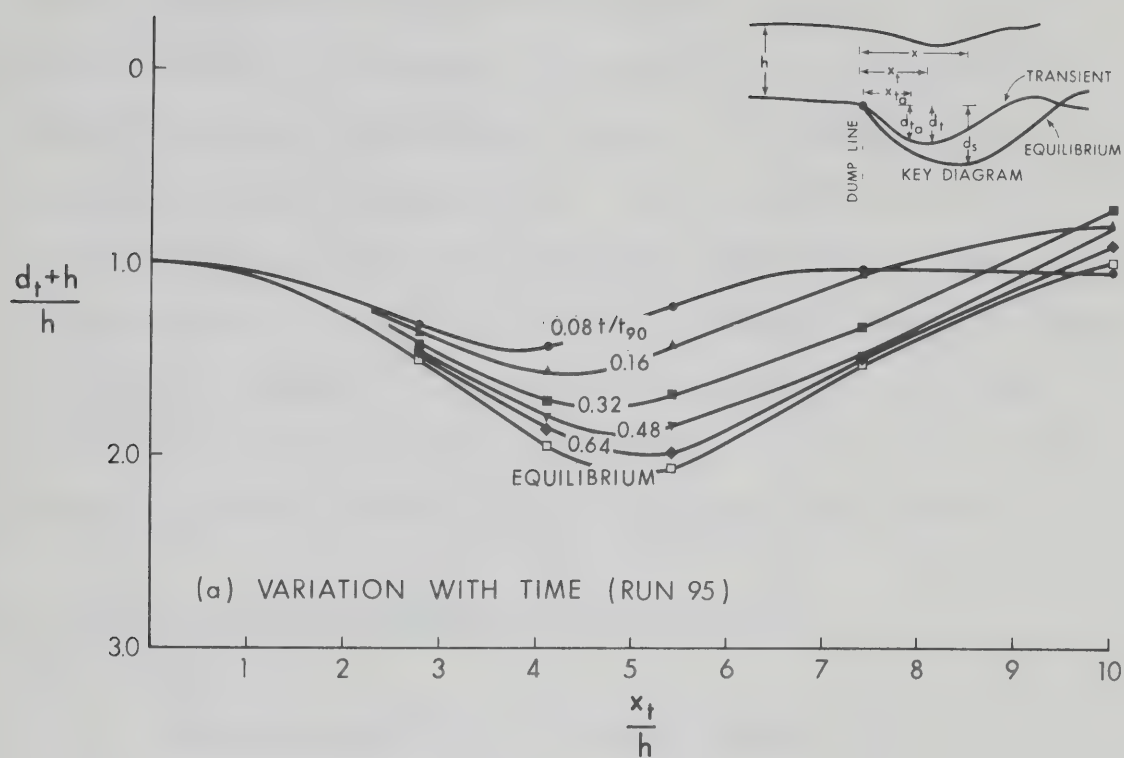


FIG. 6.11 NON-DIMENSIONAL PLOTS OF SCOUR PROFILE

location of the vena-contracta can be assessed from Figs. 5.7 and 5.9. Thus the location of the deepest scour hole can be ascertained with reasonable accuracy at any stage of closure. The configuration of the upstream end of the scour hole can then be arrived at by assuming the upstream slope of the scour hole equal to the angle of repose of the bed-sediment (Fig. 6.11a). The side slopes were observed inclined at the angle of repose in this study. The downstream slope, which both Carsten (1966) and Laursen (1963) assume to be the same as angle of repose was however observed in this study to be much flatter.

6.4 Check of Design Curves Against Previous Studies

6.4.1 General

Investigation on scour at end-dump constrictions do not appear to have been reported. Relevant studies on local scour at constrictions are chosen to conduct checks.

Two types of checks are made to verify the agreement between the data leading to the design curves developed in this study and the recommendations or data of previous studies. Data of clear water runs in this study, being considered more reliable are analysed only.

(1) The data of this study in respect of maximum scour depths are compared with

(a) Laursen's (1960,1963) design curves for i) local scour at an isolated abutment, and ii) general scour within opposing abutments.

(b) Komura's (1966) design curves for general scour at a long contraction.

- (2) The maximum scour depths measured at
- (a) vertical-edge spur-dikes (Garde et al, 1961) and at
 - (b) bridge constrictions (Liu et al, 1961) are compared with this study.

These studies did not distinguish local scour from general scour and design curves were proposed for the particular geometry of constriction studied.

6.4.2 Check Against Laursen's and Komura's Analyses

- (a) Isolated Scour Hole (due to Laursen, 1963)

A comparison of the observed d_s/h for a few typical runs of this study having m less than 0.65, (considered equivalent to an isolated abutment) is made in Fig. 6.12 with Laursen's curves (shown in Fig. 2.3). It can be seen that the maximum depths of scour obtained in this study are consistently lower (1/5 to 1/2) than the values predicted by Laursen. Thus, the maximum depth of an isolated scour hole at an end-dump dam can not be obtained from Laursen's analysis for isolated abutments.

- (b) Overlapping Scour Hole (due to Laursen, 1960 and 1963, and Komura, 1966)

The maximum depths of scour pertaining to a few typical runs of this study, having m in excess of 0.65 are considered appropriate to be analysed as data of scour in a long contraction. These are plotted in Fig. 6.13a for check against Laursen's curve and are plotted

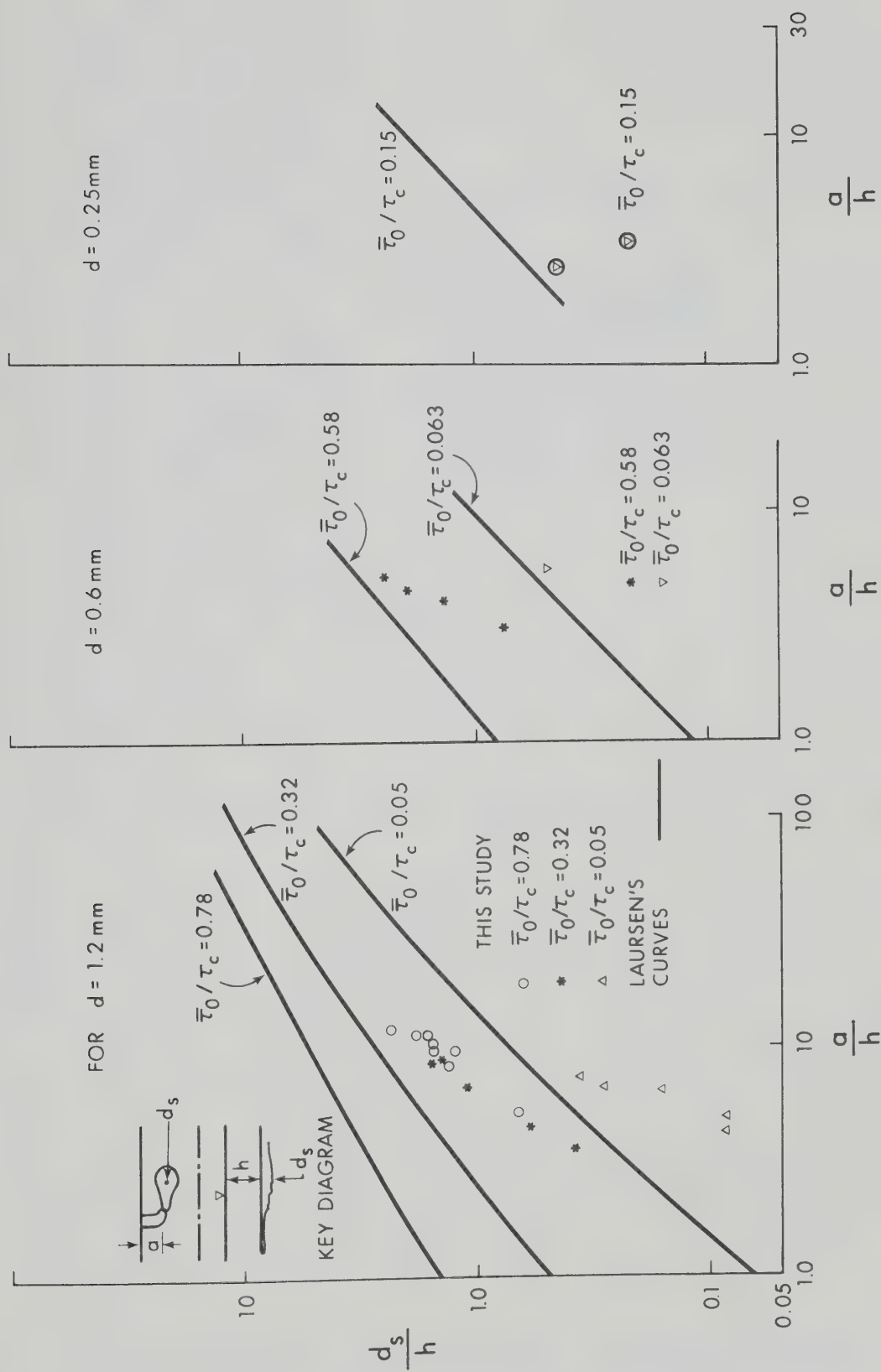


FIG. 6.12 COMPARISON OF THIS STUDY WITH LAURENSEN'S (1963) ANALYSIS FOR SCOUR AT ISOLATED ABUTMENTS

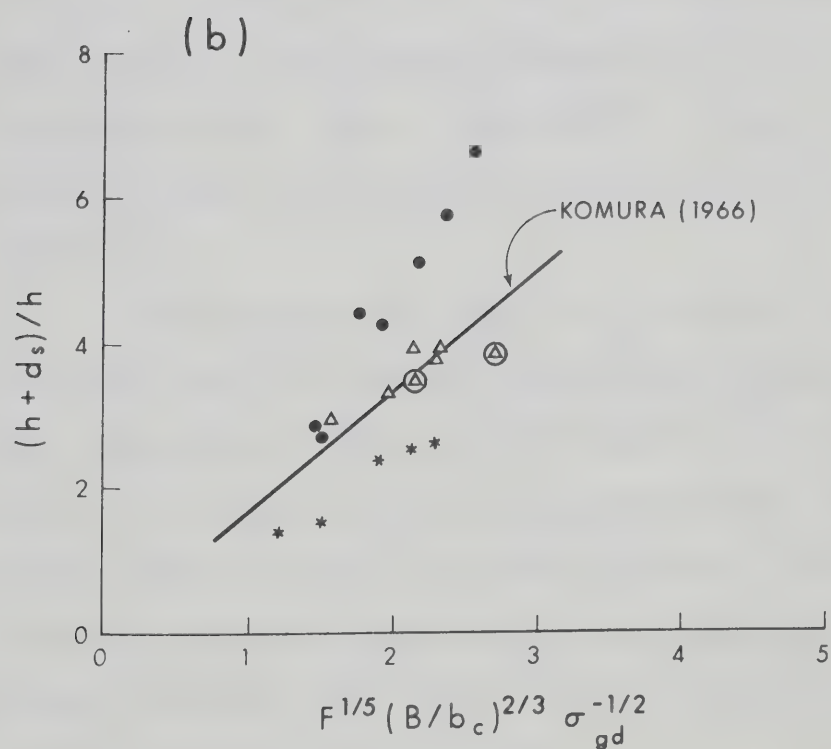
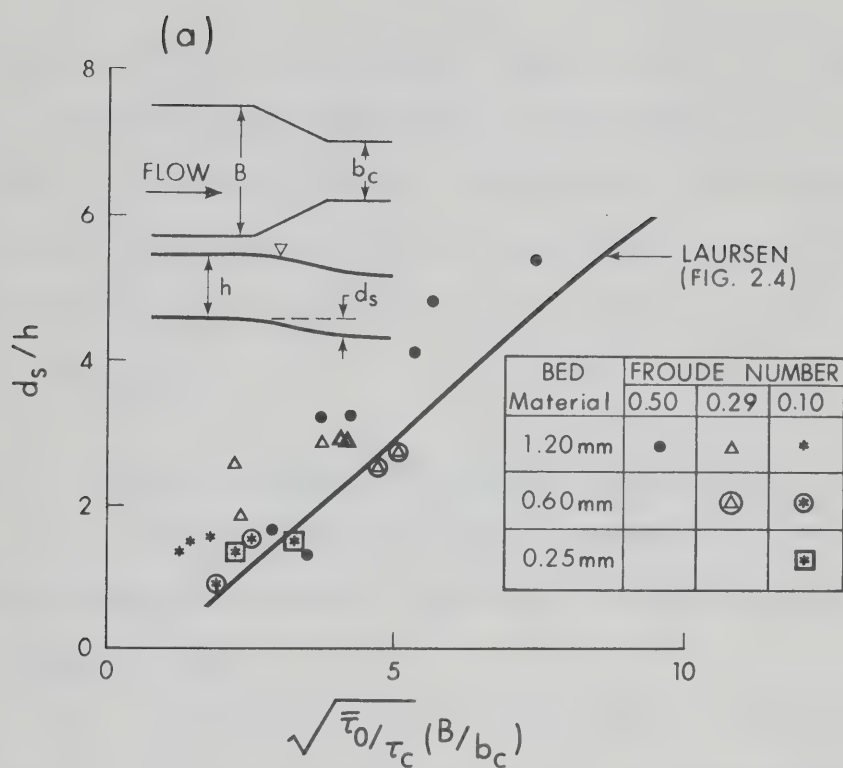


FIG. 6.13 COMPARISON OF THIS STUDY WITH a) LAURSEN'S (1963) AND b) KOMURA'S (1966) ANALYSES FOR SCOUR IN LONG CONTRACTIONS

in Fig. 6.13b for check against Komura's curve. The contracted width b_c (measured in this study) is considered equivalent to the contracted width in a long contraction. The agreement of the data both with Laursen's and Komura's curves is quite striking which indicates that an end-dump constriction behaves as a long contraction at higher contraction ratios.

6.4.3 Check of Garde et al's and Liu et al's Data

The curve in Fig. 6.3b is redrawn on Fig. 6.14 combining the non-dimensional parameters $(d_s+h)/h$, F and d/h to one parameter based on equation 3.31.

The observed maximum scour depths in a few typical runs from Garde et al's studies on bluff vertical spur-dikes and from Liu et al's (1961) studies on spill-through abutments are plotted on Fig. 6.14 for comparison with this study. The particulars of the runs chosen are detailed in Table 6.3 in which the observed and computed depths are compared.

The observed scour depths are consistently higher than the values predicted by this study, although the difference is less at higher contraction ratios. A similar trend was observed in the comparison with Laursen's curves for isolated abutments. Because an end-dump dam has a better stream-lined shape than a bluff, rigid abutment or spur-dike, a reduction in the maximum depth of scour is reasonable to expect. The results of this study, therefore, appear, compatible with the previous studies.

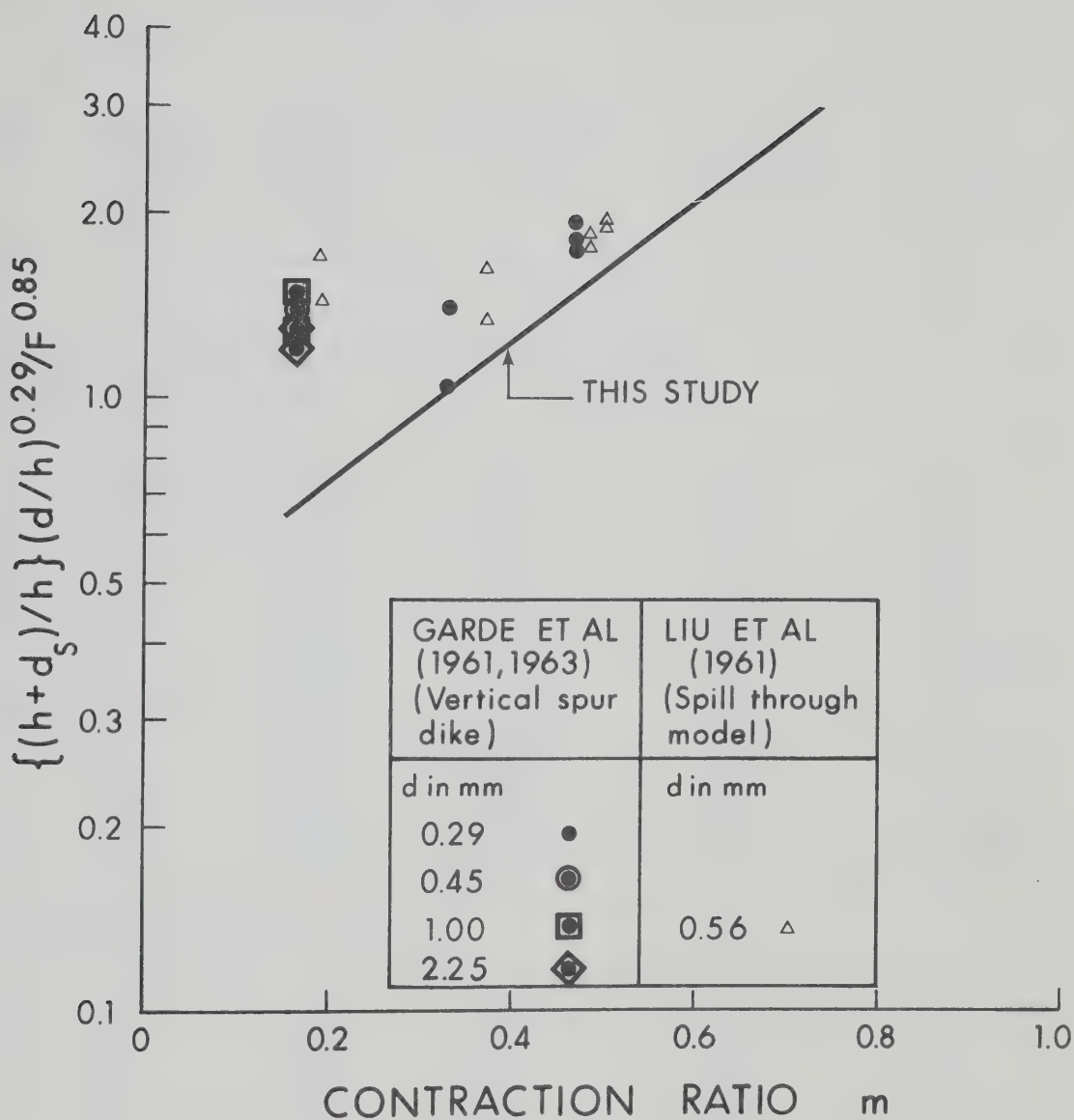


FIG. 6.14 COMPARISON OF GARDE ET AL'S (1961) DATA ON SCOUR AT VERTICAL SPUR-DIKES AND LIU ET AL'S (1961) DATA ON SCOUR AT SPILL-THROUGH ABUTMENTS, WITH THIS STUDY

TABLE 6.3
COMPARISON OF GARDE et al's (1961) DATA AND
LIU et al's DATA WITH THIS STUDY

Run No.	d Size of bed Material in mm	F Froude Number of normal Flow	m Contraction Ratio	$(h+d_s)/h$ (Observed)	$(h+d_s)/h$ Determined from Fig. 6.14
1	2	3	4	5	6
Garde, Subramanya and Nambudripad (1961, 1963) Vertical edge spur-dike					
D-9	0.29	0.14	0.47	2.08	1.72
D-10	0.29	0.284	0.47	3.28	2.60
D-12	0.29	0.23	0.47	2.57	2.20
A-3	0.29	0.165	0.33	1.11	1.10
A-10	0.29	0.12	0.33	1.38	1.02
E-1	0.45	0.148	0.165	1.29	No scour
E-3	0.45	0.225	0.165	1.79	No scour
E-7	0.45	0.272	0.165	2.00	1.08
F-2	1.00	0.172	0.165	1.27	No scour
F-3	1.00	0.24	0.165	1.68	No scour
F-6	1.00	0.318	0.165	2.17	1.05
G-1	2.25	0.182	0.165	1.02	No scour
G-2	2.25	0.408	0.165	1.61	No scour
G-3	2.25	0.476	0.165	1.80	1.06
Liu, Chang and Skinner (1961) Spill-through model					
146	0.56	0.242	0.47	2.50	1.98
148	0.56	0.323	0.47	3.03	2.55
180	0.56	0.166	0.19	1.52	No scour
182	0.56	0.299	0.19	2.63	1.15
203	0.56	0.16	0.50	1.95	2.03
206	0.56	0.394	0.50	3.82	3.15
210	0.56	0.664	0.50	5.40	4.60
232	0.56	0.203	0.37	1.73	1.25
234	0.56	0.378	0.37	3.00	2.80

6.5 Proposed Design Curves

In view of the good agreement of the experimental data with the theoretical analysis both for the clear-water and sediment-transporting flows and satisfactory checks with previous studies, Figs. 6.4, 6.5 and 6.6 are proposed as design curves for determining maximum scour depth.

The experimental data indicates F , m , ρ_s/ρ_w , d/h and $(d_s + h)/h$ to be the essential inter-related non-dimensional variables describing scour.

6.6 Maximum Backwater Rise

6.6.1 Location of Maximum Backwater

The basic data is presented in Table D.1. Typical water surface profiles through the constriction have been shown in Fig. 5.2 which indicates that although the section of maximum backwater is some distance upstream of the dump line, the level in the upstream deadwater zone at A (Fig. 5.2) very nearly corresponds to the maximum backwater level. (H is measured accordingly in contrast to h , h_1 , h_2 and h_3 (Fig. 1.2b) which are measured along the center line of flow. Difference between H and h_1 is not appreciable).

Liu et al (1957) and Biery and Delleur (1962) have correlated the length to maximum backwater L_{12} (Fig. 1.2), gap width b , Froude number F and opening ratio M . It is generally seen that the non-dimensional term L_{12}/b decreases with the increase in Froude number. It also decreases with the increase in the opening ratio.

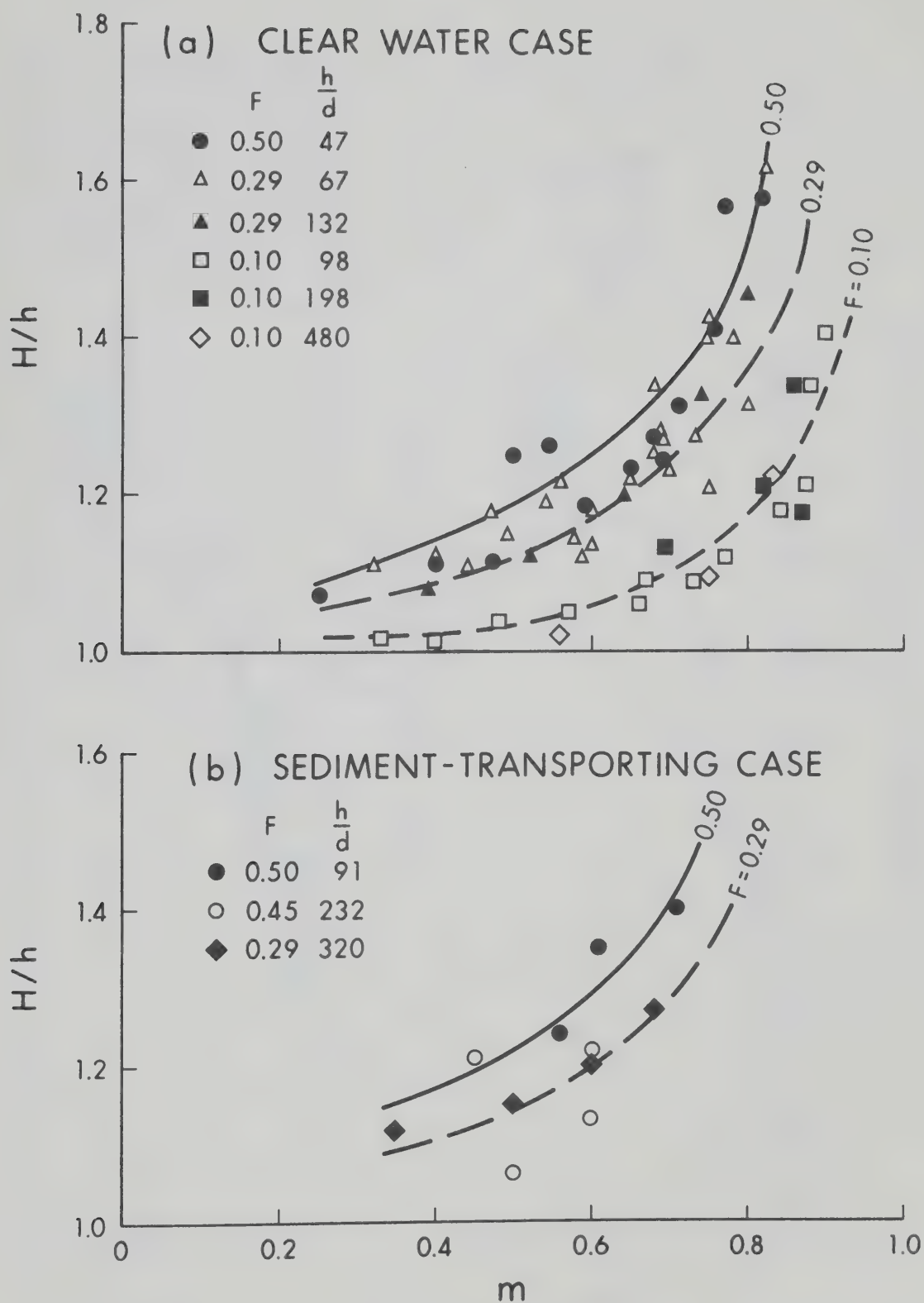
For practical purposes L_{12}/b can be considered to vary in the range 0.5 to 2.5. Carter and Tracy (1955) observed that in general L_{12}/b can be taken as unity.

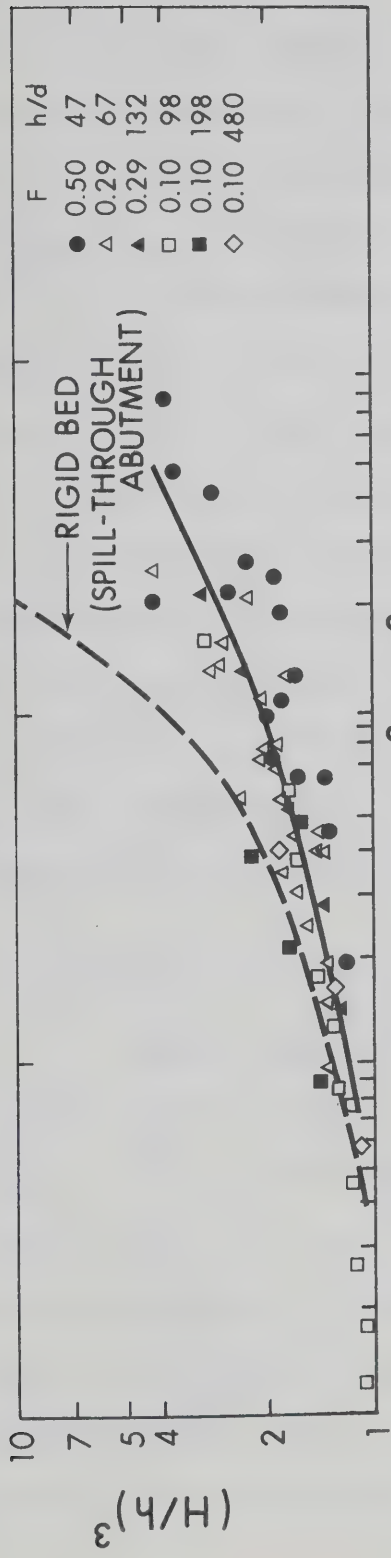
From the observation in this study, it can be stated that exactly locating the maximum backwater section is not possible, because of the extremely low variation of slope in this region. From practical considerations, the water level just upstream of the dam should be considered equal to the maximum backwater level for fixing the crest level of the dam, with suitable freeboard. The discharge capacity of any diversion arrangement, which is generally sited a short distance upstream of the dam, should be arrived at considering the maximum backwater level as the headwater level.

6.6.2 Variation of $(H/h)^3$ with $F^2(1/M^2 - 1)$

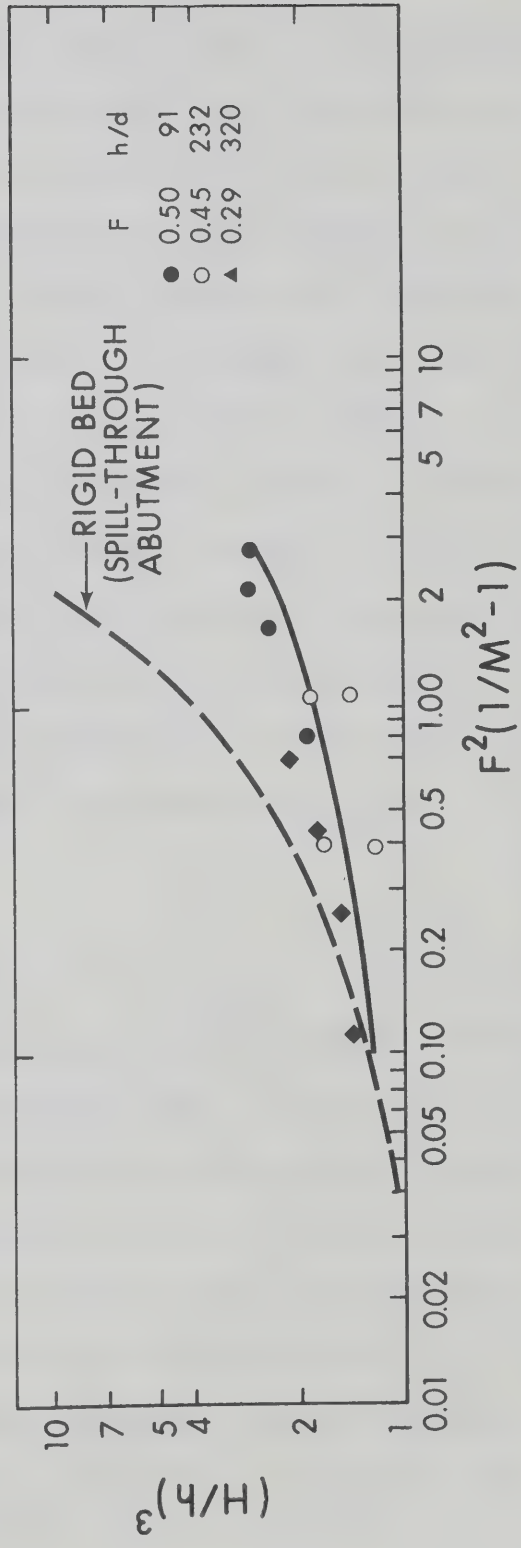
A plot of (H/h) versus m with F as the third variable is shown in Fig. 6.15. The h/d values are noted on this figure. For clarity the data points for the different sizes of closure material are not distinguished but it is seen that at the Froude numbers of 0.29 and 0.50 for the same h/d values the maximum backwater rise is slightly reduced with the larger closure material because of increased seepage through the body of the dam.

Figure 6.16 shows a plot of $(H/h)^3$ versus $F^2(1/M^2 - 1)$. The effect of h/d variation does not seem to be significant, both for the clearwater and sediment-transporting cases. In fact it is seen that an increase in h/d which results in an increase in the maximum

FIG. 6.15 VARIATION OF BACKWATER RATIO H/h , WITH CONTRACTION RATIO m



(a) CLEAR WATER CASE



(b) SEDIMENT-TRANSPORTING CASE

FIG. 6.16 RELATIONSHIPS FOR MAXIMUM BACKWATER DEPTH ON MOBILE BEDS CORRELATING $(H/h)^3$ AND $F^2(1/M^2 - 1)$

depth of scour results in a slight increase of the backwater level. A valid explanation regarding this has not been found. On the other hand the relative constancy of the maximum backwater level with varying h/d can be explained as follows. For a strictly free fall or flow down a steep slope the flow would pass through the critical before the outfall and the outfall functions as a control. Although the flow depth does not become critical so long as the bed is available for scour, the flow approaches critical condition with increase in contraction ratio. It is therefore possible that the upstream depth is primarily related to F and m at higher contraction ratios and an increase in depth of scour downstream does not significantly lower the water level upstream. But the maximum backwater rise for a mobile bed is certainly lower than that for a rigid bed, as the curve due to Liu, Bradley and Plate for spill through abutment (comparable to end-dump constriction) shown on Fig. 6.16 indicates.

6.6.3 Variation of C_m with F and m

Assuming equation 2.25 to be valid, the discharge coefficient C_m for all runs were computed. It is apparent that a correlation of C_m , F and M exists for flow through constriction on mobile beds. Omitting the data points, Fig. 6.17 is presented as a plot of C versus F with m as third parameter. Here again the effect of h/d variation has not been considered separately because the data does not indicate any systematic trend. On Fig. 6.17, the corresponding plot for flow on a rigid bed due to Valentine is shown for comparison. Figure 6.17 indi-

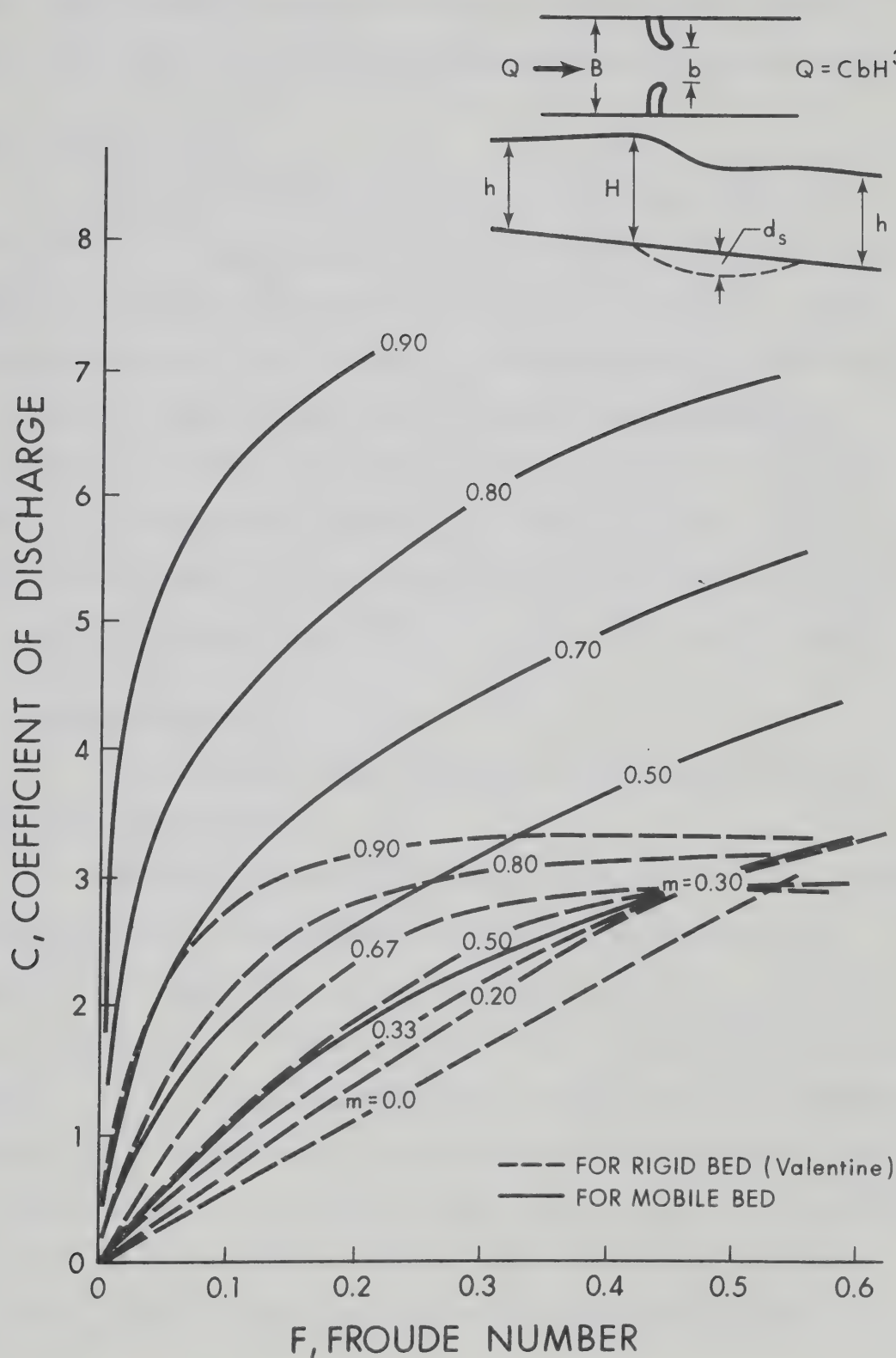


FIG. 6.17 RELATIONSHIP FOR MAXIMUM BACKWATER DEPTH ON MOBILE BEDS CORRELATING C , F AND m

cates that as the flow passes the dump line and continues down the scour hole, the coefficient is considerably increased due to suction.

6.6.4 Design Curves

Because the effect of particle size on the maximum back-water rise is not conclusively studied, the curves in Figs. 6.16 and 6.17 can not be considered as being precise but rather as useful guides in practical cases. However, the design curves are considered to have better applicability than the tentative recommendations of Liu, Chang and Skinner, who experimented with 0.56 mm sand only and stated "for the sediment involved in the tests, the water-surface drop across the embankment is approximately 60% of that in a rigid channel. It is expected, however, that this ratio varies with the bed material".

6.7 Concluding Remarks

In this chapter, the experimental data on scour and back-water have been analysed.

Assuming an exponential increase of the ratio of the maximum bed shear stress in the constricted channel to the boundary shear stress of the normal flow with the contraction ratio ($\tau'_{0_{\max}} / \bar{\tau}_0$ with m), an analysis for the maximum depth of scour was made in Chapter III, (section 3.2). The experimental data on scour supports the theoretical analysis well. Design curves for determining the maximum scour depth for the clear water and sediment-transporting flows have been proposed. Similarity in scour profiles both in respect to space and time were observed. Tentative design curves for the time history of scour have

been proposed. The size of the bed material appear to have significant influence both on the depth and rate of scour for clearwater flows. For sediment-transporting flows bed material size has less influence on the depth of scour. The most significant inter-related non-dimensional variables describing scour are the Froude number of the approach flow F , the contraction ratio m , the ratio of the bed material size to depth of flow d/h , the specific gravity ratio ρ_s/ρ_w and the ratio of scoured depth to original depth $(d_s+h)/h$.

Maximum backwater rise due to constriction on an alluvial bed was observed to be less than that for a rigid bed, as obtained in the studies of Liu, Bradley and Plate (1957) and Valentine (1958). The depth of scour does not appear to significantly affect the backwater rise (probably beyond a certain depth of scour), as does occur in the case of flow over a free fall. Definite conclusion regarding the effect of bed material size on backwater rise could not be drawn. Froude number of the approach flow F , the contraction ratio M , the coefficient of discharge C_m (assuming a weir flow through the constriction) and the non-dimensional backwater rise H/h were observed to be the significant inter-related variables.

CHAPTER VII

SUMMARY, CONCLUSIONS AND RECOMMENDATIONS

7.1 Summary and Conclusions

7.1.1 Introductory Remarks

The present study has been undertaken to develop comprehensive hydraulic design procedures for end-dump closure of alluvial channels at right angles to the flow. The primary problem in a river closure is the determination of the stable size of material (generally rockfill) at all stages of closure. The literature review indicated that the stable size is generally computed from the maximum velocity through the constriction, applying the "velocity-size" correlations developed for transverse-dump closures by Izbash (1936). This procedure was considered to be of questionable accuracy, because the flow against the sloping face of an end-dump dam is curvilinear and rapidly accelerating in contrast to the rectilinear flow over the level bed of a transverse-dump dam.

Specific studies on end-dump closure of rigid-bed channels leading to design formulae for the stable size have been reported by Pariset and Hausser (1959), and Sandover (1971). These formulae do not relate the stable size to velocity, but contain non-dimensional numbers describing the flow, fluid, and closure material. Application of Pariset and Hausser's formula requires predetermination of

the backwater rise and head loss at the constriction and the authors have not suggested any method of evaluating them. Sandover's procedure involves a trial and error solution. As such both procedures are impractical as a means of directly determining stable size during closure of alluvial channels. A systematic study on end-dump closure of alluvial channels does not appear to have been reported.

The literature review also revealed the lack of systematic investigation or specific design recommendations in respect to the associated phenomena such as the flow pattern, bed scour and the backwater rise at end-dump constrictions on alluvial channels.

An attempt has been made in the present study to formulate relationships for closure material stability, scour, and backwater, involving all of the possibly relevant variables. These relationships have been evaluated and design recommendations have been made on the basis of experimental data from laboratory tests consisting of over 120 runs. Three sizes of closure material (pebbles and chippings, 6.60 mm, 18 mm and 25 mm) and three sizes of bed material (sand, 1.20 mm, 0.60 mm and 0.25 mm) were utilized in the tests, which were carried out over three Froude numbers of the approach flow (0.50, 0.29 and 0.10).

7.1.2 Stability of Closure Material

At the outset of the experimental programme, the flow pattern was observed and the velocity distribution was obtained through an end-

dump constriction at different contraction ratios. The experimentally observed stable size was found to be consistently and substantially larger than that computed by correlation with the maximum velocity observed against the closure material. It was clearly demonstrated that neither the mean velocity through the constriction nor the maximum velocity against the closure material adequately describe the hydrodynamic effect of the curvilinear, accelerating flow.

A numerical measure termed "efficiency of closure material" has been introduced to denote the volume of closure material remaining stable within the limits of the dump line as a percentage of the quantity dumped into the flow at any stage of closure.

In Chapter III, an analysis of stability was done by assuming the closure material to become entrained after the hydrodynamic forces on the end-dump face exceed a critical value. Christensen's (1971) expression which includes the effects of particle lift, and bank slope, was used to determine the critical shear stress. A dimensional analysis was made of all the pertinent variables characterizing the flow, fluid, closure material and bed material. These analyses indicated the essential non-dimensional parameters to be the Froude number of the approach flow F , the contraction ratio m , the ratio of the closure material size to the approach flow depth D/h , and the efficiency of closure η . The form of the function which was subjected to empirical evaluation was

$$0 = f_1(F, m, D/h, \eta) \quad (7.1)$$

In Chapter V, data on the flow characteristics and material stability have been analysed. Design curves (Figs. 5.5 through 5.9) to arrive at the live stream boundary covering the flow contraction and expansion have been presented. The contraction ratio was observed to be the most important parameter describing the flow configuration. Variation of bed scour at the dump line at one contraction ratio did not appear to have appreciable effect on the stability of the closure material. In other words the bed material size, though influencing the depth of scour considerably, did not influence the stability on the end-dump face significantly. This was checked by varying h/d in the range 45-500. Similar variation of B/h in the range 10-29 did not influence the closure material stability significantly.

Design recommendations in the form of curves (Figs. 5.14 through 5.16) correlating F , m , D/h and η have been presented from which the stable size of closure material of standard shape and density can be determined directly. These curves are not recommended for use beyond a contraction ratio of 0.90. An efficiency of 0.90 was taken to adequately represent the stable design condition. The applicability of the design curves to irregular cross-sections of natural rivers has been tested by assuming the mean hydraulic radius to be representative of the normal flow depth. A few actual prototype closure data and the experimental data of Sandover have been compared with the recommendations of this study and the agreement was satisfactory. Satisfactory applicability of the design curves

to closure from one bank only was also noted.

From measured velocity distributions normal to the end-dump face, the maximum shear stress $\tau_{o_{max}}$ on the boundary was computed from boundary layer theory. The shear maxima was observed to follow the maximum velocity filament. An exponential increase of " $\tau_{o_{max}}/\bar{\tau}_o$ " with "m" was found. (Appendix C). The experimental stable size was observed to agree reasonably with the size computed to be stable against $\tau_{o_{max}}$ considering both drag and lift. For instability on the end-dump face Shields dimensionless shear stress τ_* was found to assume a value of 0.02.

7.1.3 Bed Scour

The scour patterns observed in this study confirmed that the bed scour at an end-dump constriction can be considered to be a combination of local scour (occurring at obstructions) and general scour (occurring in channel contraction). The self-formed end-dump face, however, stream-lined the flow, so that the deepest scour was observed to always occur downstream of the dump line. A reasonably two-dimensional flow was observed at the vena-contracta, where the maximum flow velocity and the associated maximum boundary shear resulted in the scour hole attaining its maximum depth. The term "maximum scour depth" represented by d_s has been used herein to denote the limiting depth of scour below the original bed in the case of clear water flow and the equilibrium depth of scour below the original bed in the case of sediment-transporting flow.

The previous studies on scour at constrictions such as spur-

dikes, and bridge abutments and at long contractions have been reviewed in Chapter III. The information was found to be deficient and inconclusive as to the effects of both the bed material size and density. Simplified analyses for arriving at the maximum depth of scour were made in this study both for the clear-water case and the sediment-transporting case by relating the rate of scour to the increased bed shear stress at the vena-contracta under an assumption of two-dimensional boundary layer flow. Maximum scour depth in clear-water flow was assumed to have been attained when the boundary shear in the scour hole is reduced to the critical value for the bed sediment, whereas in sediment-transporting flow it is attained when the rate of transport into and out of the scour hole equalizes. Dimensional analysis indicated the form of relationship for clear water flow (equation 3.31) as

$$(h+d_s)/h = f_2(F, m, h/d, \rho_w/\Delta\rho_s) \quad (7.2)$$

and for sediment-transporting flow (equation 3.43)

$$(h+d_s)/h = f_3(F, m) \quad (7.3)$$

Experimental investigations led to the correlation of the dimensionless terms in equations 7.2 and 7.3 and design curves (Figs 6.5 6.6) are presented for determining the maximum depth of scour. The applicability of the design curves has been tested for light-weight

material (coal) and 6.60 mm size pebbles as bed material. Data of other researches on scour at spur-dikes, bridge abutments and long contractions have been compared with the results of this study and are compatible with the test results obtained here.

The rate of scour during the active phase was observed to be logarithmic with time and tentative design curves have been presented to determine the transient scour depths approximately. Because the maximum depth of scour is reached asymptotically, time to attain 90% of the scoured depth, t_{90} , has been considered as a characteristic time and an important observation was that within an interval of $0.1 t_{90}$ from the commencement of scour more than 60% of the maximum scour occurred. A similarity in the scour hole configurations with respect to both space and time were observed.

7.1.4 Backwater Rise

Based on the analysis of backwater rise by previous investigators for constrictions in rigid-bed channels, two different forms of backwater rise equations were framed for experimental investigation.

$$(H/h)^3 = f_4(F^2[\frac{1}{M^2} - 1]) \quad (7.4)$$

and

$$Q = C_m \cdot b H^{3/2} \quad (7.5)$$

in which C_m , the coefficient of discharge for the flow through constriction on mobile bed was assumed as

$$C_m = f_5(F, m) \quad (7.6)$$

Dimensional analysis of all the pertinent variables also supported the equations 7.4 through 7.6.

The experimental data indicated the validity of the equations 7.4 through 7.6. It was found that the backwater rise for the constricted flow on an alluvial bed is substantially less than that on a rigid bed.

Good correlations between H/h , F and M (Fig. 6.16) and C_m , F and m (Fig. 6.17) were noted and design curves have been presented to evaluate the maximum backwater depth at any contraction ratio. The effect of the variation of the bed material size or the bed scour on the maximum backwater rise could not be conclusively studied. It was noted that backwater level decreased with increase of bed scour, but beyond a certain depth of scour, the backwater level attained a quasi-equilibrium condition and no longer decreased with increase in scour depth.

This dissertation synthesizes the procedures for comprehensive hydraulic design of end-dump closure on an alluvial channel. Because the design curves agree with prototype data and with the data of other researchers, they are considered to be of value for design and construction.

7.2 Recommendations

The following additional research studies are considered desirable to further the understanding of the complex flow phenomena in an end-dump closure and to improve the design procedures:

(1) Studies on the stability of material on end-dump closure dams inclined upstream. It is expected that due to the deflection of the high velocity zone away from the advancing face, the closure material would gain increased stability. The total quantity of closure material and the bed scour would have to be concurrently assessed.

(2) Studies to determine the effect of variation of the crest width on the stability of closure material.

(3) Studies to ascertain the effect of rate of dumping more decisively.

(4) Studies to determine the effect of the gradation and shape of closure material on the stability. These factors would also influence the seepage through the body of the dam, which in turn would change the flow through the constriction.

(5) Detailed studies involving variation of the bed material size and gradation over a wider range than heretofore,

- (a) to ascertain the effects on the stability of closure material when the bed scour is totally prevented,
- (b) to determine the required size of boulders for paving an alluvial bed prior to an end-dump closure, and

(c) to enable precise correlations between the pattern and extent of scour, and the maximum backwater with the bed material characteristics.

(6) Detailed studies of typical natural river sections to ascertain the effects on stability, scour and backwater.

(7) Since the validity of a design method must finally depend upon comparison with prototype performance, and because most river closures carried out in the past have not been well documented, there is an urgent need for collection and publication of full scale data.

LIST OF REFERENCES

1. Ahmad, M., "Experiments on Design and Behaviour of Spur-Dikes", Proceedings, 5th I.A.H.R. Congress at Minneapolis, Minnesota, 1953, pp. 145-159.
2. Albertson, M.L., Dai, Y.B., Jensen, K.A., and Rouse, H., "Diffusion of Submerged Jet", Transactions, ASCE, Vol. 115, 1950, pp. 639-697.
3. Alger, G.R., and Simons, D.B., "Fall Velocity of Irregular Shaped Particles", Journal of the Hydraulics Division, ASCE, Vol. 94, No. HY3, Proc. Paper 5949, May 1968, pp. 721-737.
4. Andru, P., "Study of Scour at Obstructions in Non-Cohesive Bed", thesis presented to the University of Alberta at Edmonton, Canada in 1956, in partial fulfillment of the requirement for the degree of Master of Science.
5. Awazu, S., "On Scour Around Spur-Dike", Proceedings 12th I.A.H.R. Congress at Fort Collins, Colorado, Vol. 3, 1967, pp. 97-104.
6. Benedict, B.A., and Christensen, B.A., "Hydrodynamic Lift on a Stream Bed", Proceedings, Sedimentation Symposium to Honour Professor H.A. Einstein. Editor H.W. Shen, Colorado State University, 1971, pp. 5-1-5-17.

7. Biery, P.F. and Delleur, J.W., "Hydraulics of Single Span Arch Bridge Constrictions", Journal of the Hydraulics Division, ASCE Vol. 88, No. HY2, Proc. Paper 3076, March 1962, pp. 75-108.
8. Blanchet, Ch., "Technique for the Construction of Rockfill Dams in Running Water", La Houille Blanche No. 1, November/December 1946, pp. 393-405, January/February 1947, pp. 41-47.
9. Blench, T., "Regime Behaviour of Canals and Rivers", Butterworth, London, 1957.
10. Breusers, H.N.C., "Time Scale of Two-Dimensional Local Scour", Proceedings 12th I.A.H.R. Congress at Fort Collins, Colorado, Vol. 3, 1967, pp. 275-282.
11. Carter, A.C., "Critical Tractive Forces on Channel Side Slopes", U.S. Bureau of Reclamation, Hydraulic Laboratory Report, NYd-366, February 1953.
12. Carstens, M.R., "Similarity Laws for Localised Scour", Journal of the Hydraulics Divisions, ASCE Vol. 92, No. HY3, Proc. Paper 4818, May 1966, pp. 13-36.
13. Chang, Y.U., "Laboratory Investigations of Flume Traction and Transportation", Transactions ASCE Vol. 65, No. 8, Pt. 2, 1939, pp. 1246-1313.
14. Chepil, W.S., "The Use of Evenly Spaced Hemispheres to Evaluate Aerodynamic Forces on a Soil Surface", Transactions, American Geophysical Union, Vol. 39, No. 3, June 1958, pp. 397-404.

15. Chitale, S.V., Discussion of "Resistance Relationships for Alluvial Channel Flow", by R.J. Garde and K.T. Rangaraju, Journal of the Hydraulics Division, ASCE, Vol. 93, No. HY2, Proc. Paper 5129, March 1967, pp. 106-108.
16. Chow, V.T., "Open Channel Hydraulics", McGraw-Hill, New York, 1959.
17. Christensen, B.A., "Incipient Motion on Cohesionless Channel Banks", Proceedings, Sedimentation Symposium to Honour Professor H.A. Einstein, Editor H.W. Shen, Colorado State University, 1971, pp. 4-1-4-18.
18. Cohen de Lara, G., "A Study of Seepage in Rockfill Dykes", Compte Rendu de Quatrieme Journées de L'Hydraulique. Société Hydrotechnique de France, Tome I, 1956 (in French).
19. Cooper, R.H., "A Study of Bed-Material Transport Based on the Analysis of Flume Experiments", thesis presented to the University of Alberta at Edmonton, Canada in 1970, in partial fulfillment of the requirement for the degree of Doctor of Philosophy.
20. Deeprose, R.K., Yaremko, E.M., Mutter, G., and Gehmlich, G., "Model Study of Rock Weirs Proposed for the Athabasca Delta Project", Department of the Environment, Alberta Water Resources Division, Edmonton, Alberta, Canada, October 1971.
21. Doddiah, D., Albertson, M.L., and Thomas, R., "Scour from Jets". Proceedings, 5th I.A.H.R. Congress at Minneapolis, Minnesota, 1953, pp. 161-169.

22. Einstein, H.A., and El-Samni, E.A., "Hydrodynamic Forces on a Roughwall", Review of Modern Physics, American Institute of Physics, Lancaster, Pa., Vol. 21, No. 3, July 1949, pp. 520-524.
23. Field, W.G., "Effects of Density Ratio on Sedimentary Similtude", Journal of the Hydraulics Division, ASCE, Vol. 94, No. NY3, Proc. Paper 5948, May 1968, pp. 705-719.
24. Forchheimer, P., "Hydraulik" Publ. Teubner Verlag, Leipzig, 1930 (in German).
25. Garde, R.J., Subramanya, K., and Nanbudripad, K.D., "Study of Scour Around Spur-Dikes", Journal of the Hydraulic Division, ASCE, Vol. 87, No. HY6, Proc. Paper 2978, November 1961, pp. 23-37.
26. Garde, R.J., Subramanya, K., and Nambudripad, K.D., Closure of "Study of Scour Around Spur Dikes", by R.J. Garde et al, Journal of the Hydraulics Division, ASCE, Vol. 89, No. HY1, Proc. Paper 3405, January 1963, pp. 167-175.
27. Govind Rao, N.S., and Sarma, K.V.N., "Scour Function", Journal of the Institution of Engineers (India), Civil Engineering Division, Vol. XLVII, January, 1967, No. 5, Pt CI3, pp. 260-286.
28. Harr, M.E., "Groundwater and Seepage", McGraw-Hill, New York, 1962.
29. Hausser, R., and Michel, B., "Stability of the Downstream Slope of Rockfill Dykes", Proceedings 8th I.A.H.R. Congress at Montreal, Vol. 4, 1959, pp. 7S₂1-7S₂6.
30. Highway Research Board, National Cooperative Highway Research Programme, Synthesis of Hwy Practice 5, "Scour at Bridge Waterways", 1970.

31. Ippen, A.T., and Drinker, P.A., "Boundary Shear Stresses in Curved Trapezoidal Channels", Journal of the Hydraulics Division, ASCE, Vol. 88, No. HY5, Proc. Paper 3273, September 1962, pp. 143-179.
32. Izbash, S.V., "Construction of Dams by Depositing Rock in Running Water", Second Congress on Large Dams, Washington, D.C., Vol. 5, 1936, p. 123.
33. Izbash, S.V., and Khaldre, K.Y., "Hydraulics of River Channel Closure, Translated from the Russian by G.L. Cairns, Butterworth, 1970.
34. Izbash, S.V. and Lebedev, I.V., "Change of Natural Streams During Construction of Hydraulic Structures", Proc. 9th I.A.H.R. Congress at Dubrovnik, September 1961, pp. 1114-1121.
35. Izzard, C.F., and Bradley, J.N., "Field Verification of Model Tests on Flow Through Highway Bridges and Culverts", Proceedings, 7th Hydraulics Conference, Iowa, 1957.
36. Kalinski, A.A., "Movement of Sediment as Bed in Rivers", Transactions, American Geophysical Union, Vol. 28, 1947, pp. 615-620.
37. Kenlegan, G.H., "Laws of Turbulent Flow in Open Channels", Journal of Research of the National Bureau of Standards, Vol. 21, December 1938, pp. 707-741.
38. Kindsvater, C.E., and Carter, R.W., "Transquil Flow Through Open Channel Constrictions", Transactions ASCE, Vol. 120, 1953, pp. 955-980.

39. Khosla, A.N., "Design of Weirs on Permeable Foundations", Publication No. 12, Central Board of Irrigation and Power, India, 1936.
40. Komura, S., "Equilibrium Depth of Scour in Long Constrictions", Journal of the Hydraulics Division, ASCE Vol. 92, No. HY5, Proc. Paper 4898, September 1966, pp. 17-37.
41. Kuul, I.S., "Experience with Damming of the Right Arm of Volga River During the Constriction of a Stream Separator", Hydrotechnical Constriction No. 1, January 1970, pp. 32-38. (Translated from Russian by ASCE).
42. Lane, E.W., "Experiments on the Flow of Water Through Contractions in an Open Channel", Transactions ASCE Vol. 83, 1919-20, pp. 1149-219.
43. Lane, E.W., and Carlson, E.J., "Some Factors Affecting the Stability of Canals Constructed in Coarse Granular Materials", Proceedings, 5th I.A.H.R. Congress at Minneapolis, Minnesota, 1953, pp. 37-48.
44. Laursen, E.M., "Observations on the Nature of Scour", Proceedings, 5th Hydraulics Conference, Iowa City, Iowa, Bulletin No. 34, June 9-11, 1952, pp. 179-197.
45. Laursen, E.M., and Toch, A., "A Generalized Model Study of Scour Around Bridge Piers and Abutments", Proceedings 5th I.A.H.R. Congress at Minneapolis, Minnesota, 1953, pp. 123-131.
46. Laursen, E.M., "Scour at Bridge Crossings", Transactions, ASCE, Vol. 127, Part I, 1962, pp. 166.

47. Laursen, E.M., "An Analysis of Relief Bridge Scour", Journal of the Hydraulics Division, ASCE, Vol. 89, No. HY3, Proc. Paper 3516, May 1963, pp. 93-118.
48. Leliavsky, S., "An Introduction to Fluvial Hydraulics", Constable, London, 1955.
49. Linford, A., "A Review of Literature on the Construction of Rockfill Dams by Dumping Stones in Running Water", TN 873, The British Hydromechanics Research Association, Cranfield, Bedford, England, 1967.
50. Liu, H.K., Bradley, J.N., and Plate, E.J., "Backwater Effects of Piers and Abutments", Colorado State University Civil Engineering Section Report CER57HKL10, October, 1957.
51. Liu, H.K., Chang, F.M., and Skinner, M.M., "Effect of Bridge Constrictions on Scour and Backwater", Colorado State University, Civil Engineering Section Report CER60HKL22, February 1961.
52. Martin, C.S., "Effect of a Porous Sand Bed on Incipient Sediment Motion", Journal of Water Resources Research, Vol. 6, August, 1970, No. 4, pp. 1162-1174.
53. Neill, C.R., Discussion of "Study of Scour Around Spur-Dikes", by R.J. Garde et al, Journal of the Hydraulics Division, ASCE, Vol. 88, No. HY2, Proc. Paper 3087, March, 1962, pp. 191-192.
54. Neill, C.R., "River Bed Scour, A Review for Bridge Engineers", Canadian Good Roads Association", Publication No. 23, December, 1964.

55. Neill, C.R., "Mean-Velocity Criterion for Scour of Coarse Uniform Bed-Material", Proceedings 12th I.A.H.R. Congress at Fort Collins, Colorado. Vol. 3, 1967, pp. 46-54.
56. Olivier, H., "Through and Overflow Rockfill Dams - New Design Techniques", Proceedings, Institution of Civil Engineers, London, Vol. 36, Paper No. 7012, March 1967, pp. 433-471.
57. Orchinnikov, V.M., "Cofferdam Closure Section at the Ust-Ilimsk Hydroelectric Project Site on the Angara", Hydrotechnical Construction, No. 8, August, 1970, pp. 699-707. (Translated from Russian by ASCE).
58. Pariset, E., and Hausser, R., "Rockfill Cofferdams Built by Toe Dumping", Proc. 8th I.A.H.R. Congress at Montreal, Vol. 4, August, 1959, pp. 8S₂1-8S₂4.
59. Parkin, A.K., "Rockfill Dams with Built-in Spillways. Hydraulic Characteristics", Water Research Foundation of Australia, Bulletin No. 6, March 1963.
60. Raudkivi, A.J., "Loose Boundary Hydraulics", Pergamon Press, Oxford, 1967, pp. 26-27.
61. Replogle, J.A., and Chow, V.T., "Tractive-Force Distribution in Open Channels", Journal of the Hydraulics Division, ASCE, Vol. 92, No. HY2, Proc. Paper 4727, March 1966, pp. 169-191.
62. Rouse, H., "Criteria for Similarity in the Transportation of Sediment", Proceedings, Hydraulics Conference, Bulletin 20, University of Iowa Studies in Engineering, 1940, pp. 33-49.

63. Sandoover, J.A., "Discharge Coefficients of Constrictions in Open Channels", *Water Power*, London, July 1969, pp. 256-261.
64. Sandoover, J.A., "Backwater Effects due to Channel Constrictions", *Water Power*, London, January, 1970, pp.
65. Sandoover, J.A., "Theories of Closure of Rockfill Dams", *Journal of the Construction Division, ASCE*, Vol. 97, No. C02, Proc. Paper 8542, Nov. 1971, pp. 313-326.
66. Shields, A., "Anwendung der Aehnlichkeitsmechanik und der Turbulenz-forschung anf die Geschiebebewegung", *Mitteilungen der Preuss, Berlin, Heft 26*, 1936; translated to English by W.P. Ott and J.C. Van Uchelen, California Inst. of Technology, Pasadena, California.
67. Simons, D.B., and Richardson, E.V., "Forms of Bed Roughness in Alluvial Channels", *Journal of the Hydraulics Division, ASCE*, Vol. 87, No. HY3, Proc. Paper 2814, May 1961, pp. 87 - 105.
68. Simons, D.B., Richardson, E.V., and Nordin, C.F., Jr., "Sedimentary Structures Generated by Flow in Alluvial Channels", Special Publication No. 12, The American Association of Petroleum Geologists, 1965, pp. 34-52.
69. Straub, L.G., "Missouri River Report", House Document 238, Corps of Engineers, U.S. Dept. of the Army, to 73rd U.S. Congress, 2nd Session, 1946, p. 1156.
70. Straub, L.G., "Dredge Fill Closure of Missouri River at Fort Randall", *Proceedings 5th I.A.H.R. Congress at Minneapolis, Minnesota*, 1953, pp. 61-75.

71. Streeter, V.L., "Fluid Dynamics", McGraw-Hill, 1948.
72. Task Committee on Preparation of Sedimentation Manual, Committee on Sedimentation., "Sediment Transportation Mechanics: Introduction and Properties of Sediment", Journal of the Hydraulics Division, ASCE, Vol. 88, No. HY4, Proc. Paper 3194, July 1962, pp. 77-107.
73. Task Committee Preparation of Sedimentation Manual, Committee on Sedimentation, "Sediment Transportation Mechanics: Erosion of Sediment", Journal of the Hydraulics Division, ASCE, Vol. 88, No. HY4, Proc. Paper 3195, July 1962, pp. 109-127.
74. Task Committee on Preparation of Sedimentation Manual, Committee on Sedimentation, "Sediment Transportation Mechanics: Initiation of Motion", Journal of the Hydraulics Division, ASCE, Vol. 92, No. HY2, Proc. Paper 4738, March 1966, pp. 291-314.
75. Taylor, D.W., "Fundamentals of Soil Mechanics", John Wiley and Sons, Inc., New York, 1957.
76. Terzaghi, K., and Peck, R.B., "Soil Mechanics in Engineering Practice", John Wiley and Sons, Inc., New York, 1948.
77. Tison, G., Jr., "Discussion of "Study of Scour Around Spur-Dikes" by R.J. Garde et al, Journal of the Hydraulics Division, ASCE, Vol. 88, No. HY4, Proc. Paper 3209, July 1962, pp. 301-306.

78. Torpen, B.E., "Large Rocks in River Control Works", Civil Engineering, September 1956, pp. 56-61.
79. Tracy, H.J., and Carter, R.W., "Backwater Effects of Open Channel Constrictions", Transactions, ASCE, Vol. 120, 1955, pp. 993-1006.
80. Tutt, D.B., "The Determination of Scour Between Bridge 15 Abutments on Gravel Bed Rivers", Thesis presented to the University of Alberta, Edmonton, Canada in 1972, in partial fulfillment of the requirement for the degree of Master of Science.
81. U.S. Army Corps of Engineers, "Hydraulic Design Criteria", Vol. II, 19, p. 712, 1970.
82. U.S. Army Engineer Division, North Pacific, Corps of Engineers, "Closure Fill and Skeleton Power House Units. The Dalles Dam, Columbia River, Oregon and Washington Hydraulic Model Investigation". Technical Report No. 57-1, May 1965.
83. Valentine, H.R., "Flow in Rectangular Channels with Lateral Constriction Plates", La Houille Blanche, No. 1, Jan/Feb. 1958. pp. 75-84.
84. Vinje, J.J., "On the Flow Characteristics of Vortices in Three-Dimensional Local Scour". Proceedings 12th I.A.H.R. Congress at Fort Collins, Colorado, Vol. 3, 1967, pp. 207-217.
85. Watkins, R.D., "Local Scour in Beds of Sand and Gravel Downstream from a Solid Apron", Civil Engineering Transactions, Institute of Engineers, Australia, April 1969, pp. 97-106.

86. Wilkins, J.K., "Flow of Water Through Rockfill and its Application to the Design of Dams", Proceedings, 2nd Australia-New Zealand Conference on Soil Mechanics and Foundation Engineering, Christchurch, N.Z., 1956, pp. 141-149.
87. Yarnell, D.L., "Bridge Piers as Channel Obstructions", U.S. Department of Agriculture, Technical Bulletin No. 442, November 1934.

APPENDIX A
CHARACTERISTICS OF NORMAL FLOW

APPENDIX A

CHARACTERISTICS OF NORMAL FLOW

A.1 Introduction

Simons and Richardson (1961) have studied and classified the bed forms due to flow in alluvial channels into ripples, dunes, anti-dunes and plane bed. These bed forms are related to the regime of the flow and particle size of the bed material. In general for sand-bed channels, after initiation of motion, ripples are formed at the low rates of transport. With increasing stream power ripples change to dunes and antidunes and eventually back to a plane bed. Simons and Richardson observed that "after beginning of motion, the plane bed changed to ripples for the sand sizes smaller than 0.5 mm and to dunes for the 0.93 mm sand".

A.2 Bed Forms

Experimental data is precise and collection of data is convenient in studies involving clear water flow over a plane bed. Theoretical considerations indicated that the effect of variation of bed material on the stability of closure material is minor. (Section 3.1.3). Although a check of the effect of bed material size on stability is made in series J through P, the design recommendations on stability are basically derived from the data of runs in series A, through G. It was decided to conduct these runs with bed material of

1.2 mm, for which there was no bed movement under normal flow conditions. Design charts on scour and backwater are of course based on the data of runs in all series covering three sizes of bed material. With 0.6 mm sand, the bed was static and plane at a Froude number of 0.10 whereas at a Froude number of 0.29, there was very little movement (plane bed to ripples) and at Froude number of 0.50, there was weak bed movement (bed form ripples). With 0.25 mm sand, there was weak bed movement (ripples at a Froude number of 0.10 and appreciable bed movement (dunes) at Froude numbers of 0.29 and 0.50). These observations are similar to those of Simons and Richardson (1961) and Cooper (1970). Figure 4.1 shows the plane bed of a normal run with 1.2 mm sand. Figure A.1 shows the duned bed with 0.25 mm sand for a run in series M.

A.3 Analysis

The computed values of boundary shear stress $\bar{\tau}_0$ for the normal runs (assuming the entire resistance to be grain resistance (Laursen, 1960, 1963) are presented in Table A.1. The computation is based on the Manning-Strickler formula which upon algebraic manipulation yields

$$\bar{\tau}_0 = \gamma_w \cdot h \cdot i = \frac{V^2 d^{1/3}}{30 h^{1/3}} \quad (A.1)$$

The computation of $\bar{\tau}_0$ from Eq. A.1 has obvious limitation for a duned or rippled bed, because the total resistance is the result of grain resistance and form resistance. The critical tractive stress

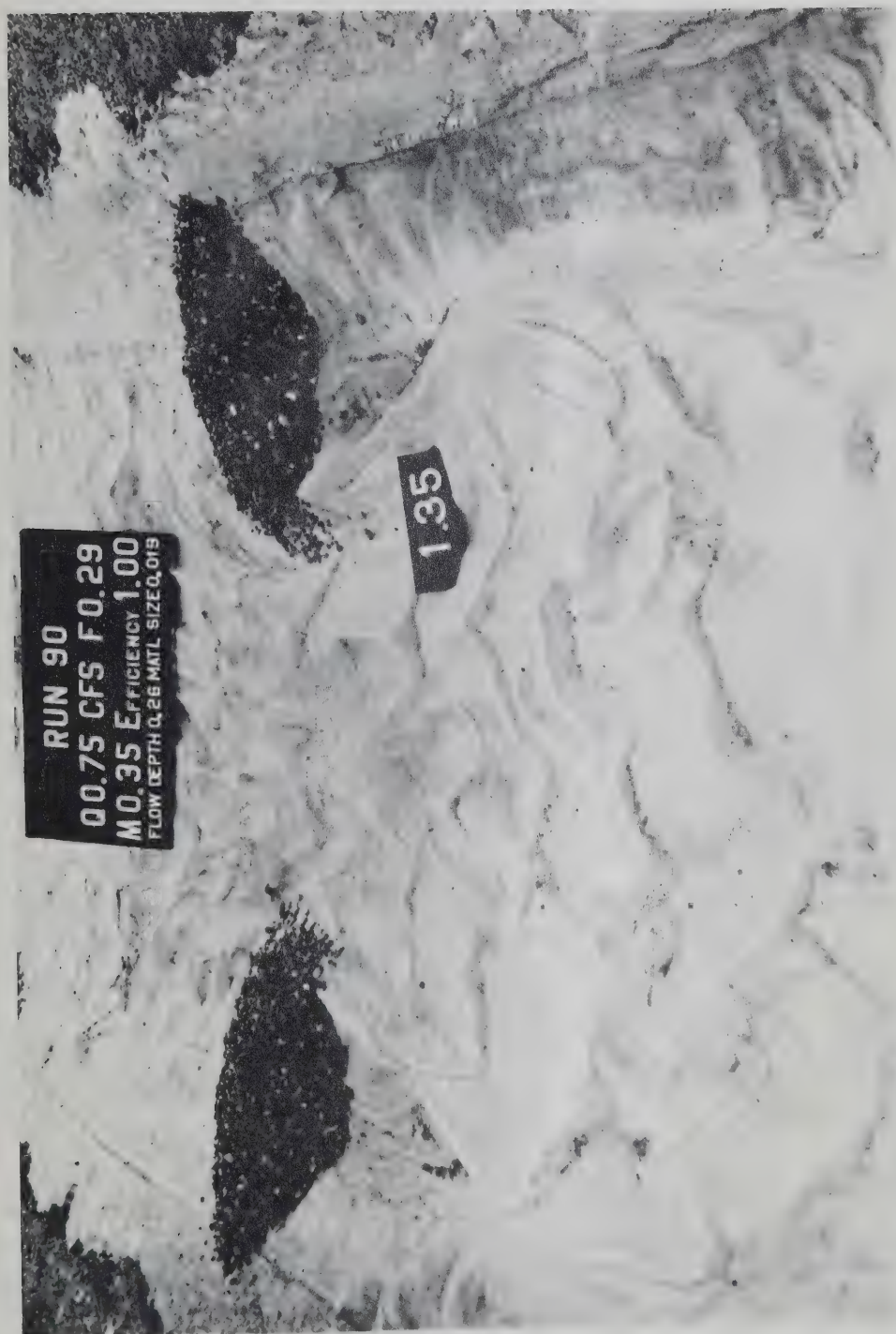


FIG. A.1 A GENERAL VIEW OF THE DUNED BED; BED MATERIAL SAND, $d_{50} = 0.25\text{mm}$
(M in photograph represents the contraction ratio)

TABLE A.1
CHARACTERISTICS OF NORMAL RUNS

F Froude number of approach flow	h Normal depth of flow in feet	V Normal velocity in fps	$\bar{\tau}_0$ Normal Shear Stress (Eq C.1) in psf	τ_c Critical Shear Stress (Eq.3.29) in psf	$\bar{\tau}_0/\tau_c$	Bed movement and form
Series B through H, d = 1.2 mm						
0.50 ^a	0.18	1.15	0.013	0.016	0.785	No movement plane bed
0.29	0.19	0.72	0.005	0.016	0.32	No movement plane bed
	0.26	0.84	0.0065	0.016	0.41	bed
0.10	0.35	0.38	0.0009	0.016	0.05	No movement plane bed
Series J, K and L, d = 0.60 mm						
0.50	0.18	1.15	0.0097	0.008	1.21	Slight movement ripples
0.29	0.26	0.84	0.0046	0.008	0.58	Very weak movement plane bed to ripples
0.10	0.35	0.38	0.0007	0.008	0.063	No movement plane bed
Series M, N and P, d = 0.25 mm						
0.50	0.18	1.15	0.0067	0.0033	2.0	Rapid movement dunes
0.29	0.26	0.84	0.0035	0.0033	1.04	Some movement ripples
0.10	0.35	0.38	0.0005	0.0033	0.15	Weak movement ripples

^aThe actual water surface slope for the normal flow was 0.0018 against the theoretical slope from Manning's formula of 0.00116 for uniform flow. (n = 0.013 for d = 1.2 mm). Detailed velocity profiles were recorded for the normal flow. From velocities measured at 0.2 depth and 0.8 depth, n was calculated assuming a logarithmic velocity distribution from boundary layer theory (Chow 1959) as 0.015

τ_c due to Shields (1936) in respect of each material is incorporated in Table A.1. It is interesting to see that bed movement was initiated at $\bar{\tau}_0/\tau_c$ values as low as 0.15 for 0.25 mm sand. Laursen (1960, 1963) also suggests beginning of sediment-transport at $\bar{\tau}_0/\tau_c$ values in the range of 0.20 to 0.80.

As indicated on Tables 4.4 and A.1, the runs in series A through H and series K were clear water runs and the rest were sediment-transporting runs. For the latter runs, sediment was fed manually at the upstream end of the flume, but this procedure can not be considered to maintain stable approach conditions, as is the case in a re-circulating flume. In other words the approach Froude number can not be considered to be strictly invariant in the sediment-transporting runs in this study. This aspect is dealt with in the analysis of data in section 6.2.3. It however needs to be mentioned that the computed value of the maximum rate of sediment discharge corresponding to the Froude number of 0.50 for the bed material of 0.25 mm, according to the design charts proposed by Cooper (1970) is only 90 parts per hundred thousand, which is indeed a low rate of transport.

APPENDIX B
TURBULENT SEEPAGE THROUGH CLOSURE DAM

APPENDIX B

TURBULENT SEEPAGE THROUGH CLOSURE DAM

B.1 Introduction

A closure dam formed of rockfill is a highly permeable structure. As closure progresses, the head differential between the upstream and downstream of the dam increases, causing considerable seepage through the body of the dam. The flow through the large voids in a prototype is turbulent. It has been established that beyond a particle Reynold's number of about 75, the flow changes from laminar to turbulent. Turbulent flow analysis has relied heavily on empirical relationships involving the porous material characteristics.

In general, the basic turbulent flow relationship has been assumed to take the form (Forcheimer, 1930).

$$i = r_1 V + r_2 V^2 + r_3 V^3 \quad (B.1)$$

or
$$i = r_4 V^\lambda$$

in which i is a representative hydraulic gradient and V is the seepage velocity through gross area.

The evaluation of constants r_1 , r_2 , r_3 and r_4 and the exponent λ has to be done empirically for the particular size and shape of the material forming the dam.

Taylor (1957) suggested a characteristic linear parameter R_m , to denote the hydraulic radius of the voids, which is the ratio of the volume of voids to the surface area of the particles.

$$\begin{aligned}
 R_m &= \frac{\text{volume of voids}}{\text{surface area of particles}} \\
 &= \frac{\text{volume of voids/volume of solids}}{\text{surface area of particles/volume of solids}} \\
 &= \frac{\text{porosity}}{\text{surface area/volume of solids}} = \frac{e}{K_t} \quad (B.2)
 \end{aligned}$$

From studies of Wilkin (1963) and Parkin (1956) the constant K_t has been evaluated to be in the range 32 - 48 from tests on crushed stones and smooth marbles ranging from 3/8" to 8". Parkin further deduced the equation

$$i = V_v^{1.85} \frac{1}{K R_m^{0.92}} \quad (B.3)$$

in which V_v represents the mean void velocity given by

$$V_v = \frac{Q_s}{A_f} \frac{(1+e)}{e} \quad (B.4)$$

in which Q = seepage discharge, A_f = gross cross-sectional area normal to flow.

Equation B.3 is similar in form to Chezy's equation

$$i = \frac{v^2}{C^2 R} \quad (B.5)$$

Izbash (1970) analysed all the variables involved in turbulent seepage from dimensional considerations and derived a similar equation

$$v_f = C_f \left(\frac{e}{1+e} \right) [D i]^{1/2} \quad (B.6)$$

in which C_f , is designated by Izbash as a "generalized Chezy coefficient".

The equation B.6 is generalized further by Izbash in the form

$$v = K_f [i]^{1/2} \quad (B.7)$$

in which K_f is the coefficient of turbulent filtration, which is primarily a function of D , the nominal size of the material and the porosity of fill. It can be seen that equations B.1, B.3 and B.7 have the same power form and involve constants which require empirical evaluation. Relevant studies in this regard have been conducted by Hausser and Michael (1959) and Cohen de Lara (1956).

In Table 5.2, the particularsof runs in which seepage discharge exceeded 10% of the uncontracted flow, have been presented. Assuming that the seepage through the closure dam follows equation B.7, an analysis is made herein to determine the coefficient of turbulent infiltration K_f for the closure materials.

B.2 Quantity of Seepage Through a Closure Dam

Referring to Fig. B.1, the information available, for the nonoverflow portion of the end-dump dam are the head difference, ΔH , the height of the dam, H_D , and the length of the dam at the base, L_b . Equations B.2, and B.4 or B.7 would not directly yield the seepage discharge, as the slope of the phreatic surface is variable in the body of the dam and the velocity of flow is not constant either longitudinally or vertically.

Step by step integration of the velocity-slope equation will lead to the formulation of total seepage discharge.

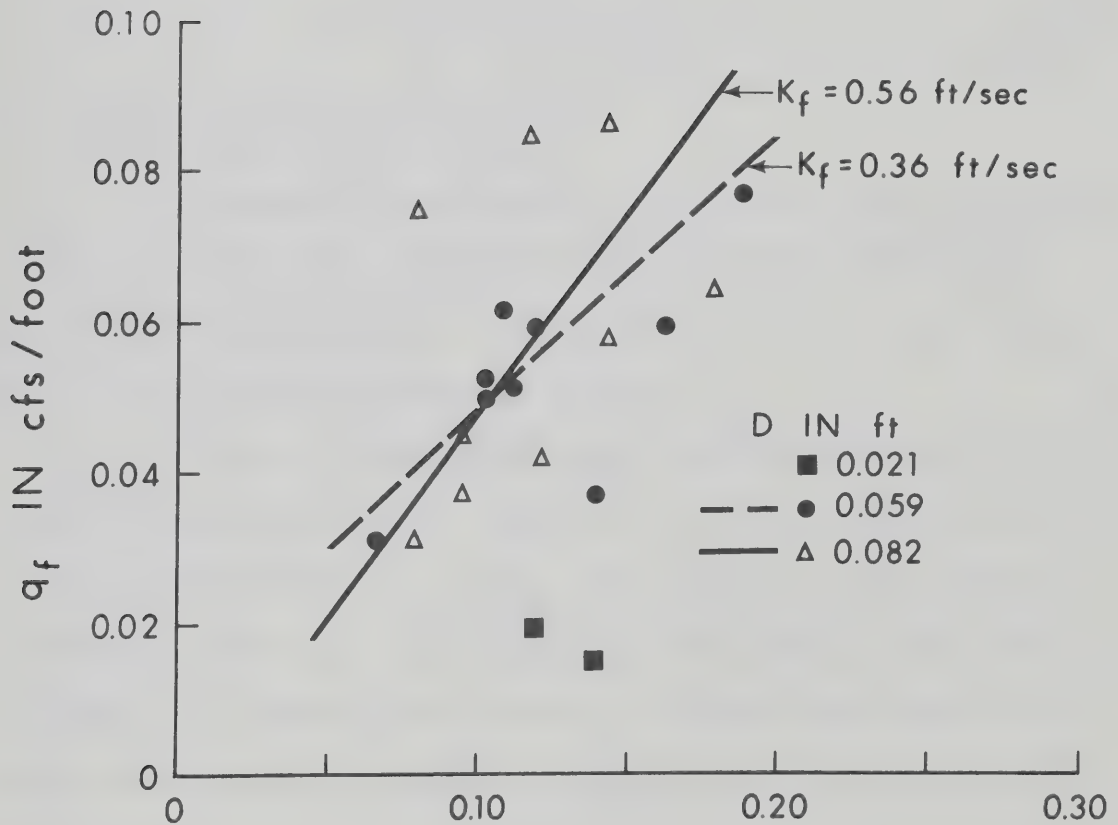
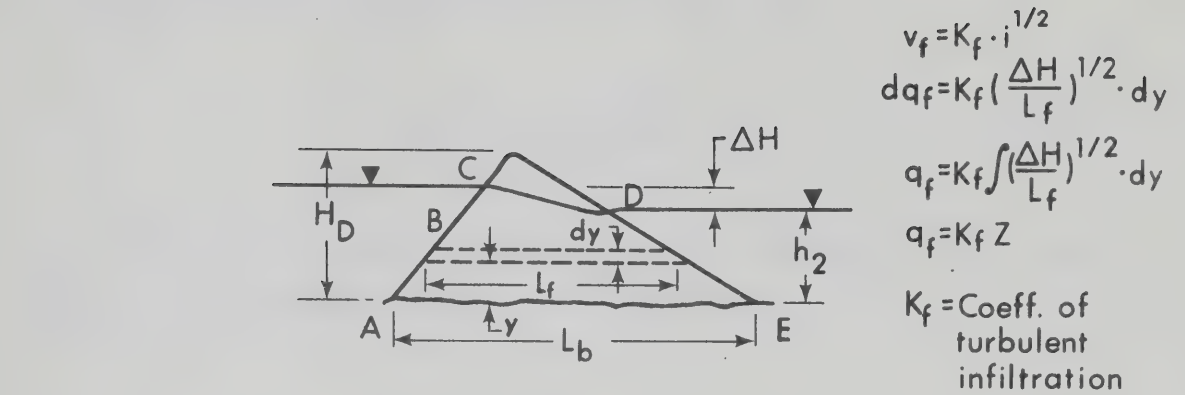
Following Izbash (1970), the saturated zone in the body of the dam (Fig. B.1) can be considered to be made of two parts, a trapezium ABDE below a horizontal line at the downstream water level and a triangle BCD above it.

From Dupuit's theory, which basically assumes that for small inclinations of the line of seepage the streamlines can be taken as horizontal, (Harr, 1962), the flow velocity is given by (Eq. B.7)

$$V_f = K_f \left(\frac{\Delta H}{L_f} \right)^{1/2} \quad (B.8)$$

By integration of Eq. B.8 with respect to depth the total seepage through the trapezoidal part is given by

$$q_{f1} = 2K_f \sqrt{\frac{H_D \cdot \Delta H}{L_b}} [\sqrt{H_D} - \sqrt{H_D - h_2}] \quad (B.9)$$



$$Z = \sqrt{\frac{H_D}{L_b}} \left\{ H_D \cdot \Delta H - 2 \sqrt{\Delta H (H_D - h_2)} + \sqrt{\frac{\Delta H^3}{3(H_D - h_2)}} \right\} \text{ in ft}$$

FIG. B.1 RELATIONSHIP FOR TURBULENT SEEPAGE THROUGH CLOSURE MATERIAL

and seepage through the triangular part is given by

$$q_{f2} = K_f \sqrt{\frac{(\Delta H)^3}{3(H_D - h_2)}} \quad (B.10)$$

q_{f2} is generally much smaller than q_{f1} . Total seepage per unit width of the dam is given by

$$q_f = q_{f1} + q_{f2} = K_f \cdot Z \quad (B.11)$$

B.3 Computation of K_f and Discussion

The hydraulic particulars (in equations B.9 and B.10) for the runs in Table 5.2 are presented in Table B.1. (Fig. B.1a is to be referred as the key diagram.) From the known values of q_f for each run, K_f is computed and presented in Table B.1.

A plot of q_f versus z for the three sizes of closure material is shown in Fig. B.1b. In spite of the scatter, the plot indicates a definite correlation of q_f and z . The slope of the line gives K_f . As shown by Parkin (Eq. B.3), K_f does not really have a unique relationship with the particle size only and depends upon porosity and shape factors which are possible reasons for scatter of the data in Fig. B.1b.

The mean values of K_f computed from the data in Table B.1 works out to 0.13, 0.36 and 0.56 ft/sec for the three closure materials of size 0.021, 0.059 and 0.082 ft. respectively. A logarithmic plot of

TABLE B.1
DATA FOR COMPUTATION OF COEFFICIENT OF TURBULENT
INFILTRATION K_f OF CLOSURE MATERIAL

Run No.	H_D in feet	ΔH in feet	h_2 in feet	L_b in feet	$\frac{z}{(Computed \text{ eq. B.9 and B.10})}$	q_f (from Table 5.2) in cfs	$K_f = q_f / z$ in ft/sec	D in feet
15	0.40	0.08	0.173	0.70	0.0612	0.025	0.385	0.059
16	0.40	0.12	0.175	0.95	0.104	0.04	0.385	0.059
20	0.38	0.096	0.164	1.05	0.079	0.032	0.406	0.08
21	0.40	0.123	0.165	1.05	0.094	0.044	0.468	0.08
30	0.51	0.065	0.375	1.40	0.12	0.019	0.15	0.059
31	0.52	0.088	0.37	1.60	0.137	0.015	0.11	0.021
33	0.45	0.02	0.377	1.30	0.065	0.03	0.458	0.021
34	0.50	0.05	0.375	1.30	0.11	0.052	0.47	0.059
35	0.63	0.125	0.37	1.30	0.163	0.059	0.362	0.059
36	0.68	0.16	0.37	1.60	0.189	0.077	0.408	0.059
45	0.38	0.073	0.25	1.00	0.104	0.053	0.51	0.059
46	0.39	0.10	0.235	1.25	0.11	0.063	0.58	0.059
48	0.36	0.06	0.257	1.15	0.085	0.075	0.90	0.082
49	0.42	0.104	0.26	1.30	0.115	0.084	0.68	0.082
57	0.39	0.095	0.255	1.10	0.119	0.059	0.496	0.059
58	0.36	0.06	0.255	0.95	0.0957	0.037	0.387	0.059
59	0.41	0.105	0.26	1.00	0.145	0.087	0.60	0.082
60	0.48	0.16	0.265	1.00	0.18	0.064	0.356	0.082
65	0.40	0.105	0.245	0.90	0.14	0.037	0.264	0.059
67	0.39	0.09	0.25	0.95	0.121	0.042	0.347	0.082
68	0.42	0.124	0.246	0.95	0.146	0.058	0.398	0.082

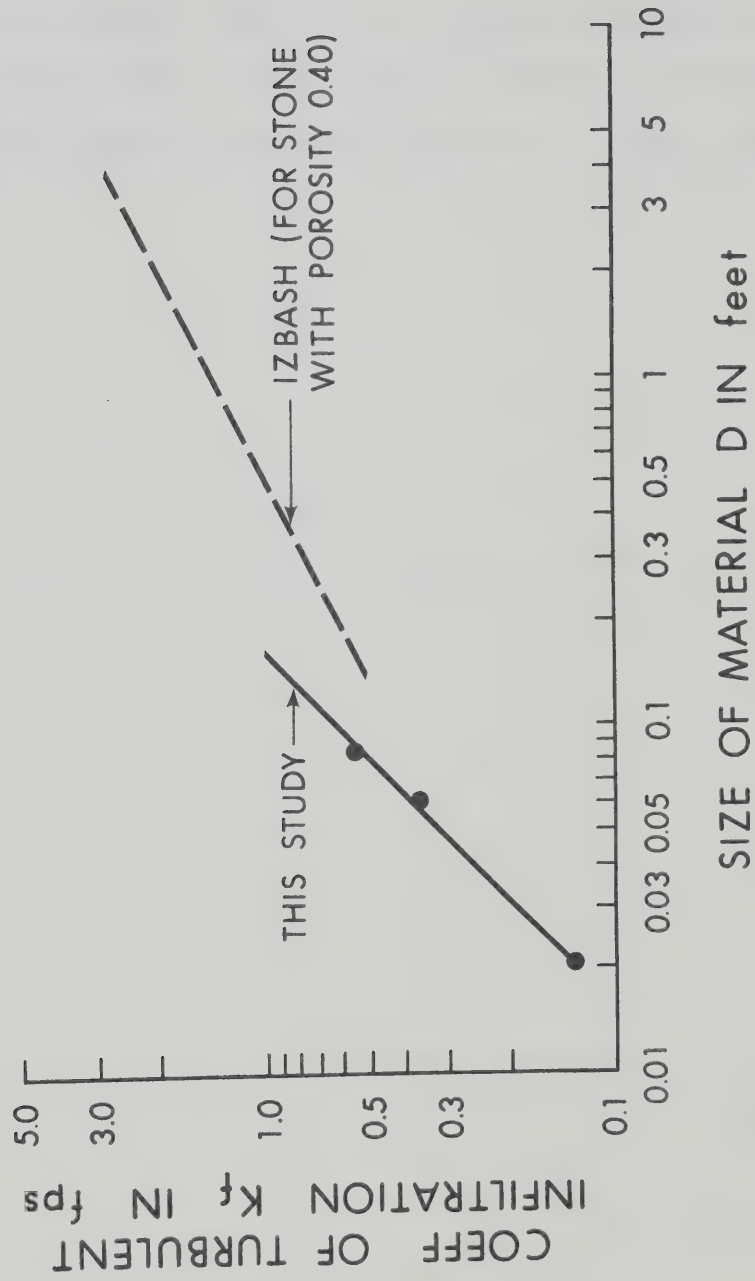


FIG. B.2 RELATIONSHIP BETWEEN COEFFICIENT OF TURBULENT INFILTRATION AND MATERIAL SIZE

K_f versus D shows a trend (Fig. B.2). Izbash's values of K_f for stone chippings are plotted on Fig. B.2. Figure B.2 is not proposed to be extrapolated or used as a design curve.

It appears that a power form of relationship between seepage velocity and the hydraulic gradient (such as equation B.7) works reasonably in the turbulent flow regime over the size range tested in this study.

APPENDIX C

ANALYSIS OF DATA BY SHEAR-STRESS STABILITY CRITERIA

APPENDIX C

ANALYSIS OF DATA BY SHEAR-STRESS STABILITY CRITERIA

C.1 Introduction

As observed in this study (section 5.5.1), the stable size of the closure material did not agree with that given by correlation (eq. 2.4) with either the mean velocity through the constriction or the maximum velocity against the closure material. It has been established in section 5.5.2 that the experimentally observed stable size agrees satisfactorily (Fig. 5.17) with the theoretical analysis, (section 3.1.3), in which the basic assumptions were

- (i) stable size can be determined by correlation with the maximum drag $\tau_{o_{\max}}$ on the face.
- (ii) $\tau_{o_{\max}} / \bar{\tau}_o$ increases exponentially with the increase of contraction ratio.

(Shear stress and drag are synonymous, denoting the hydrodynamic drag in distinction to lift).

In the course of this investigation detailed velocity measurements normal to the end-dump face have been recorded from which drag distribution on the face are obtained by assuming a boundary layer flow. Analysis and examination of the data at threshold condition are attempted herein from shear-stress stability criteria.

C.2 Experimental Measurement of Drag on Advancing Boundary

The shear stress in the flow contraction zone can be determined using the Karman-Prandtl velocity distribution for fully developed boundary layer flow over a rough bed, given by

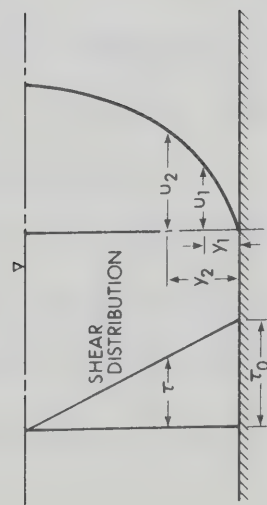
$$\frac{u}{u_*} = 5.75 \log \frac{y}{k_s} + 8.5 \quad (C.1)$$

in which u represents the velocity at a height y above the surface and u_* is the shear velocity and k_s , the roughness.

The constant 5.75 is generally applicable and constant 8.5 can be assumed for turbulent flow with particle Reynolds Number above 90, which was the case with the coarse closure material. The application of boundary layer theory is justified because the flow enters the contraction under a favourable pressure gradient and does not leave the boundary in the zone under investigation. The velocity distribution normal to the curved boundary can therefore be assumed to follow Equation C.1. Eliminating k_s and constant 8.5 by algebraic manipulation, drag on the boundary can be evaluated from the equation

$$\tau_o = \rho u_*^2 = \left(\frac{u_2 - u_1}{5.75 \log y_2/y_1} \right)^2 \quad (C.2)$$

where u_2 and u_1 represent flow velocity at depth y_2 and y_1 normal to the boundary respectively. Figure C.1 shows the definition sketch and a typical velocity-depth semilog plot.

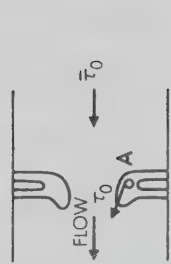


VELOCITY PROFILE FOR BOUNDARY LAYER FLOW

$$\text{LAW OF THE WALL: } \frac{u}{u_*} = 5.75 \log \frac{y}{k_s} + 8.5; \tau_0 = \rho u_*^2$$

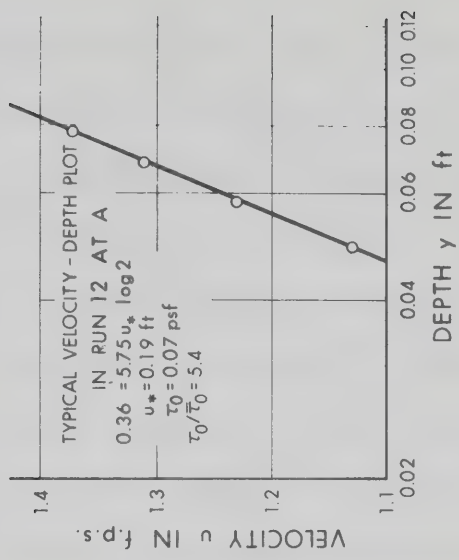
$$\text{BOUNDARY SHEAR STRESS } \tau_0 = \rho \left(\frac{u_2 - u_1}{5.75 \log_{10} \frac{y_2}{y_1}} \right)^2$$

(A)



DEFINITION SKETCH

(B)



(C)

FIG. C.1 EXPERIMENTAL MEASUREMENT OF SHEAR STRESS ON THE END-DUMP BOUNDARY

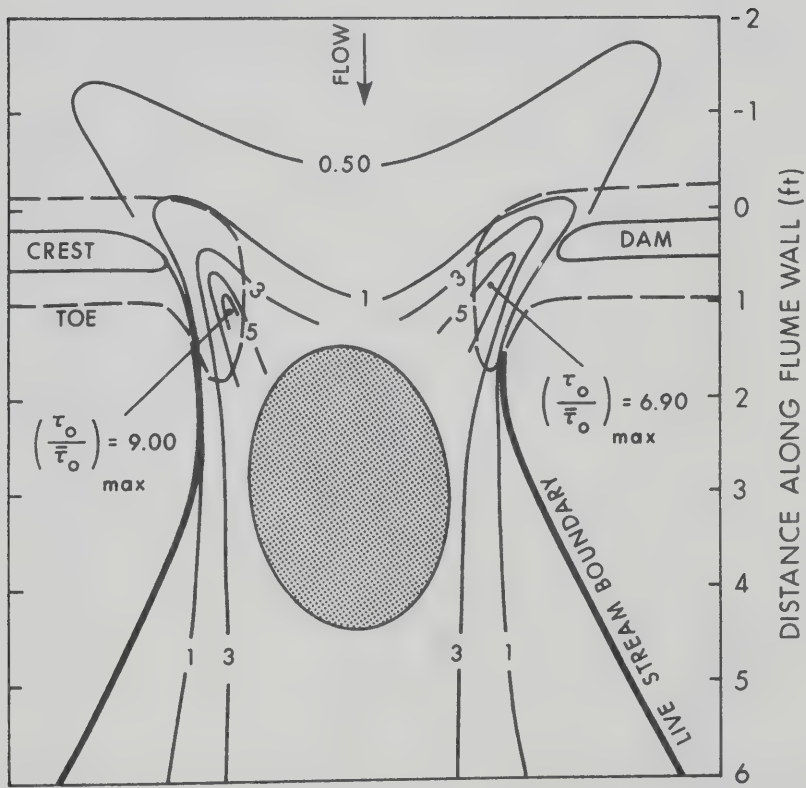
By resorting to the above procedure the shear stress distribution in the contraction zone as well as the maximum drag on the end-dump face $\tau_{0\max}$ were obtained. A typical plot of non-dimensionalized shear distribution (contours of $\tau_0/\bar{\tau}_0$) is shown in Fig. C.2. In section A, $\bar{\tau}_0$, the shear stress on the bed for uncontracted or normal flow has been evaluated for each run in this study.

Figure C.2 shows that shear stresses many times the normal occur on the advancing boundary. The locus of maximum shear has a shape similar to the live stream boundary as does the maximum velocity filament. The shear on the backwater reach and in the bed at the dump line is well below that on the slope of the dam. All these features parallel Ippen and Drinker's (1962) observations for flow along a trapezoidal channel bed.

The shear stress maxima were computed for each run. A semi-log plot of non-dimensionalised shear maxima on the advancing boundary versus the contraction ratio is shown in Fig. C.3 for all the runs in series B, C and D. The considerable scatter of the data on Fig. C.3 is to be expected, because the shear measurement based on the assumption of boundary layer flow over rough, sloping and curved boundaries, has obvious limitations.

Figure C.3, however, clearly indicates that

- (i) In the range tested, drag on the boundary increases exponentially with the contraction ratio. This attests to the validity of equation 3.6.



NOTE: IN THE SHADED REGION FLOW
SEPARATED FROM THE BOUNDARY

FIG. C.2 NON-DIMENSIONAL BOUNDARY SHEAR-STRESS
($\tau_o / \bar{\tau}_o$) DISTRIBUTION IN CONSTRICTION AT $m = 0.56$

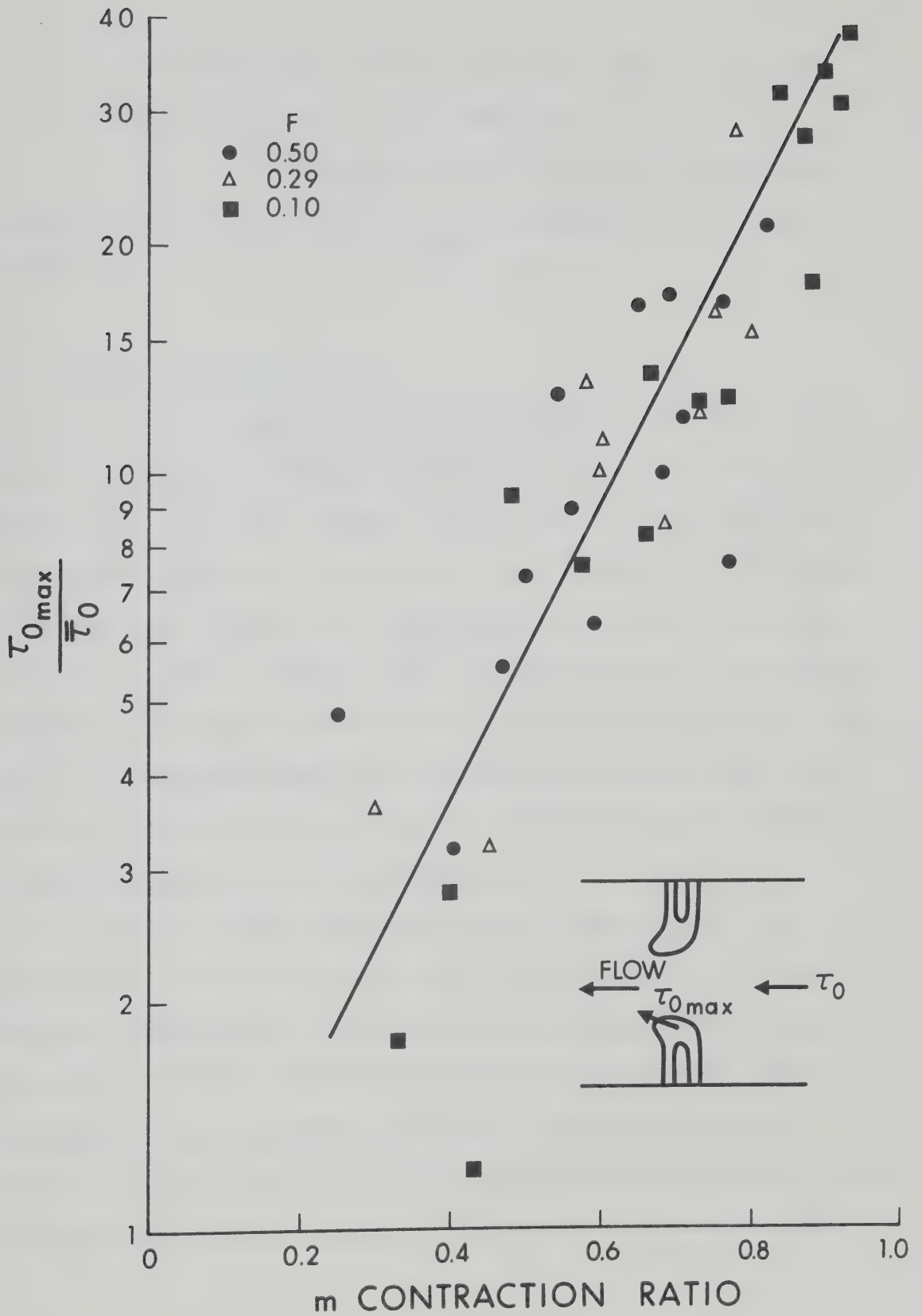


FIG. C.3 VARIATION OF NON-DIMENSIONALISED SHEAR MAXIMA $\tau_{0\max}/\bar{\tau}_0$, ON ADVANCING BOUNDARY WITH CONTRACTION RATIO m

- (ii) The effect of the variation of Froude number of approach flow on $\tau_{o_{\max}} / \bar{\tau}_o$ is not significant.

As $\bar{\tau}_o$ is known from the approach flow data, the mean curve in Fig. C.3 is used to determine $\tau_{o_{\max}}$ approximately at any stage of closure.

C.3 Effect of Hydrodynamic Lift

A.S.C.E. Task Committee on Sedimentation (1966) state "most works on initiation of motion consider only shear stress and completely ignore lift on particles, despite the fact that lift must be present". Based on the studies of Einstein and El-Samni (1949) the Task Committee concluded "that the lift is of considerable importance in entraining sediment". Studies of Chepil (1958) substantiates this. The essential feature of the studies is that lift on the top layer of particles, like drag, is also proportional to the square of the velocity close to the particle. (Einstein found u_{35} which is the velocity measured at 0.35 r_s above theoretical bed as representative).

Recent studies of Benedict and Christensen (1971), and Christensen (1971) indicate that flows in the hydrodynamically rough range will have positive values of lift. Christensen (1971), studying the state of incipient motion on cohesionless channel banks argues that "prediction of instability using the classic USBR equation based on critical drag criteria (Carter, 1953, and Lane et al 1953) and neglecting lift, must be expected to be somewhat on the unsafe side".

Christensen developed a new law for the velocity profile close to the bed (where logarithmic profile breaks down by yielding negative time-mean velocities) and deduced therefrom a relation for the lift-shear stress ratio. Christensen ultimately proposes a complex form of modification to the bank correction factor (equation 3.8) as

$$\frac{\tau_{cb(lift)}}{\tau_c} = \frac{(s^2 - \cot^2 \phi) (\cot \phi + 0.556 [\ln(\frac{10.4D_{35}}{k_s} + 1)]^2)}{0.556s [\ln(\frac{10.4D_{35}}{k_s} + 1)]^2 + \sqrt{(s^2 - \cot^2 \phi) + 0.309 [\ln(\frac{10.4D_{35}}{k_s} + 1)]^4}} \cdot \frac{1}{\cot \phi \sqrt{1+s^2}} \quad (C.3)$$

in which s = slope of the bank.

This correction factor is always less than the value obtained from equation 3.8. It will, however, approach that value when k_s/D_{35} approaches infinity. Equation C.3 has been given in graphical form for easy design use. Christensen's recommendation being relevant to the situation on the sloping end-dump face, is applied herein to determine the lift on the top layer of particles.

C.4 Stability Analysis Considering Drag and Lift

To test the hypothesis that the closure material gets entrained corresponding to a critical combination of the drag and lift

forces, the following computational steps are followed.

(1) From the design chart in Fig. 5.15, contraction ratio corresponding to a closure efficiency of 0.90 (acceptable stable condition as recommended in this study) is read out for each size of closure material at each of the three Froude numbers of 0.50, 0.29 and 0.10.

(2) $\tau_{o_{\max}}$ corresponding to the contraction ratio in Step 1 is obtained from Fig. C.3, using the known value of $\bar{\tau}_0$. (Table A.1).

(3) τ_c the critical shear stress for the closure material on a horizontal bed is computed from

$$\tau_c = 4D \text{ in fps units} \quad (C.4)$$

(4) As recommended by Christensen, $\tau_{o_{\max}}$, the actual shear stress occurring on the face should be equal to $\tau_{cb(\text{lift})} \cdot \tau_{o_{\max}} / \tau_c$ is calculated for each case.

(5) As ϕ , the angle of repose of each closure material, and s , the slope $\approx 2(\text{horizontal}):1(\text{vertical})$ is known, the design curves of Christensen based on equation C.3 are used to obtain the critical size of closure material corresponding to $\tau_{o_{\max}} / \tau_c$. (ϕ of the critical size obtained, should strictly be used and not ϕ of the actual closure material in use of the design curves. The error introduced is however insignificant).

(6) The critical size D_2 , obtained is compared with the actual size D , corresponding to design stability condition.

TABLE C.1

COMPUTATION OF STABLE SIZE CONSIDERING DRAG AND LIFT

D Closure Material	τ_c Critical Horizontal Shear for D	m Contraction Ratio at 0.9 Closure Efficiency Corresponding to Size D	$\tau_o / \bar{\tau}_o$ Corresponding to m	τ_o Corresponding to $\tau_o / \bar{\tau}_o$	τ_o / τ_c Corresponding to τ_o	D_2 Stable Size From Christensen's Curves Corresponding to τ_o / τ_c	D_3 Stable Size Corresponding to τ_o Critical Drag Stress (Eq. 3.8)
in feet	in psf	(Fig. 5.15)	(Fig. C.3)	in psf			
1	2	3	4	5	6	7	8
Series B, $F = 0.50$, $h = 0.18$, $\bar{\tau}_o = 0.013$ psf							
0.021	0.084	0.20	1.50	0.020	0.24	0.020	0.008
0.059	0.24	0.47	4.60	0.059	0.246	0.060	0.025
0.082	0.33	0.69	13.00	0.17	0.515	0.087	0.07
Series C, $F = 0.10$, $h = 0.38$, $\bar{\tau}_o = 0.009$ psf							
0.021	0.084	0.74	17.50	0.016	0.19	0.019	0.007
0.059	0.24	0.84	26.00	0.023	0.096	0.025	0.009
0.082	0.33	0.87	30.00	0.027	0.12	0.027	0.01
Series D ₁ , $F = 0.29$, $h = 0.19$, $\bar{\tau}_o = 0.0050$							
0.021	0.084	0.50	5.40	0.027	0.32	0.028	0.014
Series D ₂ , $F = 0.29$, $h = 0.26$, $\bar{\tau}_o = 0.0060$							
0.059	0.24	0.64	10.40	0.062	0.26	0.065	0.026
0.082	0.33	0.75	18.50	0.110	0.33	0.075	0.05

The observed and computed data following the above steps is presented in Table C.1. In Table C.1, the critical size D_3 , corresponding to $\tau_{0_{\max}}$ (neglecting lift) based on the USBR equation is also presented in Column 8.

The agreement between D_2 and D is indeed satisfactory, except at m values exceeding 0.80 (Series C). This is due to the possible deviation from the exponential relation between $\tau_{0_{\max}}/\bar{\tau}_0$ and m , after the two wings of the dam join at the centre which results in abnormal increase of both velocity through the constriction and shear stress on the face.

The inadequacy of neglecting lift in sediment entrainment is obvious from the consistent disagreement between D_3 (Col. 8) and D (Col. 1).

C.5 Analysis by Shields' Dimensionless Shear Stress

Shields (1936) experimental investigations of flow on a level bed, led to the generally accepted entrainment plot of the non-dimensional shear stress $\tau_* = \tau_0/(\rho_s - \rho_w)D$, versus boundary Reynolds number $R_* = u_*d/\nu$. For turbulent flow (beyond a Reynolds number of 1000) τ_* appears to be independent of R_* and takes a value of 0.04 to 0.06.

Although application of Shield's diagram to the incipient condition on the curved, sloping face of the end-dump is not justified, an analysis is made by plotting $\tau_{0_{\max}}/(\rho_D - \rho_w)D$ as abscissa against efficiency of closure, η as ordinate in Fig. C.4. The data plotted

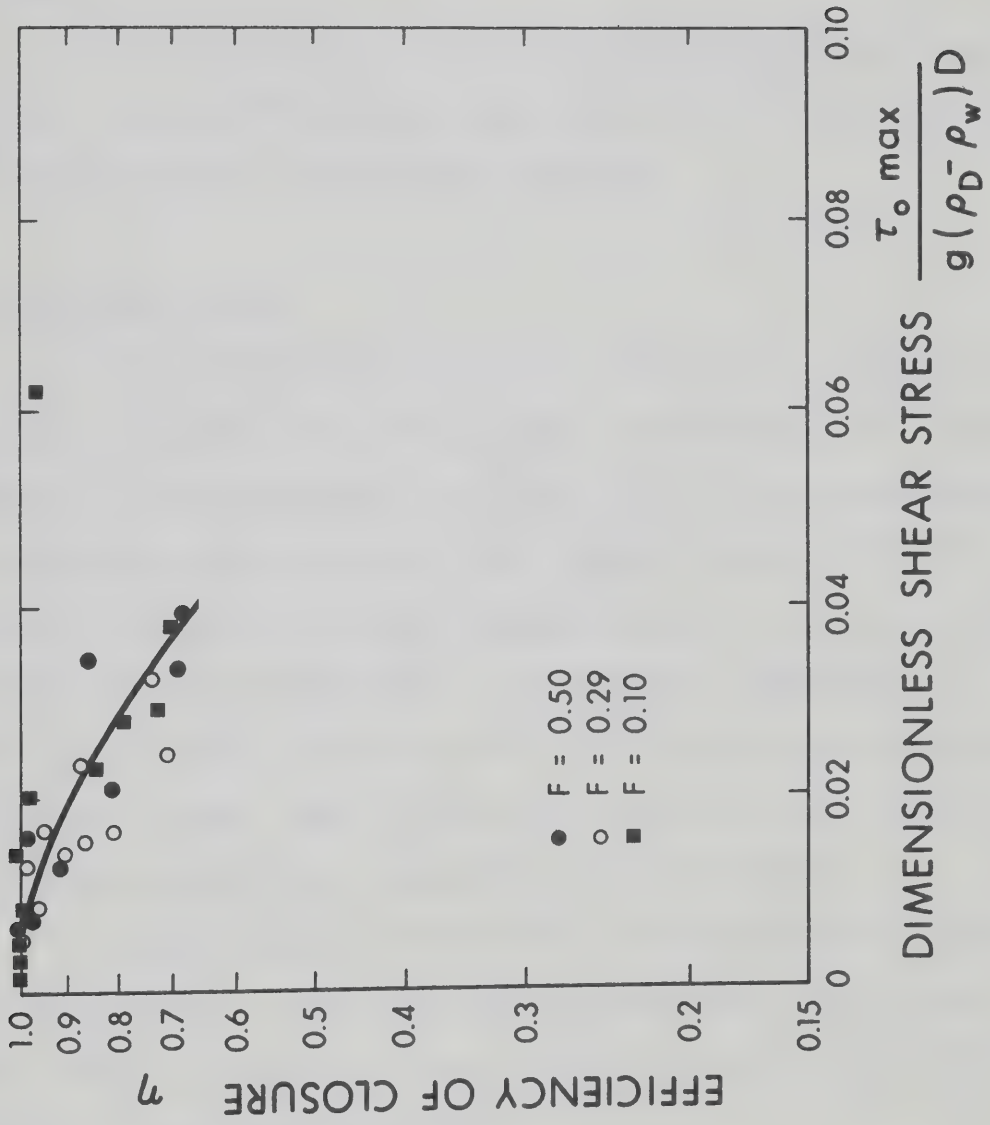


FIG. C.4 VARIATION OF EFFICIENCY OF CLOSURE η , WITH SHIELDS DIMENSIONLESS SHEAR STRESS PARAMETER τ_*

pertain to the runs in Series B, C and D, for which the efficiency of closure was above 0.70. (The measurement of $\tau_{o\max}$ at closure efficiencies below 0.70 is considered erratic, because of movement of material on the boundary).

It is interesting to note that even for highly curvilinear approach flow, Shields parameter takes a value of 0.02 at an efficiency of 0.90, considered as stable design condition.

C.6 Concluding Remarks

Maximum shear stresses occurring on the boundary have been computed from measurement of velocity normal to the end-dump face. Good agreement is observed between the critical size and the value computed by Christensen's curves correlating the size with drag and lift. An analysis in the light of Shields diagram indicated τ_* to take a value of 0.02 for the curvilinear flow on end-dump face. Correlation of stable size with drag (neglecting lift) was found to be unsatisfactory. Correlation of stable size with the value given by critical velocity criteria was observed to be unrealistic (section 5.5.1).

Although the above observations are not conclusive regarding the practicability of selecting material size on the basis of shear stress, they convincingly indicate abandonment of the velocity criterion in favour of the proposed approach.

APPENDIX D
BASIC EXPERIMENTAL DATA

TABLE D.1 BASIC EXPERIMENTAL DATA

Run No.	D Size of Closure Material in feet	b Mean Gap Width in feet	H Maximum Backwater Depth in feet	ΔH_{\max} Head Loss Between Pts A and B (Fig. 5.2) in feet	V_{\max} Maximum Velocity Against Face in f.p.s.	η Efficiency of Closure	b_c Flow Width at Vena-Contraction in feet	L_{23} Length of Contraction (Fig. 5.5) in feet	L_{34} Length of Expansion (Fig. 5.5) in feet	d_s Maximum Depth of Scour in feet	m Contraction Ratio (Computed)
1	2	3	4	5	6	7	8	9	10	11	12
Series B $Q = 1.56$ cfs, $B = 7.5$ ft., $h = 0.18$ ft., $V = 1.15$ fps, $F = 0.50$, $d = 1.2$ mm (sand)											
7	0.021	4.00	0.218	0.065	1.90	0.71	3.80	0.90	3.5	0.22	0.47
8	0.021	3.80	0.23	0.069	1.95	0.63	2.50	1.50	5.00	0.28	0.50
9	0.021	3.40	0.231	0.075	2.00	0.58	2.60	1.70	4.20	0.33	0.54
10	0.021	2.40	0.250	0.102	2.06	0.35	1.90	2.00	6.00	0.30	0.68
11	0.059	5.65	0.203	0.048	1.80	0.96	5.50	0.80	3.00	0.12	0.25
12	0.059	4.00	0.216	0.059	1.85	0.91	3.70	1.00	3.50	0.28	0.47
13	0.059	3.30	0.235	0.074	1.95	0.81	3.20	0.50	3.60	0.30	0.56
14	0.059	2.60	0.240	0.067	1.97	0.69	2.10	1.00	4.10	0.49	0.65
15	0.059	2.20	0.252	0.083	2.07	0.64	1.60	1.40	4.80	0.58	0.71
16	0.059	1.70	0.296	0.126	2.30	0.50	1.30	1.80	5.30	0.75	0.77
17	0.082	4.50	0.210	0.054	1.90	1.00	4.20	0.80	2.80	0.25	0.40
18	0.082	3.10	0.218	0.054	1.90	0.98	2.50	0.90	3.90	0.45	0.59
19	0.082	2.30	0.230	0.063	1.95	0.93	1.55	1.10	4.60	0.59	0.69
20	0.082	1.80	0.256	0.098	2.23	0.85	1.20	1.80	4.70	0.86	0.76
21	0.082	1.50	0.288	0.125	2.43	0.60	1.00	1.80	5.70	1.02	0.80

TABLE D.1 (Continued)

Run No.	D Size of Closure Material in feet	b Mean Gap Width in feet	H Maximum Backwater Depth in feet	ΔH_{\max} Head Loss Between Pts A and B (Fig. 5.2) in feet	V_{\max} Maximum Velocity Against Face in f.p.s.	n Efficiency of Closure	b_c Flow Width at Vena-Contracta in feet	L_{23} Length of Contraction (Fig. 5.5) in feet	L_{34} Length of Expansion (Fig. 5.5) in feet	d_s Maximum Depth of Scour in feet	m Contraction Ratio (Computed)
1	2	3	4	5	6	7	8	9	10	11	12
Series C $Q = 1.00$ cfs, $B = 7.5$ ft., $h = 0.38$ ft., $V = 0.35$ fps, $F = 0.10$, $d = 1.20$ mm (sand)											
24	0.002	4.30	0.38	0.016	0.80	1.00	3.80	1.00	5.00	0.00	0.43
25	0.002	2.56	0.404	0.030	1.27	0.96	2.20	0.90	6.00	0.06	0.66
26	0.002	2.03	0.414	0.035	1.40	0.62	2.00	2.30	5.00	0.14	0.73
27	0.021	5.05	0.386	0.008	0.63	1.00	4.40	1.10	5.00	0.00	0.33
28	0.021	3.90	0.393	0.015	0.86	1.00	3.00	1.50	5.00	0.01	0.48
29	0.021	2.45	0.415	0.033	1.40	0.98	2.00	1.70	5.20	0.11	0.67
30	0.021	1.20	0.446	0.073	2.07	0.67	0.90	2.10	7.00	0.53	0.84
31	0.021	0.95	0.460	0.090	2.20	0.33	0.85	2.20	--	0.43	0.87
32	0.059	4.50	0.382	0.011	0.73	1.00	3.80	1.10	6.00	0.00	0.40
33	0.059	3.20	0.397	0.021	1.04	1.00	2.40	1.10	6.00	0.00	0.57
34	0.059	1.70	0.425	0.049	1.53	0.95	1.50	1.40	7.00	0.18	0.77
35	0.059	0.90	0.50	0.128	2.17	0.82	0.88	1.50	6.50	0.58	0.88
36	0.059	0.75	0.53	0.167	2.27	0.35	0.70	--	--	0.59	0.90
37	0.082	0.60	0.55	0.183	2.63	0.72	--	--	10.00	0.59	0.92
38	0.082	0.55	0.615	0.263	3.40	0.50	--	--	--	0.60	0.93
Series D ₁ $Q = 1.00$ cfs, $B = 7.5$ ft., $h = 0.19$ ft., $V = 0.72$ fps, $F = 0.29$, $d = 1.20$ mm (sand)											
39	0.021	5.25	0.222	0.030	1.40	1.00	4.60	1.00	5.50	0.07	0.30
40	0.021	4.15	0.225	0.041	1.47	0.95	3.60	1.00	6.00	0.21	0.45
41	0.021	3.00	0.240	0.056	1.87	0.84	2.30	1.00	8.00	0.27	0.60
42	0.021	2.35	0.243	0.053	1.80	0.74	1.50	1.30	7.50	0.35	0.68

TABLE D.1 (Continued)

Run No.	D Size of Closure Material in feet	b Mean Gap Width in feet	H Maximum Backwater Depth in feet	ΔH_{\max} Head Loss Between Pts A and B (Fig. 5.2) in feet	V_{\max} Maximum Velocity Against Face in f.p.s.	η Efficiency of Closure in feet	b_c Flow Width at Vena-Contracta in feet	L ₂₃ Length of Contraction (Fig. 5.5) in feet	L ₃₄ Length of Expansion (Fig. 5.5) in feet	d_s Maximum Depth of Scour in feet	m Contraction Ratio (Computed)
1	2	3	4	5	6	7	8	9	10	11	12
Series D ₂ Q = 1.70 cfs, B = 7.5 ft., h = 0.26 ft., V = 0.87 fps, F = 0.29, d = 120 mm (sand)											
43	0.059	5.10	0.284	0.031	1.53	1.00	4.50	1.00	5.00	0.17	0.32
44	0.059	3.15	0.297	0.053	1.90	0.95	2.10	1.30	6.20	0.41	0.58
45	0.059	2.05	0.333	0.082	2.10	0.81	1.10	1.60	6.50	0.48	0.73
46	0.059	1.60	0.337	0.102	2.00	0.70	0.90	1.70	6.80	0.62	0.80
47	0.082	3.00	0.290	0.038	1.63	1.00	2.30	1.10	6.50	0.28	0.60
48	0.082	1.90	0.313	0.058	1.73	0.91	1.10	1.60	8.00	0.64	0.75
49	0.082	1.60	0.365	0.110	2.23	0.83	0.80	2.00	7.60	0.74	0.78
Series E Q = 3.00 cfs, B = 7.5 ft., h = 0.63 ft., V = 0.64 fps, F = 0.145, d = 1.20 mm (sand)											
50	0.082	1.90	0.73	0.16	2.10	0.90	--	--	--	1.17	0.75
51	0.18	1.50	0.81	0.19	2.80	0.95	--	--	--	1.28	0.80

TABLE D.1 (Continued)

Run No.	D Size of Closure Material in feet	b Mean Gap Width in feet	H Maximum Backwater Depth in feet	ΔH_{\max} Head Loss Between Pts A and B (Fig. 5.2) in feet	V_{\max} Maximum Velocity Against Face in f.p.s.	η Efficiency of Closure	b_c Flow Width at Vena-Contraction in feet	L_{23} Length of Contraction (Fig. 5.5) in feet	L_{34} Length of Expansion (Fig. 5.5) in feet	d_s Maximum Depth of Scour in feet	m Contraction Ratio (Computed)
1	2	3	4	5	6	7	8	9	10	11	12
Series F Q = 1.00 cfs, B = 4.60 ft., h = 0.26 ft., V = 0.84, F = 0.29, d = 1.20 mm (sand)											
52	0.021	2.60	0.29	--	--	0.95	--	--	--	0.15	0.435
53	0.021	1.70	0.318	--	--	0.75	--	--	--	0.38	0.65
54	0.021	1.50	0.325	--	--	0.50	--	--	--	0.49	0.68
55	0.059	2.13	0.31	--	--	0.98	--	--	--	0.26	0.54
56	0.059	1.40	0.33	--	--	0.85	--	--	--	0.53	0.69
57	0.059	1.20	0.35	--	--	0.70	--	--	--	0.56	0.74
58	0.082	1.40	0.32	--	--	0.95	--	--	--	0.48	0.70
59	0.082	1.15	0.364	--	--	0.70	--	--	--	0.56	0.75
60	0.082	0.085	0.42	--	--	0.50	--	--	--	0.57	0.82
Series G Q = 0.62 cfs, B = 2.75 ft., h = 0.26 ft., V = 0.84 fps, F = 0.29, d = 1.20 mm (sand)											
61	0.021	1.41	0.30	--	--	0.90	--	--	--	0.18	0.49
62	0.021	1.30	0.317	--	--	0.40	--	--	--	0.27	0.57
63	0.059	1.55	0.285	--	--	0.98	--	--	--	0.20	0.44
64	0.059	1.10	0.308	--	--	0.90	--	--	--	0.33	0.60
65	0.059	0.90	0.35	--	--	0.60	--	--	--	0.36	0.68
66	0.082	1.65	0.29	--	--	1.00	--	--	--	0.20	0.40
67	0.082	0.85	0.334	--	--	0.90	--	--	--	0.45	0.69
68	0.082	0.71	0.372	--	--	0.60	--	--	--	0.48	0.74

TABLE D.1 (Continued)

Run No.	D Size of Closure Material in feet	b Mean Gap Width in feet	H Maximum Backwater Depth in feet	ΔH_{\max} Head Loss Between Pts A and B (Fig. 5.2) in feet	V_{\max} Maximum Velocity Against Face in f.p.s.	η Efficiency of Closure in f.p.s.	b_c Flow Width at Vena-Contracta in feet	L_{23} Length of Contraction (Fig. 5.5) in feet	L_{34} Length of Expansion (Fig. 5.5) in feet	d_s Maximum Depth of Scour in feet	m Contraction Ratio (Computed)
1	2	3	4	5	6	7	8	9	10	11	12
Series H (One Side Closure)											
Series H ₁ Q = 0.62 cfs, B = 2.75 ft., h = 0.26 ft., V = 0.8 fps, F = 0.29, d = 1.20 mm (sand)											
69	0.021	2.35	0.29	--	--	0.90	--	--	--	0.25	0.455
70	0.059	1.10	0.317	--	--	0.90	--	--	--	0.35	0.60
Series H ₂ Q = 0.62 cfs, B = 2.75 ft., h = 0.18 ft., V = 1.22 fps, f = 0.525, d = 1.20 mm (sand)											
71	0.021	2.35	0.20	--	--	0.90	--	--	--	0.16	0.23
72	0.059	1.65	0.21	--	--	0.90	--	--	--	0.33	0.40
73	0.082	0.95	0.24	--	--	0.90	--	--	--	--	0.65
Series H ₃ Q = 0.36 cfs, B = 3.10 ft, h = 0.38 ft., V = 0.35 fps, F = 0.10, d = 1.2 mm (sand)											
74	0.021	0.80	0.44	--	--	0.90	--	--	--	--	0.74

TABLE D.1 (Continued)

Run No.	D Size of Closure Material	b Mean Gap Width	H Maximum Backwater Depth	ΔH_{\max} Head Loss Between Pts A and B (Fig. 5.2)	V_{\max} Maximum Velocity Against Face	η Efficiency of Closure	b_c Flow Width at Vena-Contracta	L_{23} Length of Contraction (Fig. 5.5)	L_{34} Length of Expansion (Fig. 5.5)	d_s Maximum Depth of Scour	m Contraction Ratio (Computed)
	in feet	in feet	in feet	in feet	in f.p.s.		in feet	in feet	in feet	in feet	
Series J $Q = 0.94$ cfs, $B = 4.15$ ft., $h = 0.26$ ft., $V = 0.84$ fps, $F = 0.29$, $d = 0.60$ mm (sand)											
75	0.021	2.52	0.28	--	--	0.98	--	--	--	0.18	0.39
76	0.059	1.62	--	--	--	0.90	--	--	--	0.55	0.61
78	0.082	0.93	0.345	--	--	0.90	--	--	--	0.68	0.74
79	0.059	1.50	0.313	--	--	0.90	--	--	--	0.70	0.65
80	0.082	0.85	0.38	--	--	0.80	--	--	--	0.72	0.80
81	0.082	1.98	0.29	--	--	1.00	--	--	--	0.35	0.52
Series K $Q = 0.56$ cfs, $B = 4.25$ ft., $h = 0.38$ ft., $V = 0.35$ fps, $F = 0.10$, $d = 0.60$ mm (sand)											
82	0.059	1.32	0.43	--	--	1.00	--	--	--	0.20	0.69
83	0.059	0.75	0.46	--	--	0.90	--	--	--	0.35	0.82
85	0.082	0.55	0.45	--	--	1.00	--	--	--	0.57	0.87

TABLE D.1 (Continued)

Run No.	D Size of Closure Material in feet	b Mean Gap Width in feet	H Maximum Backwater Depth in feet	ΔH_{\max} Head Loss Between Pts A and B (Fig. 5.2) in feet	V_{\max} Maximum Velocity Against Face in f.p.s.	η Efficiency of Closure	b_c Flow Width at Vena-Contracta in feet	L ₂₃ Length of Contraction (Fig. 5.5) in feet	L ₃₄ Length of Expansion (Fig. 5.5) in feet	d_s Maximum Depth of Scour in feet	m Contraction Ratio (Computed)
Series L Q = 0.82 cfs, B = 3.80 ft., h = 0.18 ft., V = 1.15 fps, F = 0.50, d = 0.60 mm (sand)											
86	0.021	2.54	--	--	--	0.80	--	--	--	0.14	0.33
87	0.059	1.85	0.223	--	--	0.95	--	--	--	0.44	0.51
88	0.059	1.48	0.243	--	--	0.60	--	0	--	0.60	0.61
89	0.082	1.10	0.253	--	--	0.95	--	--	--	0.73	0.71
Series M Q = 0.75 cfs, B = 3.40 ft., h = 0.26 ft., V = 0.84 fps, F = 0.29, d = 0.25 mm (sand)											
90	0.021	2.20	0.292	--	--	0.98	--	--	--	0.21	0.35
91	0.021	1.70	0.30	--	--	0.90	--	--	--	0.34	0.50
92	0.059	1.35	0.315	--	--	0.95	--	--	--	0.42	0.60
93	0.082	1.10	0.33	--	--	0.95	--	--	--	0.56	0.68
Series N Q = 0.48 cfs, B = 3.60 ft., h = 0.38 ft., V = 0.35 fps, F = 0.10, d = 0.25 mm (sand)											
94	0.021	1.60	0.385	--	--	1.00	--	--	--	0.17	0.56
95	0.021	0.90	0.415	--	--	0.90	--	--	--	0.53	0.75
96	0.059	0.60	0.465	--	--	0.90	--	--	--	0.57	0.83
Series P Q = 0.72 cfs, B = 3.40 ft., h = 0.19 ft., V = 1.10 fps, F = 0.45, d = 0.25 mm (sand)											
98	0.059	1.40	0.215	--	--	0.80	--	--	--	0.33	0.58
99	0.059	1.95	0.23	--	--	1.00	--	--	--	0.24	0.43
100	0.082	1.30	0.23	--	--	0.95	--	--	--	0.46	0.62

TABLE D.1 (Continued)

Series R	-	Runs 101 through 106	-	Qualitative Observations were made on the effect of rate of dumping on the closure material stability.
Series S	-	Runs 107 through 111	-	Applicability of the design curves on stability to irregular cross-section of natural rivers was tested by undistorted modelling (Details in Table 5.6).
Series T ₁ and T ₂	-	Runs 112 through 127	-	Design curves on scour were verified for large bed material (pebbles 6.60 mm), and light weight bed material (coal, 1.60 mm) (Details in Table 6.1).

B30038